USGS
science for a changing world

In Cooperation with the Bureau of Land Management

Geochemistry of Surface and Ground Water in Cement Creek from Gladstone to Georgia Gulch and in Prospect Gulch, San Juan County, Colorado

By Raymond H. Johnson, Laurie Wirt, Andrew H. Manning, Kenneth J. Leib, David L. Fey, and Douglas B. Yager

Open-File Report 2007-1004

U.S. Department of the Interior
U.S. Geological Survey

U.S. Department of the Interior
DIRK KEMPTHORNE, Secretary

U.S. Geological Survey
Mark D. Myers, Director

U.S. Geological Survey, Reston, Virginia 2007

For product and ordering information:
World Wide Web: http://www.usgs.gov/pubprod
Telephone: 1-888-ASK-USGS

For more information on the USGS—the Federal source for science about the Earth,
its natural and living resources, natural hazards, and the environment:
World Wide Web: http://www.usgs.gov
Telephone: 1-888-ASK-USGS

Suggested citation:
Johnson, R.H., Wirt, L., Manning, A.H., Leib, K.J., Fey, D.L, and Yager, D.B, 2007, Geochemistry of surface and ground water in Cement Creek from Gladstone to Georgia Gulch and in Prospect Gulch, San Juan County, Colorado: U.S. Geological Survey, Open-File Report 2007-1004.

Contents

Figures

Sample Locations

Streamflow

Temporal Geochemistry at the Mouth of Prospect Gulch

Temporal Geochemistry in Cement Creek

Temporal Ground-Water Geochemistry

Maps of Stream and Ground-Water Geochemistry

Noble Gas Data

Tables

Appendix Files

Conversion Factors

Inch/Pound to SI

Multiply	By	To obtain
Length		
inch (in.)	2.54	centimeter (cm)
inch (in.)	25.4	millimeter (mm)
foot (ft)	0.3048	meter (m)
mile (mi)	1.609	kilometer (km)
yard (yd)	0.9144	meter (m)
Volume		
ounce, fluid (fl. oz)	0.02957	liter (L)
pint (pt)	0.4732	liter (L)
quart (qt)	0.9464	liter (L)
gallon (gal)	3.785	liter (L)
gallon (gal)	0.003785	cubic meter (m^3)
cubic inch (in^3)	0.01639	liter (L)
cubic foot (ft^3)	0.02832	cubic meter (m^3)
cubic yard (yd^3)	0.7646	cubic meter (m^3)
Flow rate		
foot per second (ft/s)	0.3048	meter per second (m/s)
cubic foot per second (ft^3/s)	0.02832	cubic meter per second (m^3/s)
Mass		
ounce, avoirdupois (oz)	28.35	gram (g)
pound, avoirdupois (lb)	0.4536	kilogram (kg)
Pressure		
atmosphere, standard (atm)	101.3	kilopascal (kPa)

Temperature in degrees Fahrenheit (°F) may be converted to degrees Celsius (°C) as follows:
°C=(°F-32)/1.8
Vertical coordinate information is referenced to the North American Vertical Datum of 1929 (NAVD 29).
Horizontal coordinate information is referenced to the North American Datum of 1927 (NAD 27).

SI to Inch/Pound

Multiply	By	To obtain
Length		
centimeter (cm)	0.3937	inch (in.)
millimeter (mm)	0.03937	inch (in.)
meter (m)	3.281	foot (ft)
kilometer (km)	0.6214	mile (mi)
meter (m)	1.094	yard (yd)
Volume		
liter (L)	33.82	ounce, fluid (fl. oz)
liter (L)	2.113	pint (pt)
liter (L)	1.057	quart (qt)
liter (L)	0.2642	gallon (gal)
cubic meter (m^3)	264.2	gallon (gal)
liter (L)	61.02	cubic inch (in^3)
cubic meter (m^3)	35.31	cubic foot (ft^3)
cubic meter (m^3)	1.308	cubic yard (yd^3)
Flow rate		
meter per second (m/s)	3.281	foot per second (ft/s)
cubic meter per second (m^3/s)	35.31	cubic foot per second (ft^3/s)
Mass		
gram (g)	0.03527	ounce, avoirdupois (oz)
kilogram (kg)	2.205	pound avoirdupois (lb)
Pressure		
kilopascal (kPa)	0.009869	atmosphere, standard (atm)

Temperature in degrees Celsius (°C) may be converted to degrees Fahrenheit (°F) as follows:
°F=(1.8×°C)+32
Vertical coordinate information is referenced to the North American Vertical Datum of 1929 (NAVD 29).
Horizontal coordinate information is referenced to the North American Datum of 1927 (NAD 27).

Abbreviations

mg/L = milligrams per liter

µg/L = micrograms per liter

cfs = cubic feet per second

Geochemistry of Surface and Ground Water in Cement Creek from Gladstone to Georgia Gulch and Prospect Gulch, San Juan County, Colorado

By Raymond H. Johnson, Laurie Wirt, Andrew H. Manning, Kenneth J. Leib, David L. Fey, and Douglas B. Yager

Abstract

In San Juan County, Colo., the effects of historical mining continue to contribute metals to ground water and surface water. Previous research by the U.S. Geological Survey identified ground-water discharge as a significant pathway for the loading of metals to surface water in the upper Animas River watershed from both acid-mine drainage and acid-rock drainage. In support of this ground-water research effort, Prospect Gulch was selected for further study and the geochemistry of surface and ground water in the area was analyzed as part of four sampling plans: (1) ten streamflow and geochemistry measurements at five stream locations (four locations along Cement Creek plus the mouth of Prospect Gulch from July 2004 through August 2005), (2) detailed stream tracer dilution studies in Prospect Gulch and in Cement Creek from Gladstone to Georgia Gulch in early October 2004, (3) geochemistry of ground water through sampling of monitoring wells, piezometers, mine shafts, and springs, and (4) samples for noble gases and tritium/helium for recharge temperatures (recharge elevation) and ground-water age dating. This report summarizes all of the surface and ground-water data that was collected and includes: (1) all sample collection locations, (2) streamflow and geochemistry, (3) ground-water geochemistry, and (4) noble gas and tritium/helium data.

Introduction

In the late nineteenth century, San Juan County, Colo., was the center of a metal mining boom in the San Juan Mountains. Although most mining activity ceased by the 1990's, the effects of historical mining continue to contribute metals to ground water and surface water. While streams in this area have low pH and elevated metal loads due to acid-rock drainage, the influence of acid-mine drainage due to historical mining activities has degraded preexisting ground-water and surface-water quality (Church and others, 2006). As a result, viable fish and aquatic habitat is now more limited than what existed before mining (Besser and others, 2006). Since the 1990s, an increased population and a local economic base that is shifting away from hard-rock mining toward recreational tourism have increased the demand for clean water. Determining the ground-water flow and associated dissolved-metal transport is critical in protecting ground-water and surface-water resources.

Because of historical mining and degraded water quality, many surface-water samples and other data were collected in the upper Animas River watershed (fig. 1) by the U.S. Geological

Survey (Church and others, 2006; *http://amli.usgs.gov/reports/*). Three goals of this watershed characterization project are to (1) characterize the surface-water quality, (2) identify abandoned mines that contribute the greatest amount of metals to surrounding surface waters, and (3) determine premining water quality. The resulting data will provide the necessary scientific information for public land managers to select effective remedial approaches that will improve the water quality.

Ground-water discharge has been identified as a significant pathway for metal loading to surface water from both acid-mine drainage and from acid-rock drainage (Church and others, 2006; Mast and others, 2006; Kimball and others, 2002; Kimball and others, 2006). Understanding the ground-water flow and dissolved metal transport is essential in determining whether sampled metal concentrations in streams are related to acid-mine drainage or acid-rock drainage, and thus, whether or not an identified source of metals should be remediated.

In an effort to understand the ground-water flow system in the upper Animas River watershed, Prospect Gulch (figs. 1 and 2) was selected for further study because of the large amount of previously collected data (Church and others, 2006). These data included stream tracer dilution studies (Kimball and others, 2002; Wirt and others, 1999, 2001) and detailed maps of hydrothermal alteration (Bove and others, 2006). Stream tracer dilution studies provide information on water quality and quantity within the streams and from ground-water inflows. Maps of hydrothermal alteration indicate areas of mineralization that are source areas for acid-rock drainage. Many of the inactive mines within Prospect Gulch are on land managed by the Bureau of Land Management (BLM), who will use the data from this area to make decisions regarding remedial efforts. The geochemistry of surface and ground water was analyzed as part of four sampling plans: (1) ten streamflow and geochemistry measurements at five stream locations (four locations along Cement Creek plus the mouth of Prospect Gulch, table 1 and fig. 2) from July 2004 through August 2005, (2) detailed stream tracer dilution studies in Prospect Gulch and in Cement Creek from Gladstone to Georgia Gulch in early October, 2004 (figs. 3–5), (3) geochemistry of ground water through sampling of monitoring wells, piezometers, mine waters and selected springs (figs. 6–10), and (4) samples of noble gases plus tritium/helium for the determination of recharge temperatures (elevation) and ground-water age (table 2). The data from these sampling plans will be used to support the calibration of a ground-water flow model and provide the basis for a holistic model of the hydrogeochemistry of Prospect Gulch. This report summarizes all of the surface and ground water data that was collected and includes (1) all sample collection locations, (2) streamflow and geochemistry, (3) ground water geochemistry, and (4) noble gas and tritium/helium data. In addition, a grouping of the ground-water samples based on geochemistry is provided to allow for a better understanding of the ground-water flow pathways.

Geologic Setting

Prospect Gulch is part of the 28.2-Ma San Juan caldera, coincident with and (or) postdating formation of the 27.8-Ma Silverton caldera (Yager and Bove, 2002). Intermediate- to felsic-composition igneous rocks and minor volcaniclastic sedimentary rocks that were deposited on the flanks of volcanic vents predominate and are part of the Silverton Volcanics described by Lipman and others (1973). The Silverton Volcanic lavas and volcaniclastic sediments shed from the adjacent volcanoes infilled the San Juan caldera depression to nearly a kilometer in thickness over an approximately 14-km-diameter area. Primary minerals of the Silverton Volcanics intermediate-composition porphyritic lavas include, in relative order of abundance, plagioclase, quartz, hornblende, pyroxene, ± biotite, and opaque oxide minerals.

Regional-scale propylitic alteration affected much of the study area following caldera formation and was contemporaneous with the deposition of the Silverton Volcanics (Burbank, 1960). Propylitic alteration occurred as the large thickness of lavas that infilled the San Juan caldera cooled and degassed, altering the primary igneous mineral assemblage to a secondary assemblage containing quartz, chlorite, ± epidote, ± calcite, ± pyrite, fine-grained muscovite, and iron oxide minerals. This propylitic assemblage was shown to have some acid-neutralizing capacity where it was not further altered by later hydrothermal alteration (Yager and others, 2005).

Prospect Gulch is located on the margin of the historic Red Mountain mining district, which was actively mined during the late 1870's for precious metals and is located near the northwest structural margins of the San Juan and Silverton calderas. Several alteration types formed contemporaneously with or shortly after felsic intrusive activity at approximately 21 Ma, overprinting the regional propylitic assemblage and locally eliminating any acid-neutralizing capacity while introducing acid-generating minerals, especially pyrite. These assemblages are particularly evident in the vicinity of Red Mountain No. 3 (figs. 1 and 2) whose slopes drain into Prospect Gulch. The summit and slopes of Red Mountain No. 3 are stained red, yellow, and brown with secondary mineral coatings that are caused mainly by the oxidation and weathering of pyrite.

The geology of the area and types of alteration vary substantially from north to south across the Prospect Gulch subbasin (Bove and others, 2006). The majority of intensely altered terrain is exposed along the northern part of the subbasin on south-facing slopes along and beneath the ridge that separates Dry Gulch from Prospect Gulch (fig. 2). Acid sulfate mineralization is exposed near Red Mountain No. 3 and is characterized by a high sulfidization mineral assemblage that includes quartz, alunite, pyrophyllite (QAP assemblage), and pyrite. Pervasive silicification accompanied the acid sulfate alteration where it forms highly resistant ridges such as those exposed on Red Mountain No. 3. Poorly indurated and more easily weathered argillic (ARG assemblage) alteration occurs on the margins of the quartz-alunite-pyrophyllite assemblage (QAP assemblage); dickite (a waxy clay mineral in outcrop) is commonly associated with both assemblages. Areas of pervasive quartz-sericite-pyrite (QSP assemblage) alteration, locally containing 10–20 volume percent pyrite, is the most extensive alteration type exposed in Prospect Gulch. The QSP assemblage commonly crops out topographically below or adjacent to the QAP and ARG assemblages. Similar to the ARG assemblage, the QSP assemblage is more readily weathered than the QAP assemblage. Surficial deposits including debris cones and talus have formed below Red Mountain No. 3 and incorporate clasts of the upslope QAP, ARG, and QSP assemblages.

In the southern part and lower one-third of Prospect Gulch, regional propylitic alteration dominates, although it is locally overprinted by narrow, more intensely altered zones of QAP and QSP assemblages that are exposed in northeast-trending gulleys in the upper part of the subbasin that drain toward the north into Prospect Gulch. Locally, surficial deposits involving mainly propylitically altered clasts, whose source is located along the ridge that separates Georgia Gulch from Prospect Gulch, are volumetrically important.

A general structural geologic fabric is evident in and around Prospect Gulch based on interpretation of mapped veins (D.J. Bove, unpub. data, 2005; Bove and others, 2006). Northwest-, north-, and northeast-trending veins are evident along with another prominent set of east-trending veins. These veins may have formed along existing faults or formed contemporaneously with mineralization along structural zones of weakness. Definitive evidence at the surface of faulting related to vein emplacement, however, is sparse. East-west-trending veins are not as common as their north-trending counterparts, but they do occur. Major structures, if present, are obscured largely by the intense hydrothermal alteration that has affected much of the northern subbasin.

Hydrologic Setting

The stream in Prospect Gulch is approximately 2.4 km in length with an elevation change of 800 m from headwaters to the mouth. Average annual precipitation is about 114 cm with 94 cm occurring as snowfall, as confirmed by measurements at Gladstone, Colo. (2 miles north of Prospect Gulch, fig. 2) by Sunnyside Gold Corporation (Wirt and others, 2001). As a result, the majority of water available for recharge into the ground-water system occurs in late May and early June during the spring snow melt. Late June through September is dominated by summer thunderstorms, producing rainfall that provides additional water for ground-water recharge (Wirt and others, 1999). Snow generally covers the ground surface in most of Prospect Gulch from October through early May, with the frozen conditions preventing any significant recharge to the ground water system.

Sampling Methods

The installation methods and construction details for piezometers and monitoring wells used for sampling are discussed in Johnson and Yager (2006). A stream tracer dilution study was completed in Prospect Gulch on October 4, 2004, using a lithium bromide (LiBr) injection. A second tracer was completed in Cement Creek from Gladstone to Georgia Gulch using a sodium bromide (NaBr) injection on October 6, 2004. The procedures for these tracers were the same as described by Wirt and others (2001) and Kimball and others (2002). Direct streamflow measurements were done using a velocity meter and the stream's cross-sectional area following the methods described by Rantz (1982). Direct streamflow measurements and concurrent stream water sampling were always done during times when surface runoff was minimal (some snow melt water could not be avoided). Information of the sampling and analysis methods for noble gases and tritium/helium are presented in the section discussing that data.

Samples for water analyses were analyzed using inductively coupled plasma-mass spectrometry (ICP-MS, Lamothe and others, 1999), inductively coupled plasma-atomic emission spectrometry (ICP-AES, Briggs and Fey, 1996), ion chromatography (IC, d'Angelo and Ficklin, 1996), the ferrozine method for iron species (Bangthanh To and others, 1999), and titrated in the laboratory for alkalinity. Water samples for ICP-MS and ICP-AES analyses were left unfiltered or filtered in the field using a 0.45-micron capsule filter and all samples were acidified to a pH<2 with ultra pure nitric acid. Water samples for IC and alkalinity were left unfiltered or filtered in the field to 0.45 microns and all samples were refrigerated for preservation.

A detailed review of which analysis to use (ICP-MS versus ICP-AES) was done to determine which method provided the best data in terms of accuracy and precision. The precision for both methods appeared to be very good; however, the accuracy of the ICP-MS decreased for some elements at high concentrations, especially iron and aluminum. This accuracy was assessed based on a comparison of iron concentrations from the ferrozine method (Bangthanh To and others, 1999) versus ICP-MS and ICP-AES. In addition, certain wells and springs with very consistent metal concentrations were used to evaluate measurement accuracy. The plots in this report use data from the ICP-AES measurements with the exception of arsenic, copper, nickel, lead, and vanadium, which often require the lower detection limit provided by ICP-MS analyses. In addition, sulfate data from the ICP-MS method was used rather than the IC method, and rubidium data was only provided by ICP-MS.

Data Presentation

The sample locations for the five stream locations, two stream tracer injection studies, tracer inflows, and all monitoring wells, piezometers, mine shafts, and springs are shown in a series of figures. The main intent of this report is to release all of the temporal streamflow data (table 1), noble gas and helium/tritium data (table 2), and all geochemistry data (appendix A) in a format that can be easily understood via tables, graphs, and maps. These tables, graphs, and maps do not always present every analysis that was completed (all map data were created based on the file "sample points and dates used in mapping.xls" in appendix B), and the reader is referred to the file "sample locations and geochemistry.xls" in appendix A for the unabridged data set. Additional details on the calculated synoptic streamflow from the stream tracer injection studies will be provided in an additional U.S. Geological Survey Open-File Report. The resulting series of graphs and maps are extensive and a full printout of this report is not necessary for the average reader. Each section title is designed to provide a key to the type of figures that can be found in each section and the table of contents can be used to identify individual figures. All of the underlying data in these figures can be found in the appendices.

Streamflow in Cement Creek and Prospect Gulch

Streamflow and geochemistry measurements for the five locations in figure 2 were collected ten times during the period from August 2004 through August 2005. Streamflows at these five locations and the streamflows at the mouth of Cement Creek (USGS gauge 09358550) are in table 1 and shown in figures 11 and 12. Figure 11 gives a comparison with daily flow rates at the mouth of Cement Creek and figure 12 gives a comparison with the flow rate at the mouth of Cement Creek only on the direct measurement days. A comparison of streamflows at the mouth of Cement Creek versus each of the five direct measurement locations is in figures 13–17 with a best fit regression line provided on each figure. The streamflow measurement in Cement Creek above Prospect Gulch (CCPG1) in January 2005 was effected by snow plow operations damming up Cement Creek, so the flow from the regression analysis was used to provide the values in table 1 and figures 11 and 12. Snow from an avalanche prevented a measurement in Cement Creek below Georgia Gulch (CCBG) in January 2005 from being taken at the original measurement location, so this measurement was taken on Cement Creek just before the mouth of Georgia Gulch. At the measurement time, there was no evidence that Georgia Gulch was flowing, but the streamflow at this location in table 1 and figures 11 and 12 is based on the regression analysis in figure 17.

Temporal Geochemistry at the Mouth of Prospect Gulch

A series of graphs are provided that present the geochemistry of Prospect Gulch through time. Because of the low pH of the stream water (generally less than 4.0), variations of geochemistry between the filtered and unfiltered samples were generally similar and within analytical error. Since the goal of this research is to identify ground-water geochemistry (filtered) and not suspended in-stream precipitates (unfiltered), only the filtered concentrations are graphed. Plots of geochemistry through time and calculated loads (streamflow times concentration) are provided for the mouth of Prospect Gulch (figs. 18–24). An extra water sample at the mouth of Prospect Gulch was collected on February 17, 2005. This sample is included in the Prospect Gulch plots, and loads are calculated using the regression curve in figure 15. Of all the elements that were analyzed, only the rare earth elements, chloride, and any elements that were near or below detection

limits are not plotted. All the rare earth elements had very low concentrations. The chloride data was not deemed acceptable because of its detection in blank samples.

For Prospect Gulch, many elements showed similar trends and were grouped into categories based on the three temporal geochemical signatures. Field measurements of pH and electrical conductivity are not considered in these categories and are plotted separately (fig. 18). The elements Ba, Cu, and Pb show trends of higher concentrations during high streamflow. A reverse trend is seen for Si, Fe, Al, As, Ni, K, and Rb where stream concentrations are lower during low streamflow (baseflow). Since sampling was not done during times of surface runoff, all stream water quality represents a combination of snow melt, shallow ground-water discharge to surface water, and deep ground-water discharge to surface water. Field testing of snow melt that flowed overland directly into streams showed very low electrical conductivities and is assumed to have little to no dissolved constituents. Shallow and deep are relative terms, but generally represent flow in unconsolidated material (0 to 100 feet) versus flow in bedrock (100 feet plus). Deep ground-water discharge to streams generally has constant quantity and quality (confirmed by springs and monitoring wells near Cement Creek). The remaining streamflow quantity and quality is more variable, since it is derived from shallow ground water and snow melt. Water table measurements in monitoring wells and piezometers confirm a significant drop in the water levels within shallow monitoring points during stream baseflow conditions. As a result, the high concentrations of the elements Ba, Cu, and Pb seen in times of high streamflow are derived from transport in the shallow ground water. Likewise, the elements Si, Fe, Al, As, Ni, K, and Rb in streams are derived from transport in the deeper ground water. This relatively constant discharge of deeper ground water to the streams is diluted by snow melt and shallow ground-water discharges during times of higher streamflow.

Concentrations of the shallow ground-water indicators (Ba, Cu, and Pb) are in figure 19 and the resulting loads are in figure 20. Concentrations of the deep ground-water indicators (Si, Fe, Al, As, Ni, K, and Rb) are in figure 21 and the resulting loads are in figure 22. Elements that are found in both shallow and deep ground waters (inconclusive indicators) include Ca, Na, Mn, Sr, Zn, SO_4, and Mg. These elements show less variation throughout the year because of their ubiquitous occurrence and are only diluted during the spring snow melt (fig. 23). Of these inconclusive indicators, Zn has a trend slightly more similar to shallow ground water and Mg has a trend slightly more similar to deep ground water. The corresponding loads for the inconclusive ground water indicators are in figure 24.

Temporal Geochemistry in Cement Creek from Gladstone to Renoux Bridge

A series of graphs are provided that present the geochemistry of Cement Creek through time. Through the end of September 2004, minor liming was occurring at a treatment plant near Gladstone (no liming occurred after the end of September 2004). This treatment had the potential to lower some of the metal concentrations seen in Cement Creek for the August and September 2004 samples. Again, because of the low pH of the stream water (generally near 4.0), variations of geochemistry between the filtered and unfiltered samples were within analytical error and only the filtered concentrations are graphed. Plots of geochemistry through time and calculated loads presented in downstream order: Gladstone, Above Prospect, and Renoux Bridge are shown in figures 25–62 (sample locations are in figure 2). Because the concentrations and streamflow in Cement Creek at the Renoux Bridge and below Georgia Gulch are very similar, data in Cement Creek at Georgia Gulch are not plotted to make the graphs easier to read. In addition, the

constituent concentration and load data from Prospect Gulch are plotted on the Cement Creek graphs for comparison.

To provide a more logical figure organization, all of the Cement Creek plots (figs. 25–62) are grouped in the same way as the Prospect Gulch plots, first with shallow ground-water indicator elements followed by deep ground-water and inconclusive indicator elements. However, the Cement Creek geochemistry does not necessarily follow these same groups. Figures 25–62 provide one plot for each constituent showing the concentration and load changes through time and space within Cement Creek compared to the mouth of Prospect Gulch. While a detailed interpretation is beyond the scope of this report, the elements Cu, Zn, Fe, and Al are noteworthy. The main source of elements like Cu and Zn must have their main source in an area above Gladstone because these elements are diluted in concentration with a minimal change in load as Cement Creek flows past Prospect Gulch. However, Fe and Al must have a large source in and around Prospect Gulch because of the large increase in Fe and Al concentrations and loads as Cement Creek flows from the Above Prospect to the Renoux Bridge sampling locations. In addition, the Fe and Al concentrations at the mouth of Prospect Gulch are consistently at or above those seen in Cement Creek.

Temporal Ground-Water Geochemistry

Ground-water geochemistry was derived from monitoring wells and piezometers installed in 2004 (Johnson and Yager, 2006), springs, mine shafts, and a subclass of springs created by shallow one foot holes dug in bogs and fens to sample the shallow ground water (monitoring holes). All ground-water samples are appropriately classified in appendix A. In general, the samples that represent deep ground-water have the most stable geochemistry through time, whereas samples that represent shallow to intermediate ground-water have more variable geochemical conditions through time. A time series of Al, As, Fe, and Zn concentrations for several representative locations that sample the deeper ground water is in figures 63–66. These locations were selected because they had the most data through time. Likewise, a time series of Al, Cu, Fe, and Zn concentrations for locations that sample shallow ground water are in figures 67–70 with the samples at SP-2 (deep ground-water source) shown for comparison. In addition, a time series for the lower Prospect Gulch well (LPG-D) is given in figures 71–75 for Al, As, Cu, Fe, and Zn concentrations. These elements were selected because they are critical elements for stream water quality due to their influence on the viability of aquatic organisms (Besser and others, 2006). Many other element concentrations in ground water are available in appendix A.

Maps of Stream Geochemistry

During the stream tracer dilution studies, detailed geochemical data was collected from surface water and ground water. Figures 76–129 show the results for filtered concentrations of elements measured by ICP-MS or ICP-AES as outlined in the methods section, with stream samples in one figure followed by ground-water samples (discussed in the next section, but figures are put together for easy comparison). These maps can be used as companion figures to the graphs of stream geochemistry. The benefit of using a map view is an easy visualization of the changing geochemistry downstream. However, these results are limited to a snapshot in time based on geochemistry collected during the stream tracer dilution studies. Readers are referred to the graphs of stream geochemistry for temporal information (figs. 25–62). The constituents are grouped in the same manner as provided in the temporal stream concentration data to highlight shallow, deep, and inconclusive ground-water indicators. Filtered concentrations of shallow ground-water indicators

Cu, Ba, and Pb are given in figures 82–87. Filtered concentrations of deep ground-water indicators Al, Fe (ferrous and ferric), Si, Ni, Rb, K, and As are given in figures 88–107 and filtered concentrations of intermediate indicators Ca, Na, Mn, Sr, Zn, SO_4, and Mg are given in figures 108–121.

The results for Li (fig. 124) and Br (fig. 128) show the higher stream concentrations at the upstream injection points that are then diluted via inflows of ground water and other tributaries (minimal background source of Li and Br). In addition, NO_3 (fig. 126), As (fig. 106), and Se (no figure) concentrations show similar trends to Li and Br. This similarity occurred because the analytical methods for detecting As and Se are prone to interference from high Li and Br concentrations (information provided by Ruth Wolf, the analytical chemist who oversees the ICP-MS laboratory). The source of NO_3 cannot be confirmed, but is likely from fertilizer contamination in the plastic tank that was used to mix the tracer solution.

As mentioned previously, Cu and Zn show distinct sources above Gladstone with the dilution of Cu and Zn in Cement Creek as it flows past Prospect Gulch (figs. 82 and 116, respectively). Cu is also found in Prospect Gulch stream water, but it is diluted in concentration at the base of Prospect Gulch. Al and Fe show reverse trends, where the greatest Al and Fe concentrations occur at the base of Prospect Gulch and in Cement Creek below Prospect Gulch (figs. 88 and 90, respectively). Discussion of other metal concentrations is beyond the scope of this report.

Maps of Ground-Water Geochemistry

Ground-water samples include inflows sampled during the stream tracer dilution studies and samples taking during "well" sampling (includes wells, piezometers, monitoring holes, springs, seeps, and mine shafts). Maps of the ground-water geochemistry provide data on pH, conductivity, temperature, and constituents with significant concentrations (figs. 76–129, paired with stream sampling for easy comparison). The data mapped in figures 76–129 are provided in appendix B because only one date for the well sampling was included on the maps. An attempt was made to use the June 2005 sampling data when available. In addition, several wells have multilevel sampling points (Johnson and Yager, 2006) and the maps only show the analytical data from the deepest point. Again, the constituents are grouped in the same manner as provided in the temporal stream concentration data to highlight shallow, deep, and inconclusive ground-water indicators. Filtered concentrations of shallow ground-water indicators Cu, Ba, and Pb are given in figures 82–87. Filtered concentrations of deep ground-water indicators Al, Fe (ferrous and ferric), Si, Ni, Rb, K, and As are given in figures 88–107 and filtered concentrations of intermediate indicators Ca, Na, Mn, Sr, Zn, SO_4, and Mg are given figures 108–121. In addition, the same series of maps are provided for fluoride, which was found by Bove and others (2006) to be an indicator of vein mineralization in the Eureka Graben area near Gladstone (figs. 122 and 123).

Box Plots of Geochemistry in Ground-Water Categories

As previously discussed, the geochemistry of samples in Prospect Gulch indicated a separation of ground waters with deep, shallow, and inconclusive sources. These categories are expanded for comparison purposes for all ground-water samples (stream inflows, wells, piezometers, springs, and mine shafts) by assigning a category (mine, deep, intermediate, or shallow) on the basis of dissolved oxygen concentrations, changes in geochemistry throughout the year (when available), and the concentration of Al, Cu, Fe, Ba, Si, and Zn. Deep ground waters are characterized by having little to no oxygen, high concentrations of Al, Fe, and Si, (approximately

20, 60, and 50 mg/L, respectively) and little to no Cu (because Cu is not mobile in anoxic conditions). Shallow ground waters are characterized by having high oxygen concentrations, very low metal concentrations, yet high concentrations of Ba (approximately 40 μg/L) and copper (up to 800 μg/L). The intermediate ground waters were identified as having changing geochemical conditions and intermediate concentrations of Al, Fe, Si, (approximately 5, 15, 20 mg/L, respectively), Cu (10 μg/L), and Ba (15 μg/L). Mine waters were easily identified by extremely high Al, Cu, Fe, and Zn concentrations and very low Ba concentrations. These are approximate indicators for the categorization of different ground waters where the final category was selected as a best interpretation. Graphs of varying geochemistry using these different categories are given in figures 130–139 with the inclusion of the stream geochemistry for Prospect Gulch (PG stream) and Cement Creek (CC stream) from the stream tracer dilution studies.

Trends of Downstream Ground Water with a Deep Source

In the ground water with a deep source, trends of several constituents are plotted to look at spatial variation at the base of Prospect Gulch. A map of the selected monitoring points for downstream trends analyses at the base of Prospect Gulch is provided (fig. 140). Downstream trends for Al, Fe, Mg, Na, Mn, Zn, Ca, Sr, temperature, conductivity, As, and V are provided and constituents are grouped by elements that were similar in concentration and could thus be conveniently plotted together. The resulting trends are provided as a chart showing chemical concentrations at the selected monitoring points going downstream along Cement Creek (figs. 141–145) followed by maps of the same constituents at all identified deep ground-water sample sites (figs. 146–157).

Noble Gas Analyses and Tritium/Helium Data

Analyses of dissolved noble gases and tritium/helium were completed within Prospect Gulch to provide data on ground water age, recharge temperatures, and excess air levels. Summary results are provided in table 2. Complete analytical and modeling results are found in appendix C. Dissolved gas samples were collected from springs using passive diffusion samplers similar to those described in Sanford and others (1996). Additional explanation of the method of sampling dissolved gases with diffusion samplers and a total dissolved gas pressure probe is provided by Manning and others (2003). The diffusion samplers were placed directly within the spring orifice to insure that the sampled water had not re-equilibrated with the atmosphere. Dissolved gas samples were collected from wells and piezometers in clamped copper tubes as described in Stute and Schlosser (2000). A description of noble gas analytical techniques, along with tritium sampling and analytical methods, can be found in Stute and Schlosser (2000) and Solomon and Cook (2000). Recharge parameters were derived using inverse modeling as described by Aeschbach-Hertig and others (1999, 2000). Figure 158 shows a comparison of Prospect Gulch sample initial tritium (^{3}H) values (measured ^{3}H + modeled tritiogenic ^{3}He) with the precipitation ^{3}H record for Albuquerque, N. Mex. and the PG-Snow-1 sample. Sample initial tritium values are plotted against the apparent recharge year as indicated by the apparent ^{3}H/^{3}He age. Samples that plot below the precipitation ^{3}H line contain a component of water that recharged prior to 1950.

Summary

The data presented in this report is extensive and covers the geochemistry of surface and ground water from data collected in and around Prospect Gulch. This report has descriptive section

titles to guide readers to specific data and figures of interest. While the interpretive component of this report is minimal, for presentation purposes, geochemistry data for assumed water categories are provided to assist in simplifying the data results. In addition, major source areas for Cu and Zn above Gladstone and Al and Fe in and around Prospect Gulch are highlighted as significant interpretations from the stream geochemistry. Many other constituents provide insight into the surface and ground water interactions and geochemistry, but additional interpretation is beyond the scope of this report.

References Cited

Aeschbach-Hertig, W., Peeters, F., Beyerle, U., and Kipfer, R., 1999, Interpretation of dissolved atmospheric noble gases in natural waters: Water Resources Research, v. 35, p. 2779–2792.

Aeschbach-Hertig, W., Peeters, F., Beyerle, U., and Kipfer, R., 2000. Paleotemperature reconstruction from noble gases in ground water taking into account equilibration with entrapped air: Nature, v. 405, p. 1040–1043.

Bangthanh To, T., Nordstrom, D.K., Cunningham, K.M., Ball, J.W., and McCleskey, R.B., 1999, New method for the direct determination of dissolved Fe(III) concentration in acid mine waters: Environmental Science and Technology, v. 33, p. 807–813.

Besser, J.M., Finger, S.E., and Church, S.E., 2006, Impacts of historical mining on aquatic ecosystems—An ecological risk assessment*, in* Church, S.E., von Guerard, Paul, and Finger, S.E., eds., Integrated investigations of environmental effects of historical mining in the Animas River watershed, San Juan County, Colorado: U.S. Geological Survey Professional Paper 1651.

Bove, D.J., Mast, M.A., Dalton, J.B., Wright, W.G., and Yager, D.B, 2006, Major styles of mineralization and hydrothermal alteration and related solid- and aqueous-phase geochemical signatures, *in* Church, S.E., von Guerard, Paul, and Finger, S.E., eds., Integrated investigations of environmental effects of historical mining in the Animas River Watershed, San Juan County, Colorado: U.S. Geological Survey Professional Paper 1651.

Briggs, P.H., and Fey, D.L., 1996, Twenty-four elements in natural and acid mine waters by inductively coupled plasma-atomic emission spectrometry, *in* Arbogast, B.F., ed., Analytical methods manual for the Mineral Resources Surveys Program: U.S. Geological Survey Open-File Report 96-525, p. 95–101.

Burbank, W.S., 1960, Pre-ore propylitization, Silverton Caldera, Colorado, *in* Geological Survey Research 1960: U.S. Geological Survey Professional Paper 400–B, article 6, p. B12–B13.

Church, S.E., von Guerard, Paul, and Finger, S.E., eds., 2006, Integrated investigations of environmental effects of historical mining in the Animas River Watershed, San Juan County, Colorado: U.S. Geological Survey Professional Paper 1651, 6 plates, 1 DVD.

Johnson, R.H., and Yager, D.B., 2006, Completion reports, core logs, and hydrogeologic data from wells and piezometers in Prospect Gulch, San Juan County, Colorado: U.S. Geological Survey Open-File Report 2006–1030, http://pubs.usgs.gov/of/2006/1030/.

Kimball, B.A., Runkel, R.L., Walton-Day, K.W., and Bencala, K.E., 2002, Assessment of metal loads in watersheds affected by acid mine drainage by using tracer injection and synoptic sampling — Cement Creek, Colorado, USA: Applied Geochemistry, v. 17, p. 1183–1207.

Kimball, B.A., Walton-Day, Katherine, and Runkel, R.L., 2006, Quantification of metal loading by tracer injection and synoptic sampling, 1996–2000, *in* Church, S.E., von Guerard, Paul, and Finger, S.E., eds., Integrated investigations of environmental effects of historical mining in the Animas River Watershed, San Juan County, Colorado: U.S. Geological Survey Professional Paper 1651.

Lamothe, P.J., Meier, A.L., and Wilson, S.A., 1999, The determination of forty four elements in aqueous samples by Inductively Coupled Plasma—Mass Spectrometry: U.S. Geological Survey Open-File Report 99-151, 14 p.

Lipman, P.W., Steven, T.A., Luedke, R.G., and Burbank, W.S., 1973, Revised volcanic history of the San Juan, Uncompahgre, Silverton, and Lake City calderas in the western San Juan Mountains, Colorado: U.S. Geological Survey Journal of Research, v. 1, p. 627–642.

Manning, A.H., Solomon, D.K., and Sheldon, A.L., 2003. Applications of a total dissolved gas pressure probe in ground water studies: Ground Water, v. 41, p. 440–448.

Mast, M.A., Verplanck, P.L., Wright, W.G., and Bove, D.J., 2006, Characterization of background water quality, *in* Church, S.E., von Guerard, Paul, and Finger, S.E., eds., Integrated investigations of environmental effects of historical mining in the Animas River Watershed, San Juan County, Colorado: U.S. Geological Survey Professional Paper 1651.

Rantz, S.E., 1982, Measurement and computation of streamflow (2 v.): U.S. Geological Survey Water-Supply Paper 2175, 631 p.

Sanford, W.E., Shropshire, R.G., and Solomon, D.K., 1996, Dissolved gas tracers in groundwater — Simplified injection, sampling, and analysis: Water Resources Research, v. 32, no. 6, p. 1635–1642.

Solomon, D.K., and Cook, P.G., 2000, ^{3}H and ^{3}He, *in* Cook, P.G. and Herczeg, A.L., eds., Environmental Tracers in Subsurface Hydrology: Boston, Kluwer Academic Publishers, p. 397–424.

Stute, M., and Schlosser, P., 2000, Atmospheric noble gases, *in* Cook, P.G. and Herczeg, A.L., eds., Environmental Tracers in Subsurface Hydrology: Boston, Kluwer Academic Publishers, p. 349–377.

Wirt, L., Leib, K.J., Bove, D.J., Mast, M.A., Evans, J.B., and Meeker, G.P., 1999, Determination of chemical-constituent loads during base-flow and storm-runoff conditions near historical mines

in Prospect Gulch, upper Animas River watershed, southwestern Colorado: U.S. Geological Survey Open-File Report 99–159, 39 p.

Wirt, L., Leib, K.J., Bove, D., and Melick, R., 2001, Metal loading assessment of point and non-point sources in a small alpine sub-basin characterized by acid drainage—Prospect Gulch, upper Animas River watershed, Colorado: U.S. Geological Survey Open-File Report 2001–0258, 36 p.

Yager, D.B., and Bove, D.J., 2002, Generalized geologic map of part of the upper Animas River watershed and vicinity, Silverton, Colorado: U.S. Geological Survey Miscellaneous Field Studies Map MF–2377, scale 1:48,000.

Yager, D.B., McCafferty, A.E., Stanton, M.R., Diehl, S.F., Driscoll, R.L., Fey, D.L., and Sutley, S.J., 2005, Net acid production, acid neutralizing capacity, and associated geophysical, mineralogical, and geochemical characteristics of Animas River watershed rocks near Silverton, Colorado: U.S. Geological Survey Open-File Report 2005, 78 p.

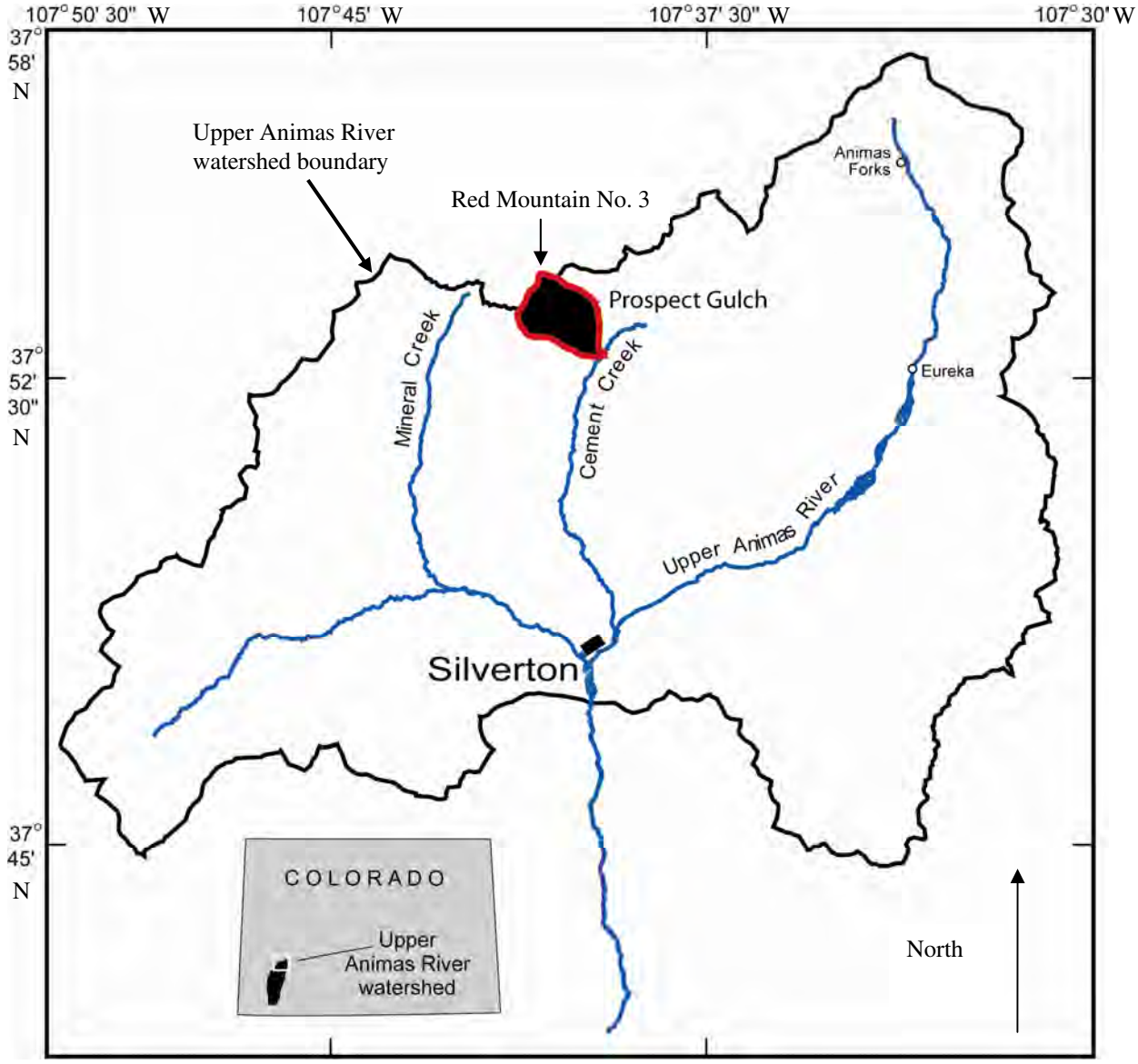

Figure 1. Location of Prospect Gulch in the upper Animas River watershed.

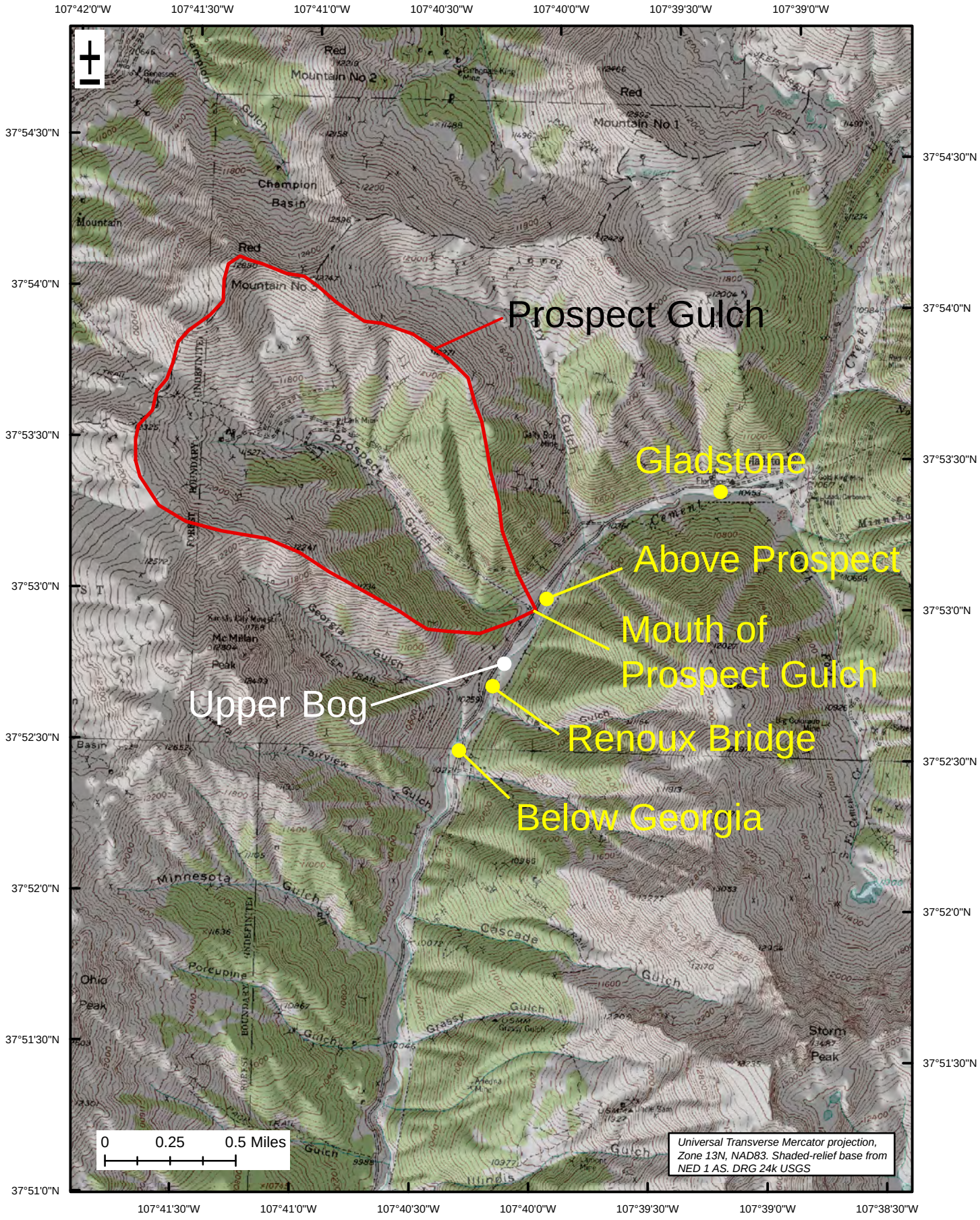

Figure 2: Detailed view of Prospect Gulch with surrounding topography, the Upper Bog (in white), and streamflow measurement locations (in yellow).

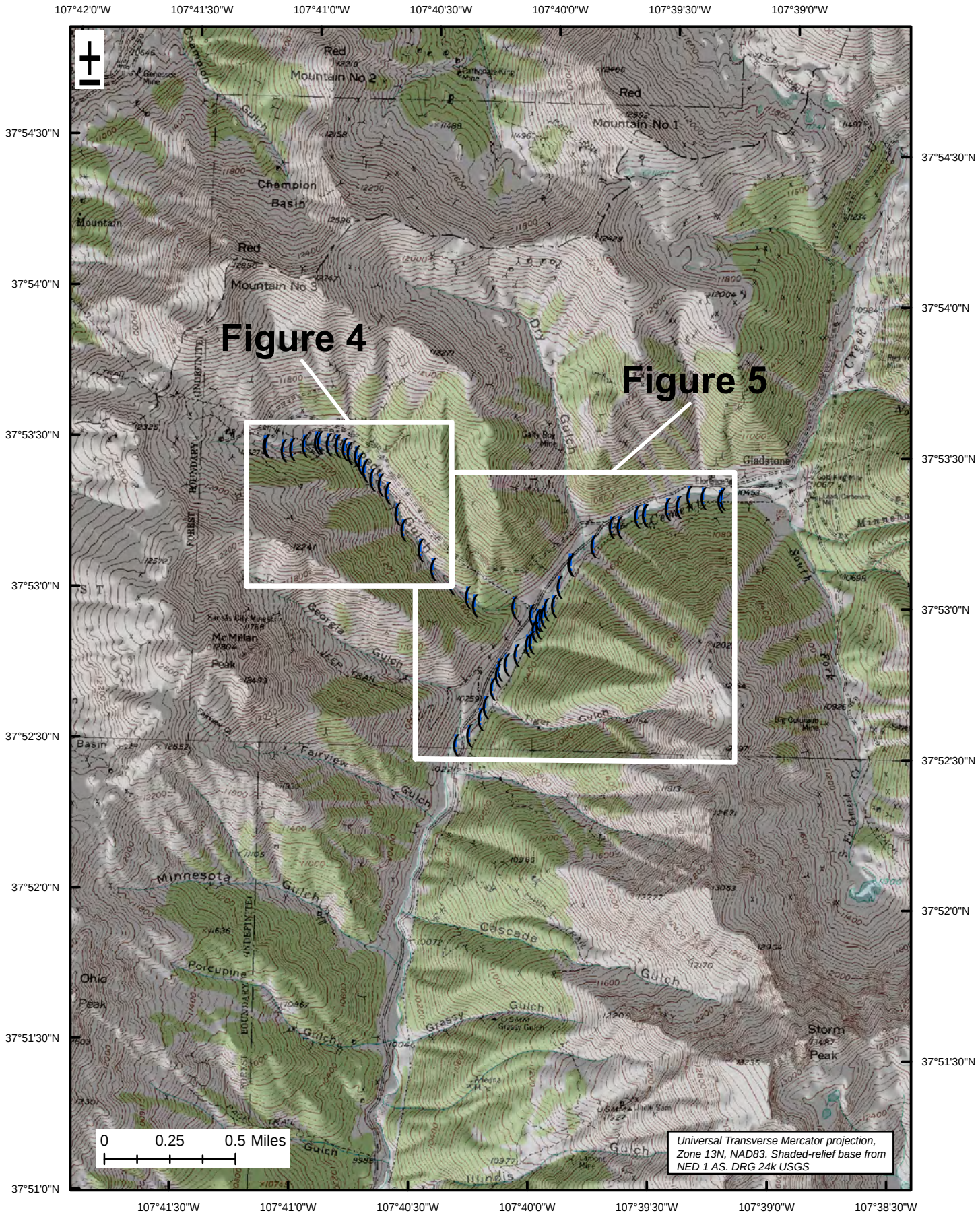

Figure 3: Locations of subsequent figures with instream sample locations.

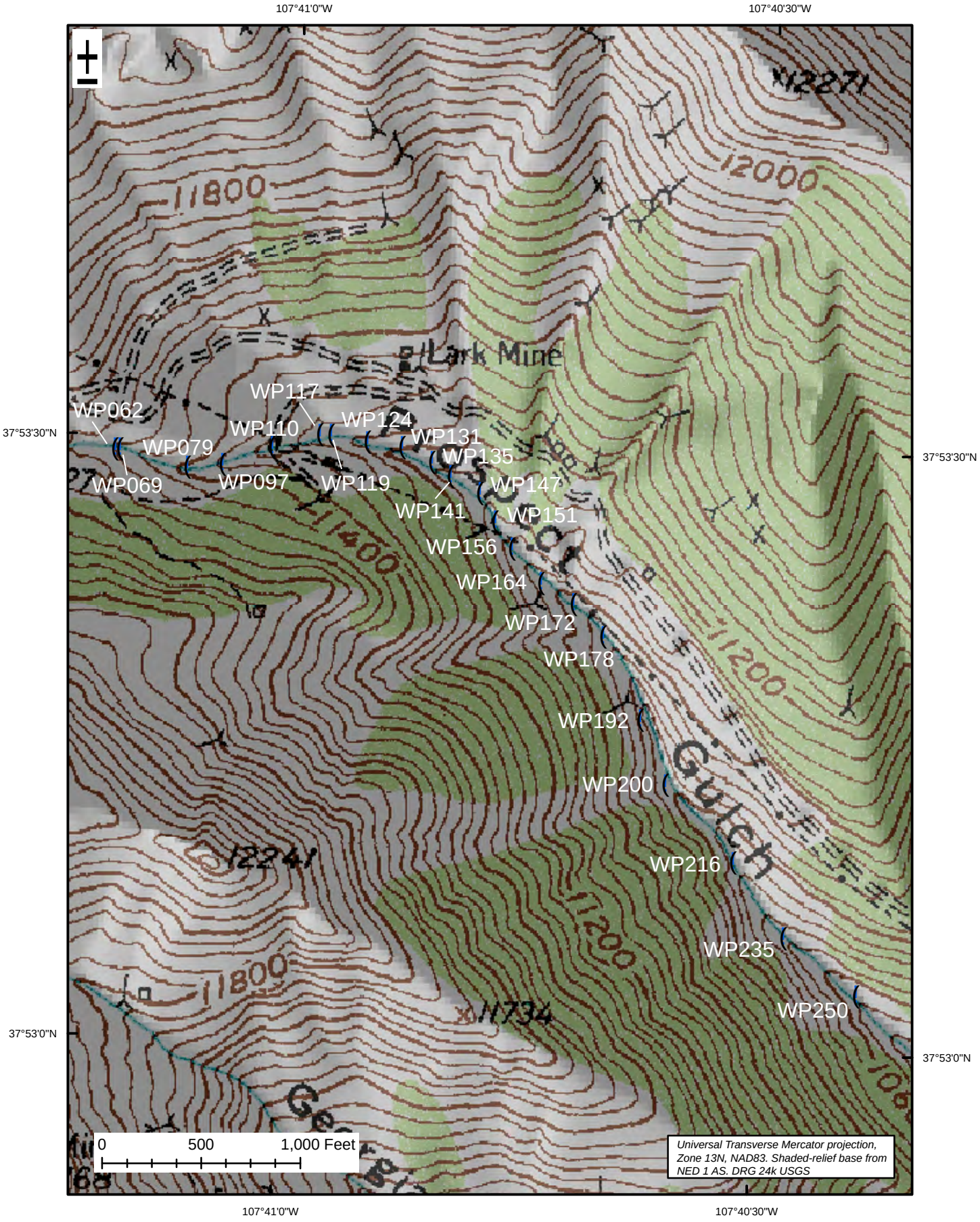

Figure 4: Instream sample locations in Prospect Gulch.

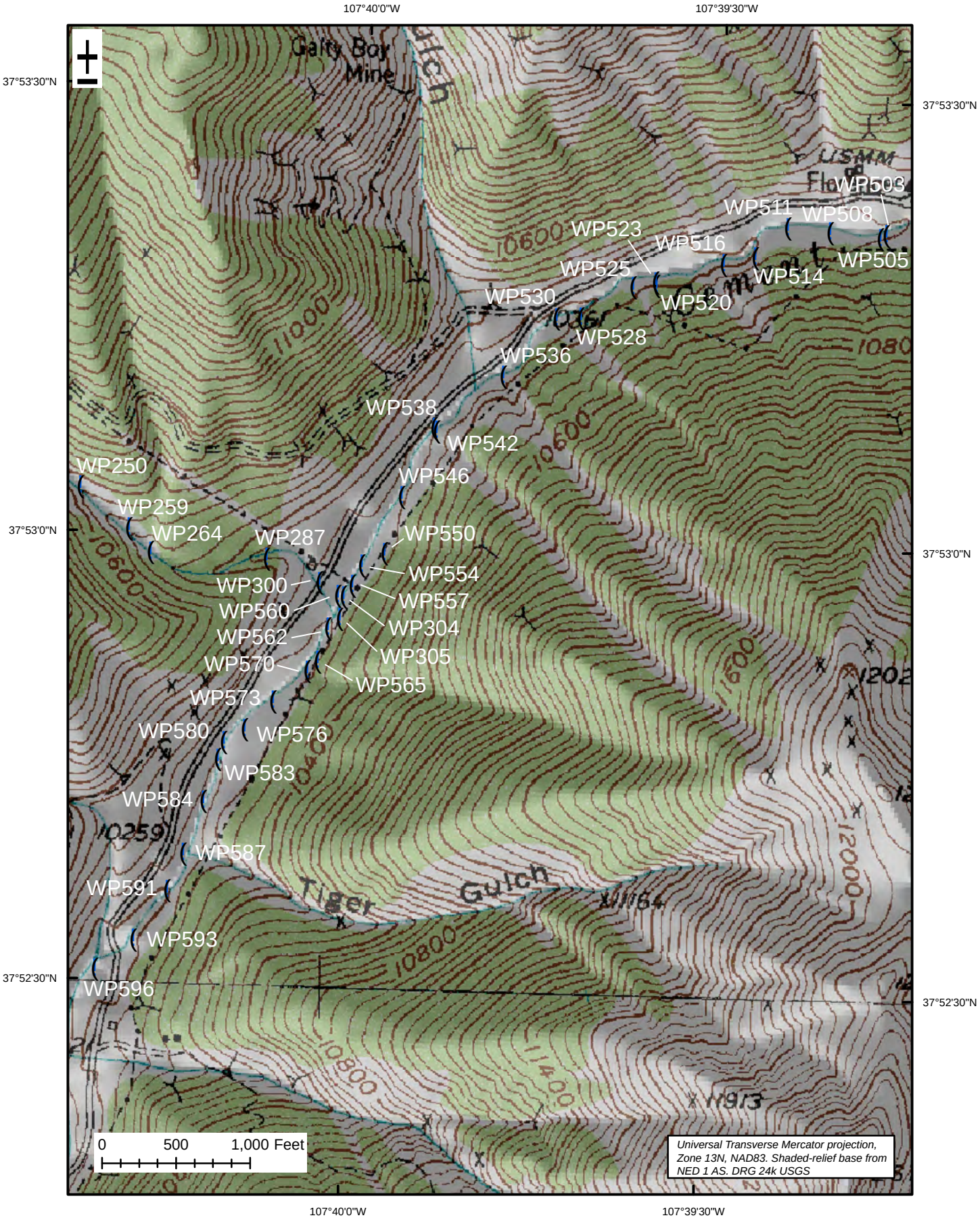

Figure 5: Instream sample locations in Cement Creek and mouth of Prospect Gulch.

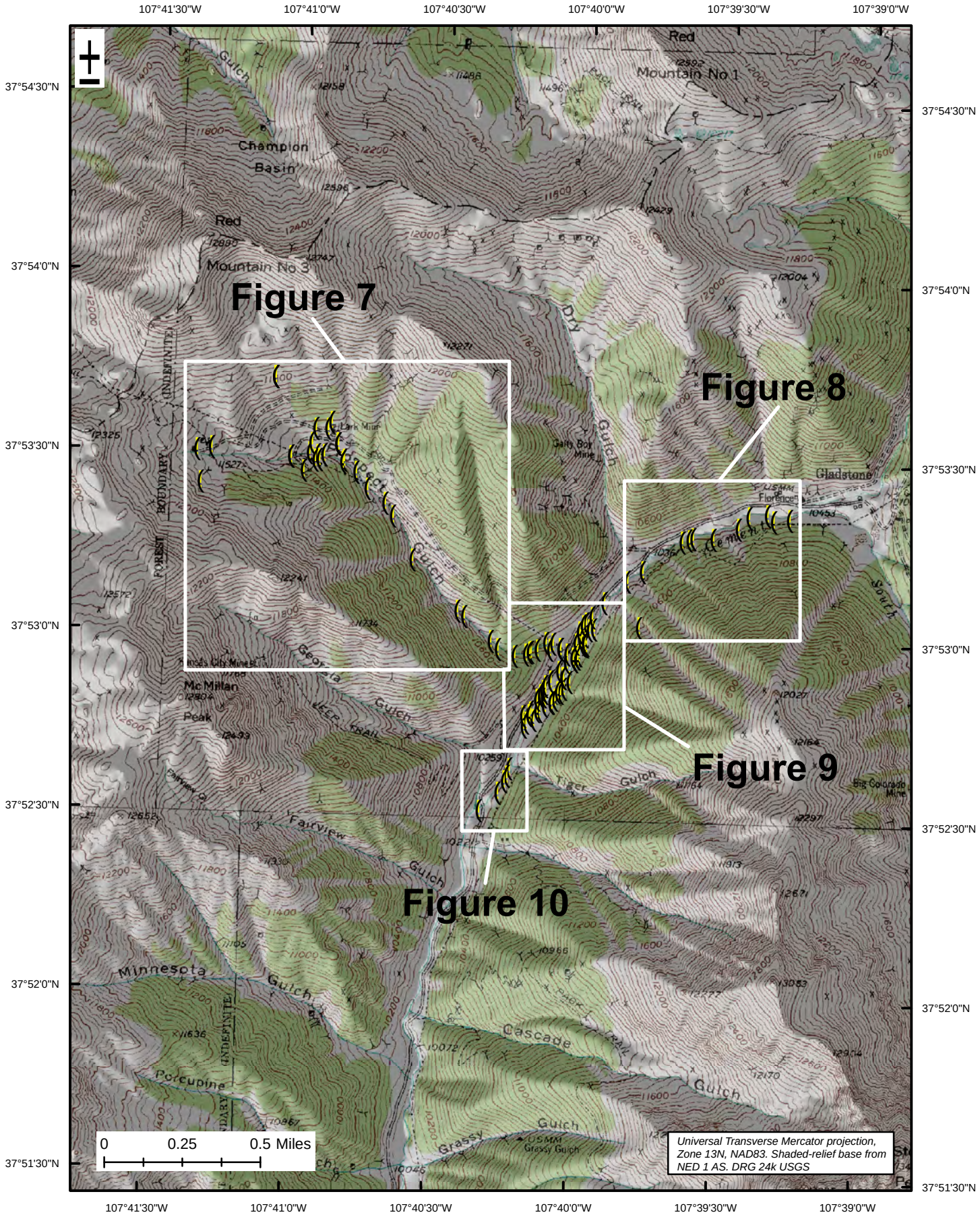

Figure 6: Locations of subsequent figures with ground-water sample locations.

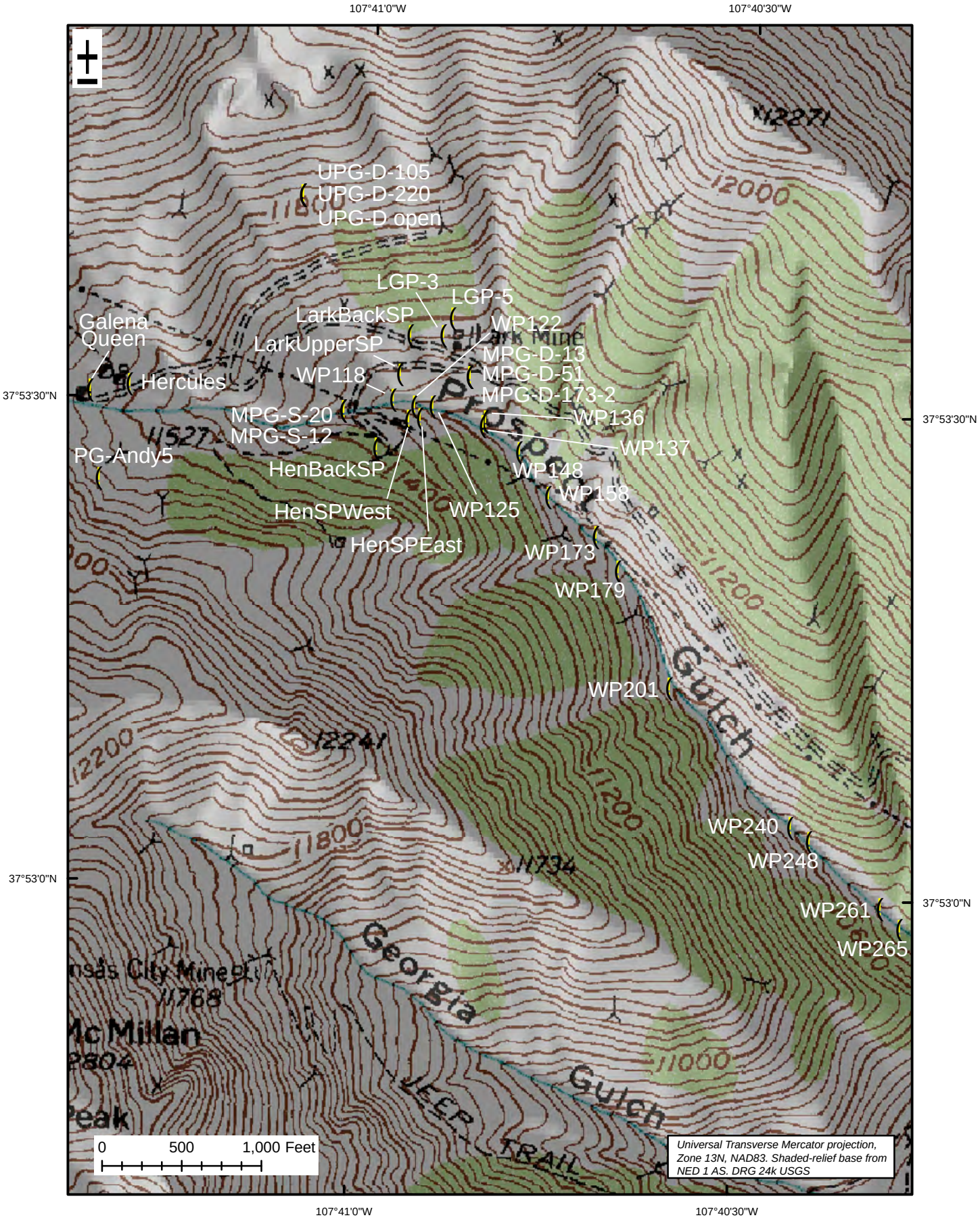

Figure 7: Ground-water sample locations in Prospect Gulch.

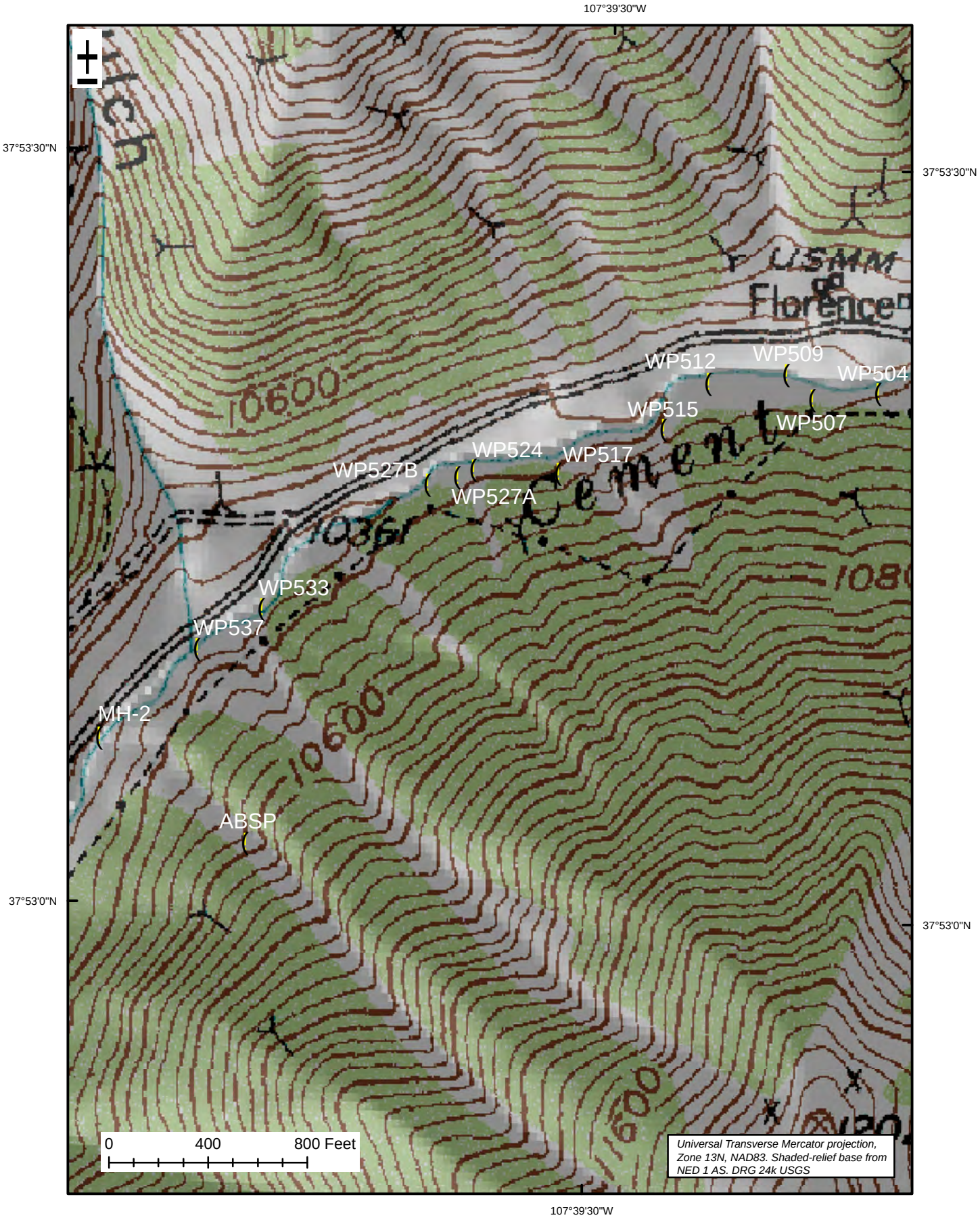

Figure 8: Ground-water sample locations in Cement Creek near Gladstone.

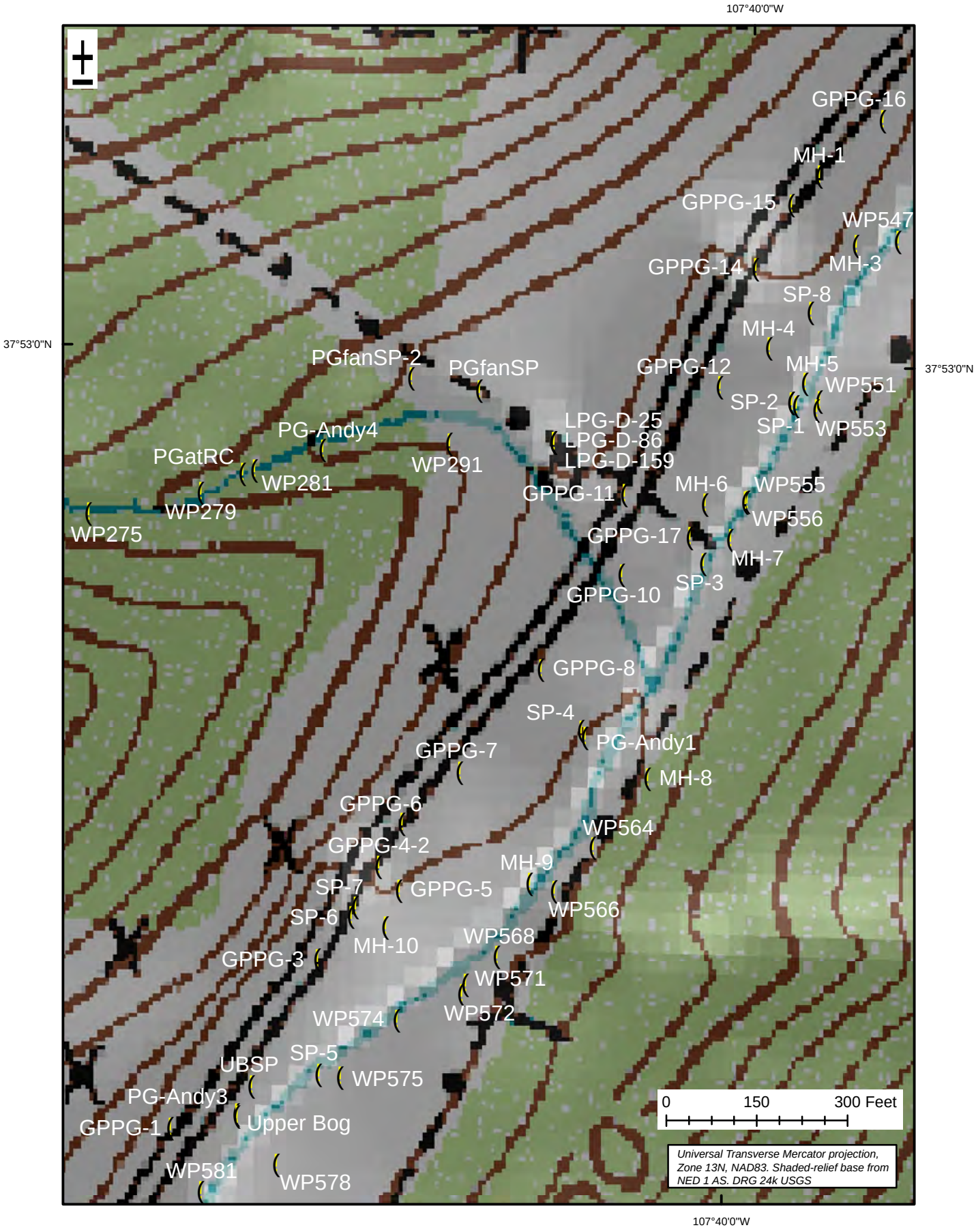

Figure 9: Ground-water sample locations in Cement Creek near Prospect Gulch.

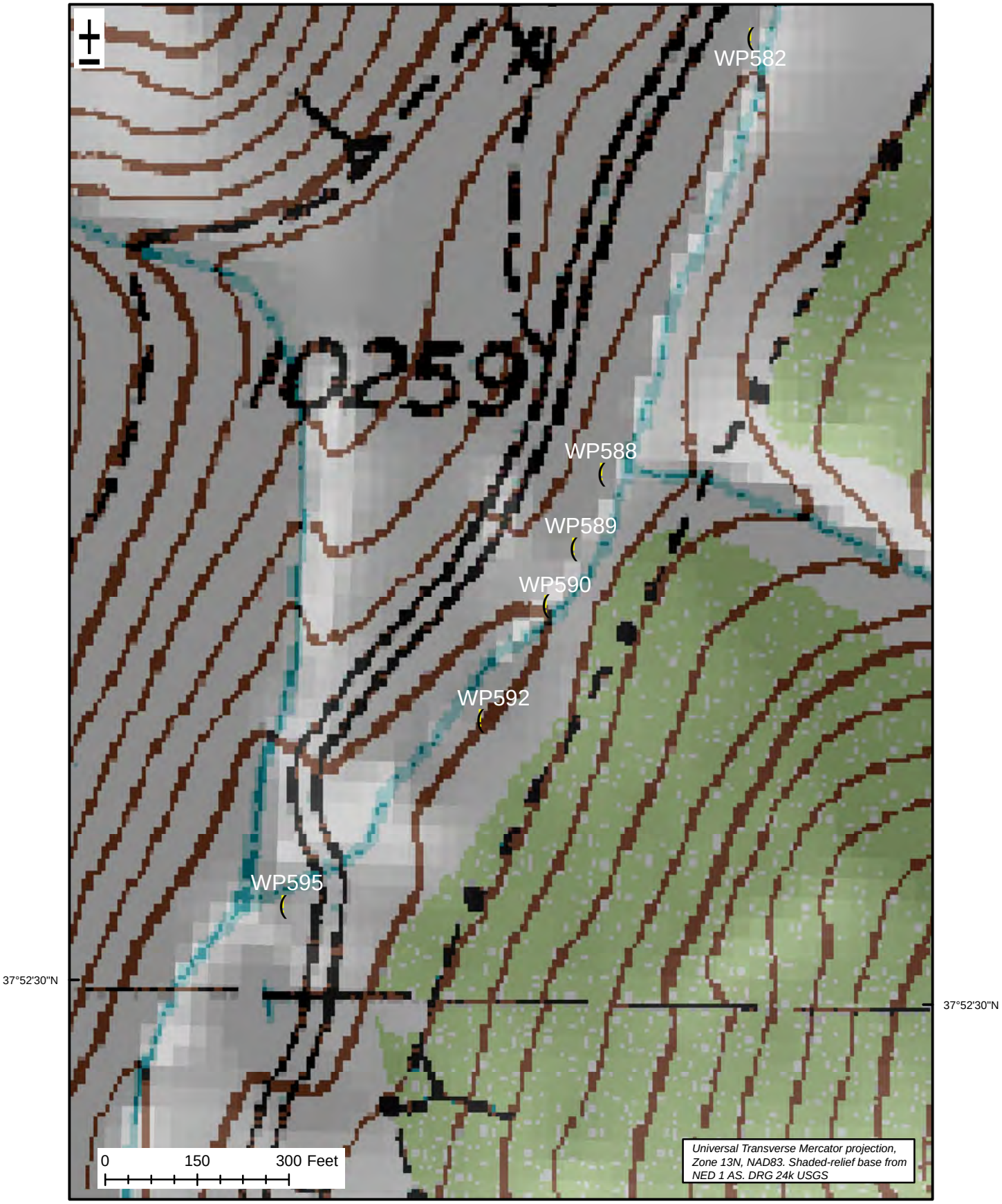

Figure 10: Ground-water sample locations in Cement Creek near Georgia Gulch.

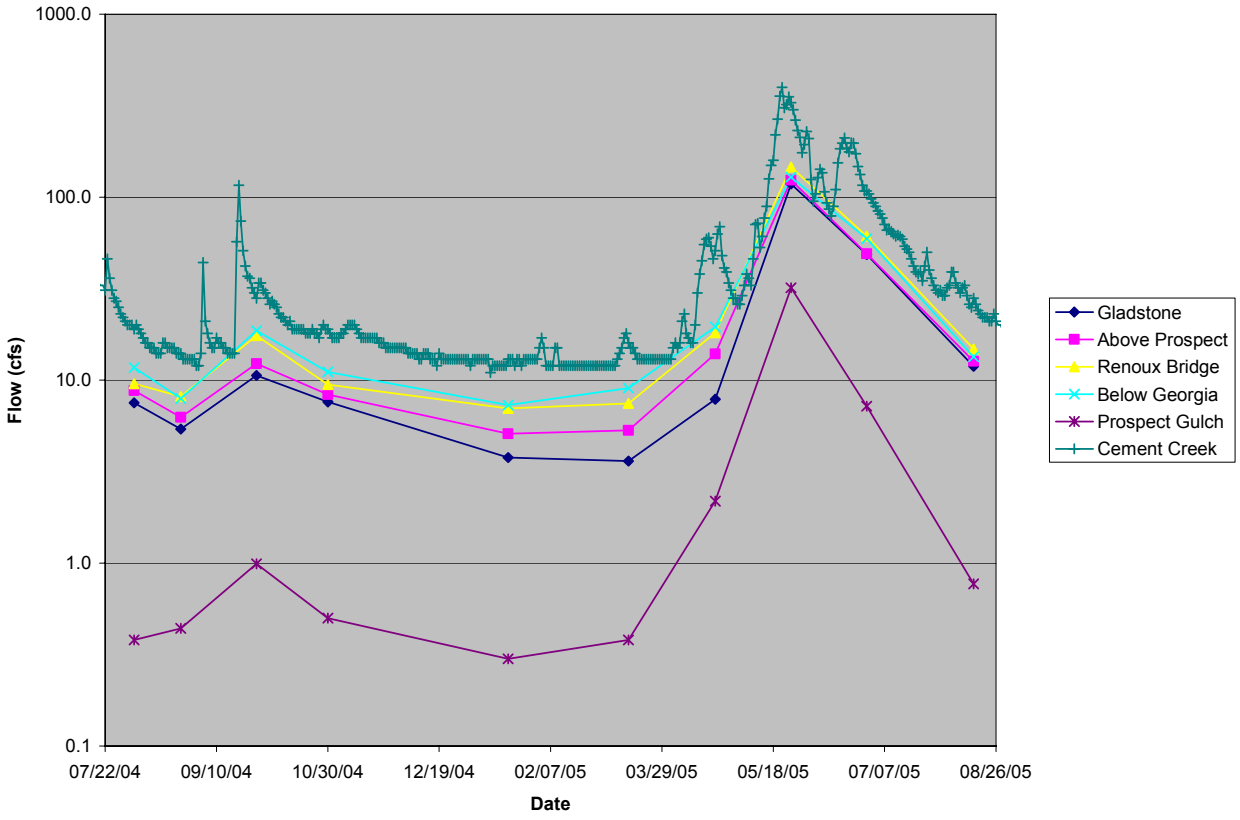

Figure 11: Streamflow at the five selected locations in Cement Creek on measurement days and the mouth of Cement Creek on a daily basis.

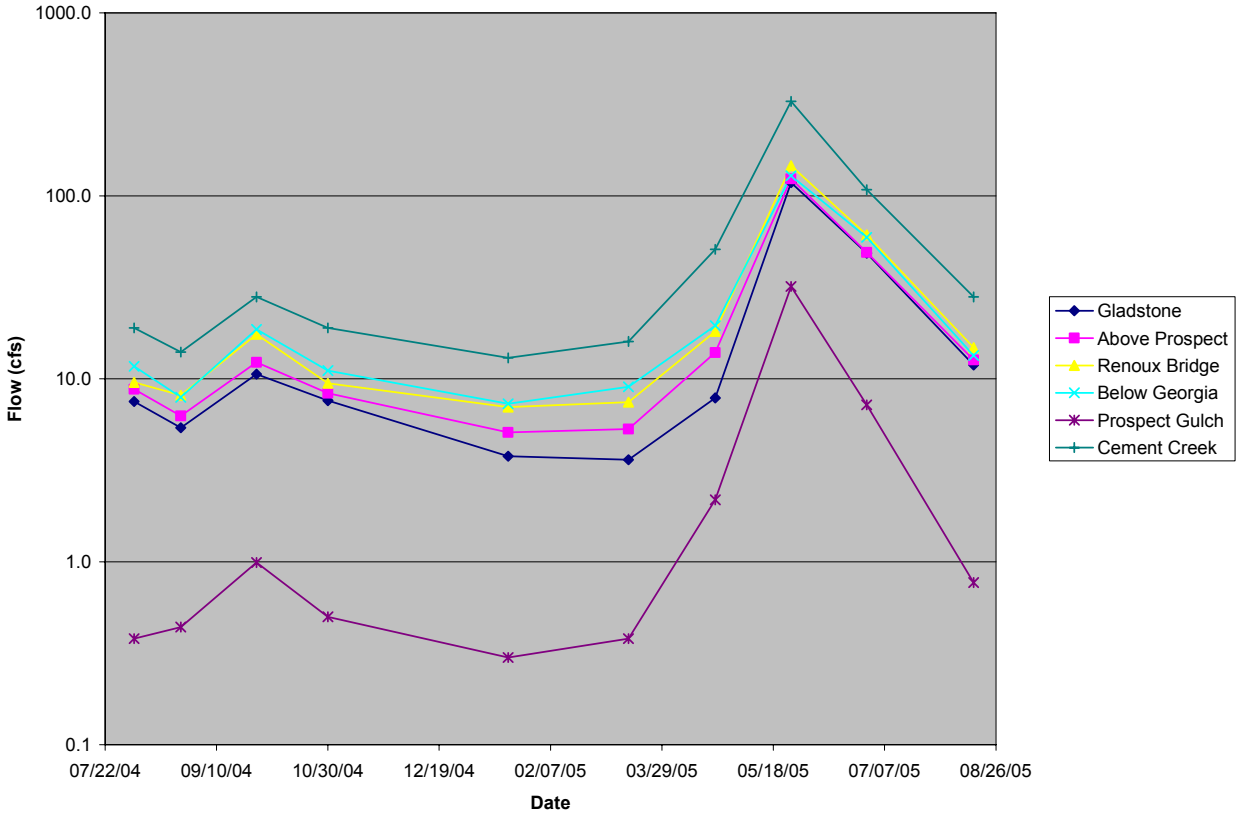

Figure 12: Streamflow at the five selected locations in Cement Creek and the mouth of Cement Creek on measurement days.

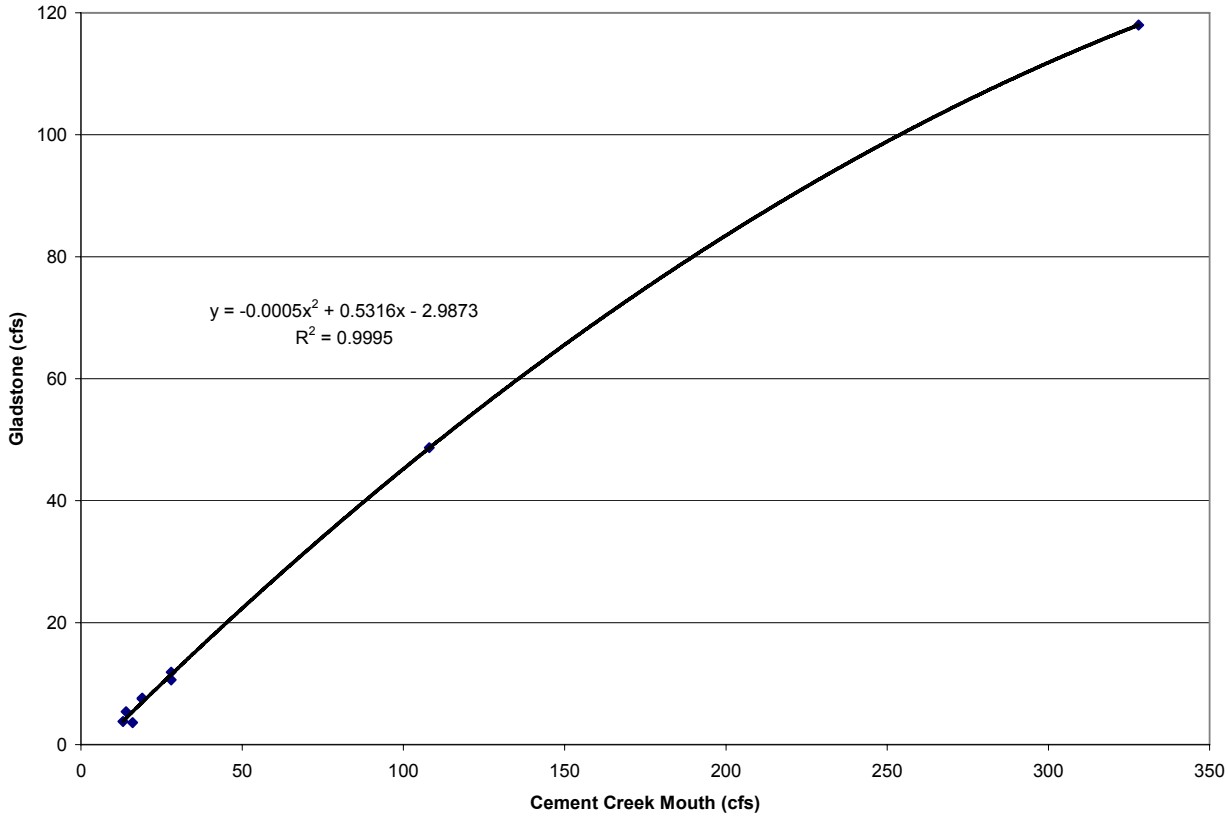

Figure 13: Streamflow with regression analysis for the mouth of Cement Creek versus Cement Creek at Gladstone.

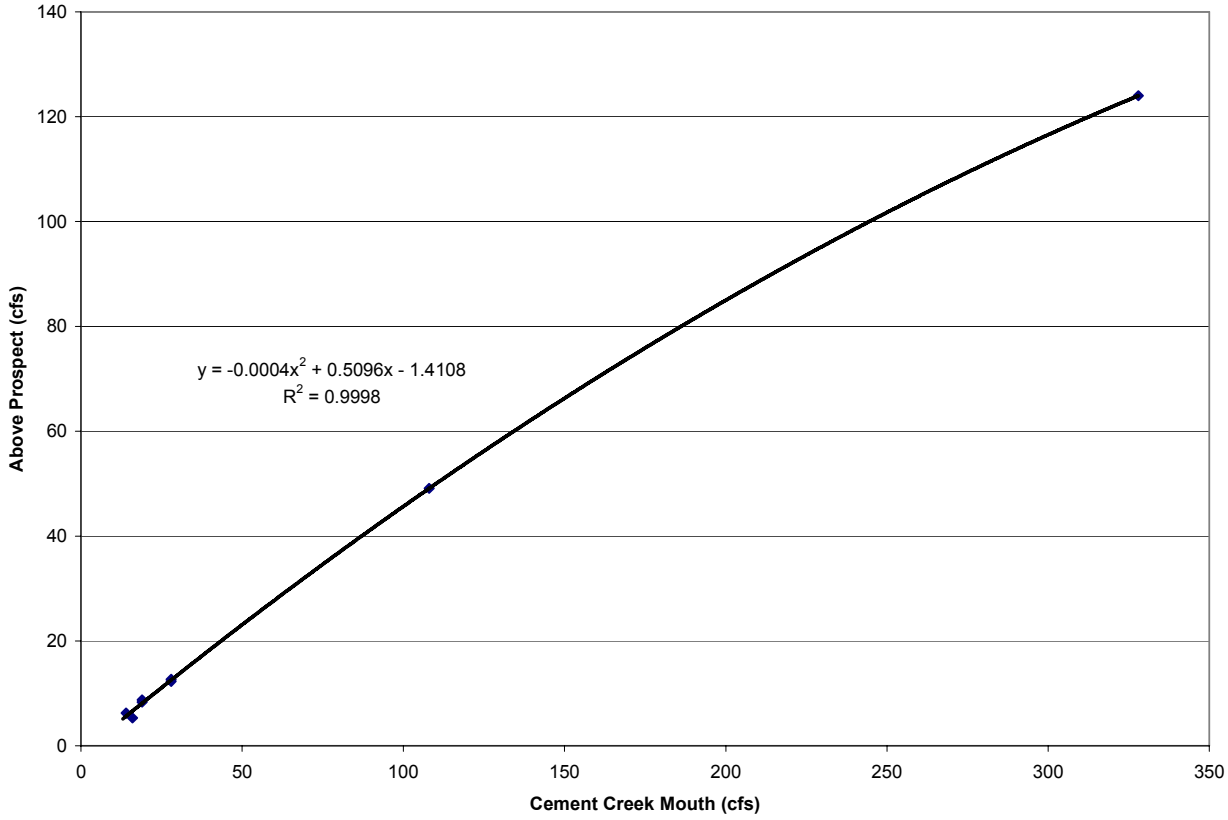

Figure 14: Streamflow with regression analysis for the mouth of Cement Creek versus Cement Creek above Prospect.

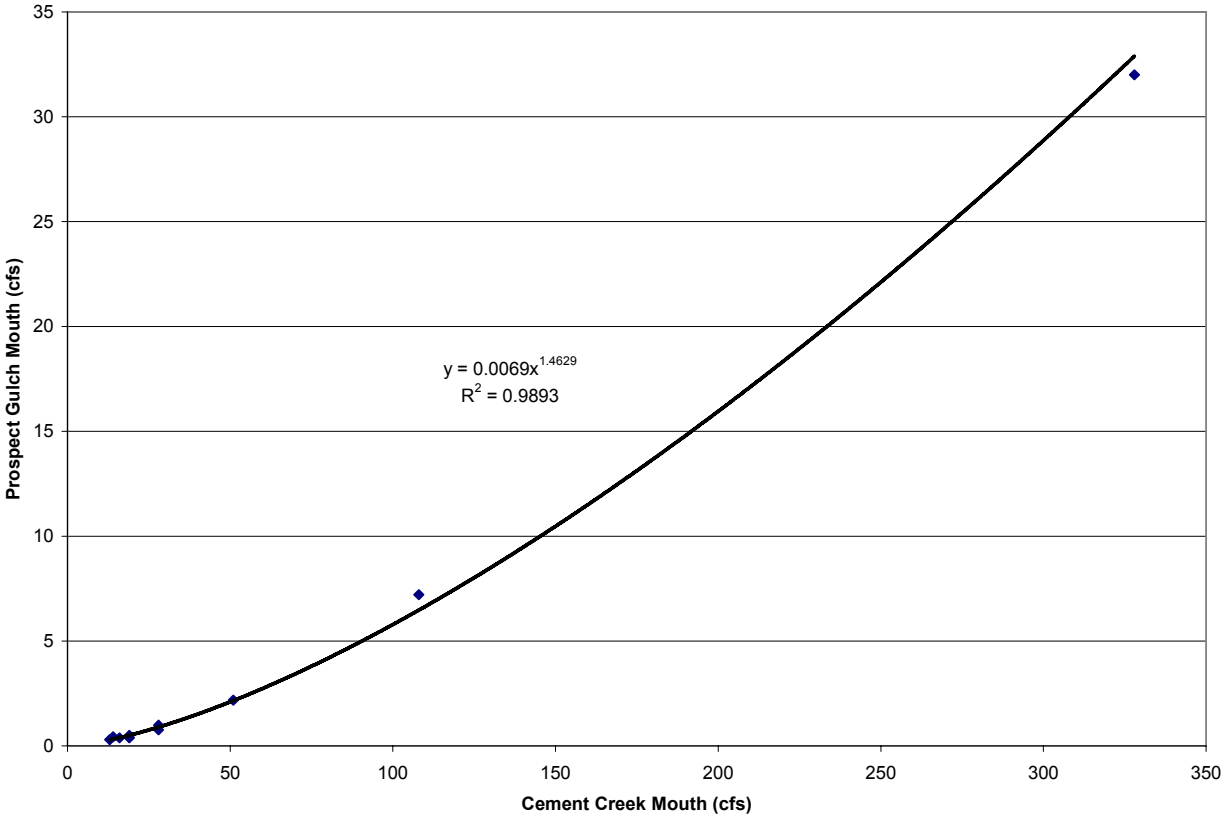

Figure 15: Streamflow with regression analysis for the mouth of Cement Creek versus the mouth of Prospect Gulch.

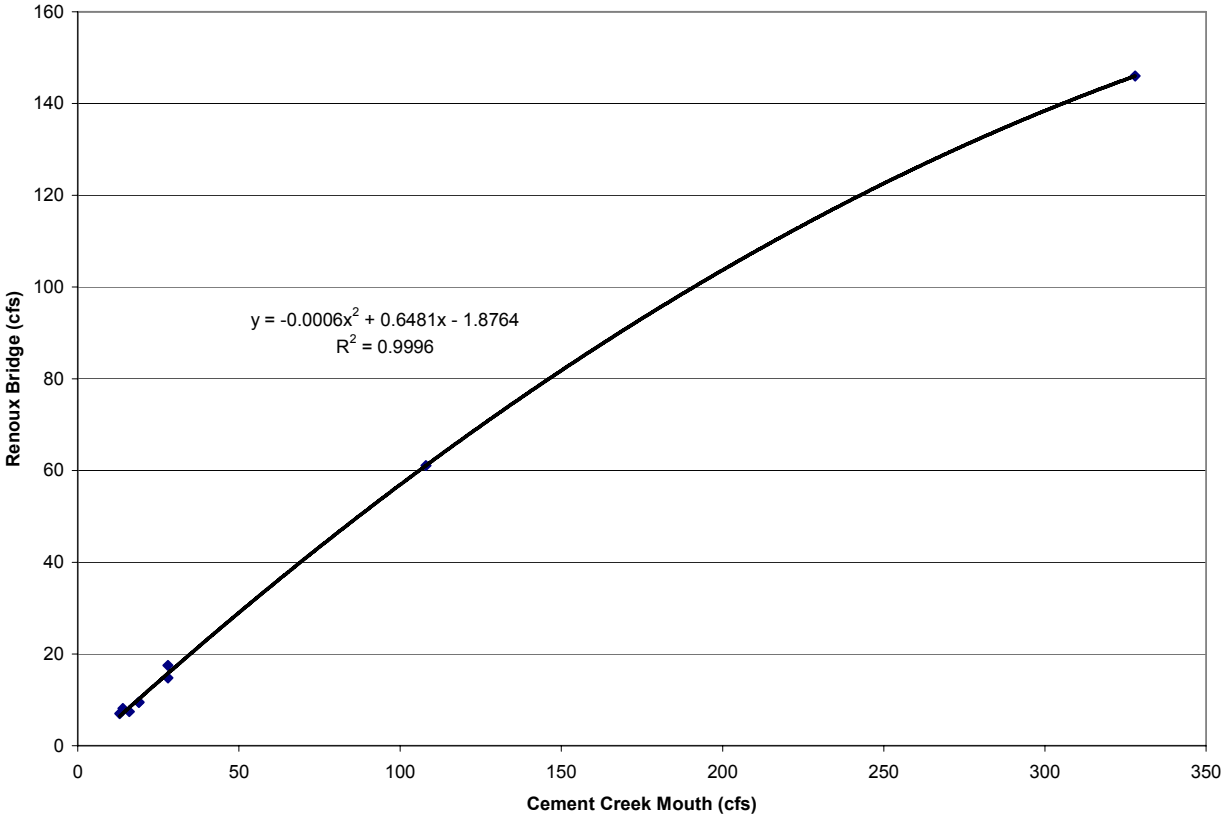

Figure 16: Streamflow with regression analysis for the mouth of Cement Creek versus Cement Creek at the Renoux Bridge.

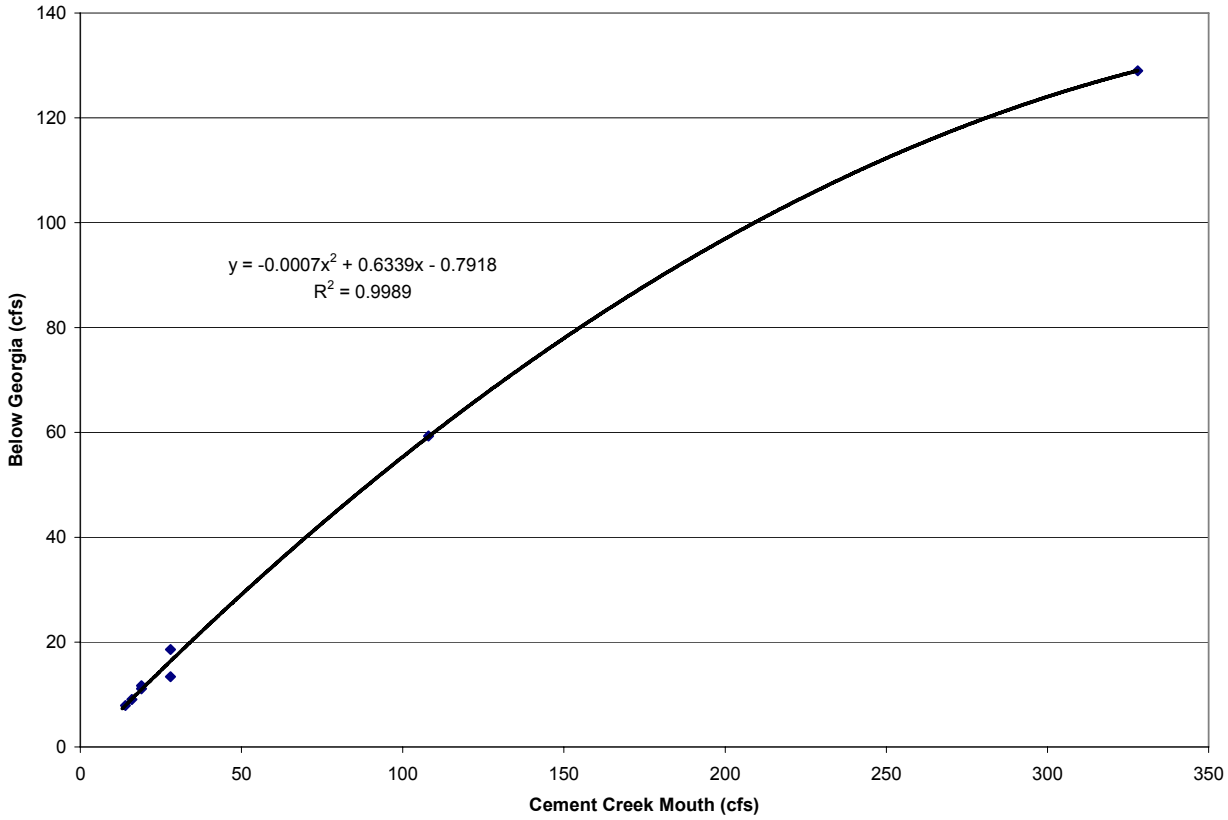

Figure 17: Streamflow with regression analysis for the mouth of Cement Creek versus Cement Creek below Georgia Gulch.

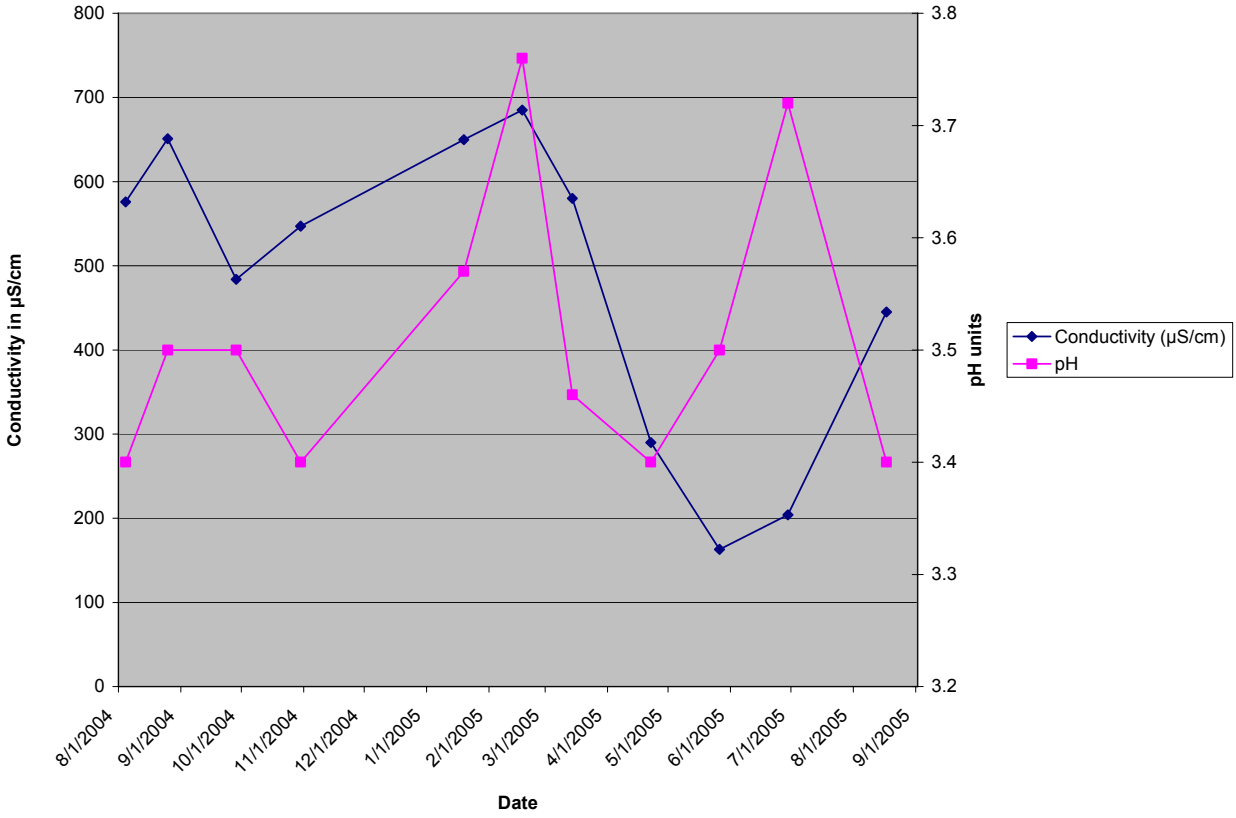

Figure 18: Conductivity and pH at the mouth of Prospect Gulch.

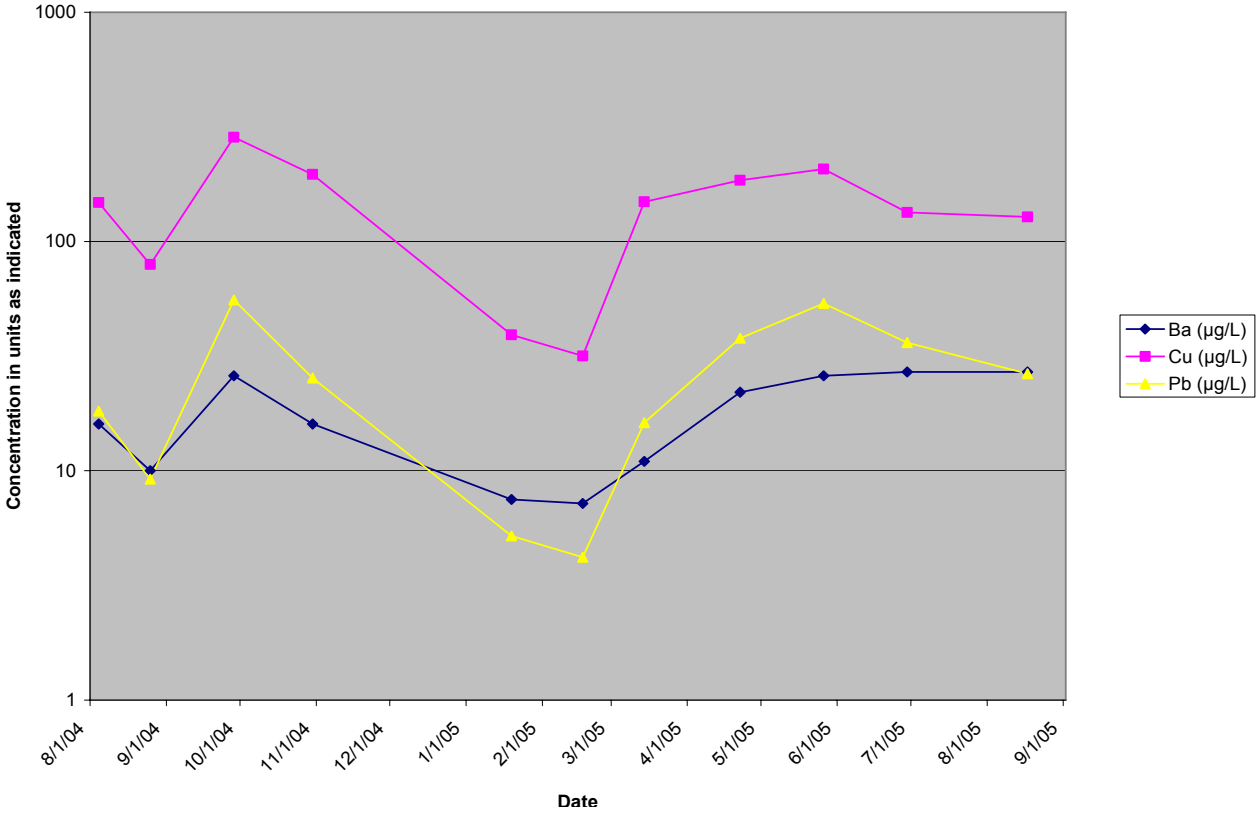

Figure 19: Concentrations of shallow ground-water indicators at the mouth of Prospect Gulch.

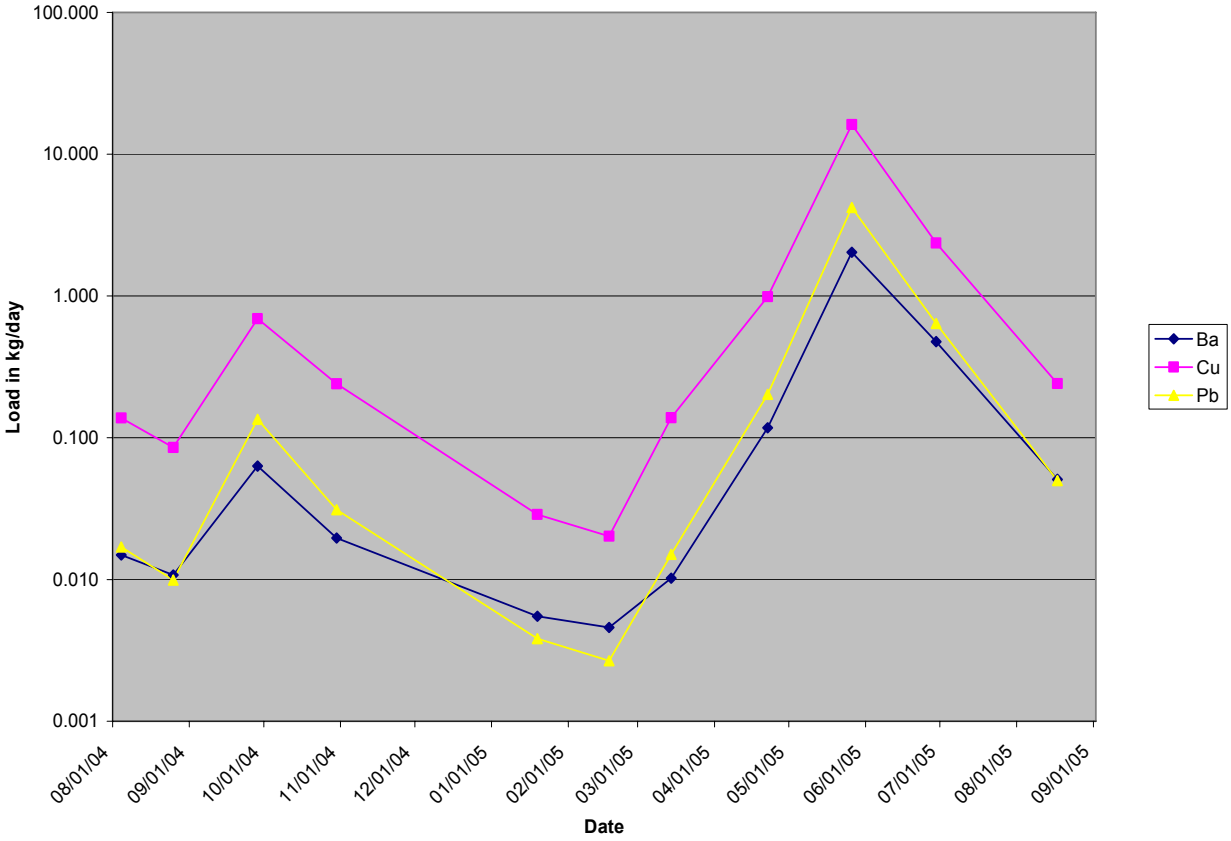

Figure 20: Loads for shallow ground-water indicators at the mouth of Prospect Gulch.

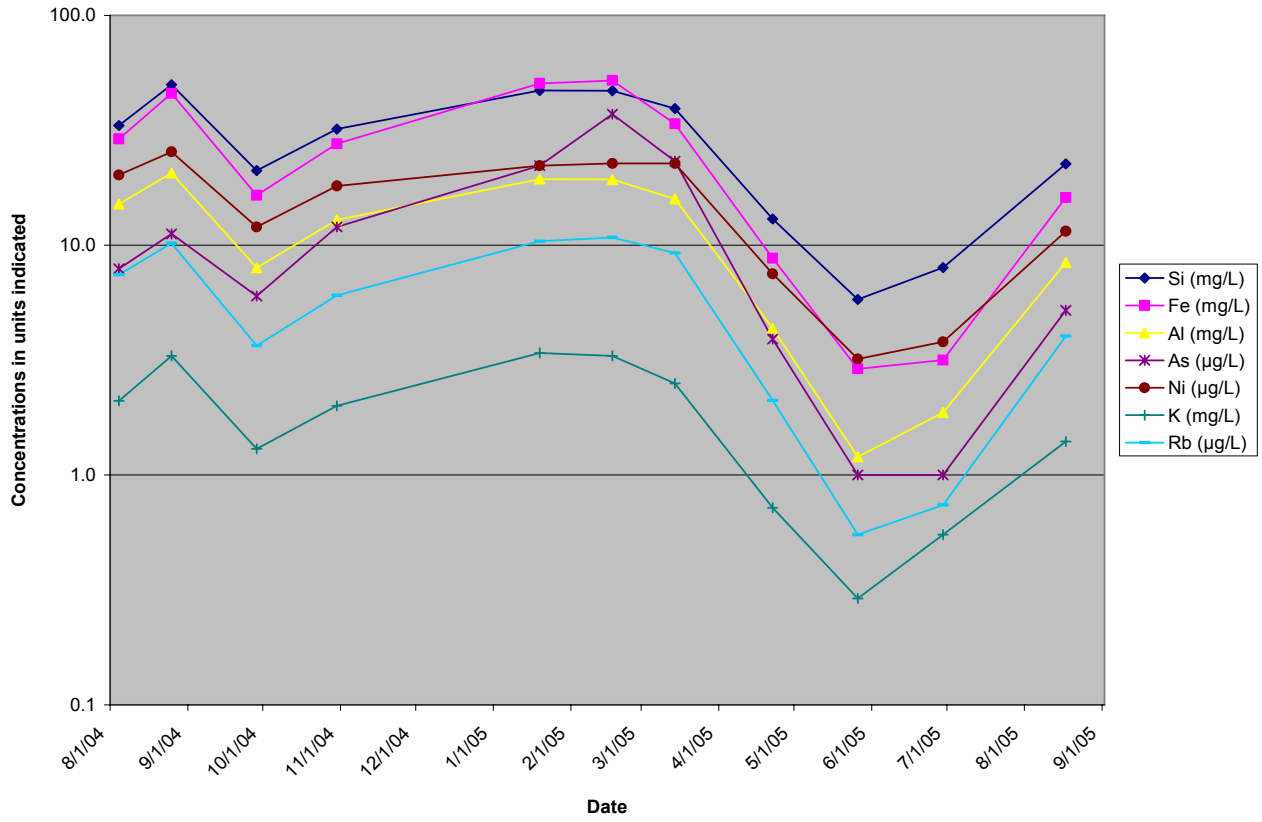

Figure 21: Concentrations of deep ground-water indicators at the mouth of Prospect Gulch.

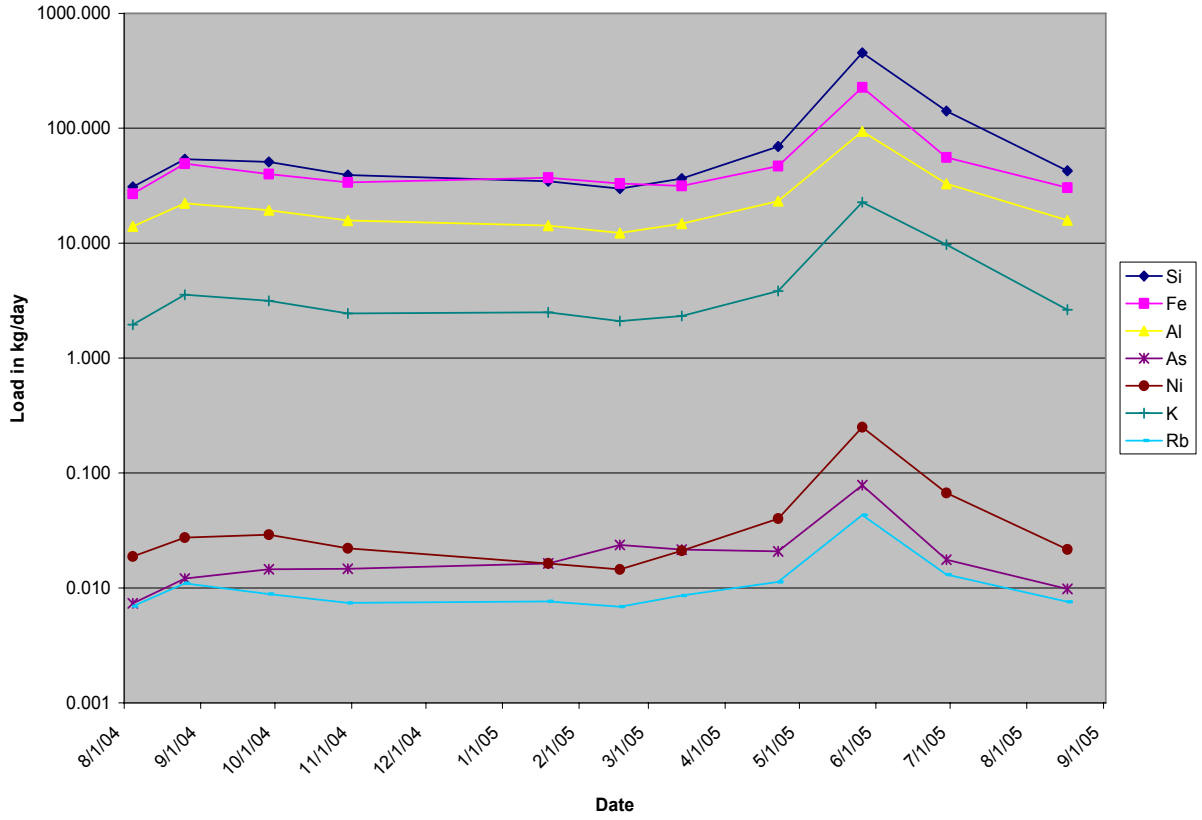

Figure 22: Loads for deep ground-water indicators at the mouth of Prospect Gulch.

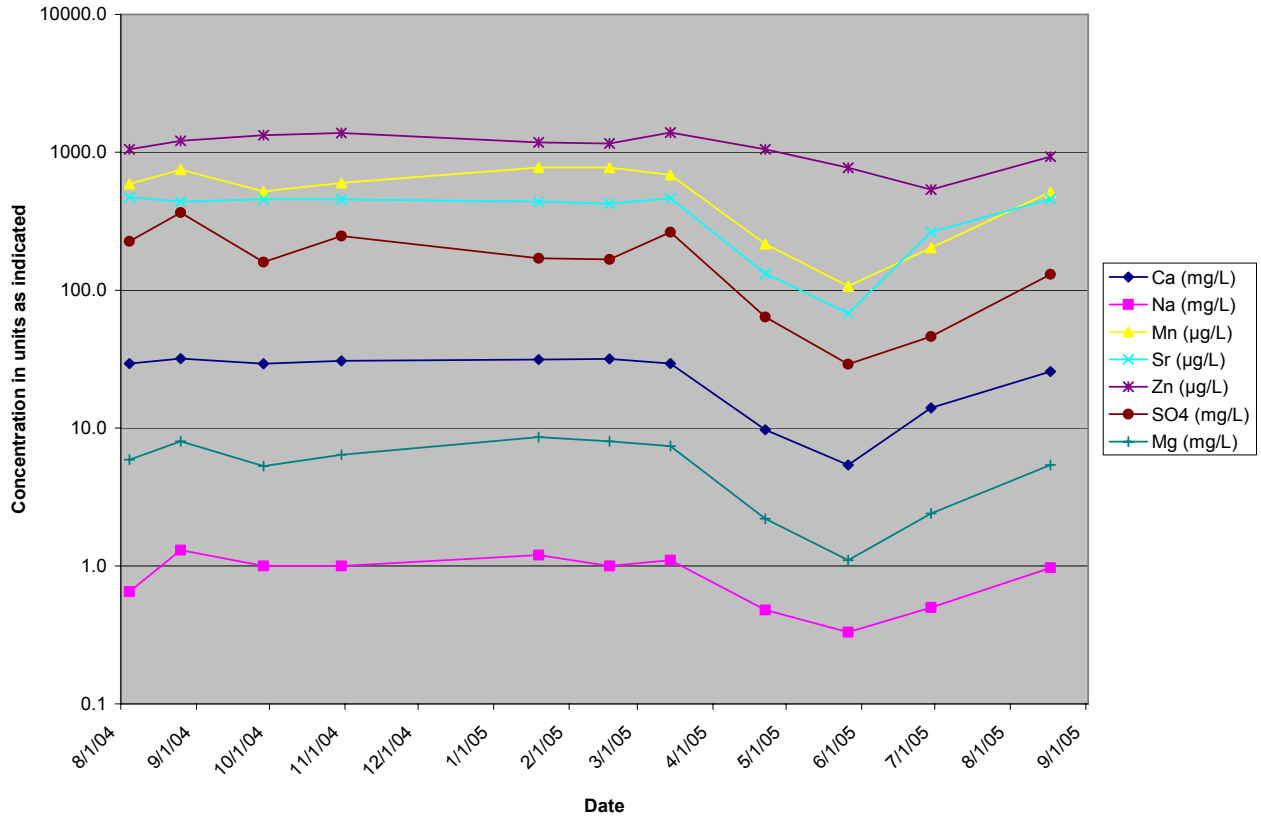

Figure 23: Concentrations of inconclusive ground-water indicators at the mouth of Prospect Gulch.

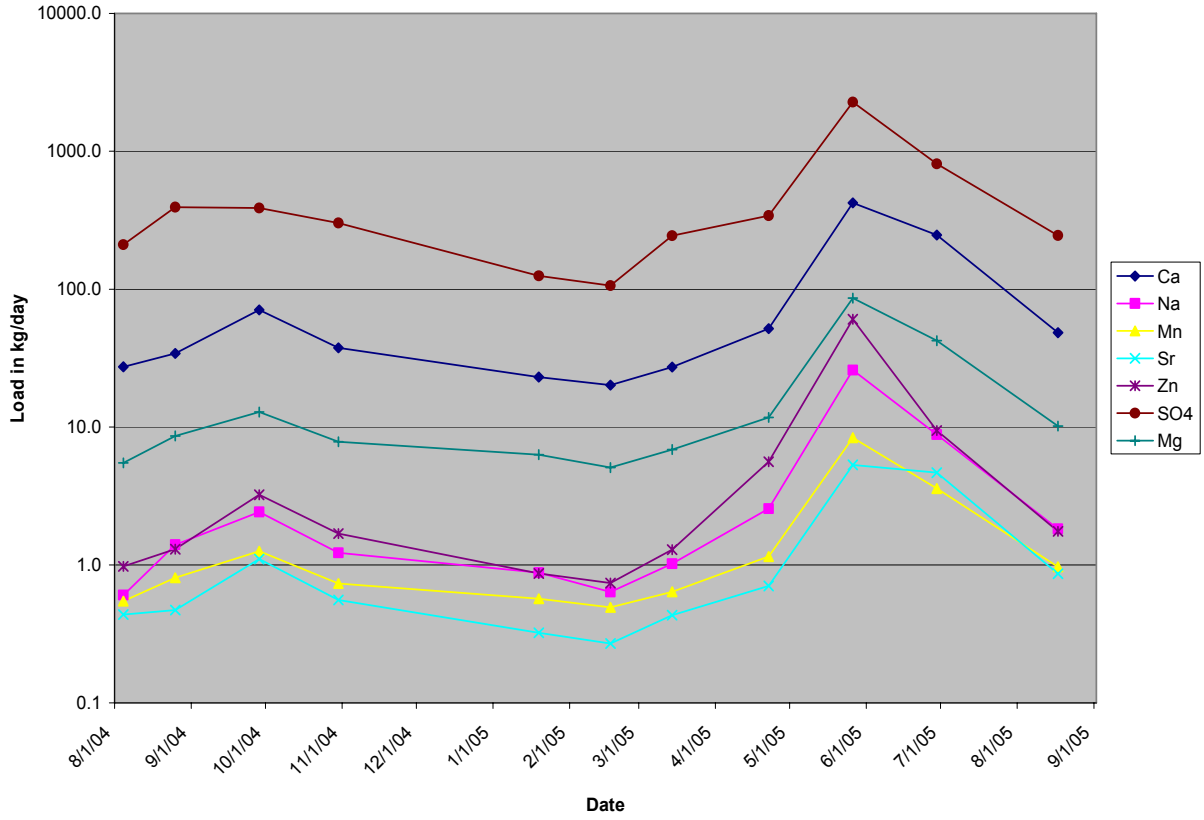

Figure 24: Loads for inconclusive ground-water indicators at the mouth of Prospect Gulch.

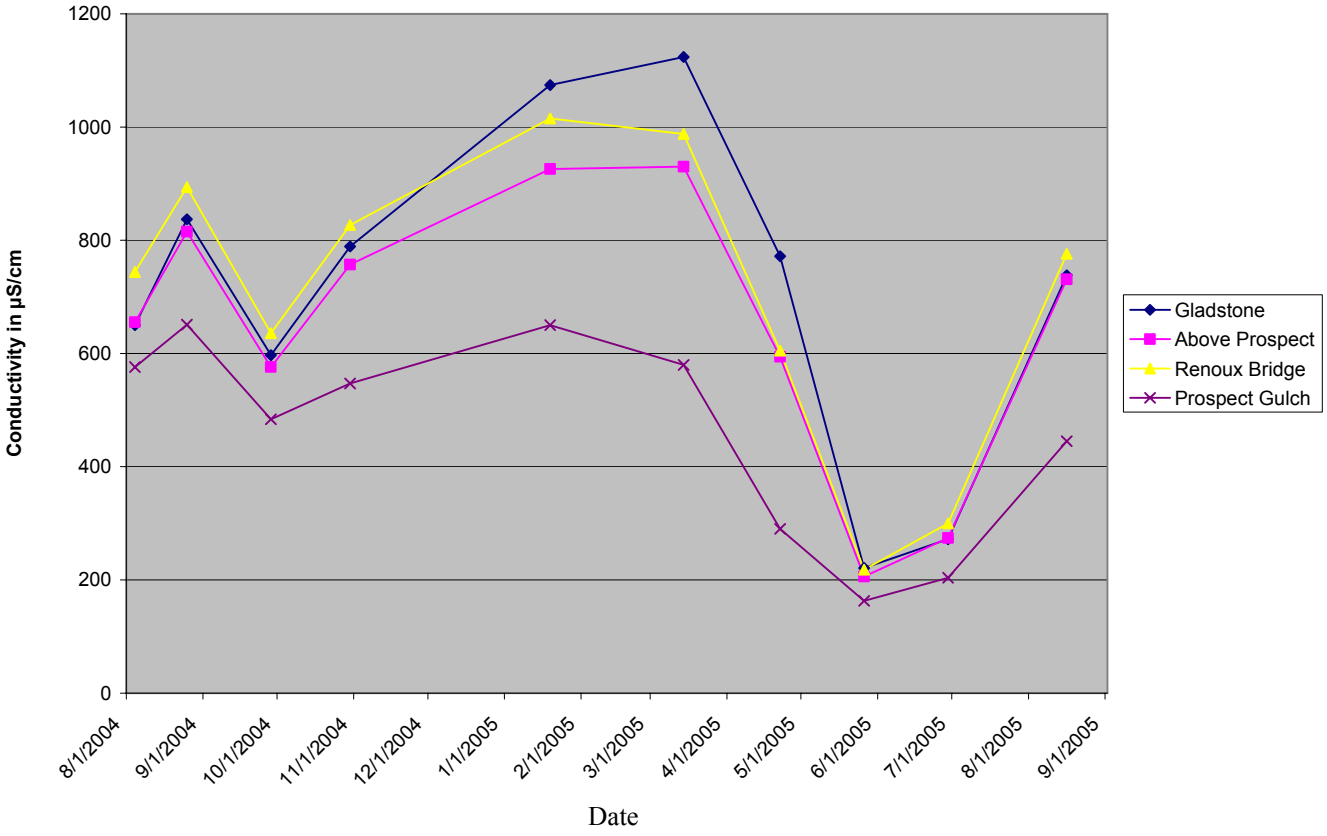

Figure 25: Temporal conductivity in Cement Creek and Prospect Gulch.

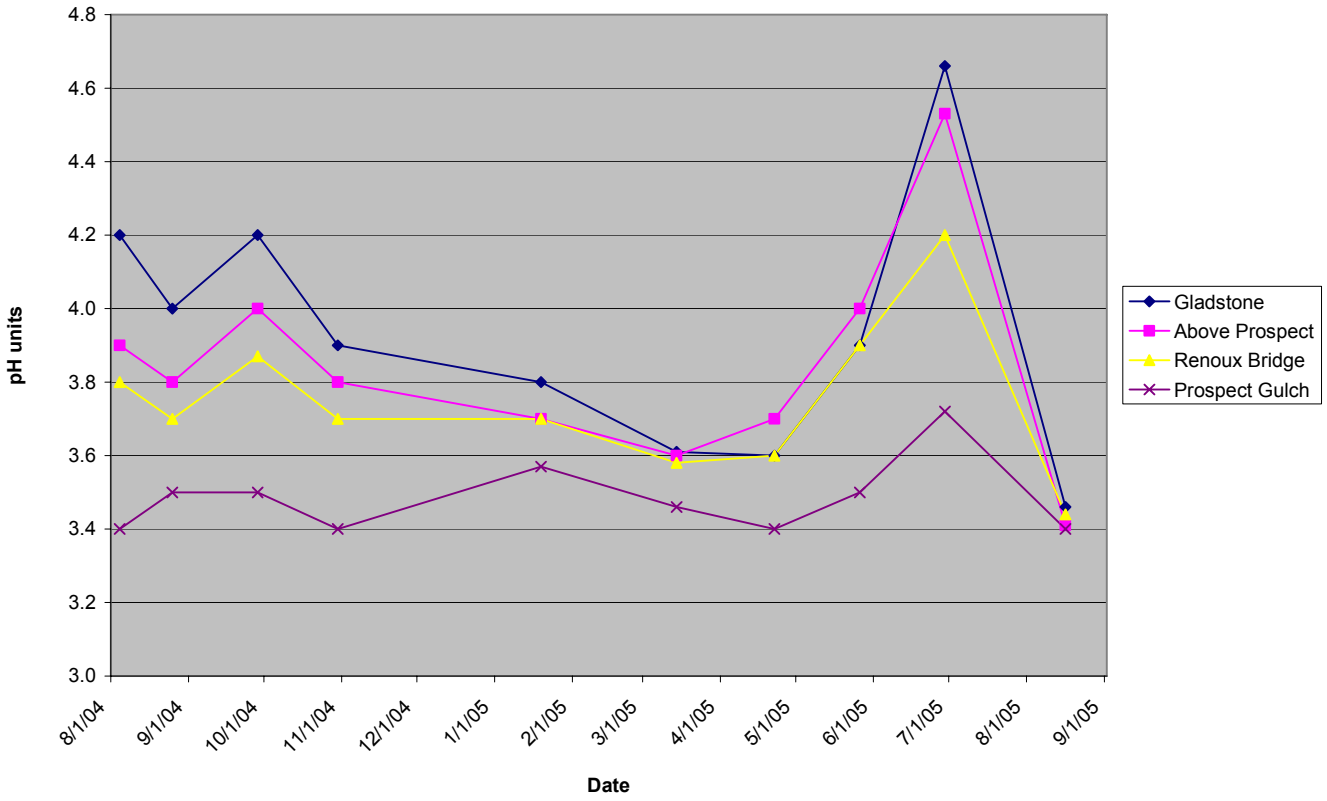

Figure 26: Temporal pH values in Cement Creek and Prospect Gulch.

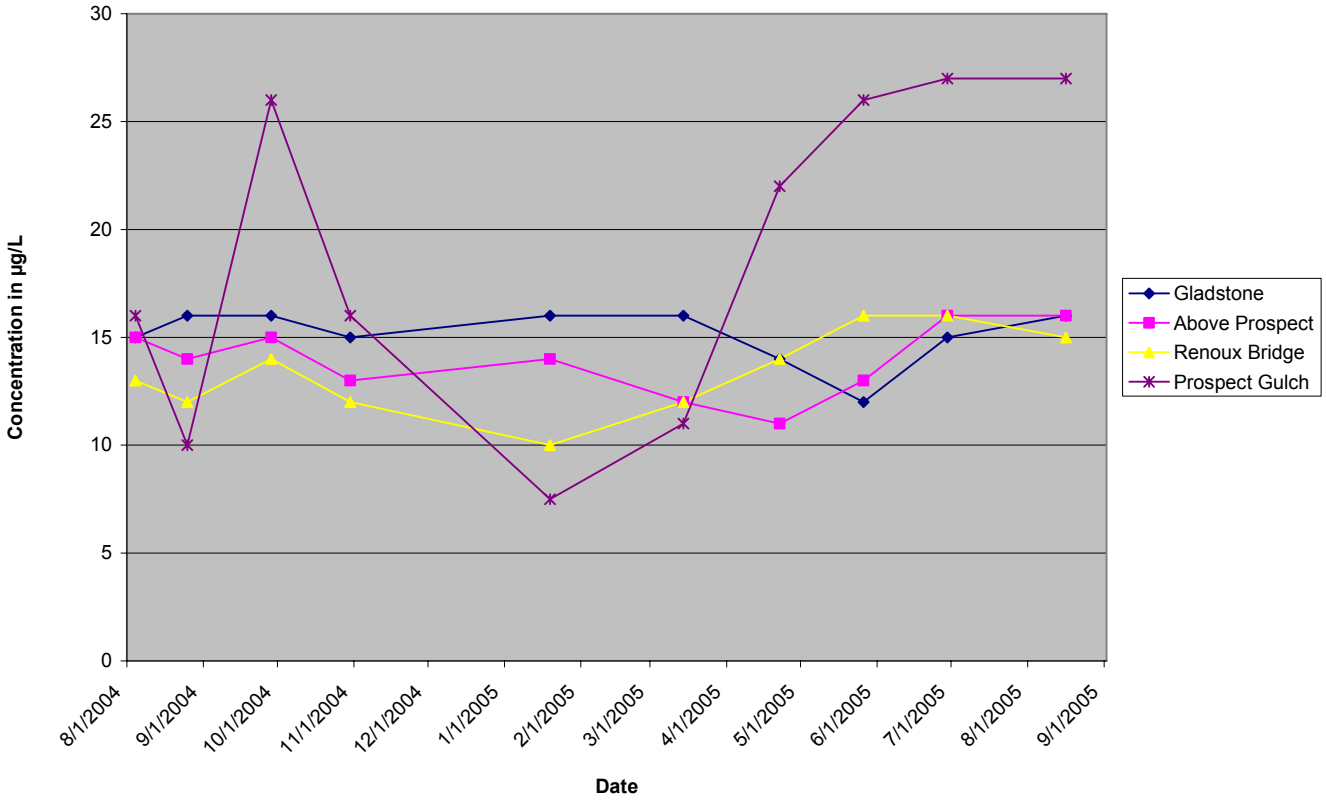

Figure 27: Temporal barium concentrations in Cement Creek and Prospect Gulch.

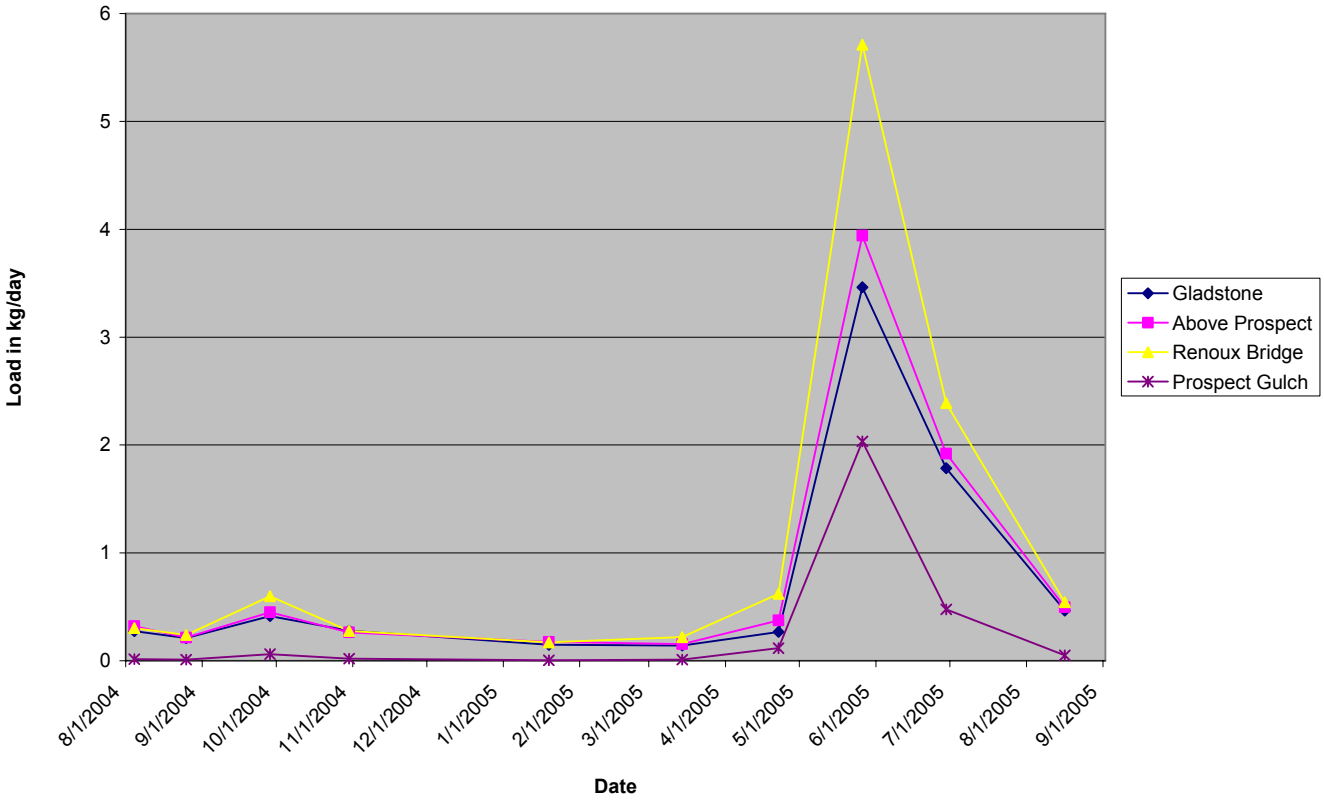

Figure 28: Temporal barium loads in Cement Creek and Prospect Gulch.

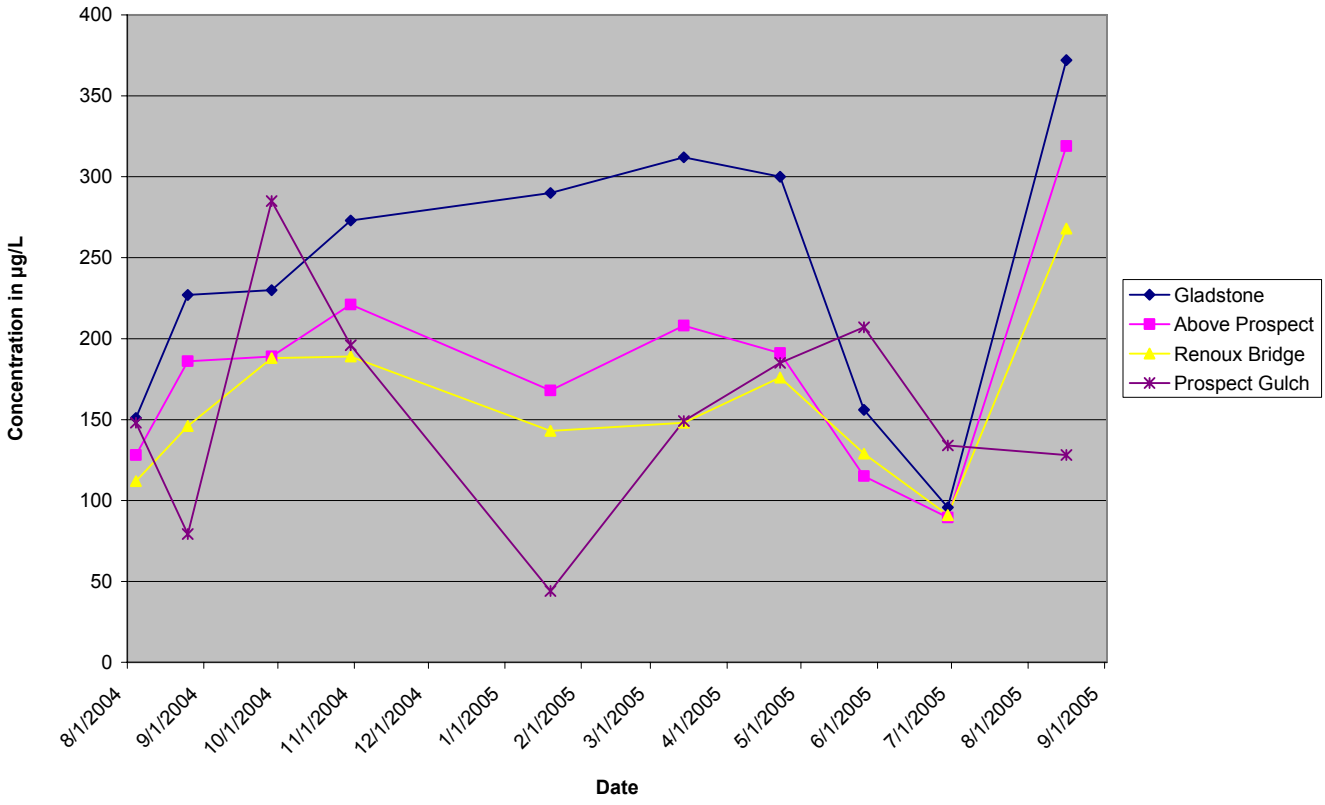

Figure 29: Temporal copper concentrations in Cement Creek and Prospect Gulch .

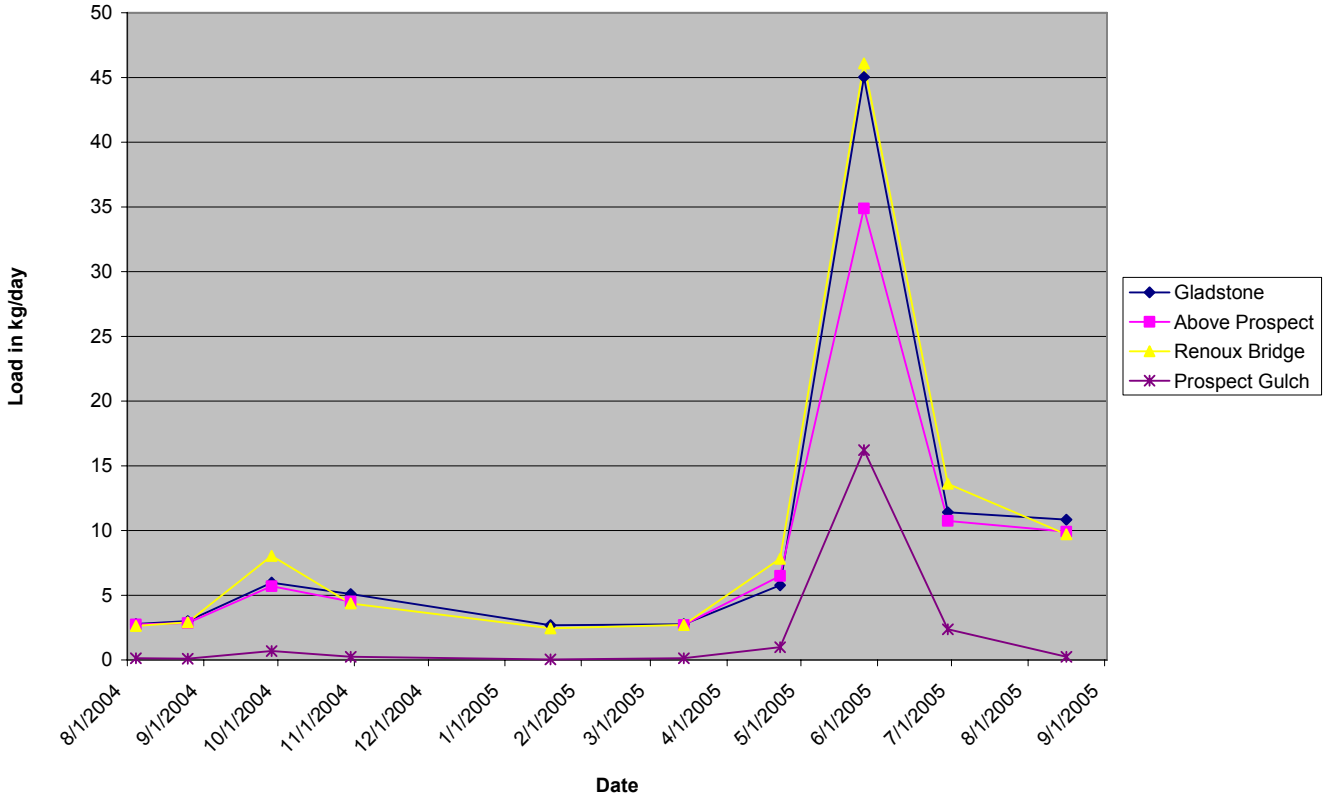

Figure 30: Temporal copper loads in Cement Creek and Prospect Gulch.

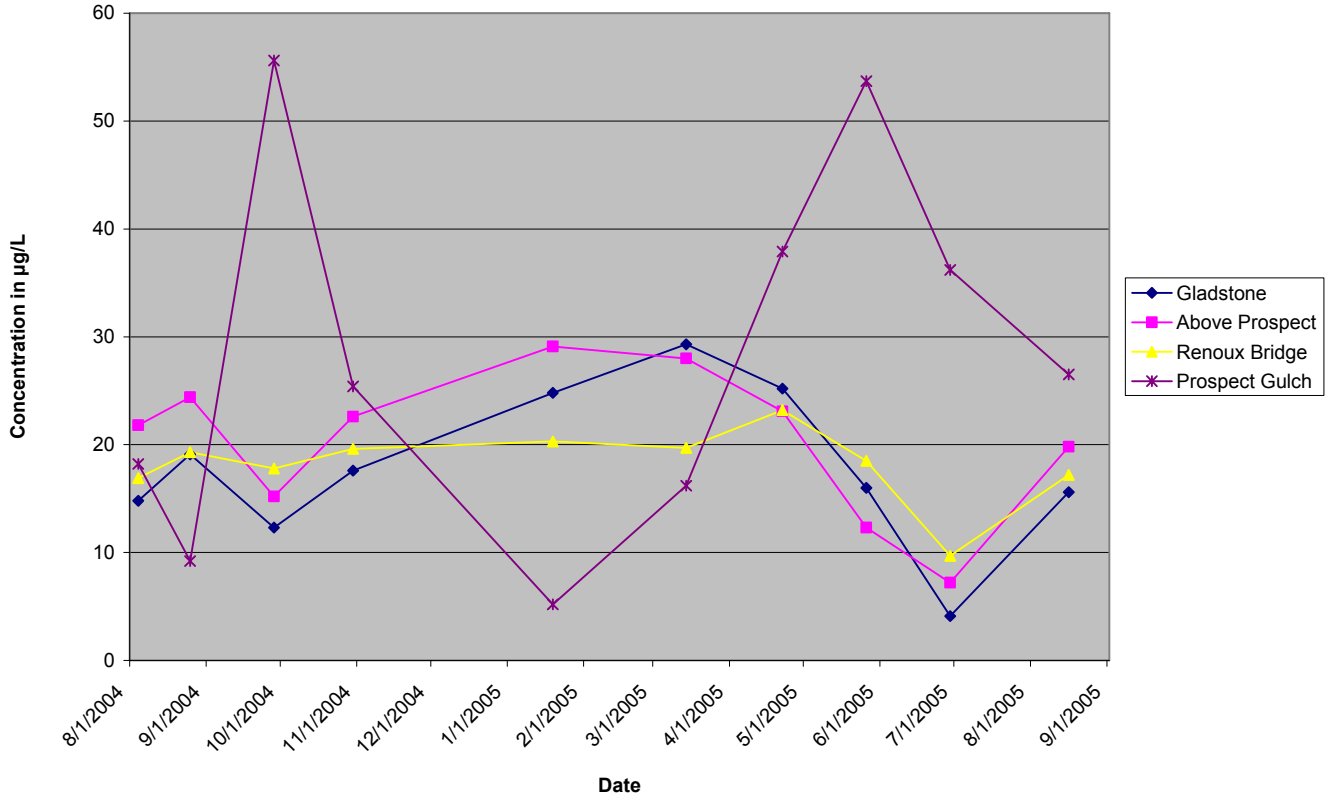

Figure 31: Temporal lead concentrations in Cement Creek and Prospect Gulch.

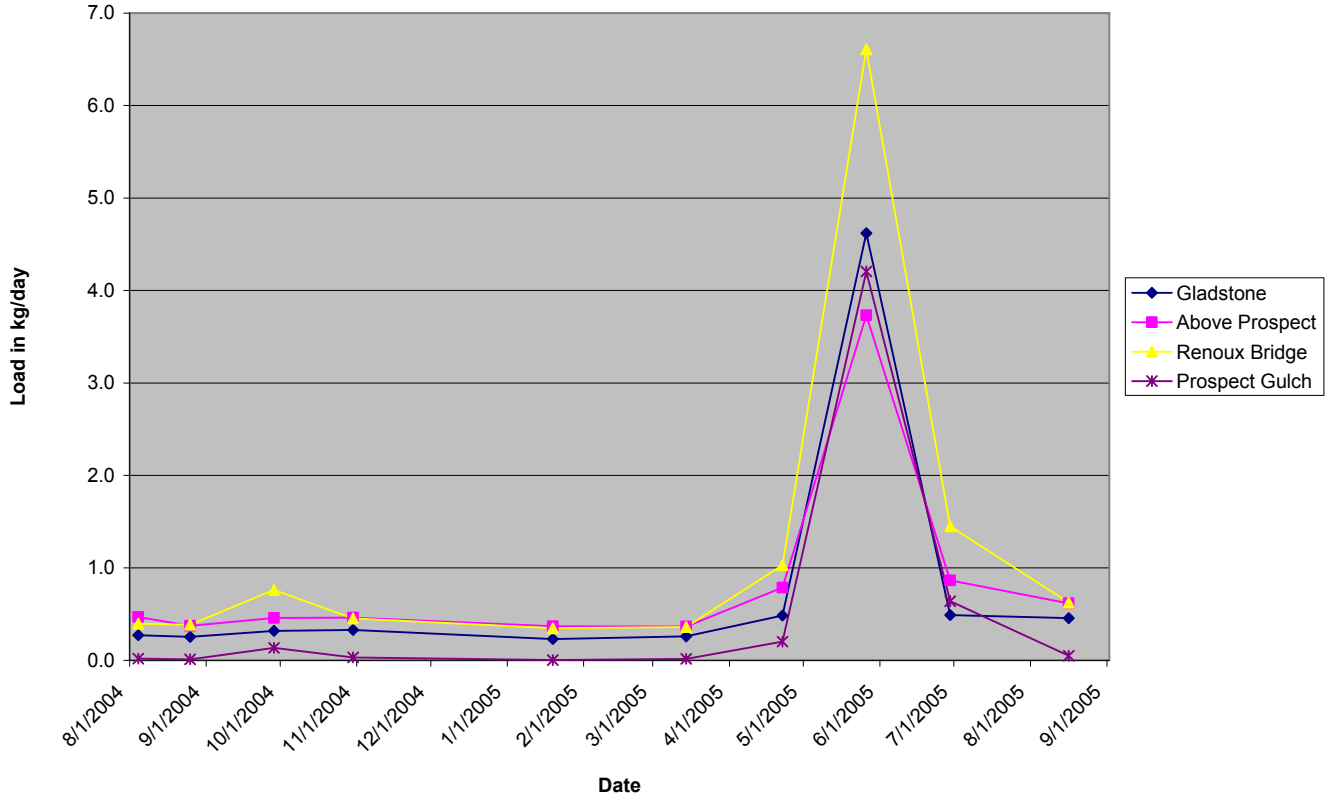

Figure 32: Temporal lead loads in Cement Creek and Prospect Gulch.

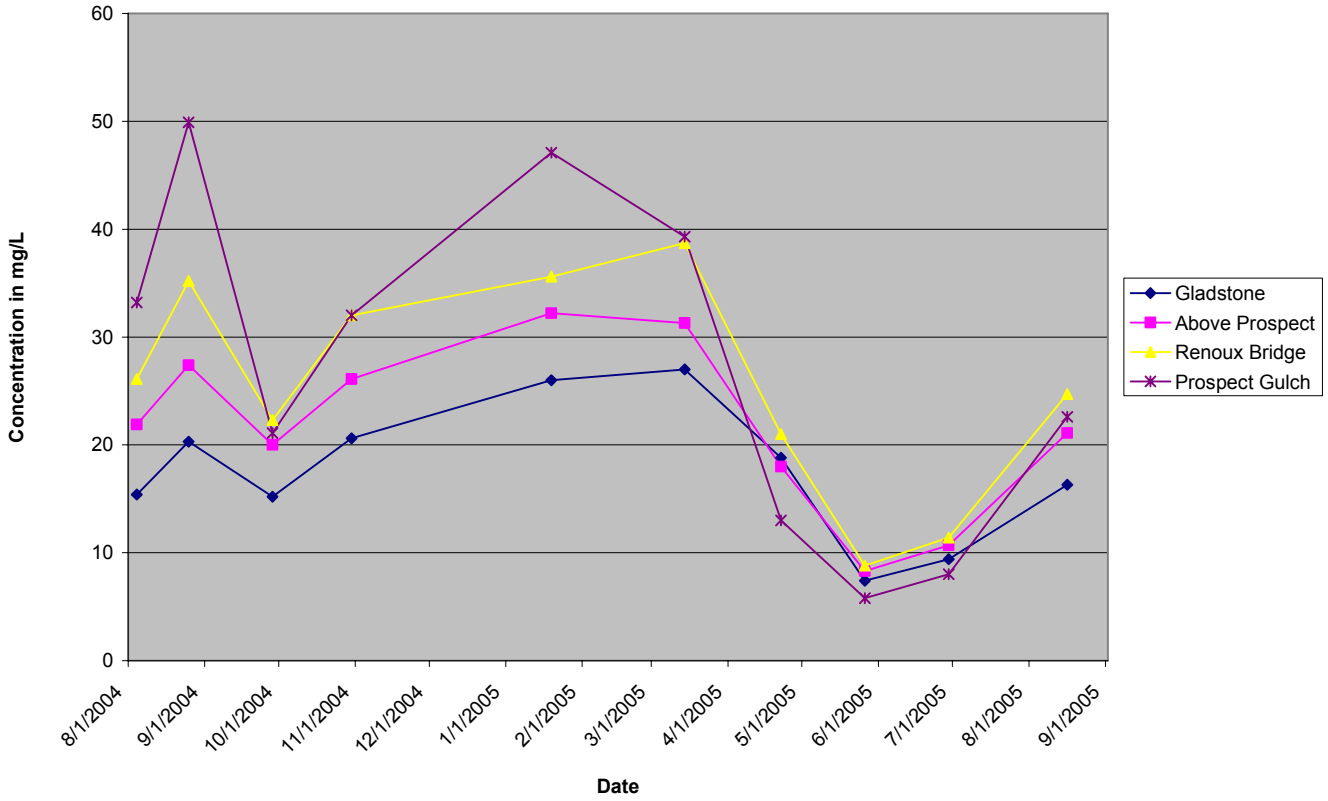

Figure 33: Temporal silica concentrations in Cement Creek and Prospect Gulch.

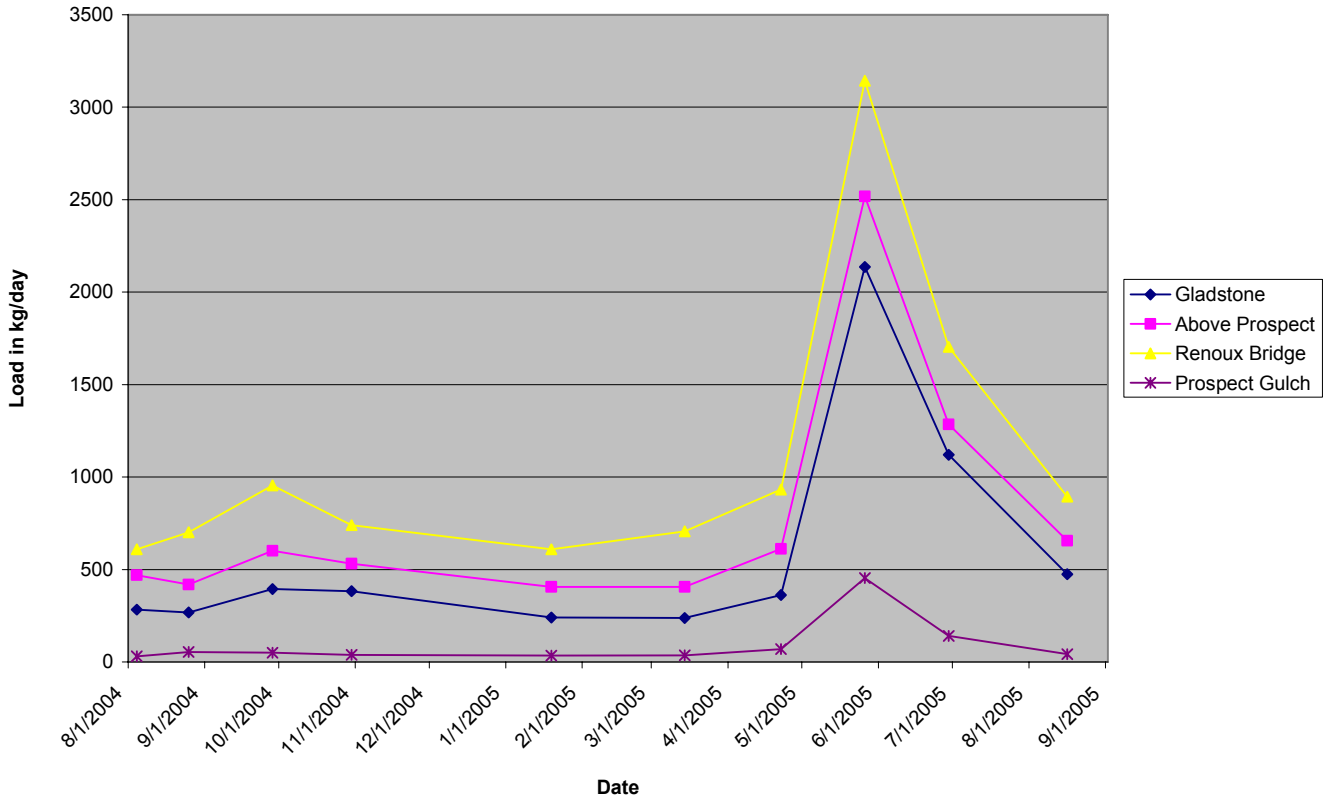

Figure 34: Temporal silica loads in Cement Creek and Prospect Gulch.

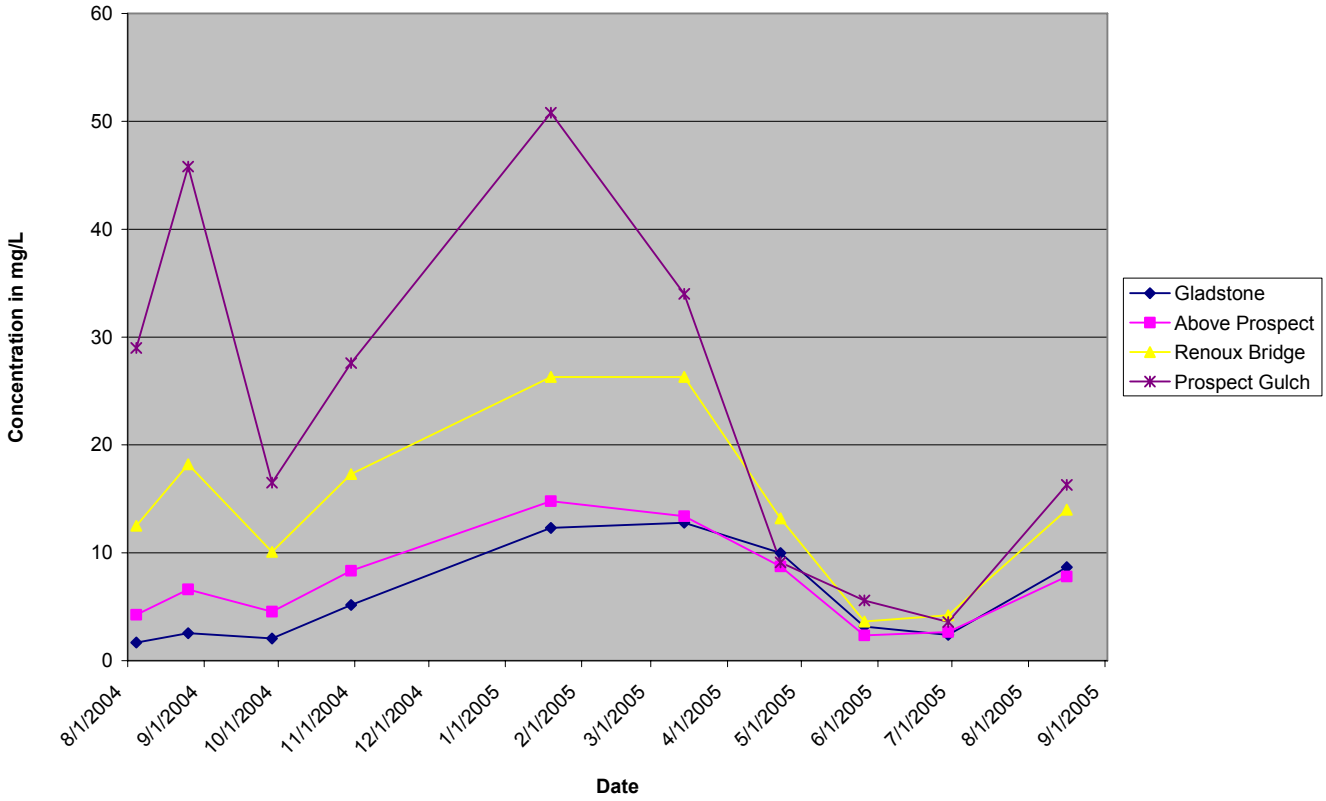

Figure 35: Temporal iron concentrations in Cement Creek and Prospect Gulch.

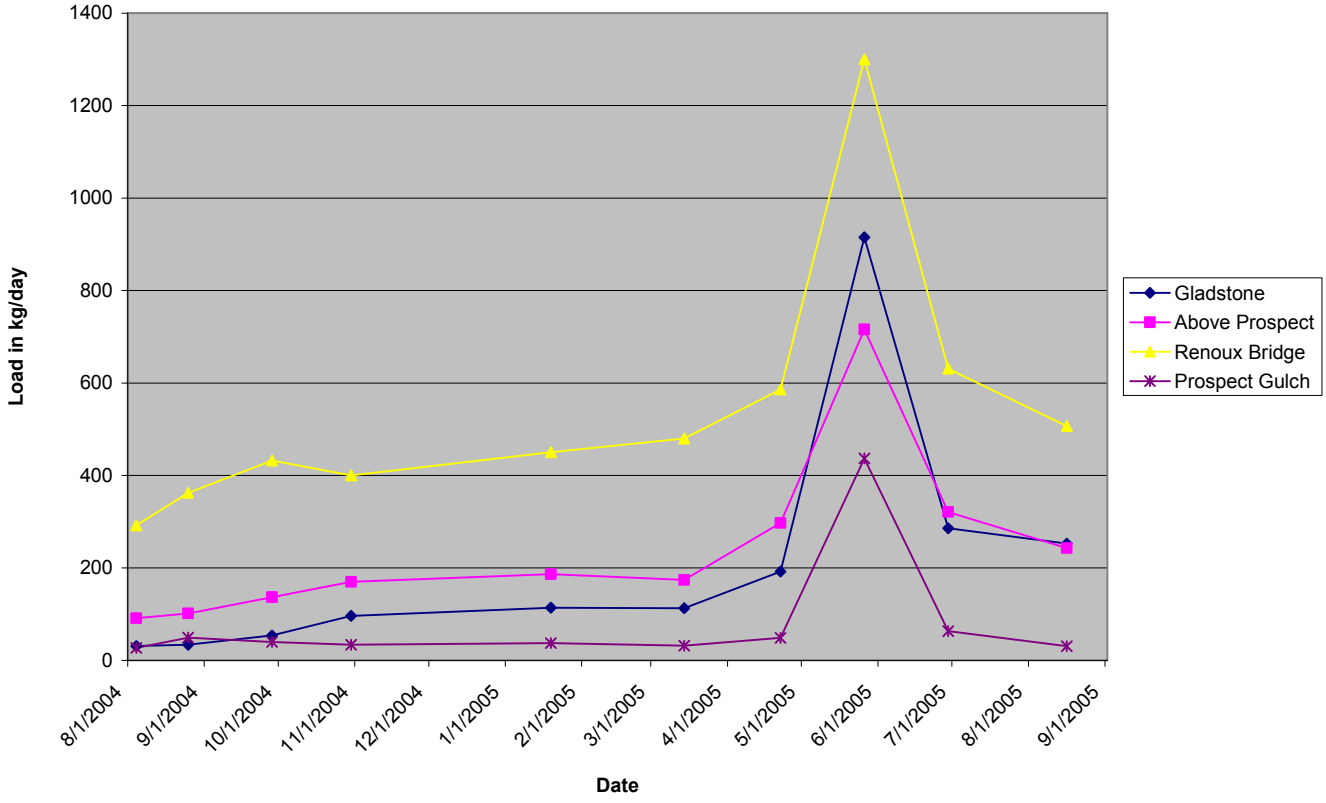

Figure 36: Temporal iron loads in Cement Creek and Prospect Gulch.

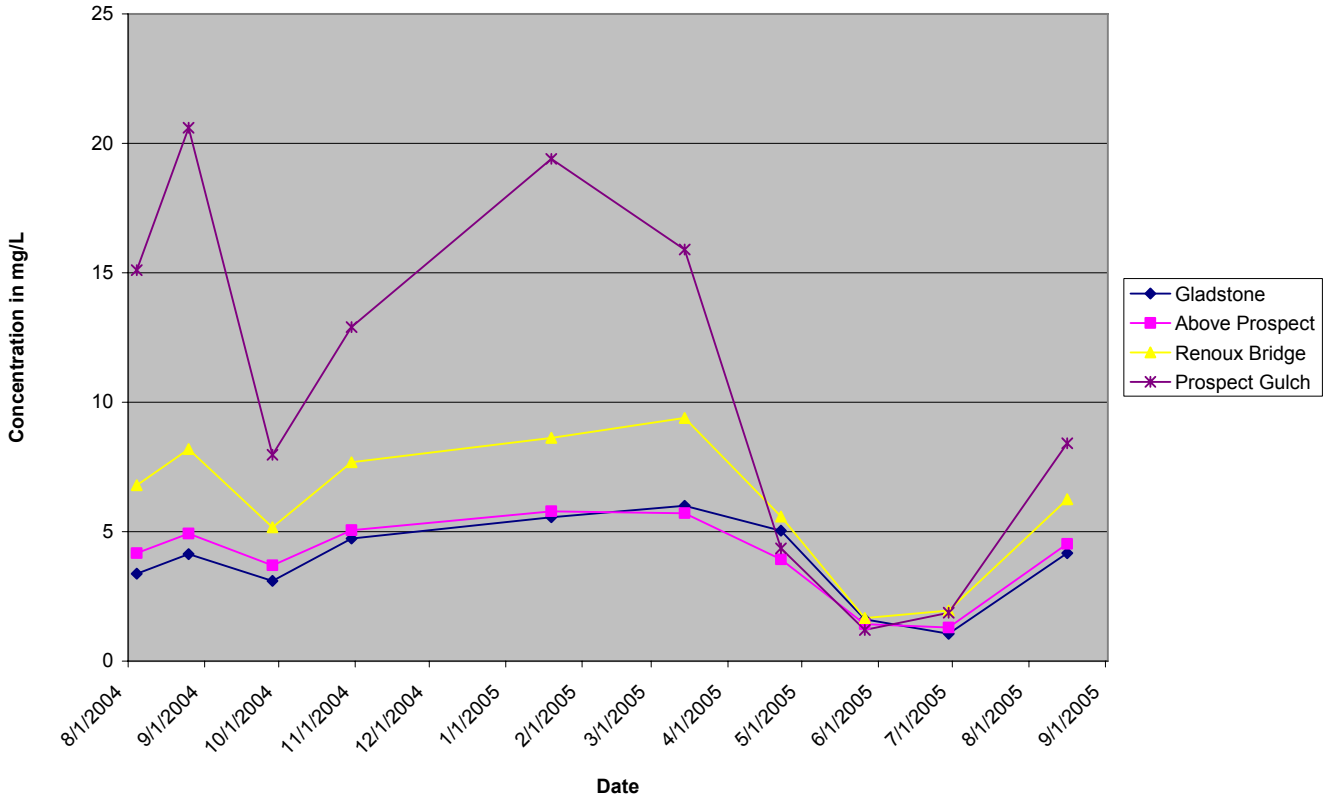

Figure 37: Temporal aluminum concentrations in Cement Creek and Prospect Gulch.

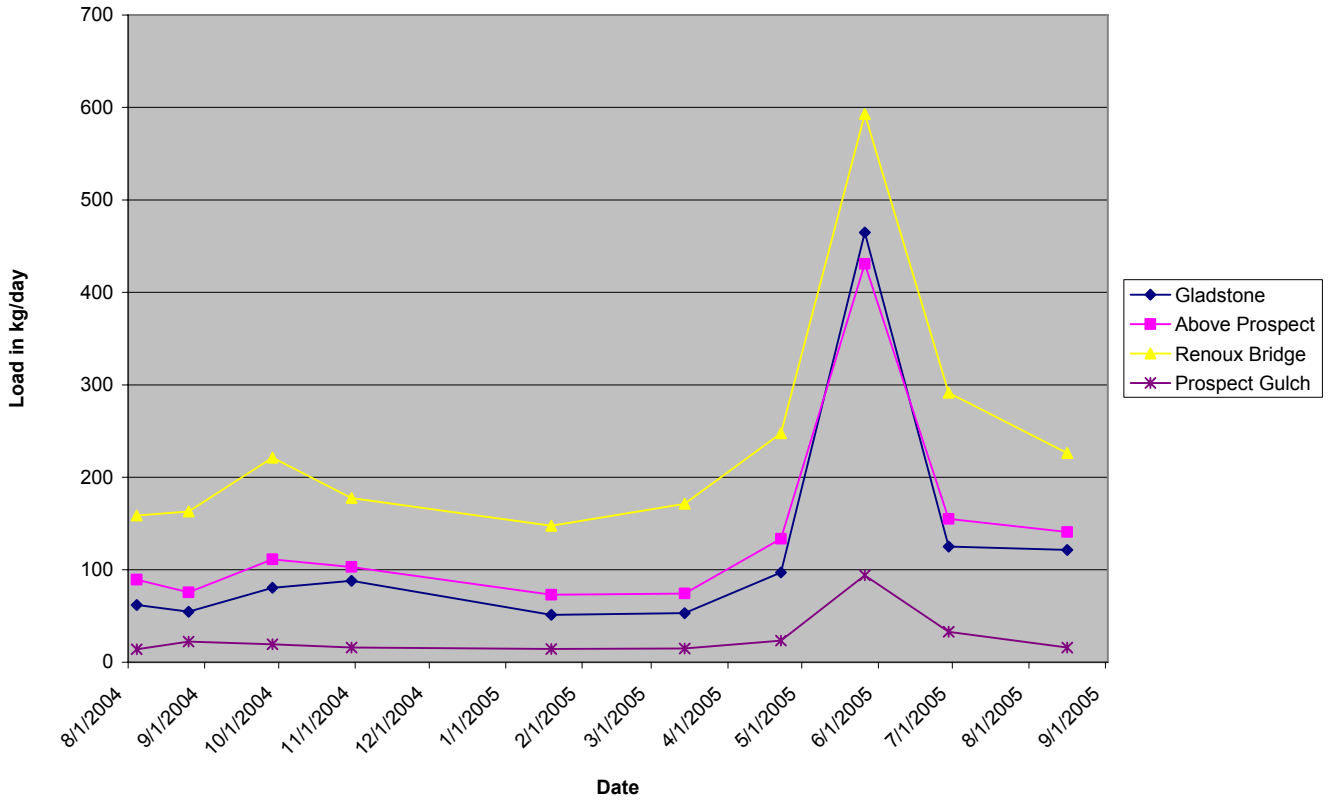

Figure 38: Temporal aluminum loads in Cement Creek and Prospect Gulch.

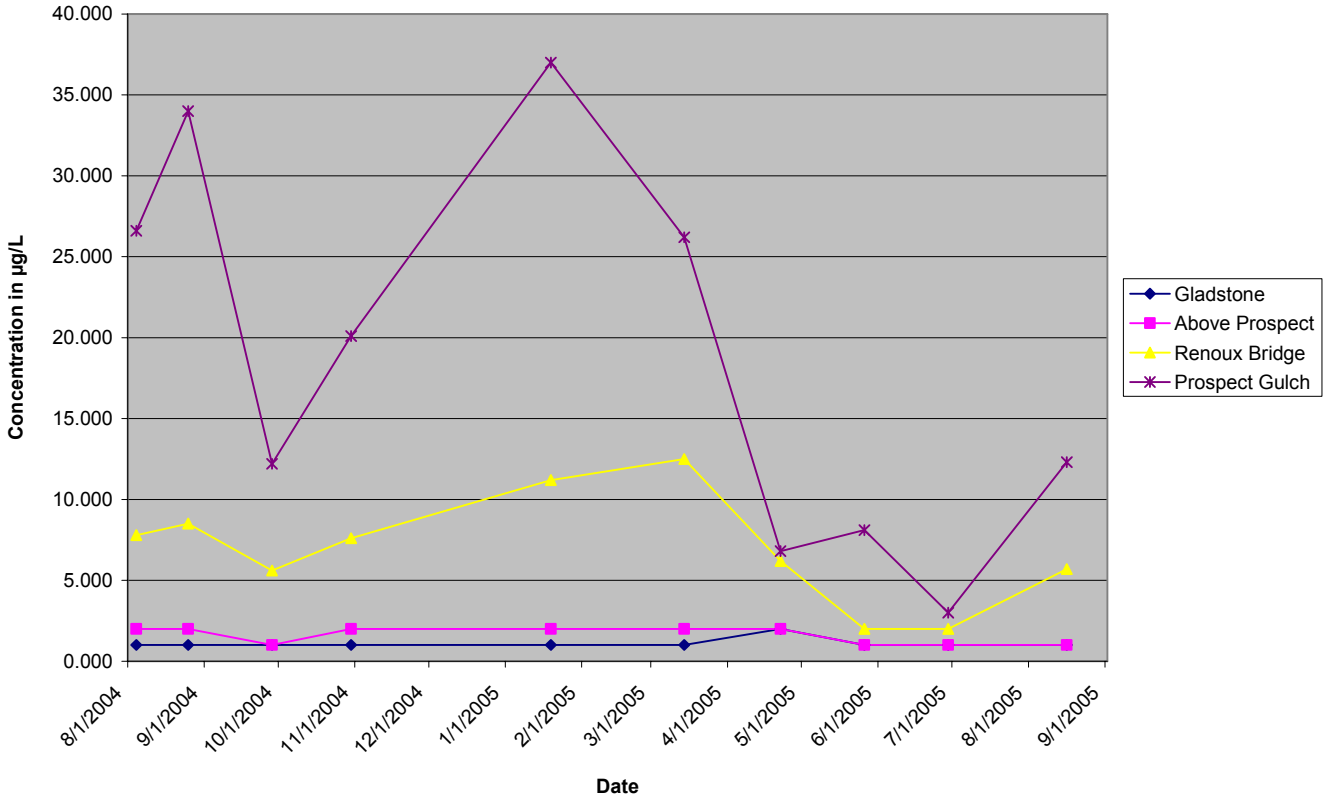

Figure 39: Temporal arsenic concentrations in Cement Creek and Prospect Gulch.

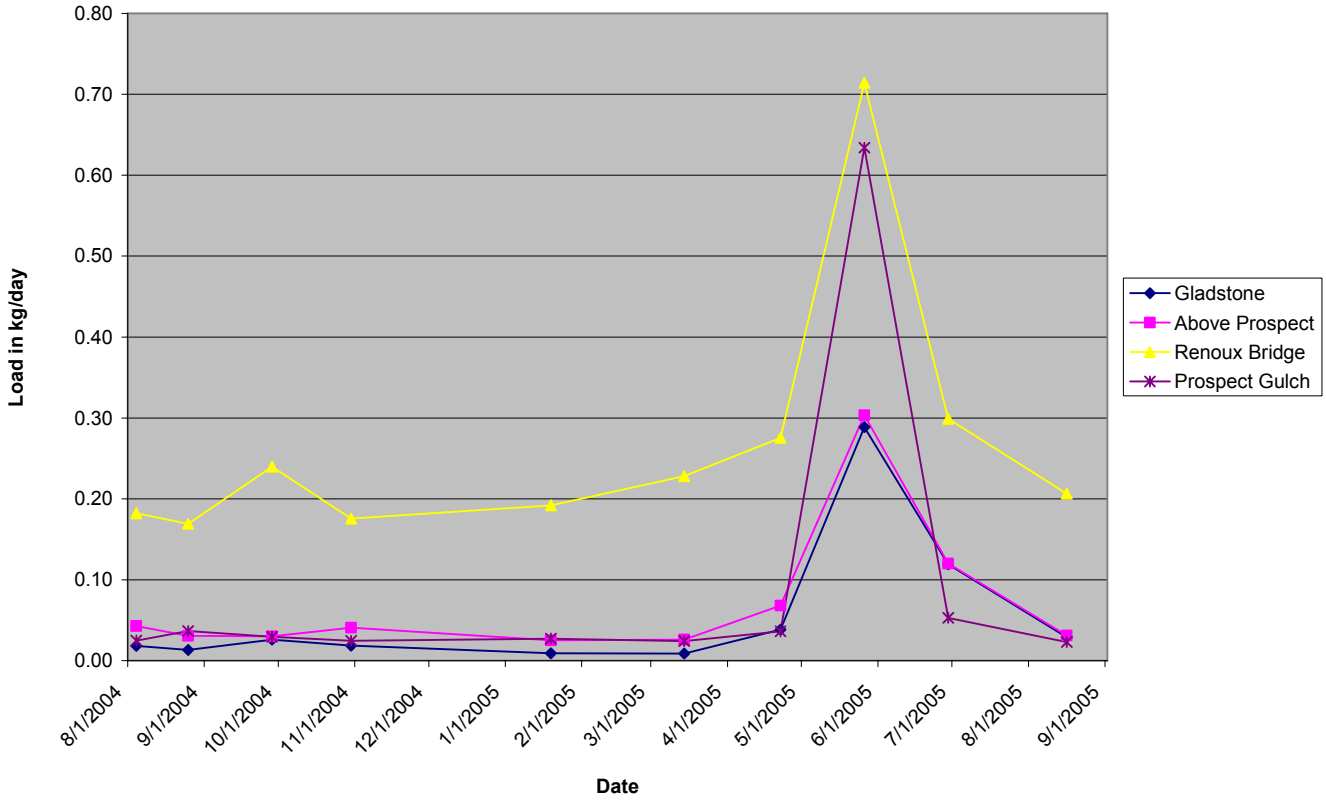

Figure 40: Temporal arsenic loads in Cement Creek and Prospect Gulch.

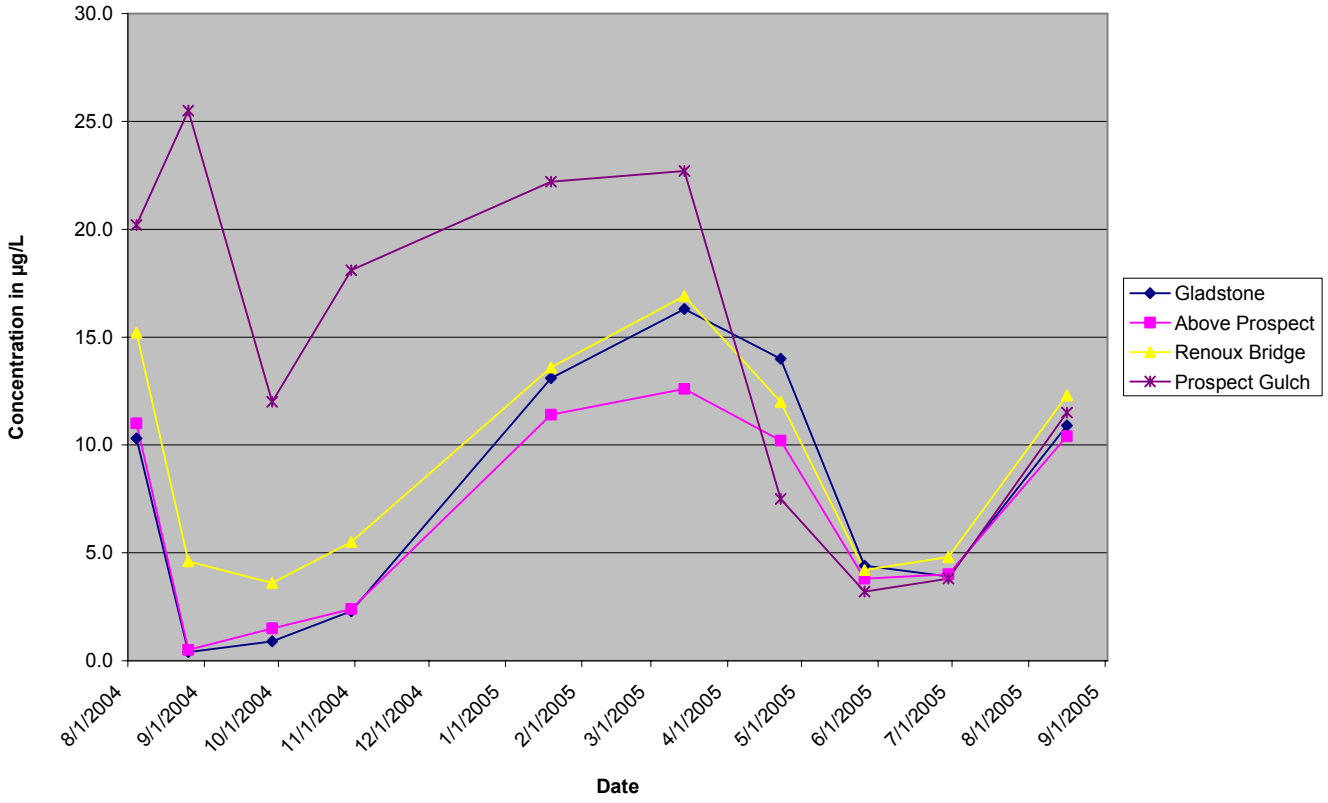

Figure 41: Temporal nickel concentrations in Cement Creek and Prospect Gulch.

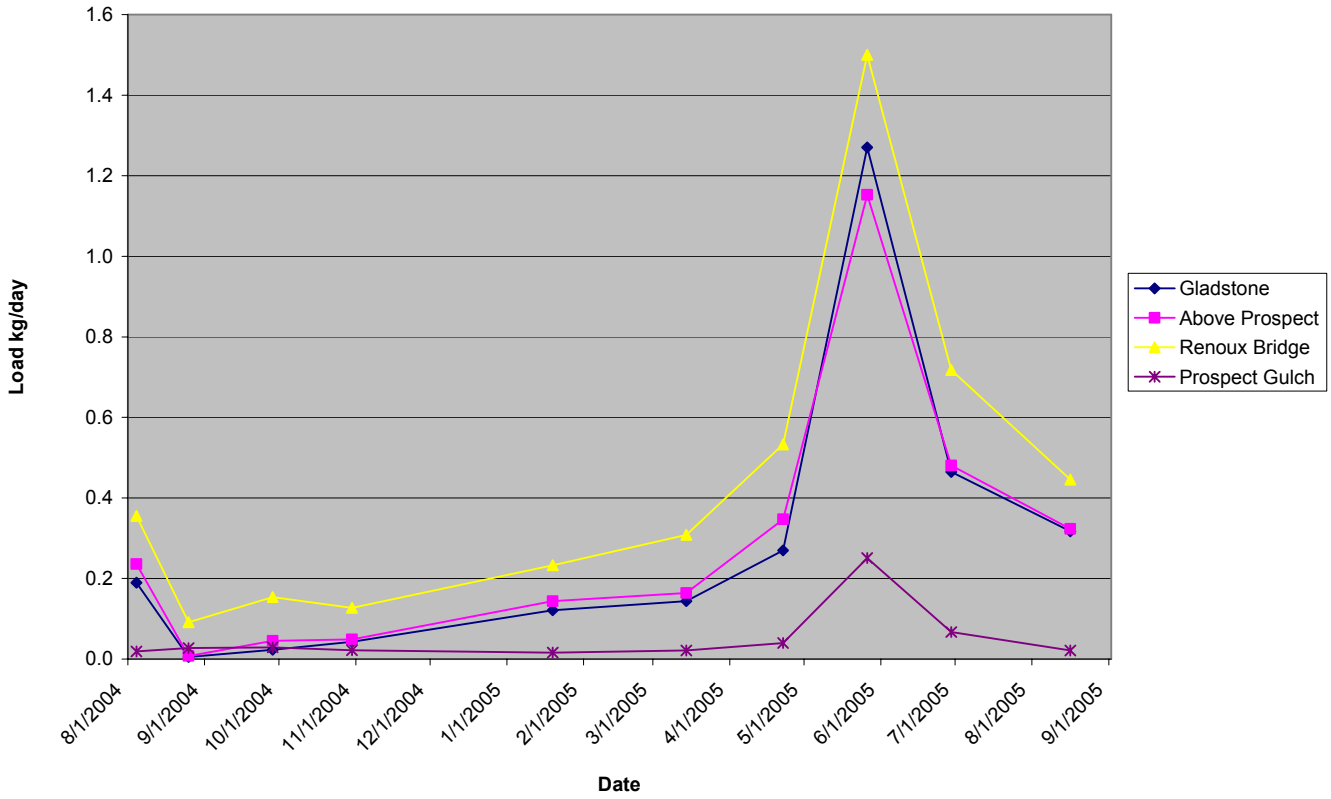

Figure 42: Temporal nickel loads in Cement Creek and Prospect Gulch.

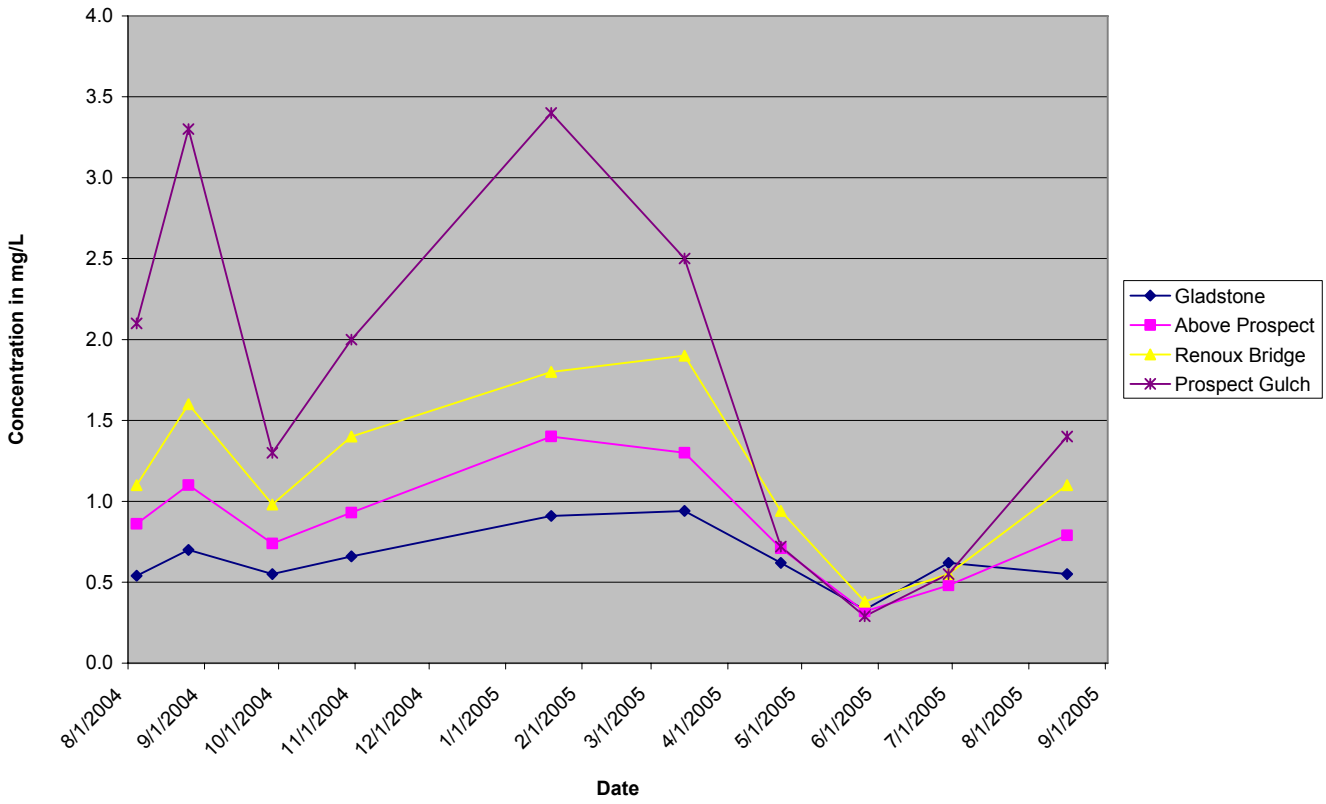

Figure 43: Temporal potassium concentrations in Cement Creek and Prospect Gulch.

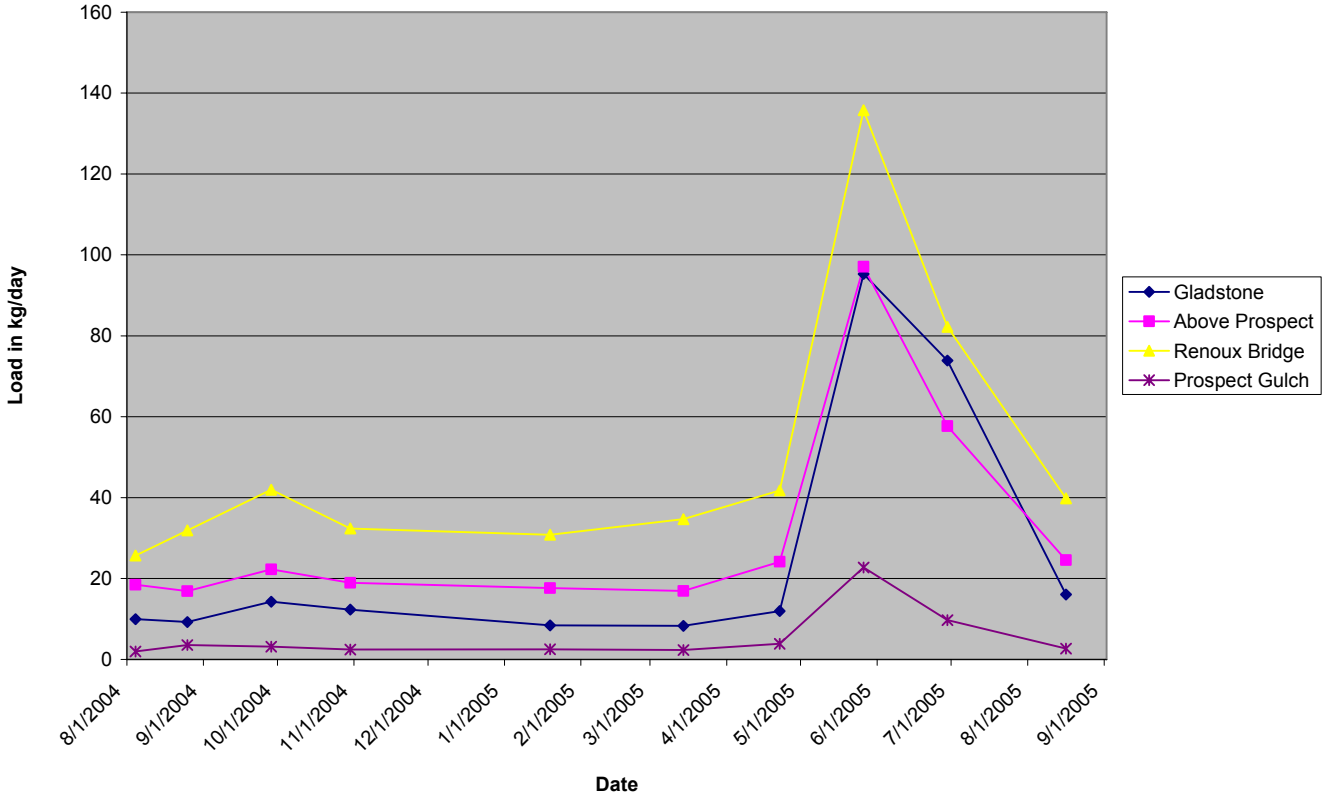

Figure 44: Temporal potassium loads in Cement Creek and Prospect Gulch.

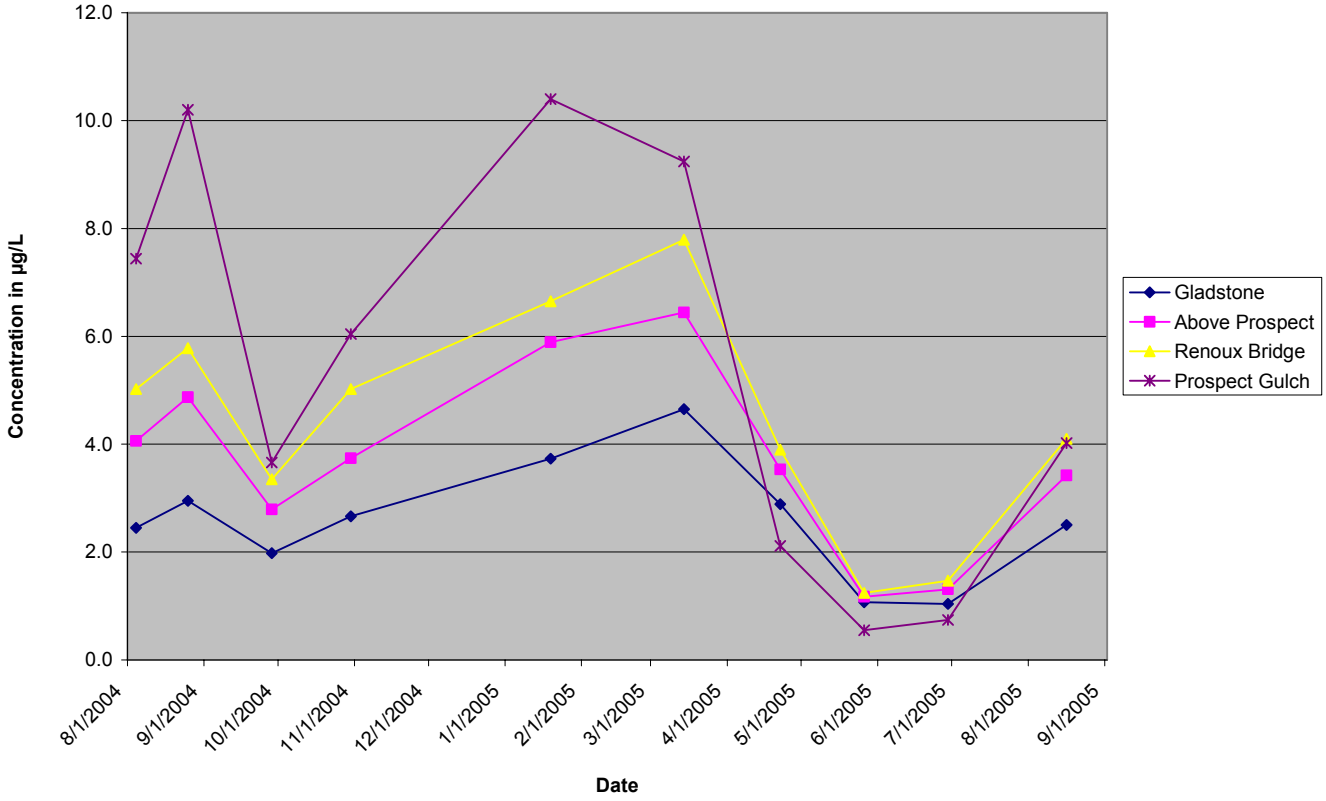

Figure 45: Temporal rubidium concentrations in Cement Creek and Prospect Gulch.

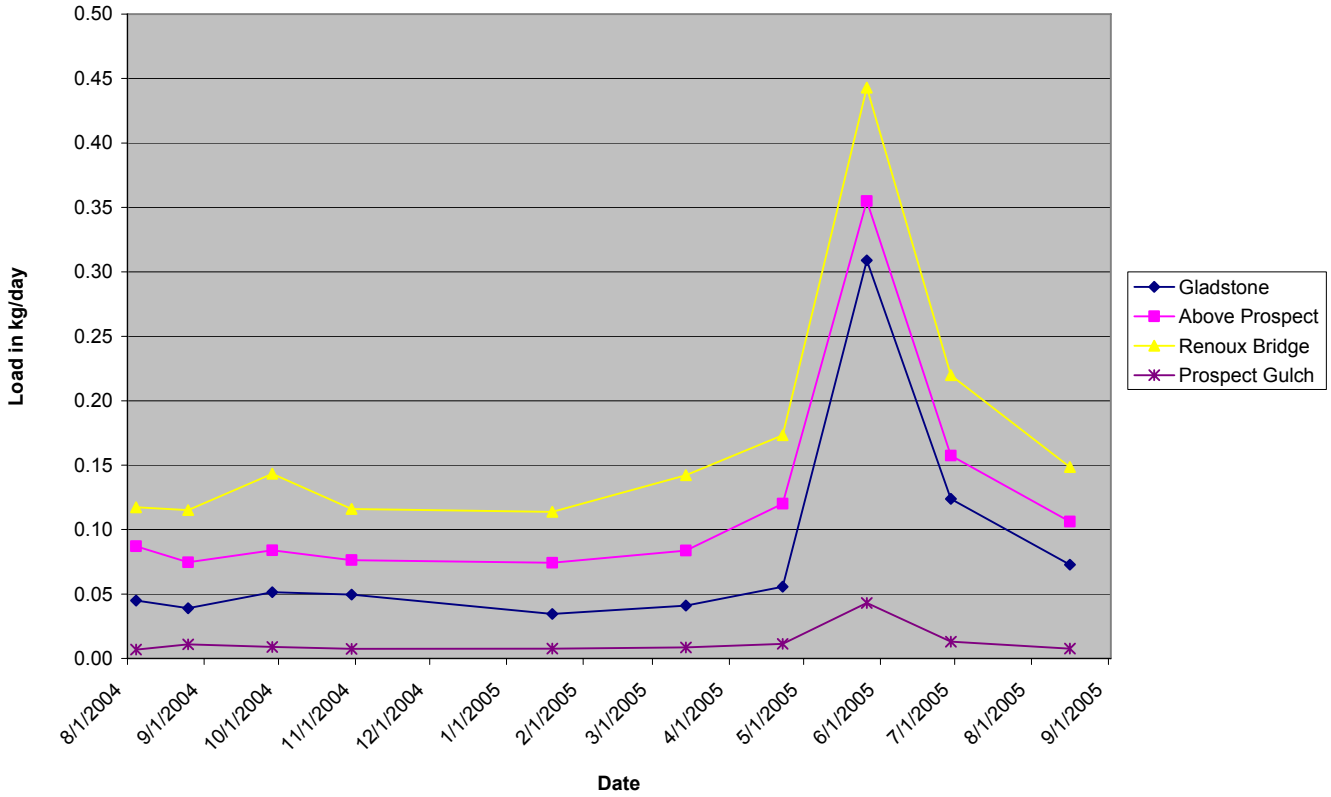

Figure 46: Temporal rubidium loads in Cement Creek and Prospect Gulch.

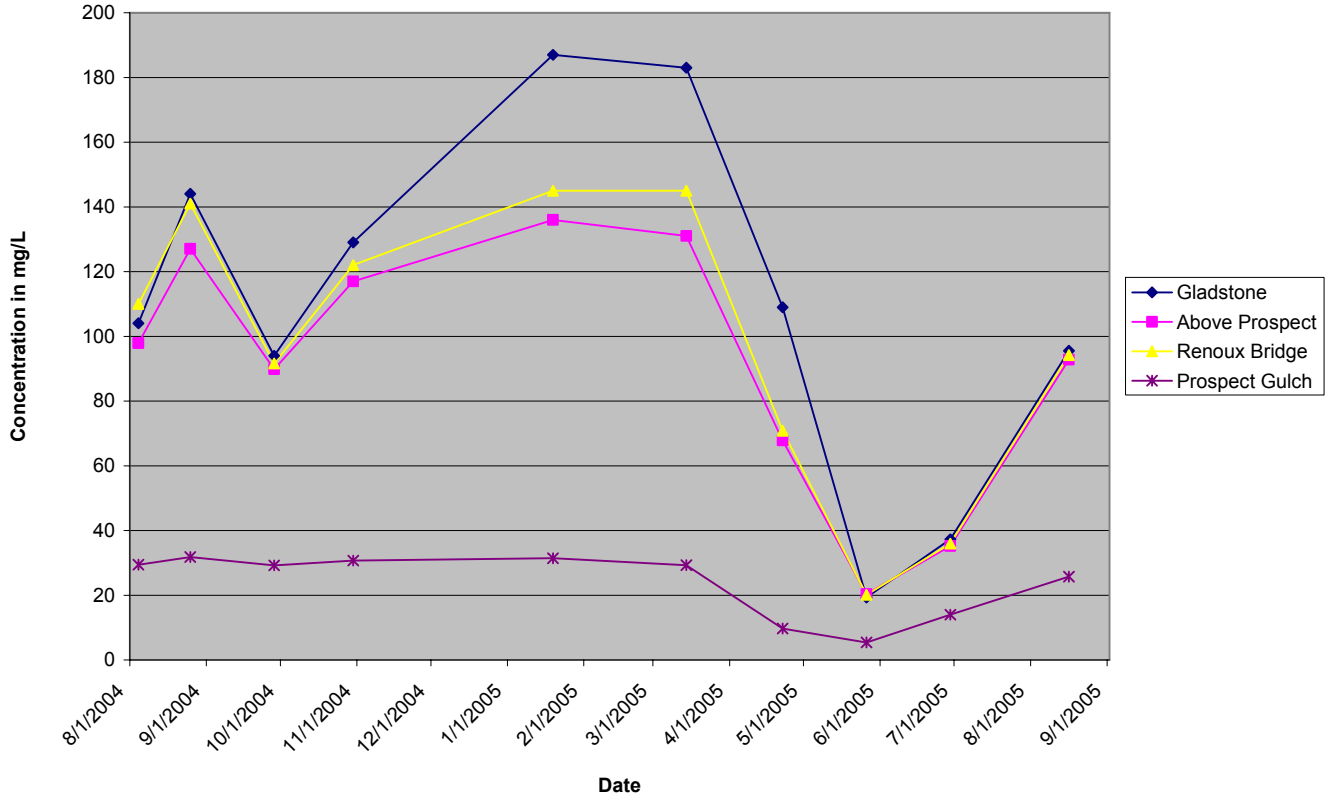

Figure 47: Temporal calcium concentrations in Cement Creek and Prospect Gulch.

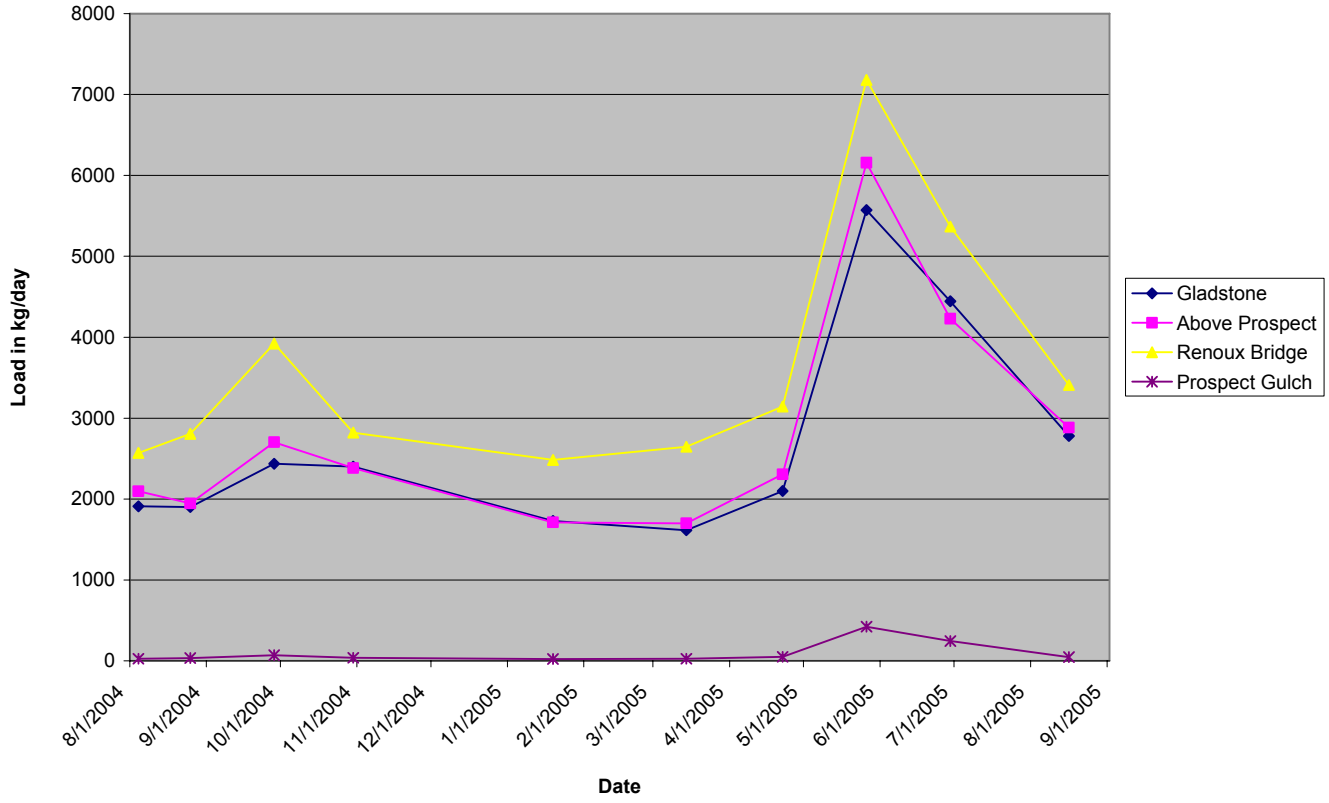

Figure 48: Temporal calcium loads in Cement Creek and Prospect Gulch.

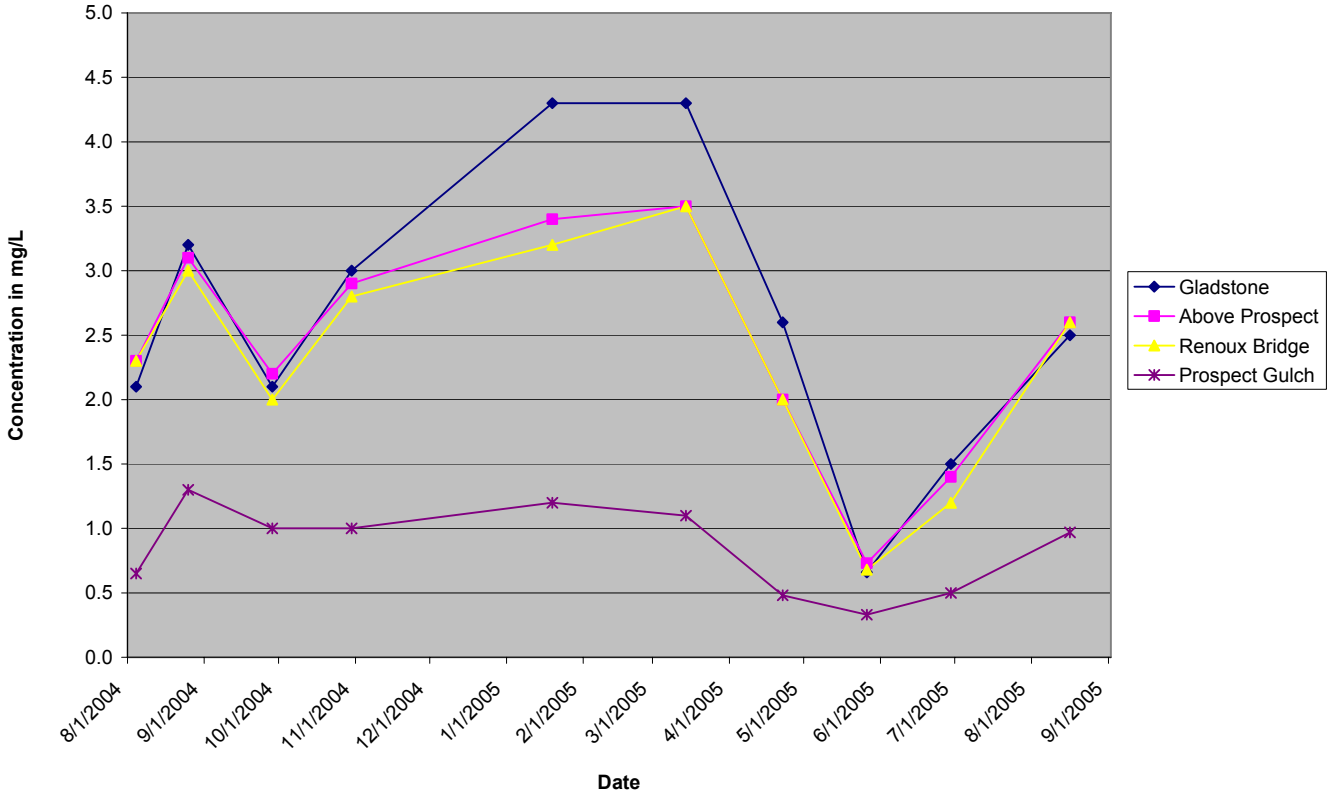

Figure 49: Temporal sodium concentrations in Cement Creek and Prospect Gulch.

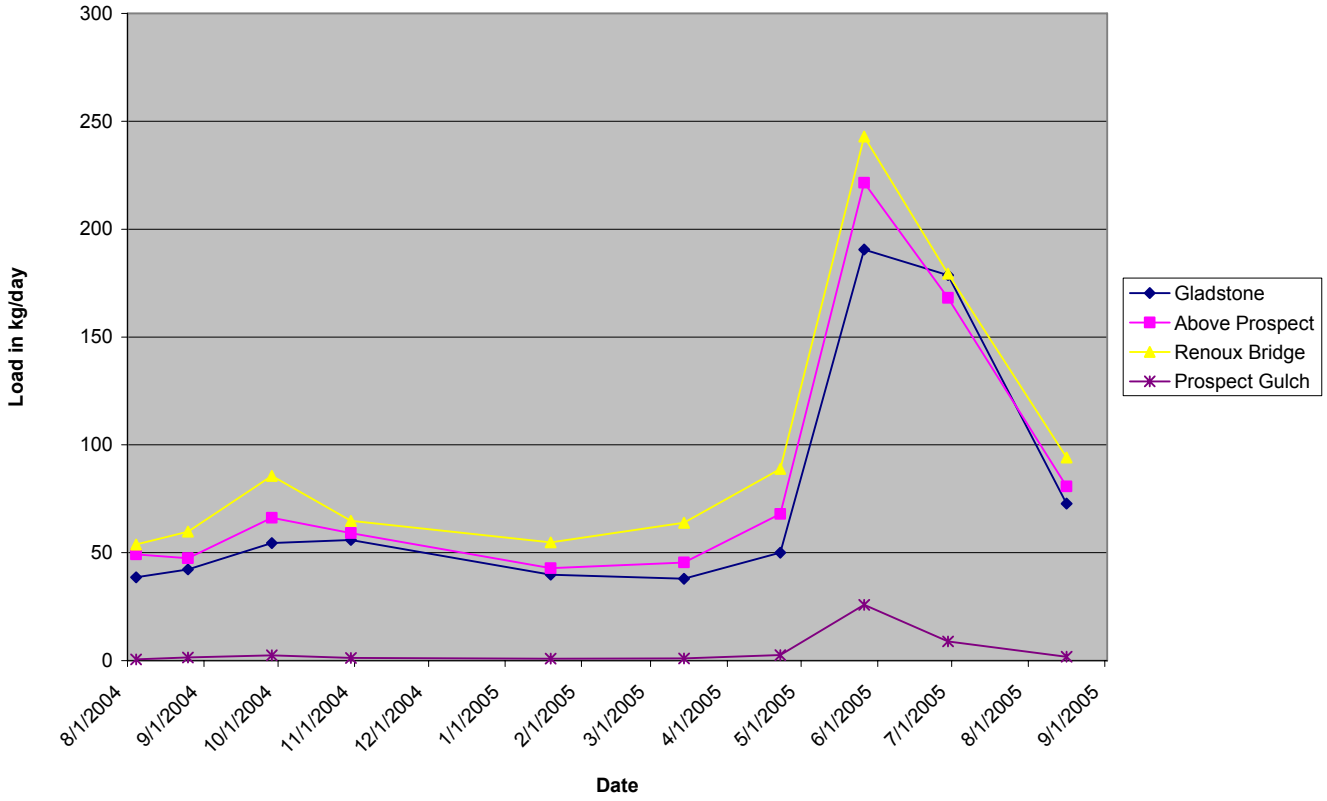

Figure 50: Temporal sodium loads in Cement Creek and Prospect Gulch.

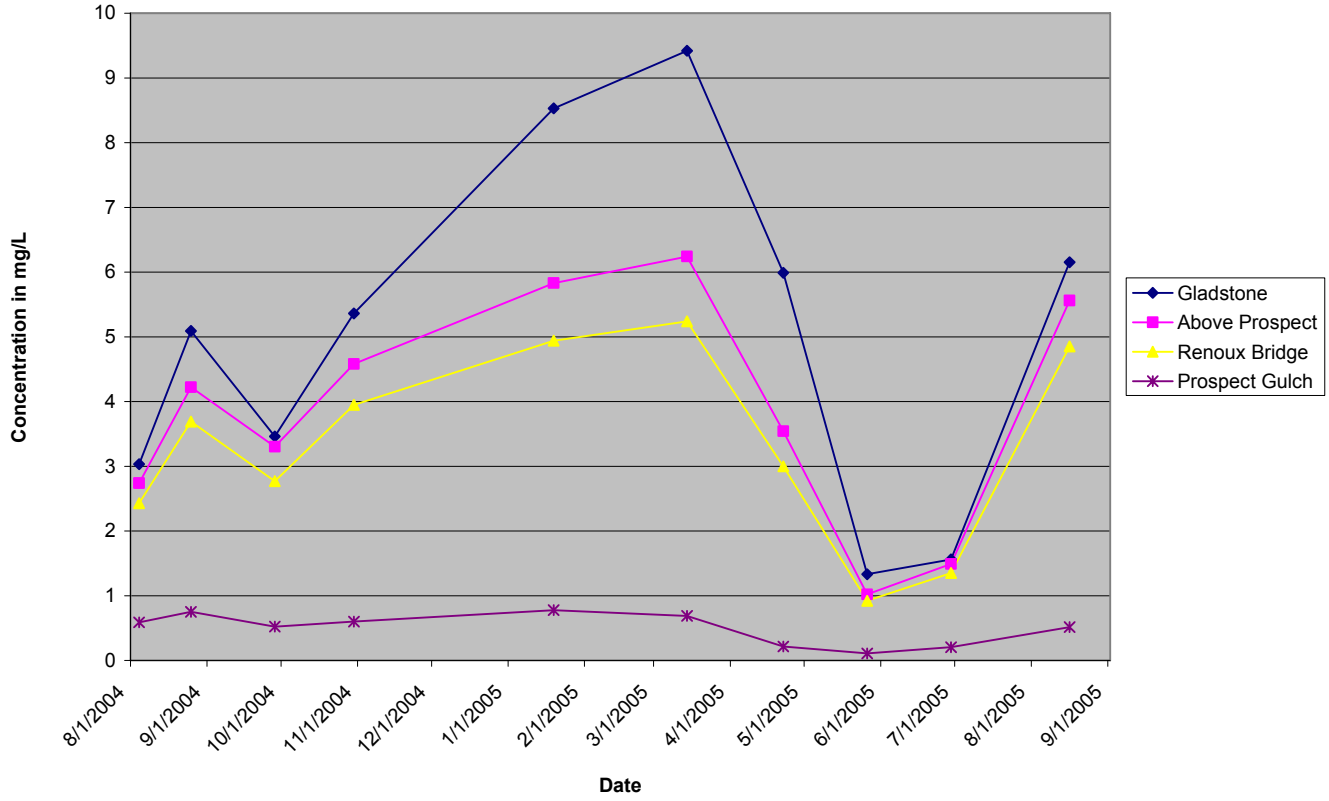

Figure 51: Temporal manganese concentrations in Cement Creek and Prospect Gulch.

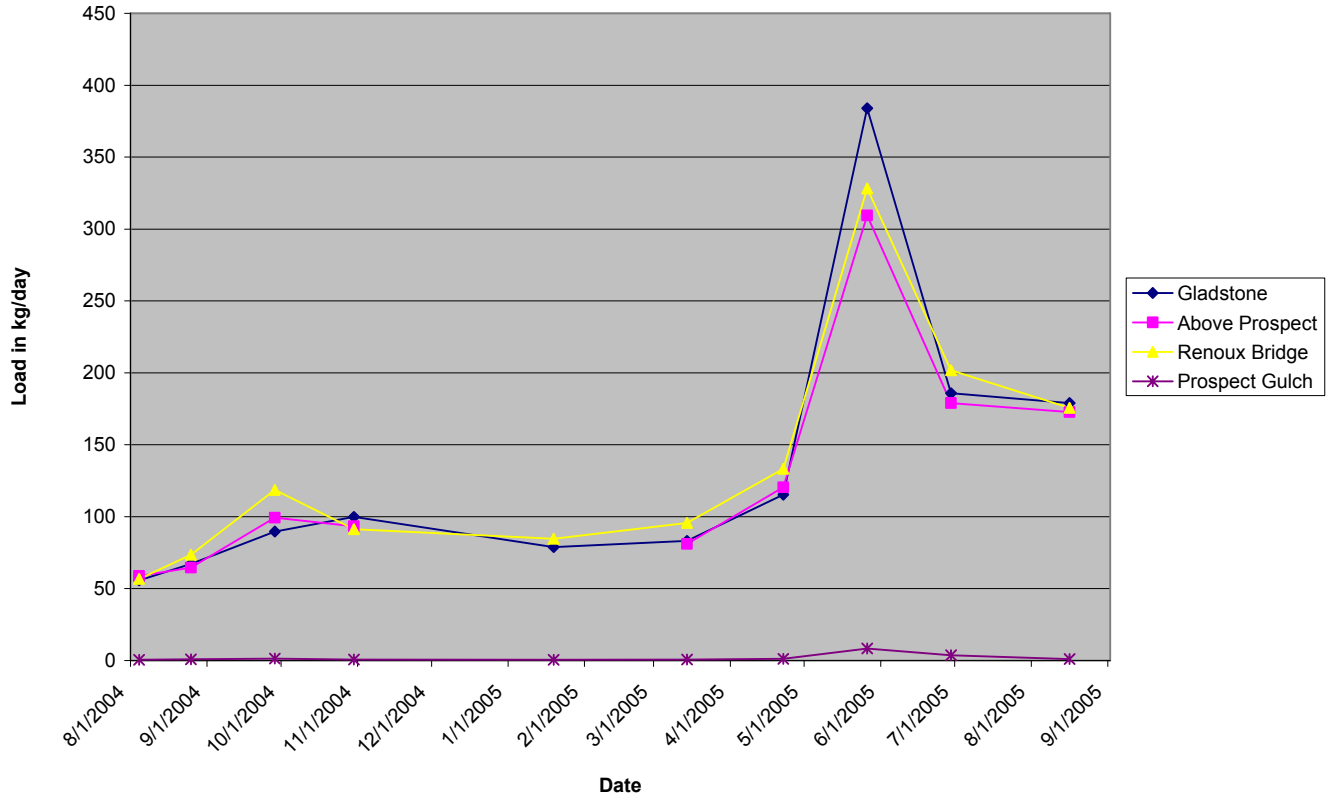

Figure 52: Temporal manganese loads in Cement Creek and Prospect Gulch.

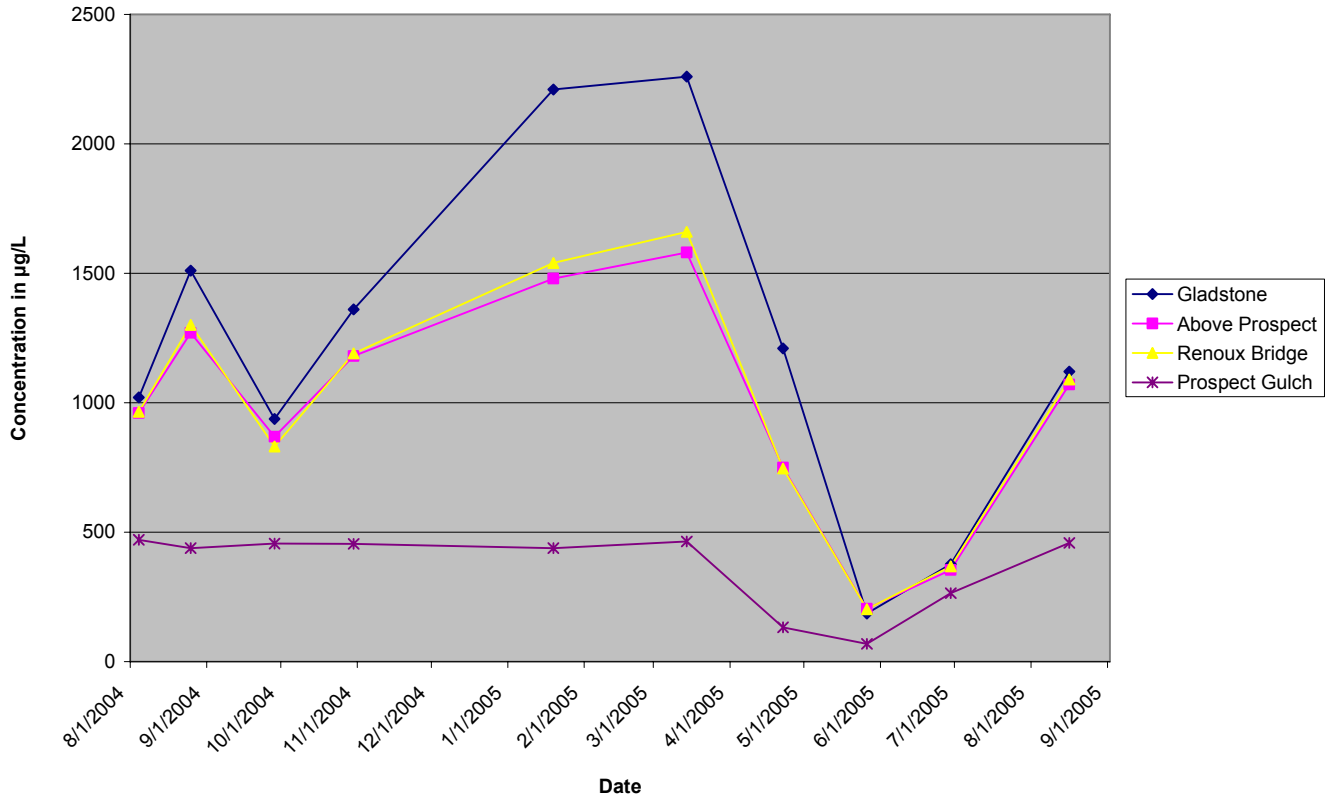

Figure 53: Temporal strontium concentrations in Cement Creek and Prospect Gulch.

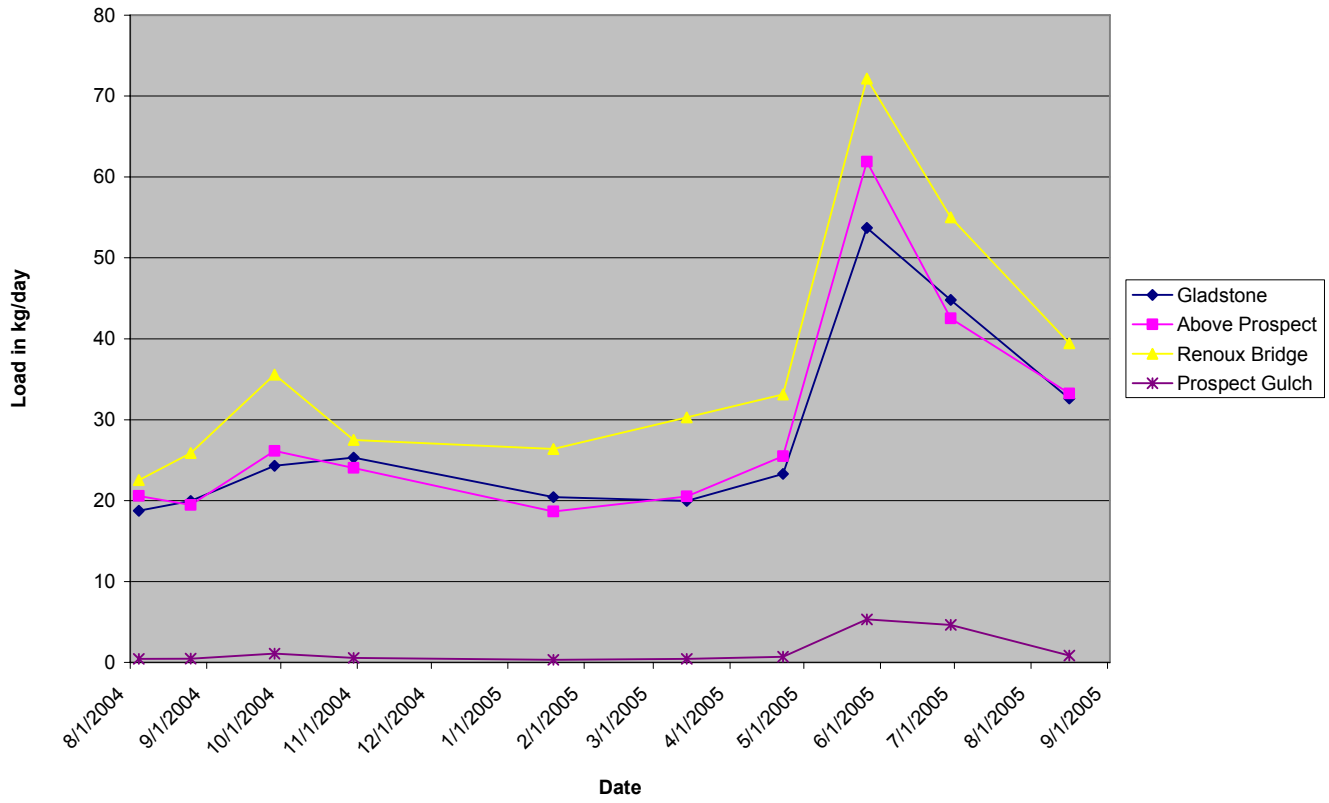

Figure 54: Temporal strontium loads in Cement Creek and Prospect Gulch.

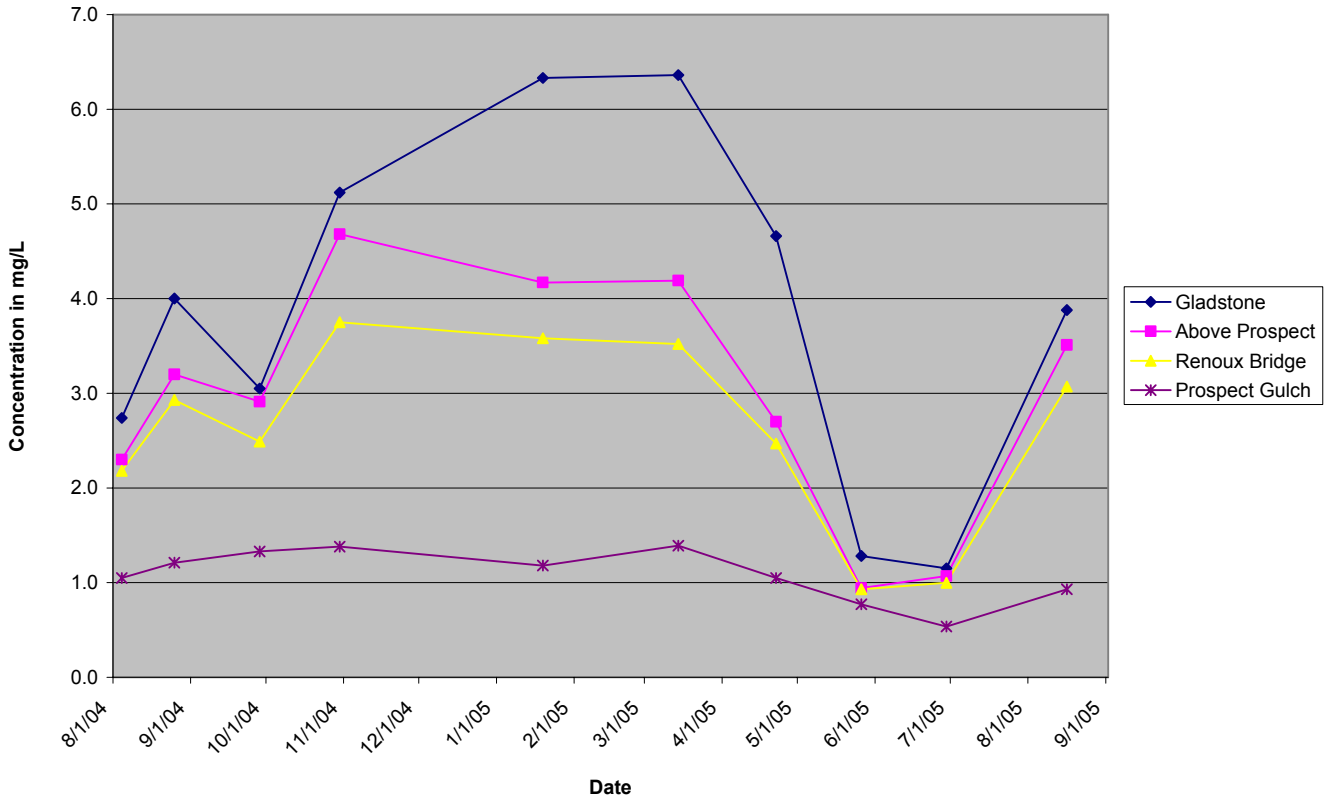

Figure 55: Temporal zinc concentrations in Cement Creek and Prospect Gulch.

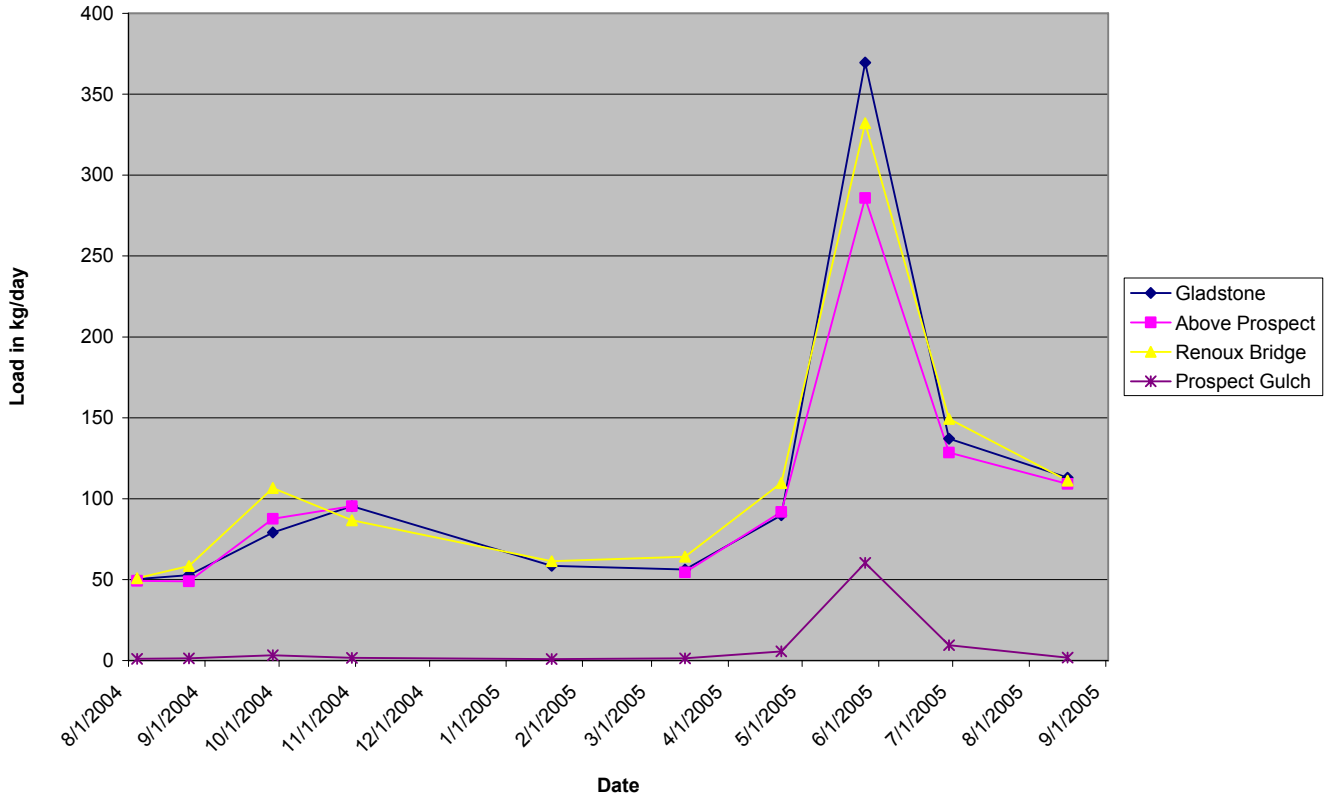

Figure 56: Temporal zinc loads in Cement Creek and Prospect Gulch.

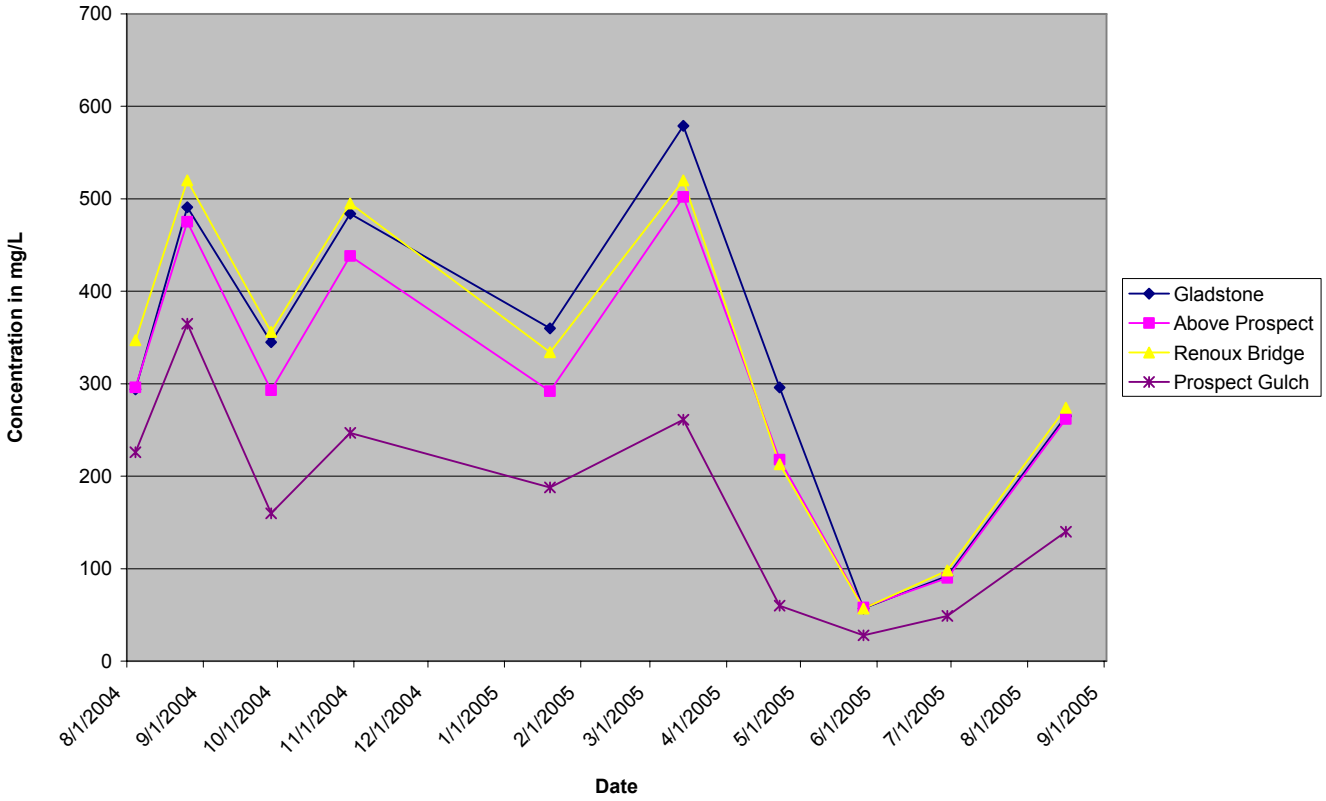

Figure 57: Temporal sulfate concentrations in Cement Creek and Prospect Gulch.

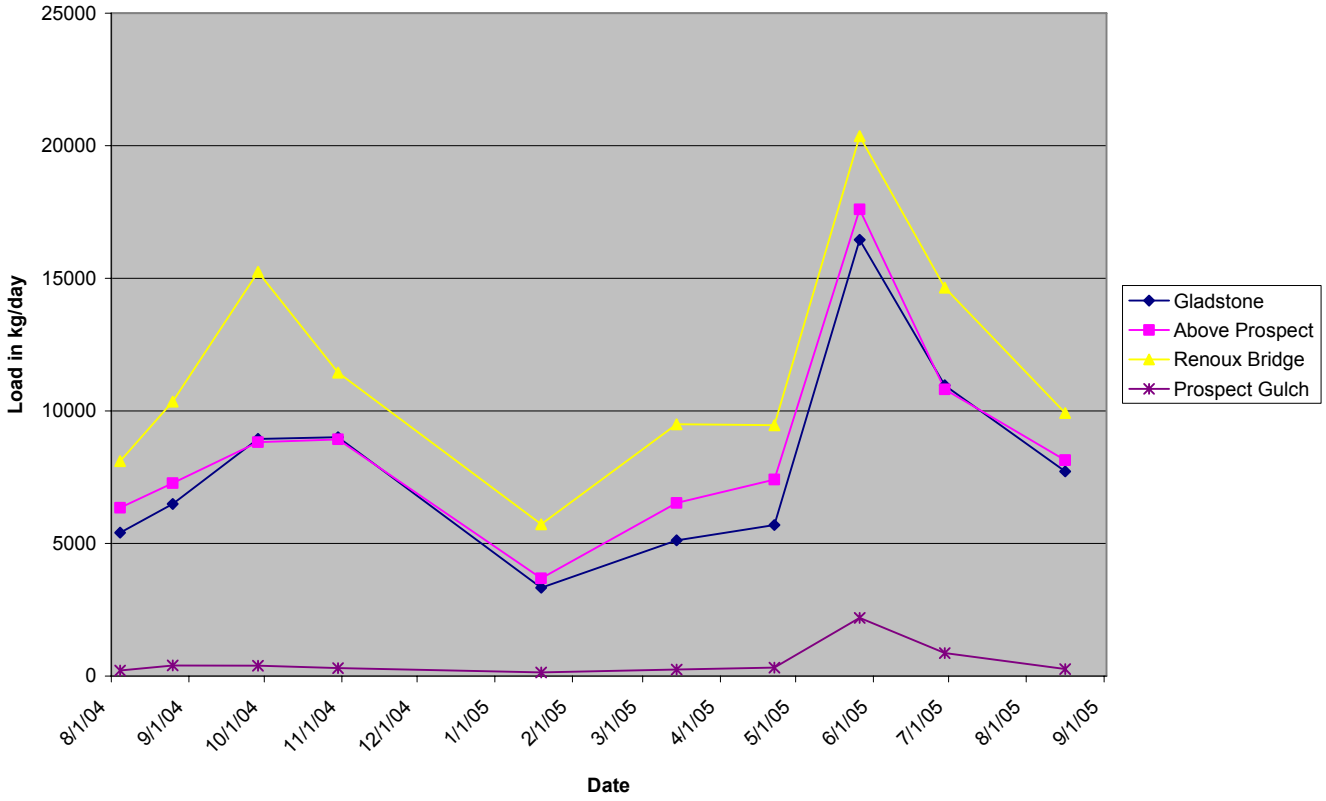

Figure 58: Temporal sulfate loads in Cement Creek and Prospect Gulch.

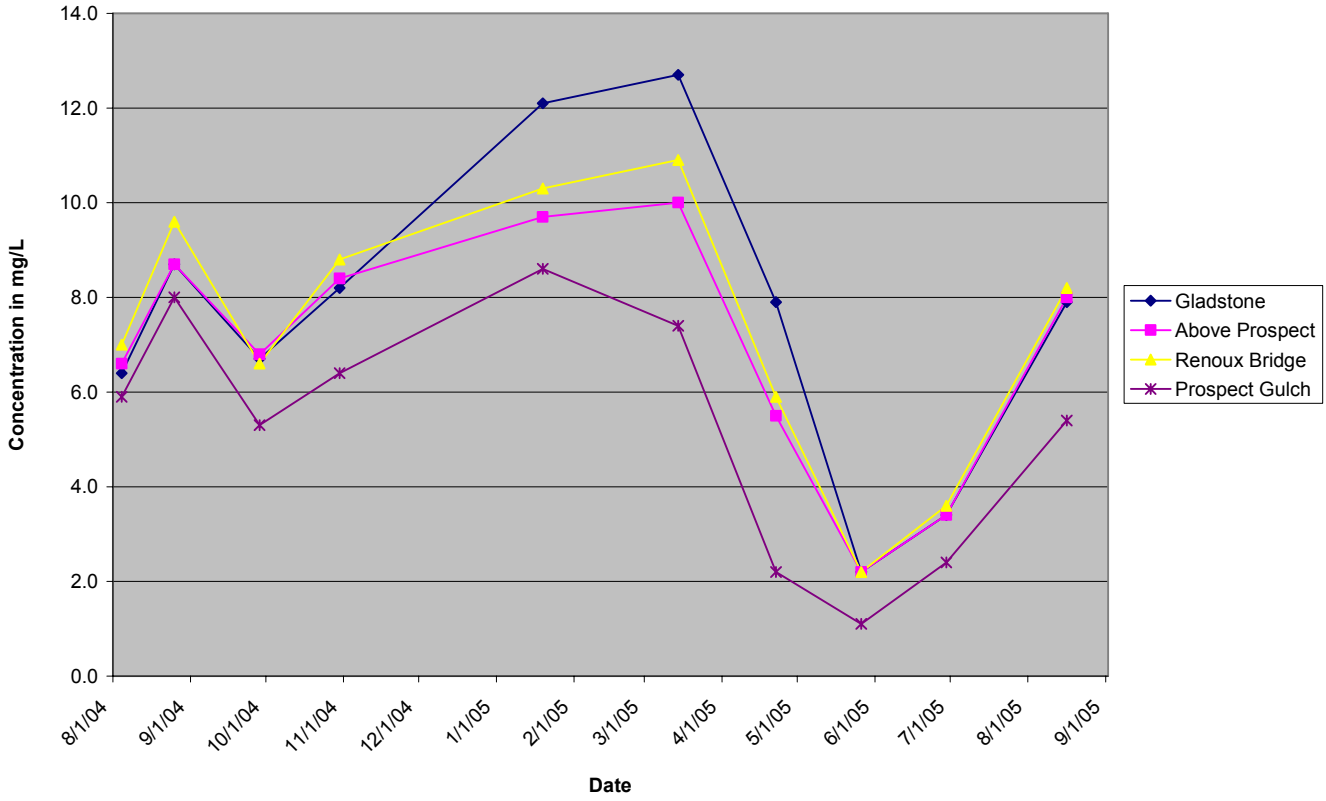

Figure 59: Temporal magnesium concentrations in Cement Creek and Prospect Gulch.

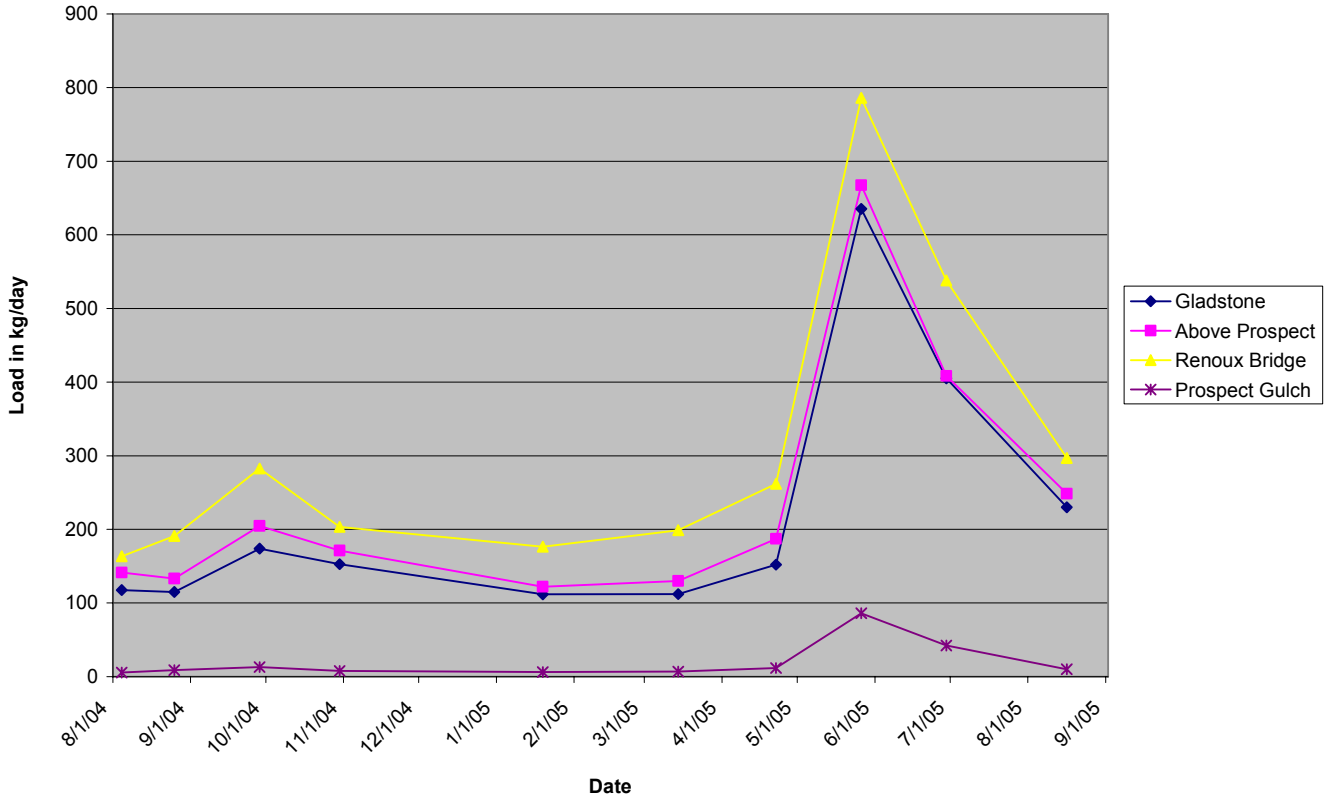

Figure 60: Temporal magnesium loads in Cement Creek and Prospect Gulch.

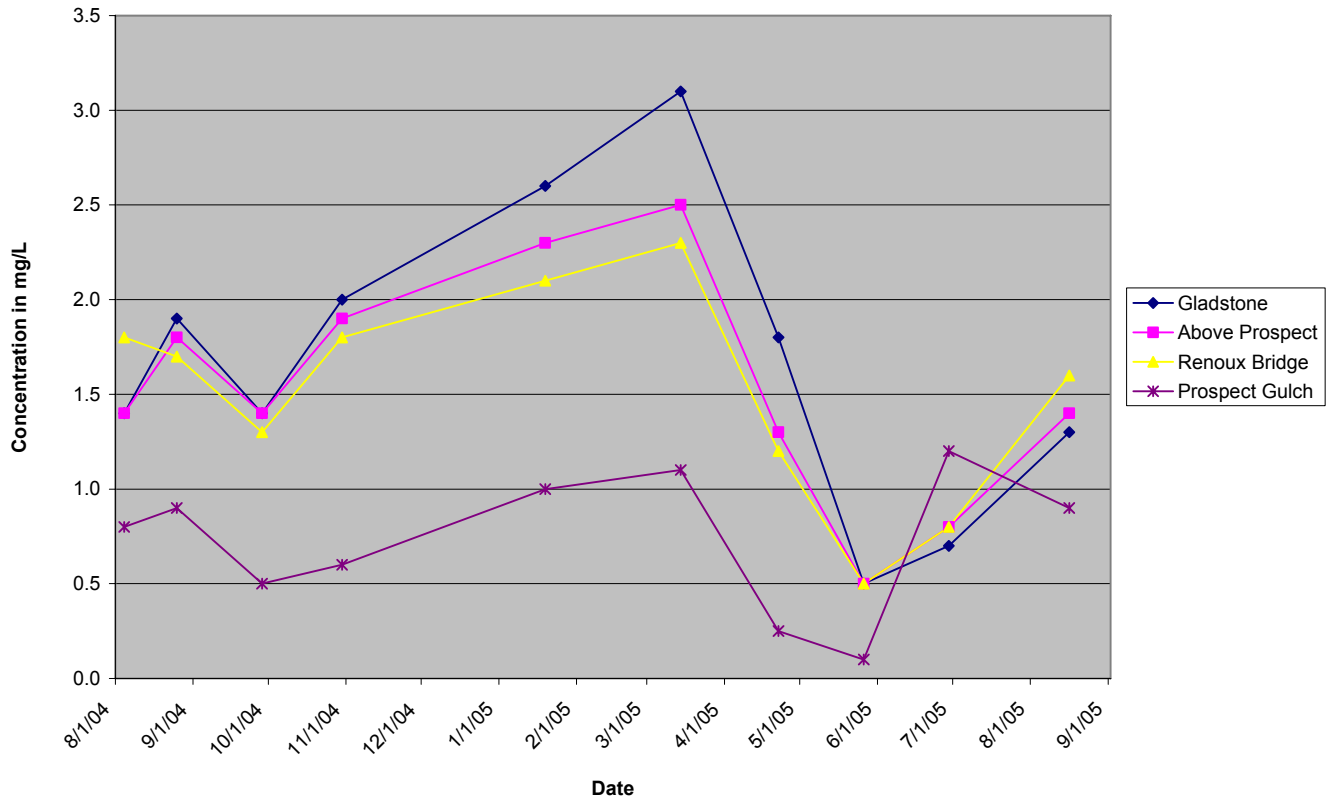

Figure 61: Temporal fluoride concentrations in Cement Creek and Prospect Gulch.

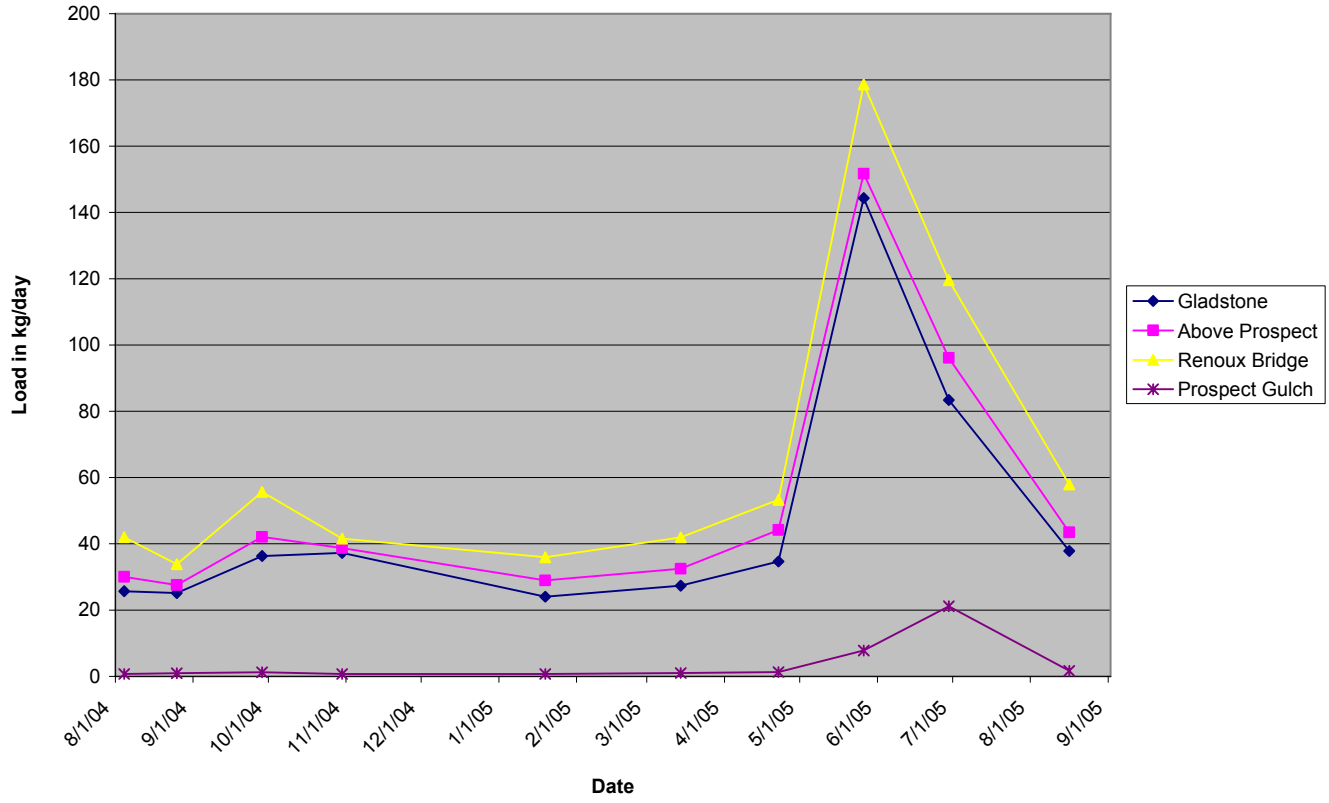

Figure 62: Temporal fluoride loads in Cement Creek and Prospect Gulch.

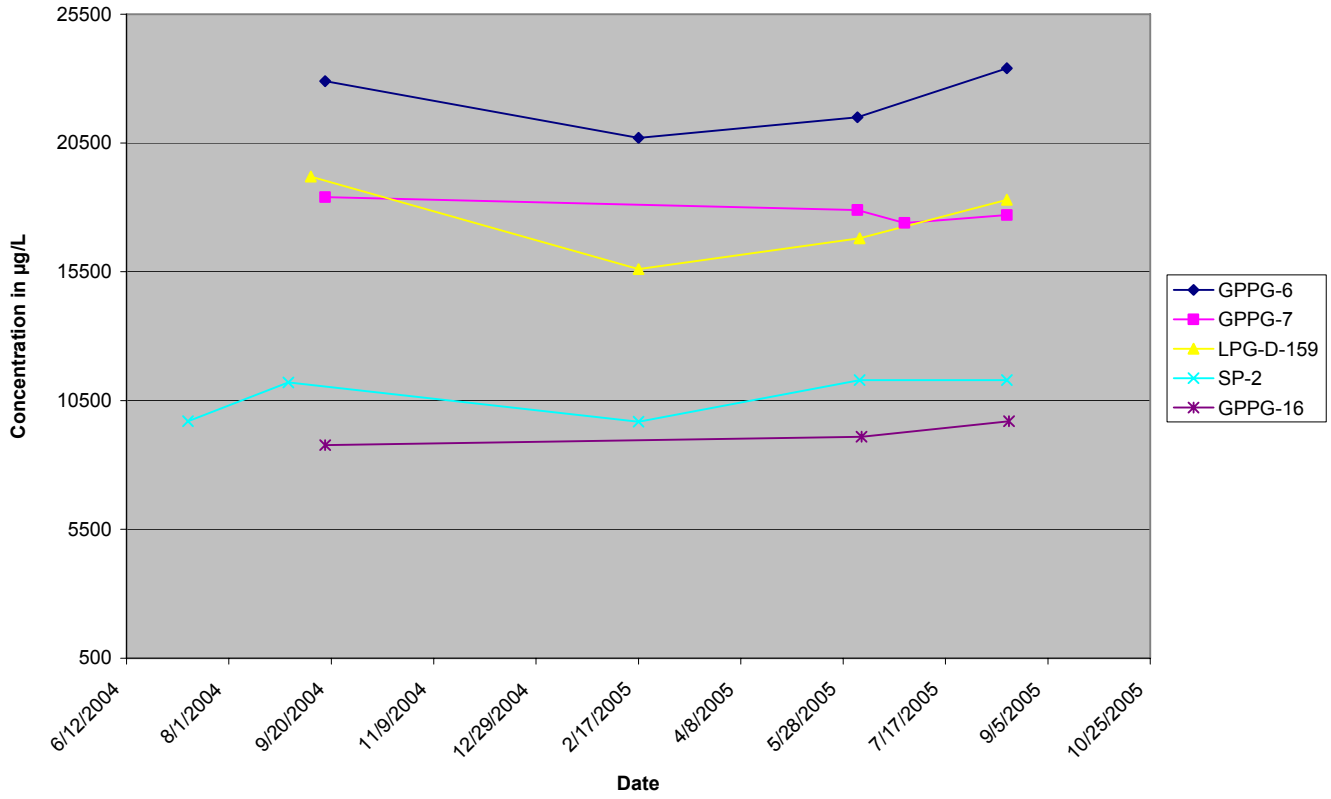

Figure 63: Aluminum concentrations in deep ground water.

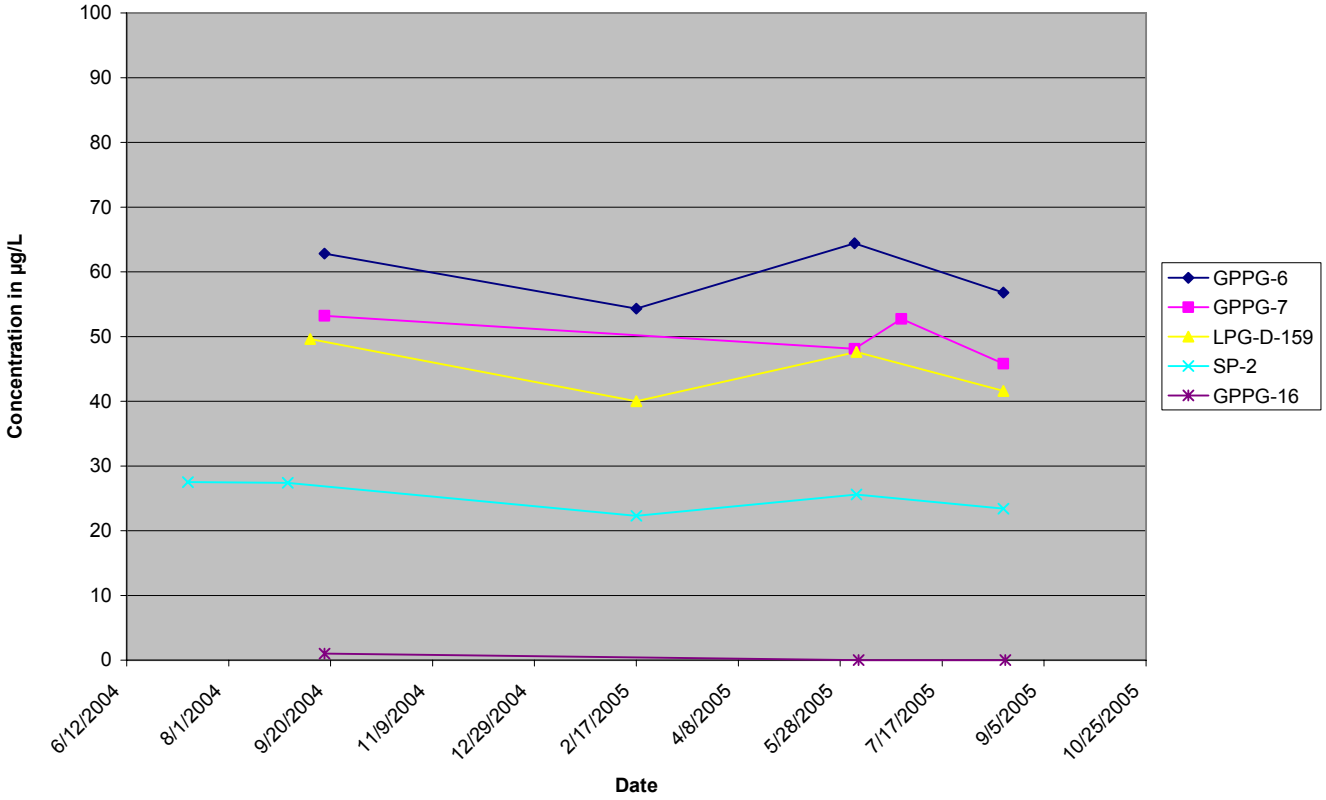

Figure 64: Arsenic concentrations in deep ground water.

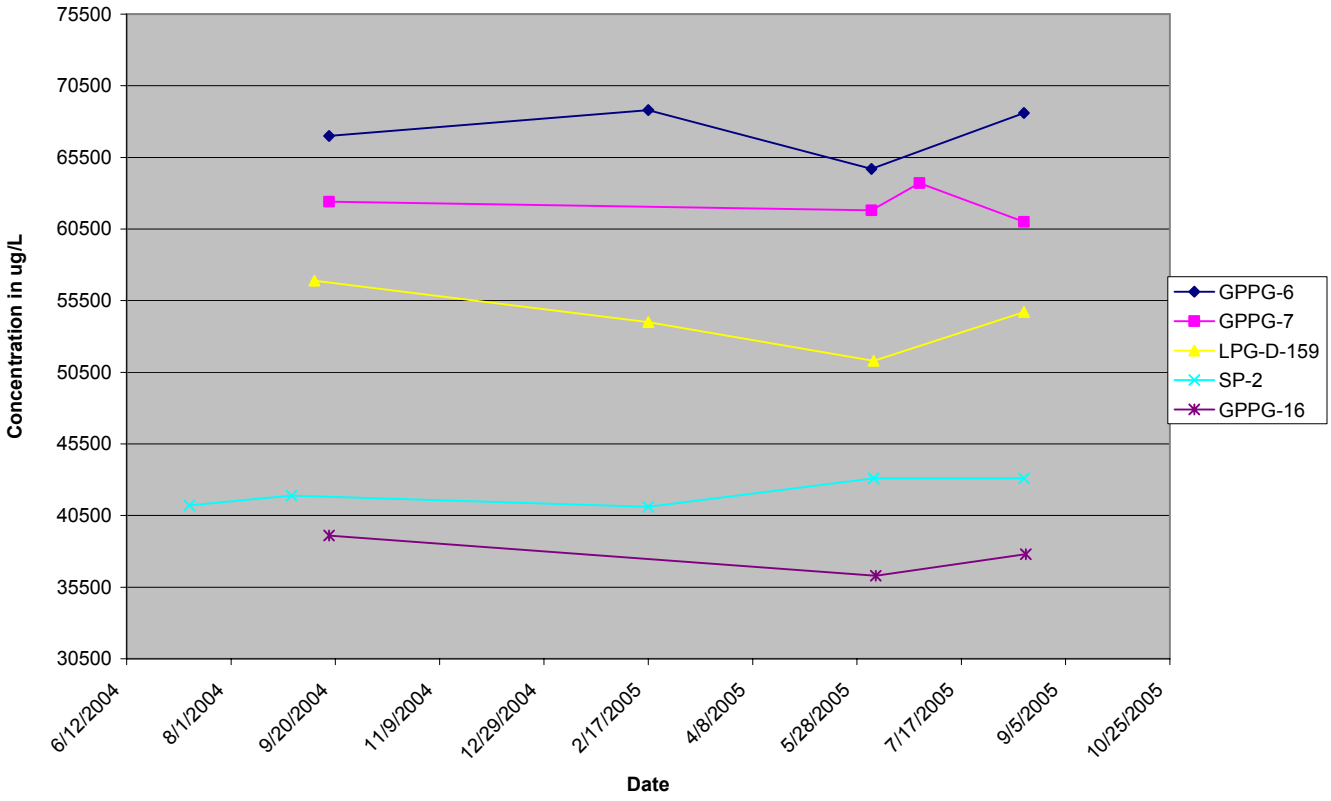

Figure 65: Iron concentrations in deep ground water.

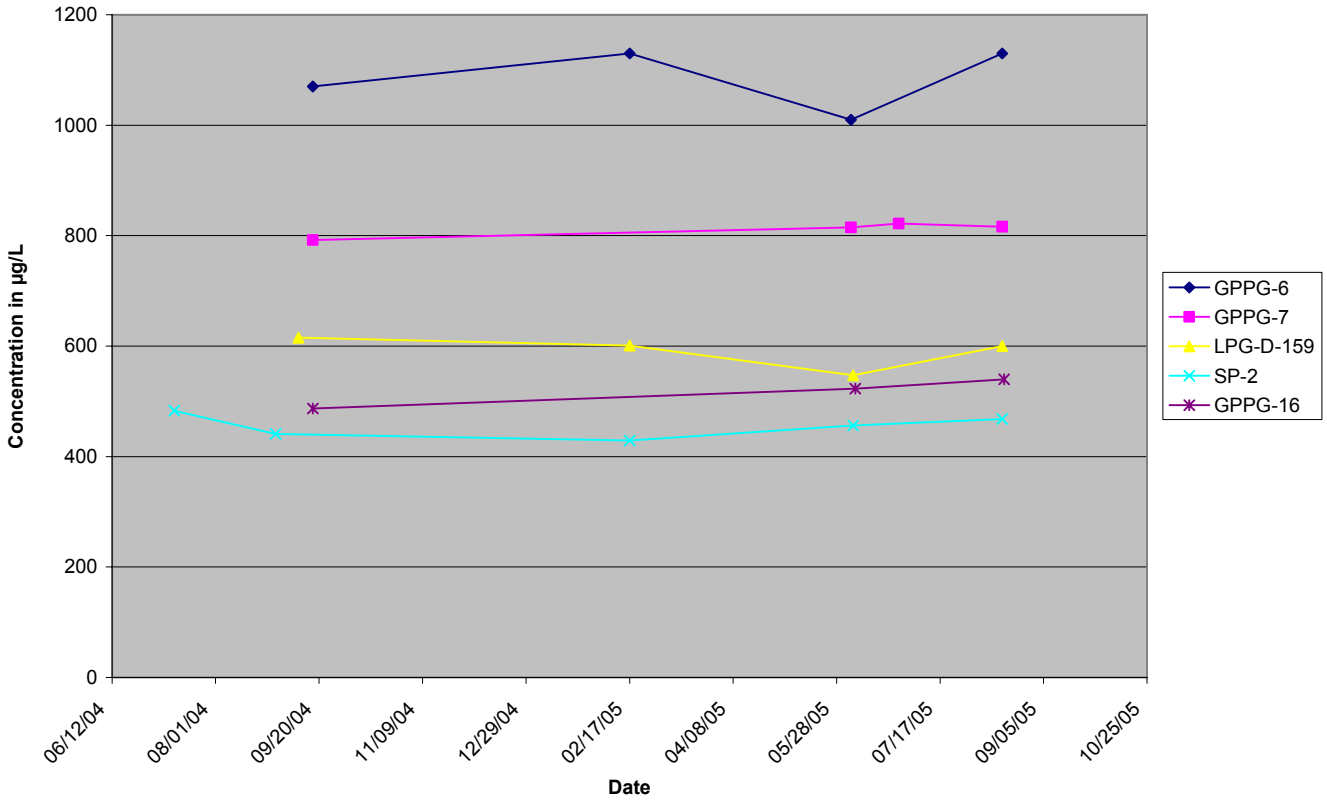

Figure 66: Zinc concentrations in deep ground water.

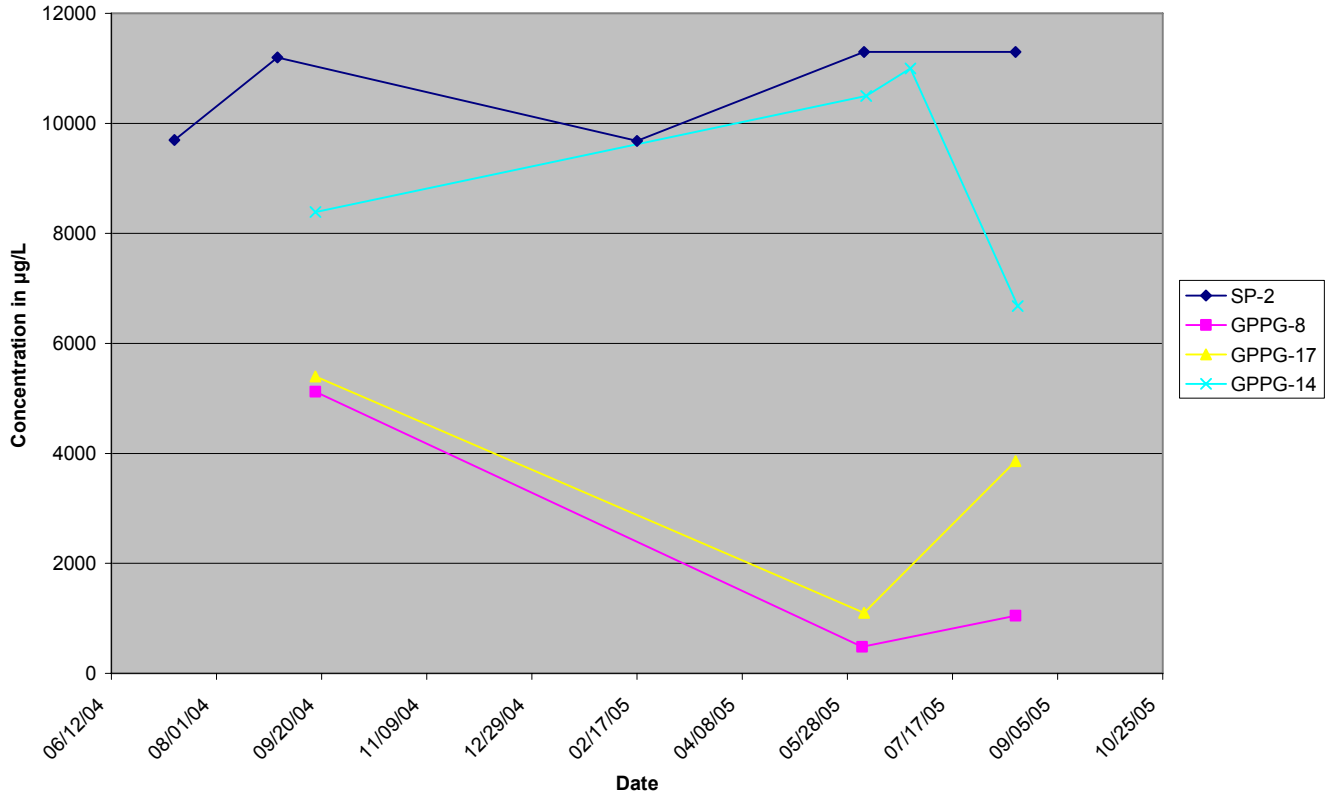

Figure 67: Aluminum concentrations in shallow ground water and SP-2.

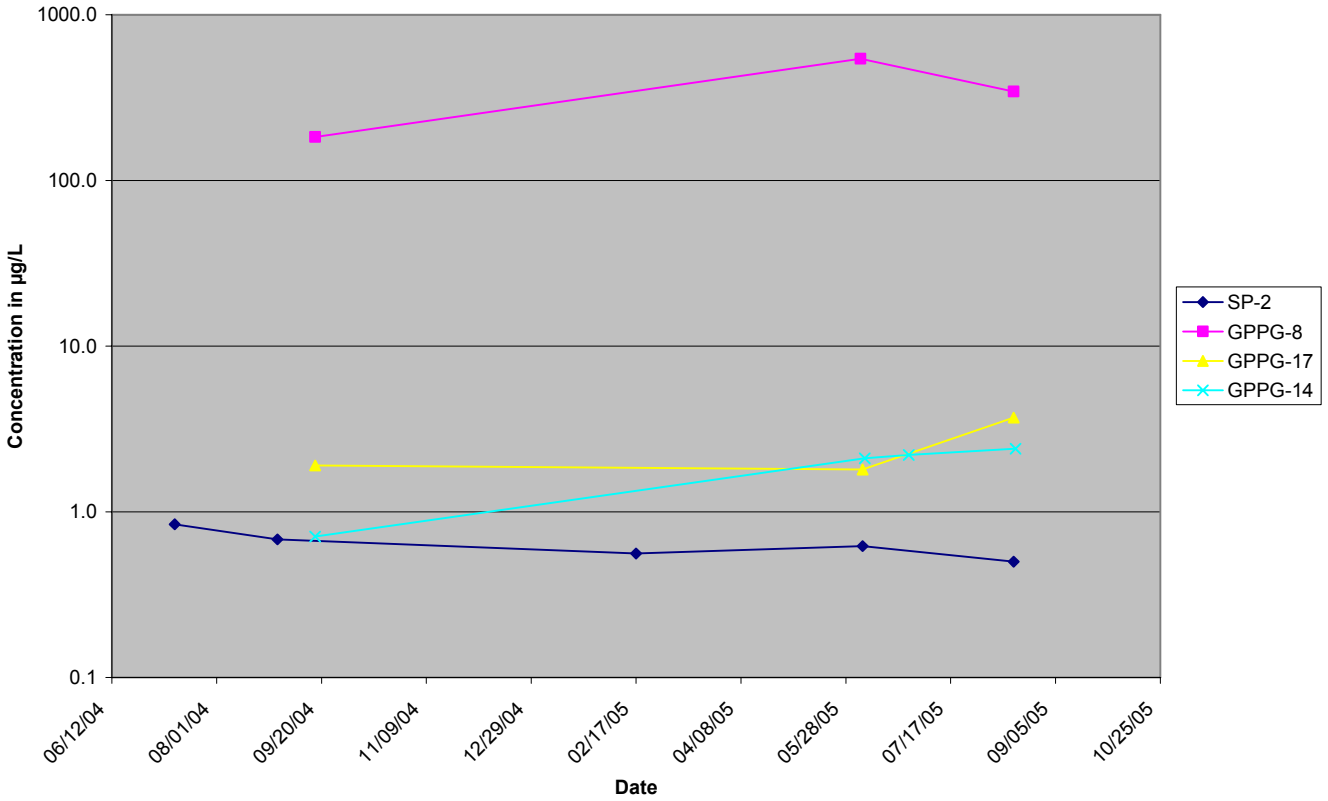

Figure 68: Copper concentrations in shallow ground water and SP-2.

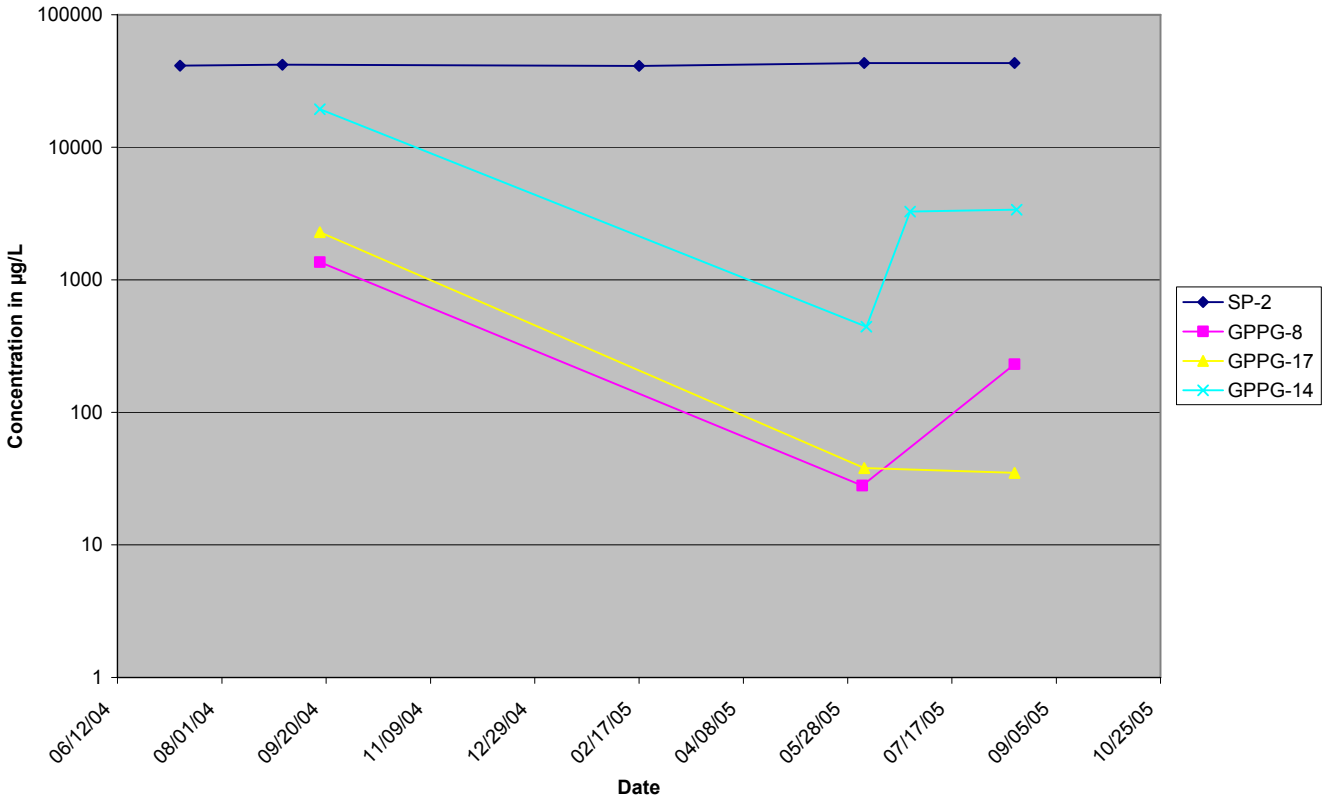

Figure 69: Iron concentrations in shallow ground water and SP-2.

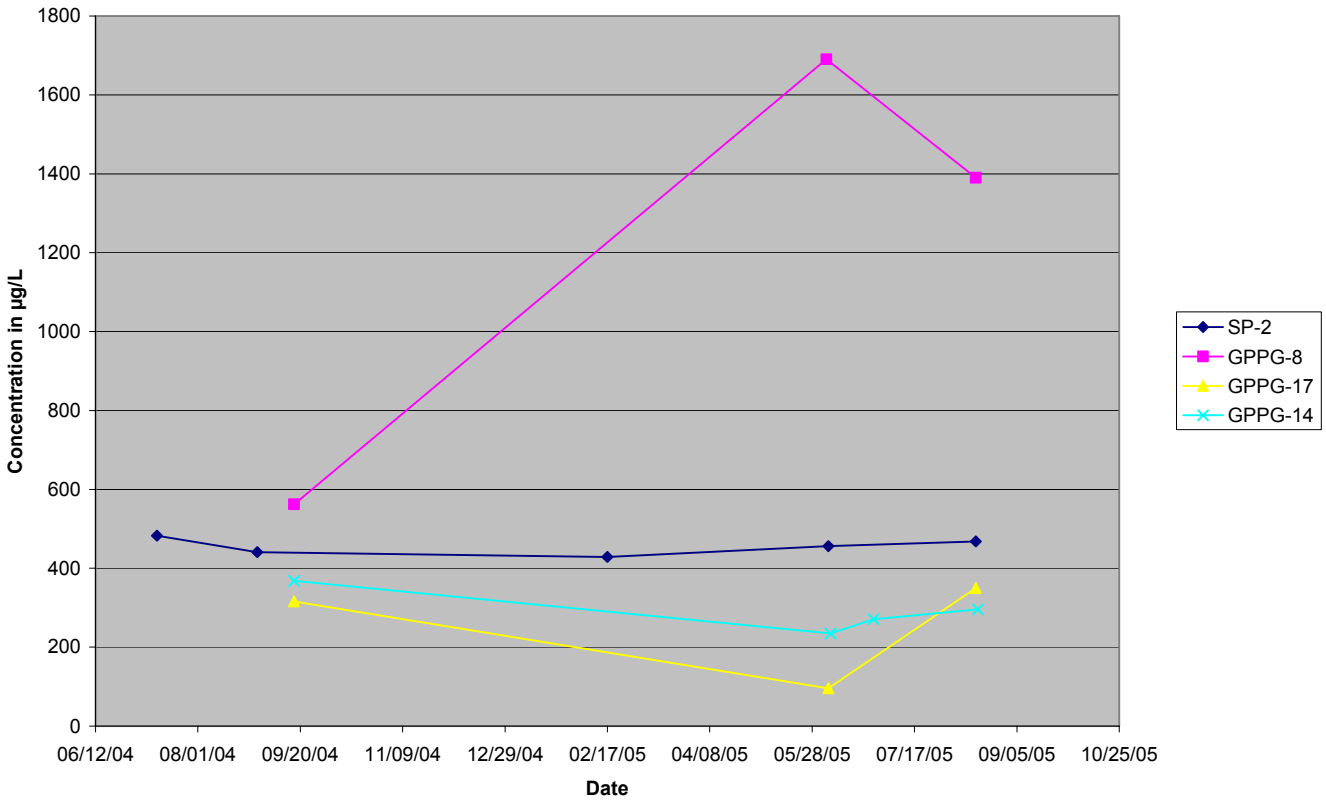

Figure 70: Zinc concentrations in shallow ground water and SP-2.

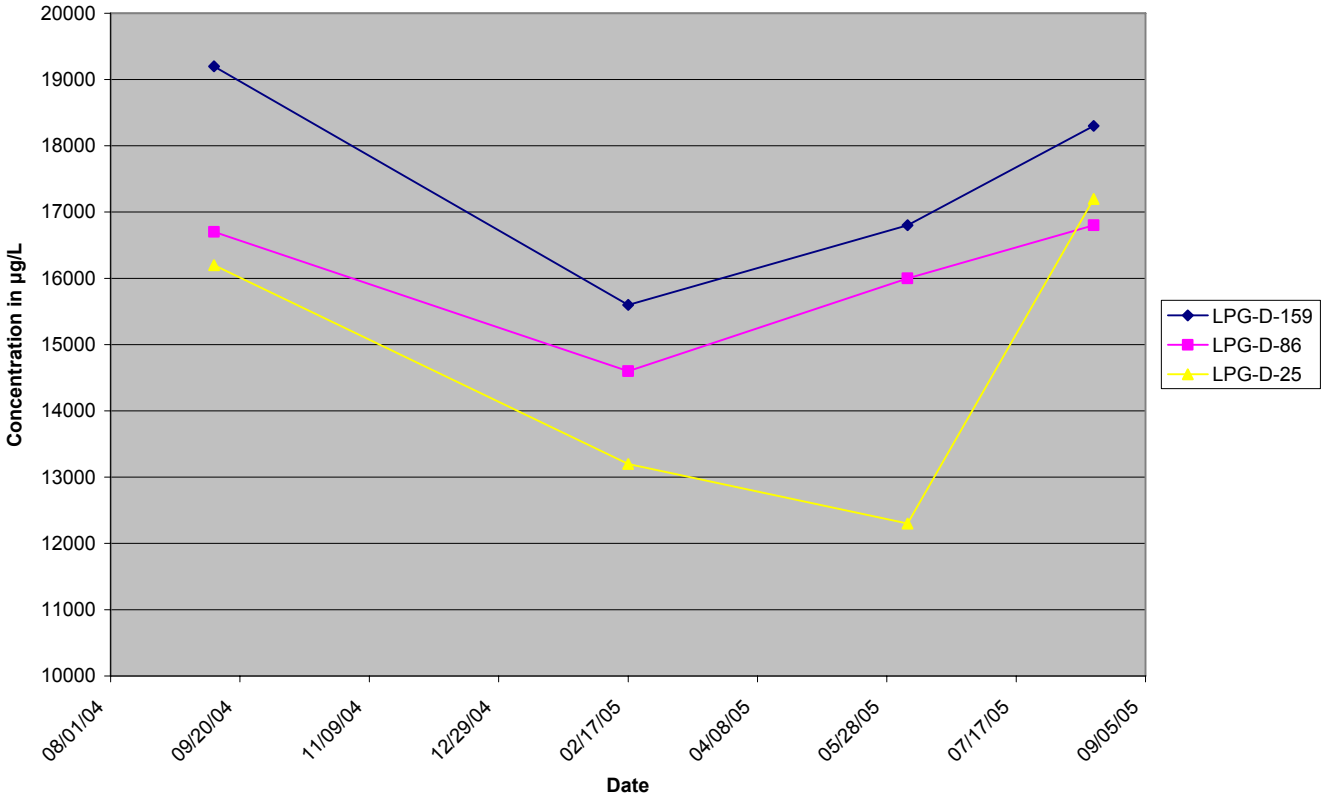

Figure 71: Aluminum concentrations well LPG-D.

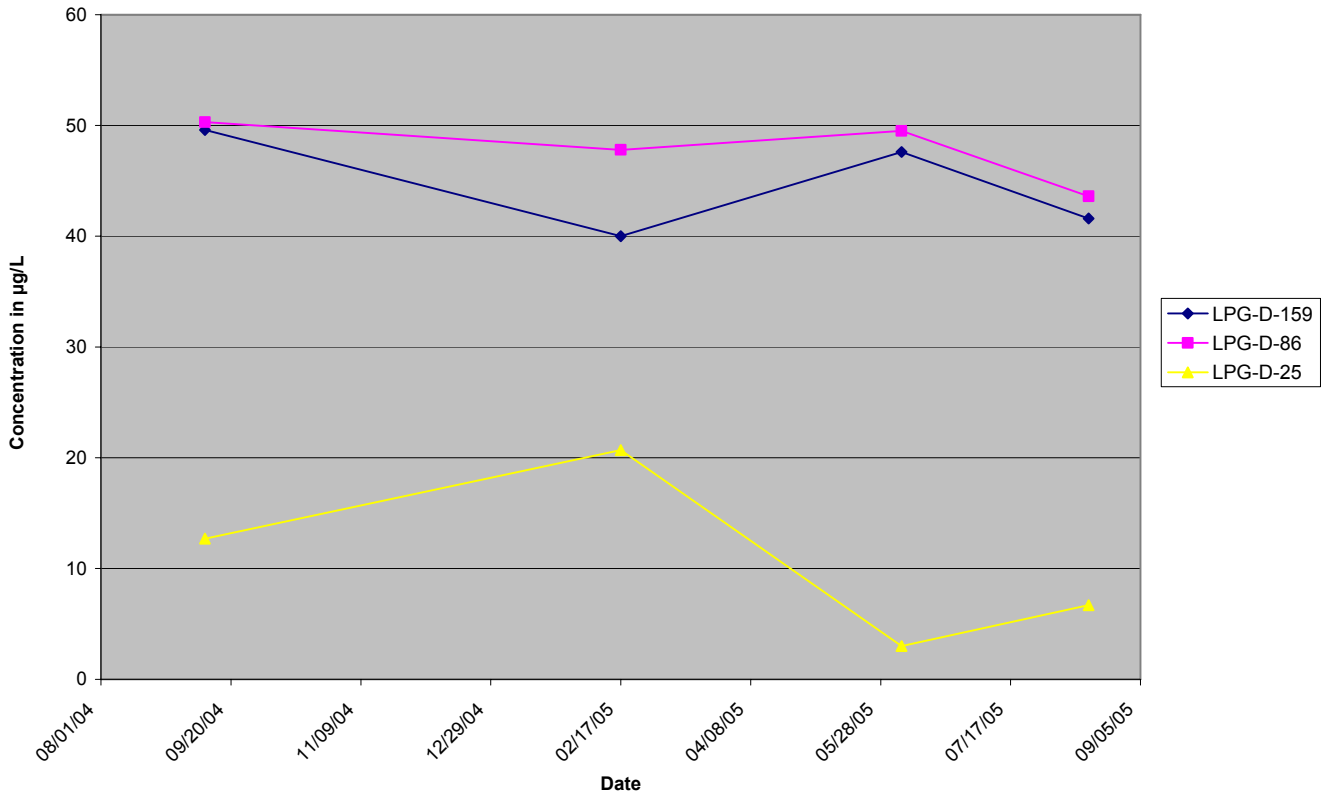

Figure 72: Arsenic concentrations well LPG-D.

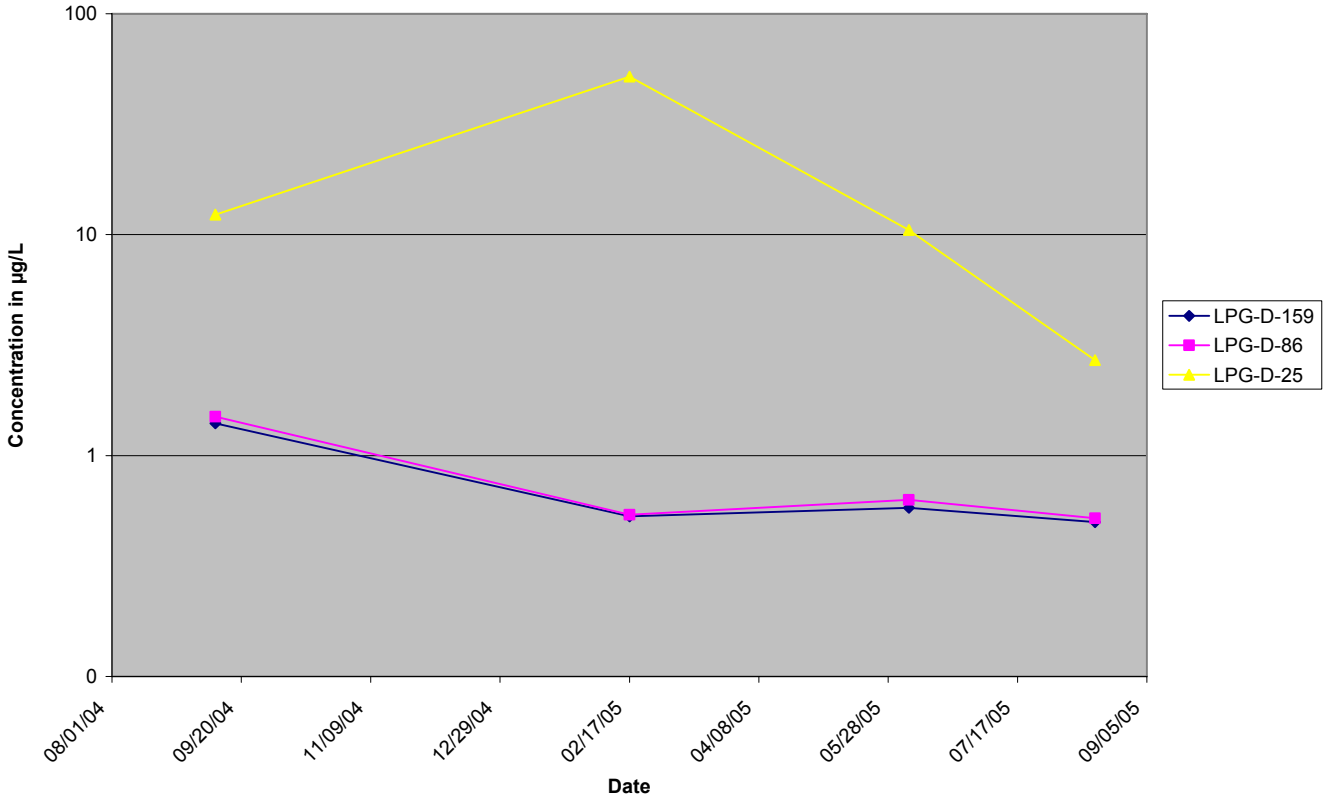

Figure 73: Copper concentrations well LPG-D.

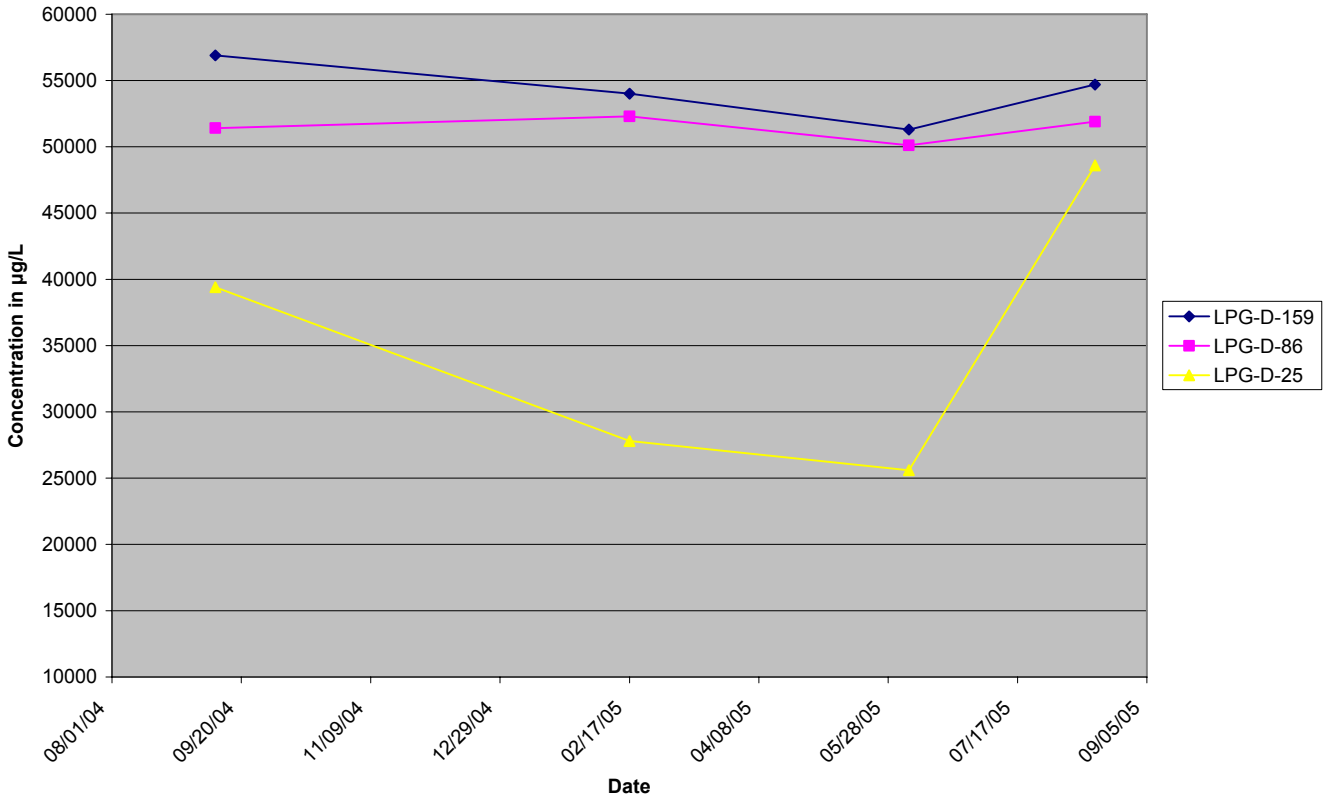

Figure 74: Iron concentrations well LPG-D.

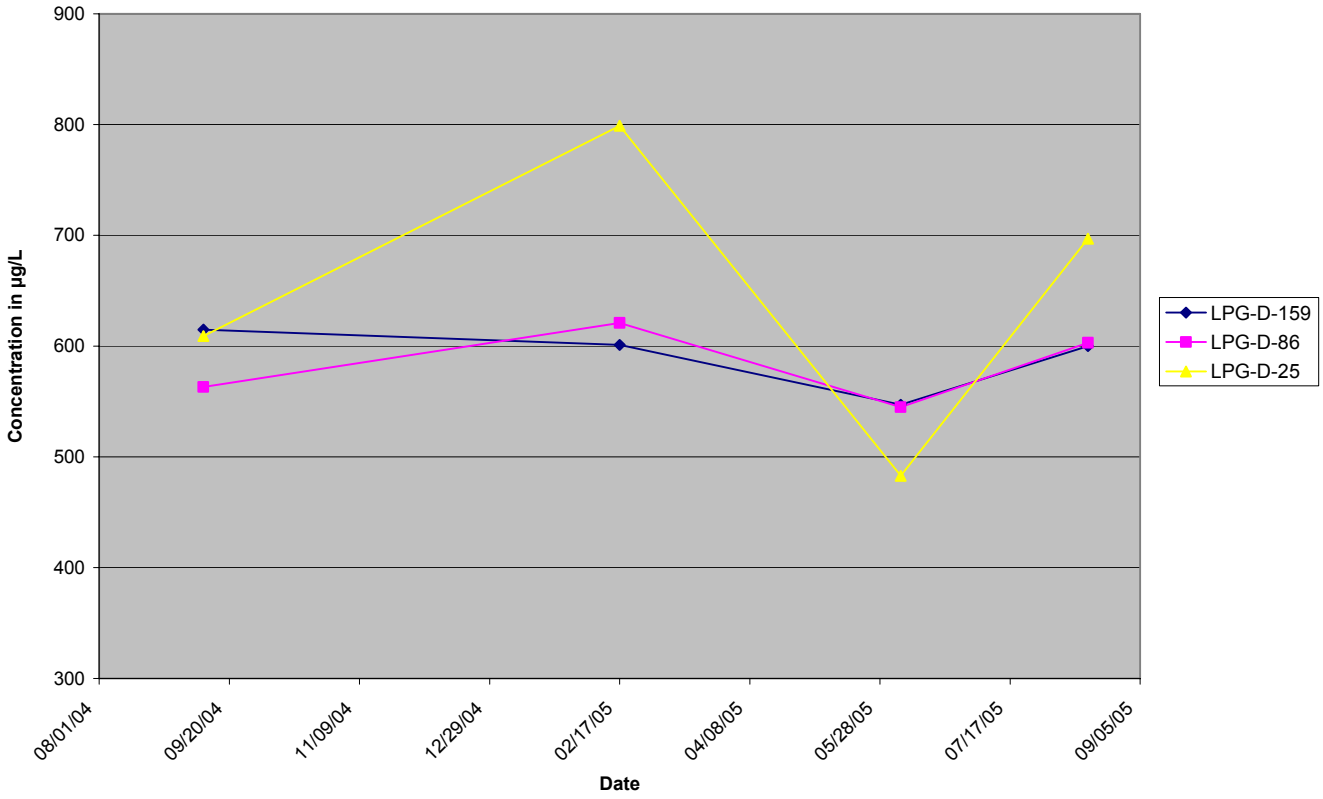

Figure 75: Zinc concentrations well LPG-D.

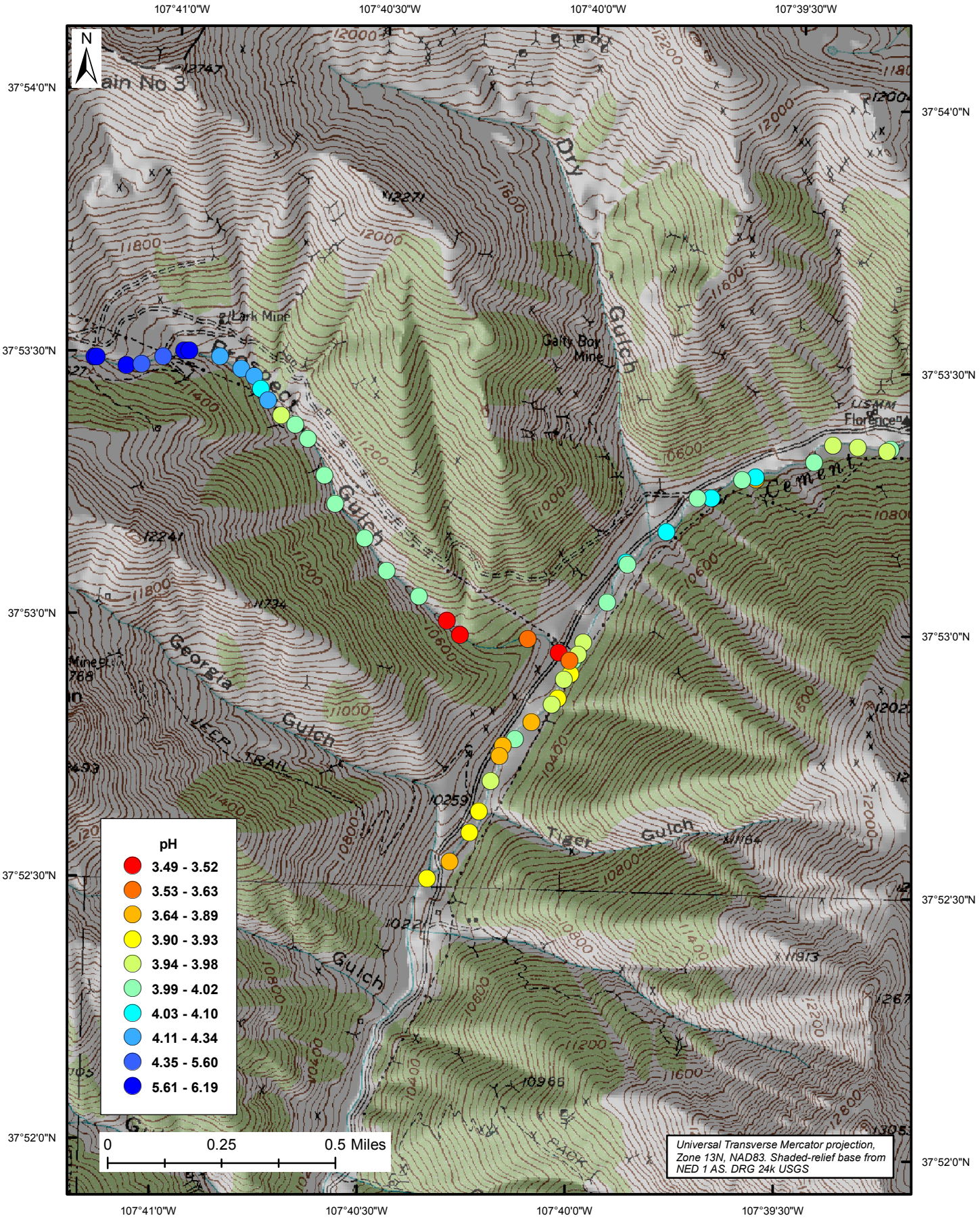

Figure 76: Instream pH values.

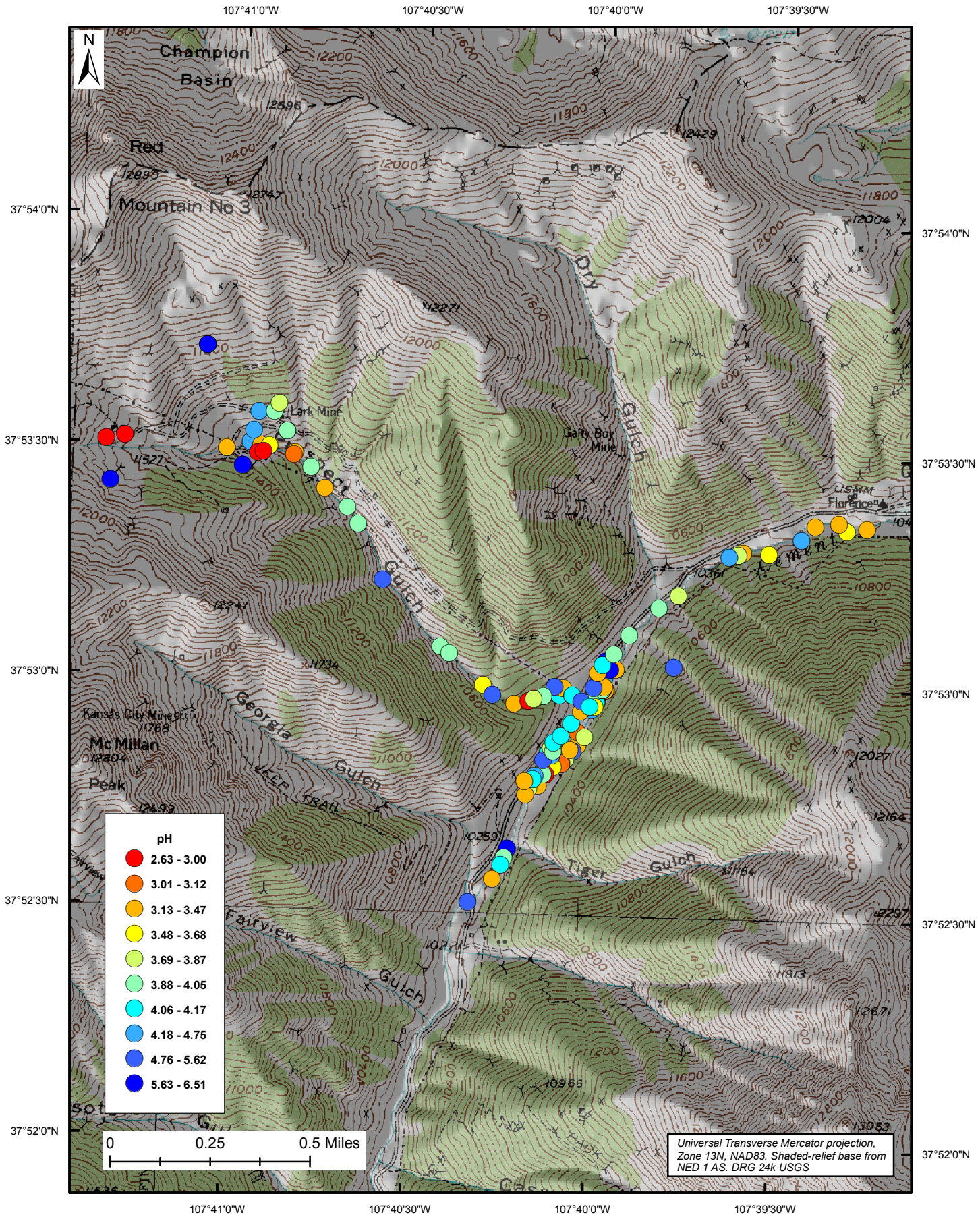

Figure 77: Ground-water pH values.

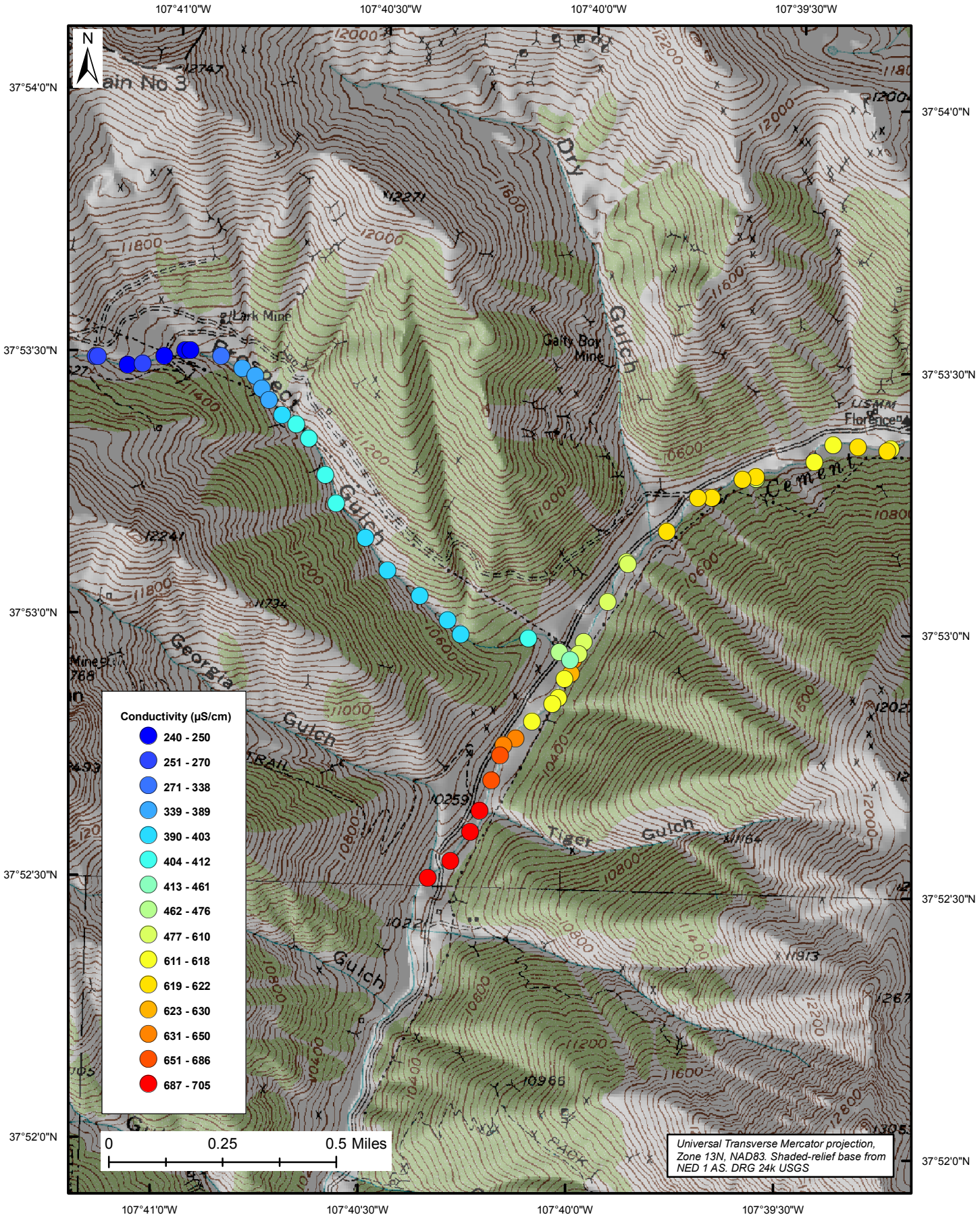

Figure 78: Instream conductivity in µS/cm.

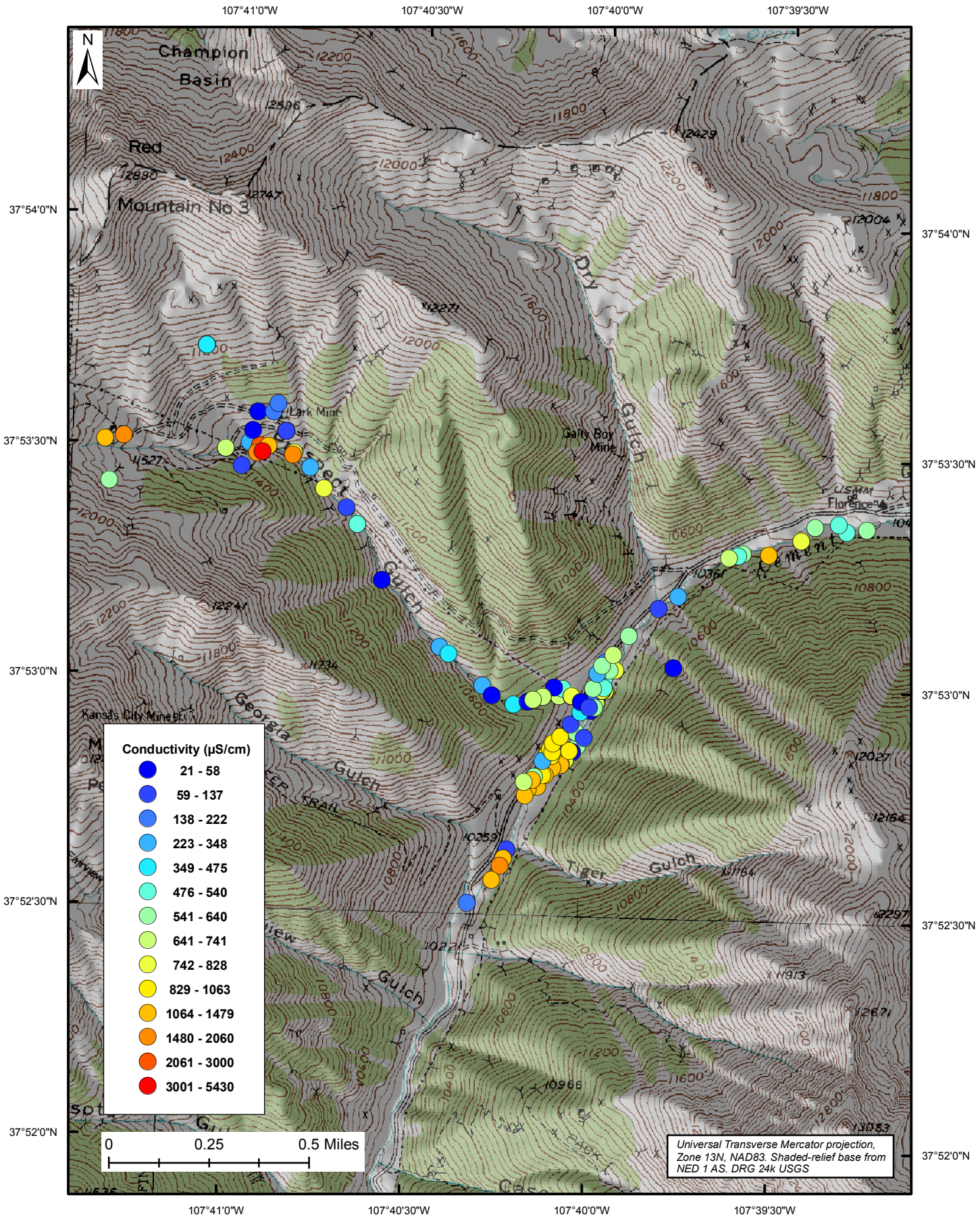

Figure 79: Ground-water conductivity in µS/cm.

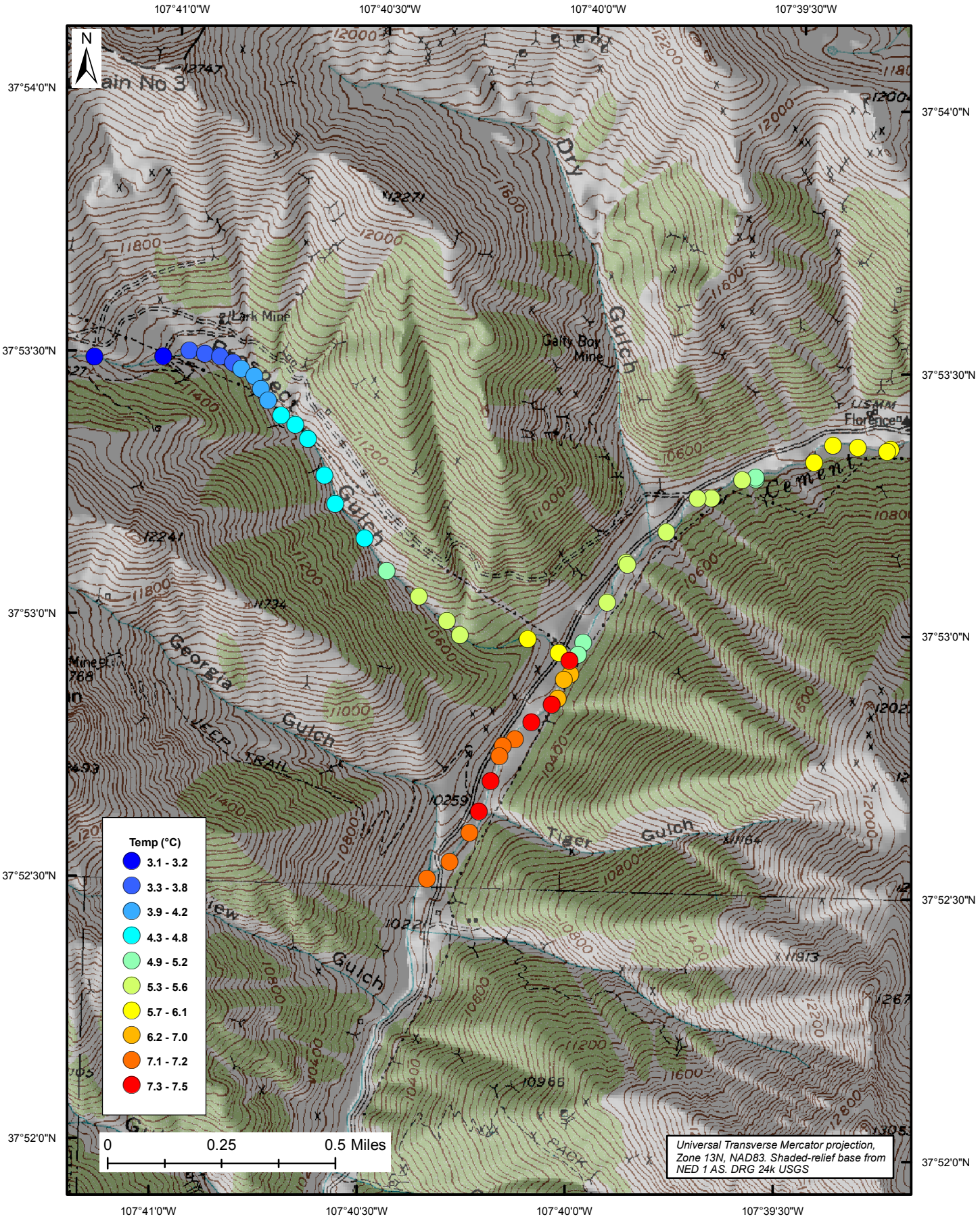

Figure 80: Instream temperature in °C.

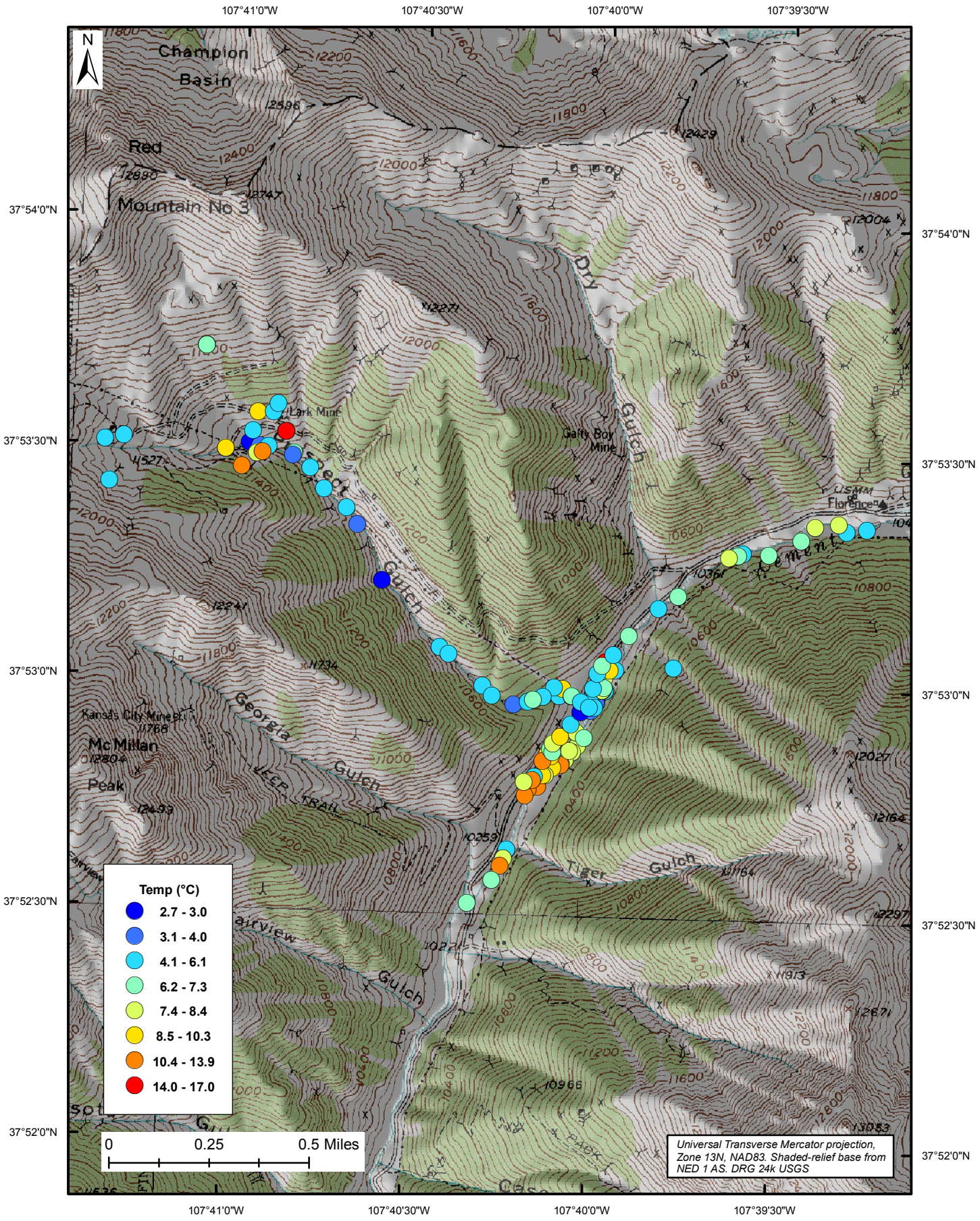

Figure 81: Ground-water temperature in °C.

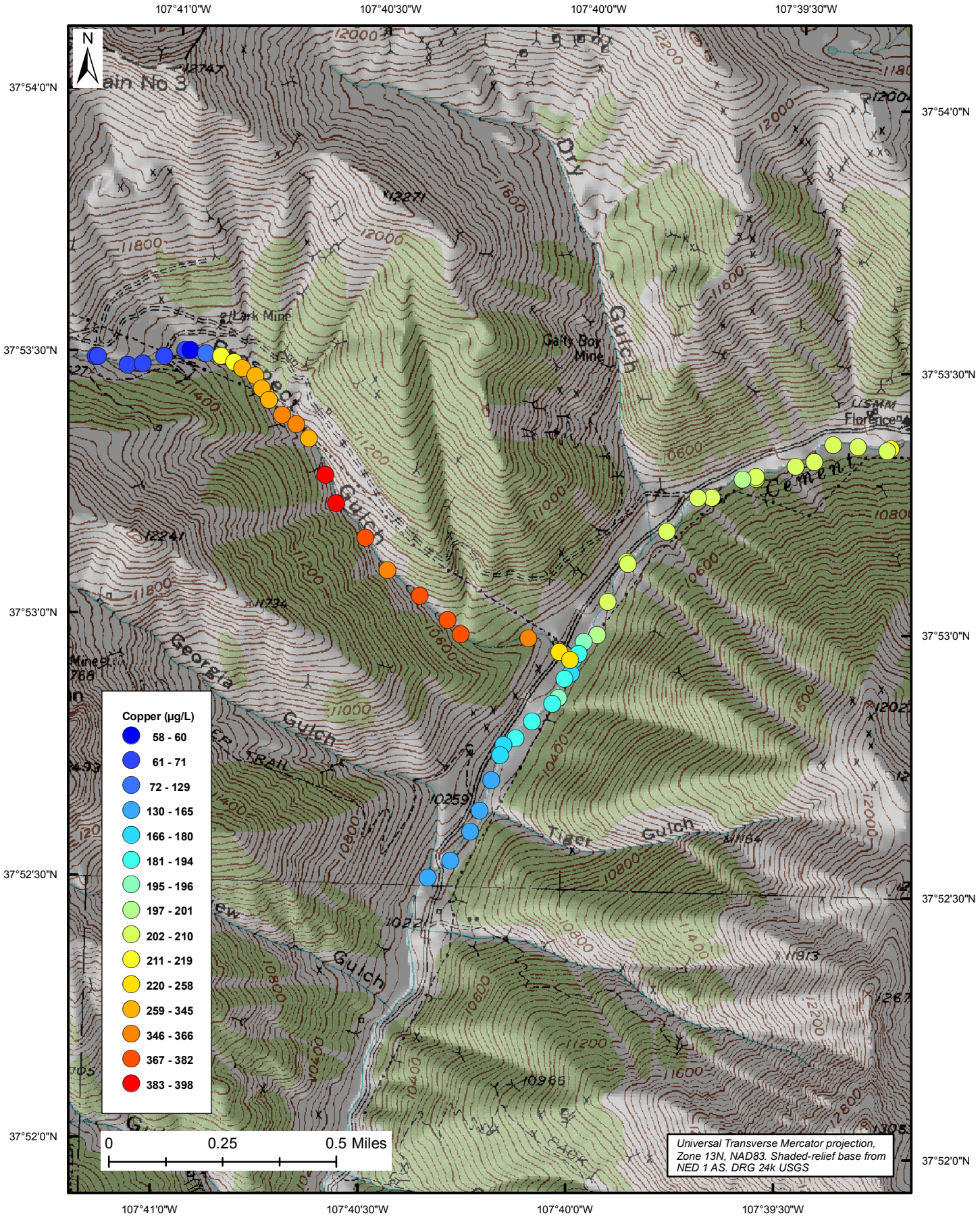

Figure 82: Instream copper concentrations in µg/L.

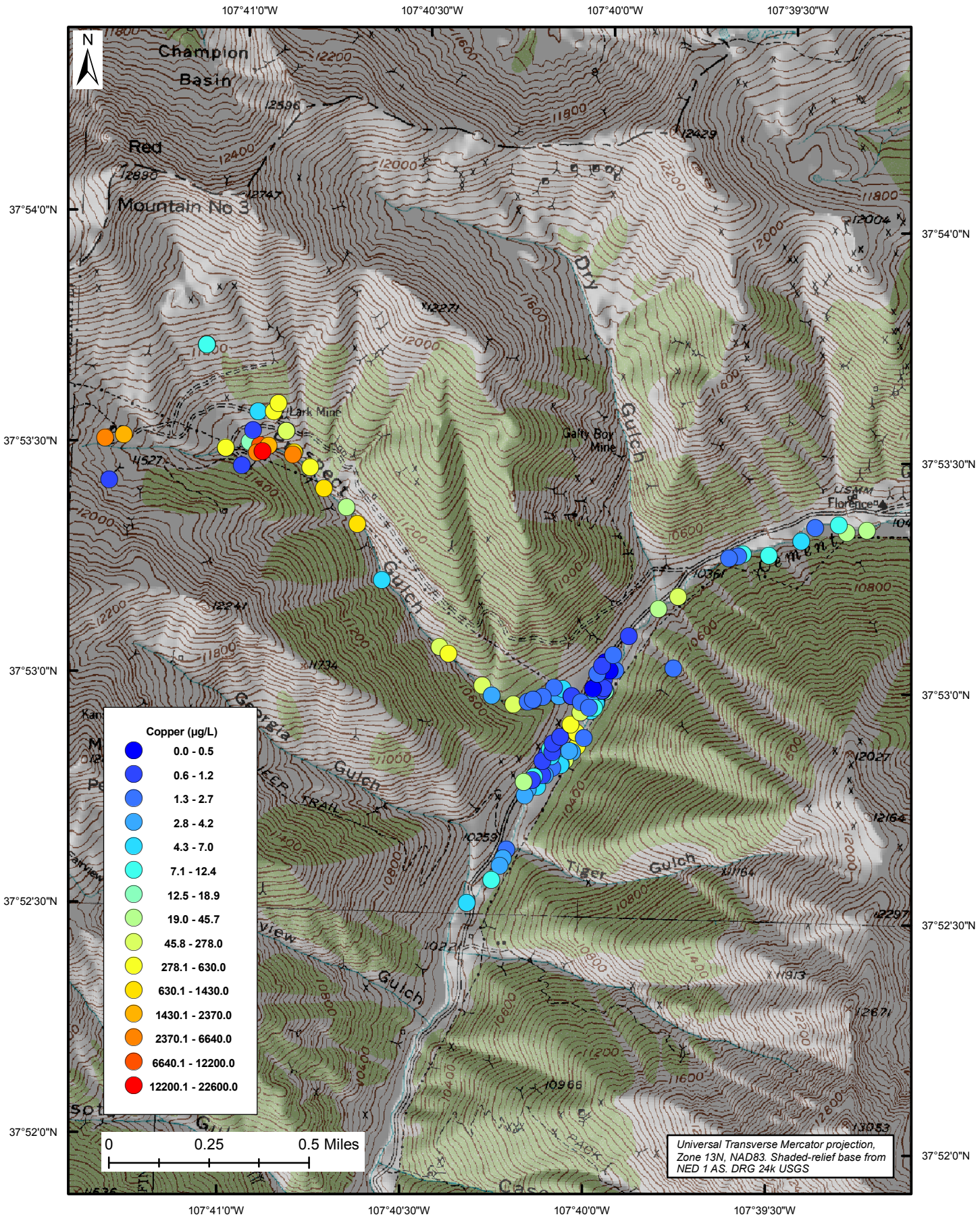

Figure 83: Ground-water copper concentrations in µg/L.

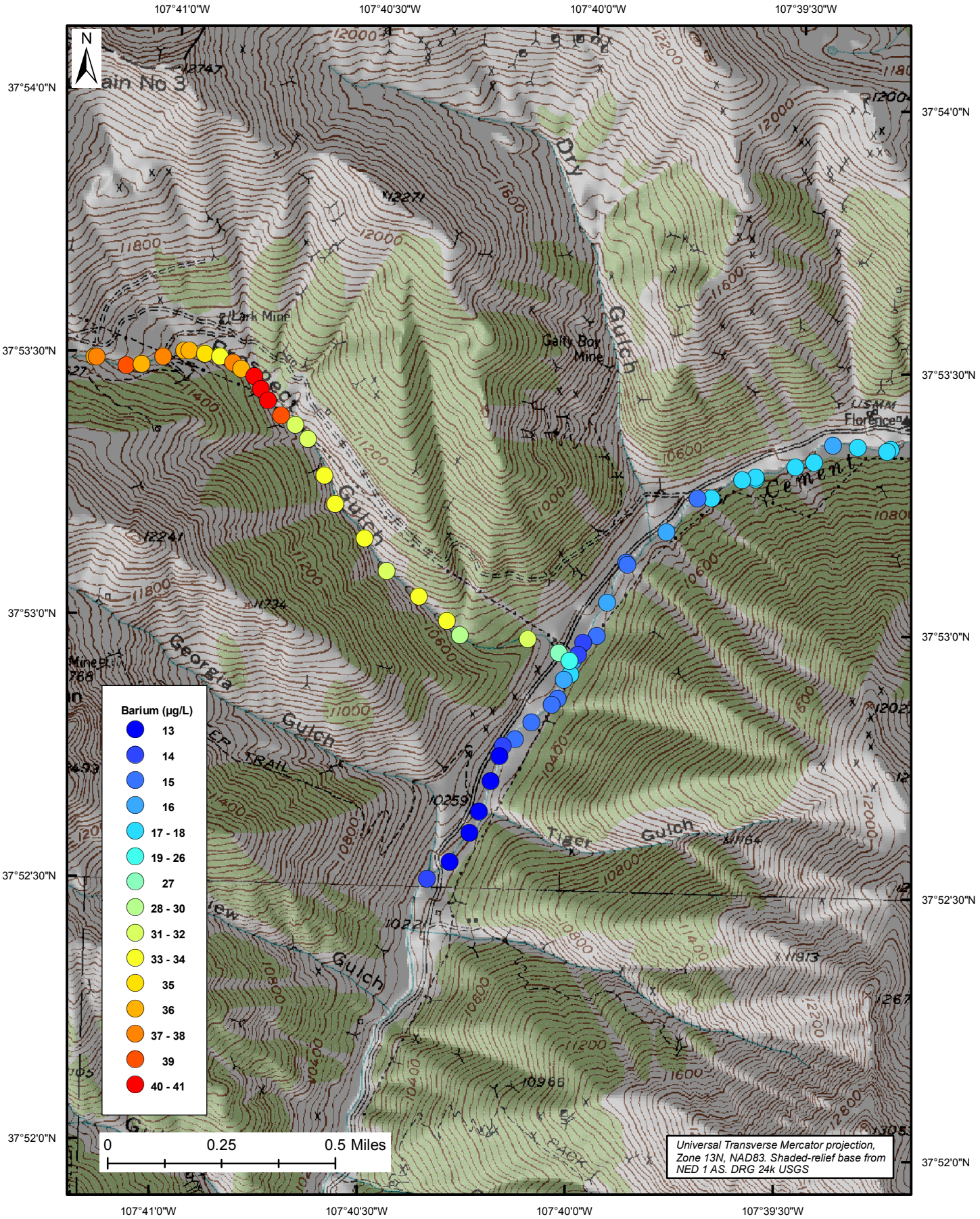

Figure 84: Instream barium concentrations in µg/L.

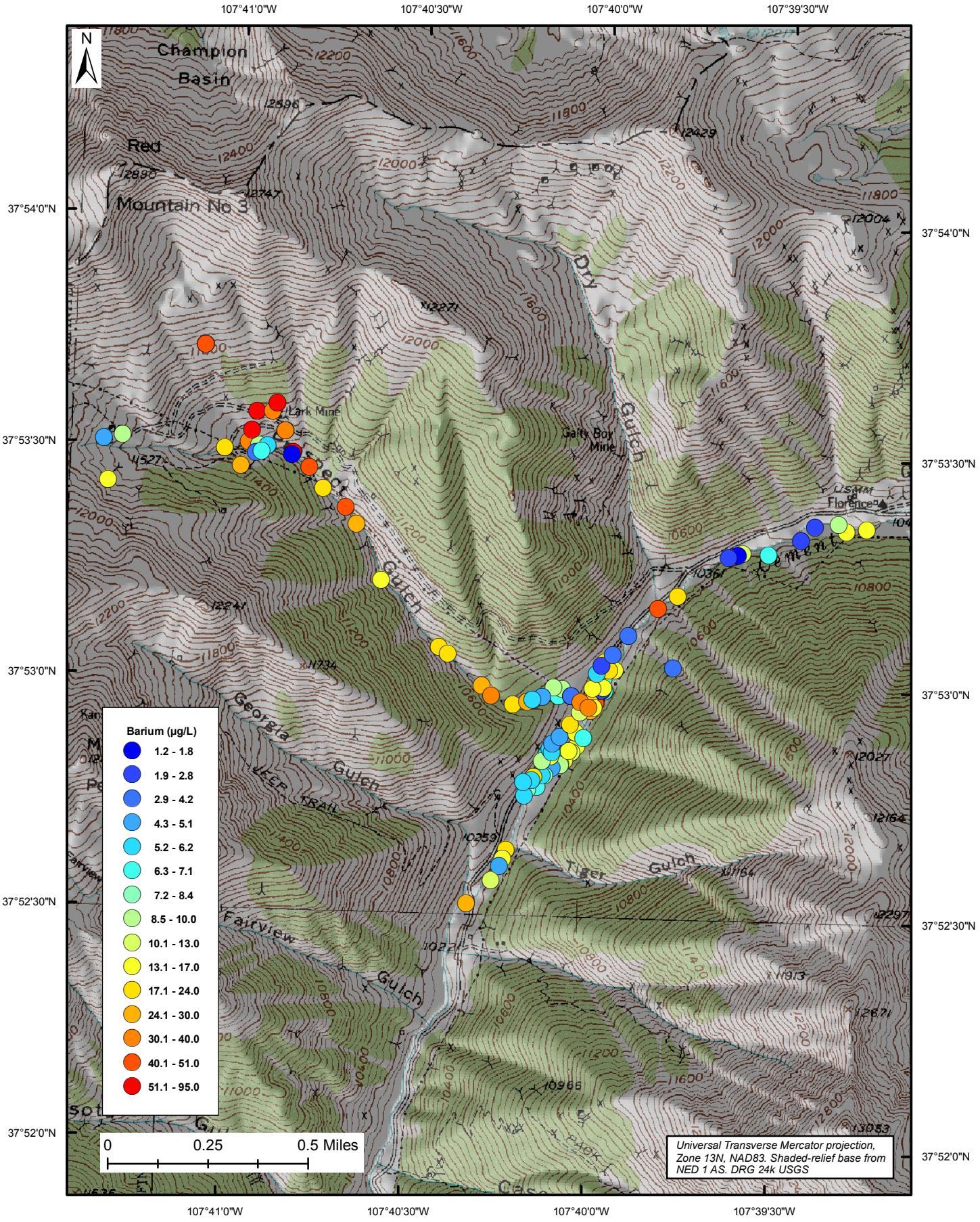

Figure 85: Ground-water barium concentrations in µg/L.

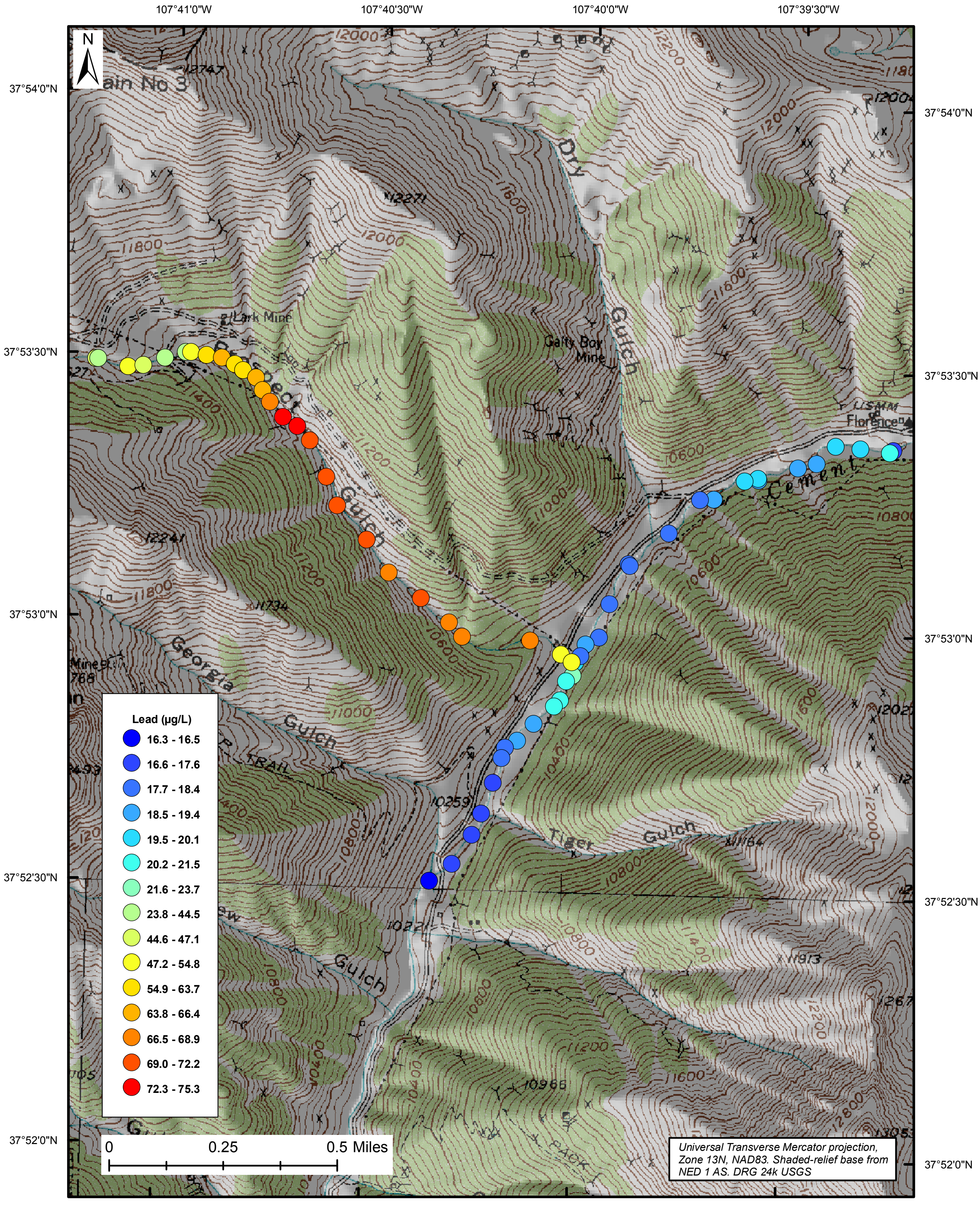

Figure 86: Instream lead concentrations in µg/L.

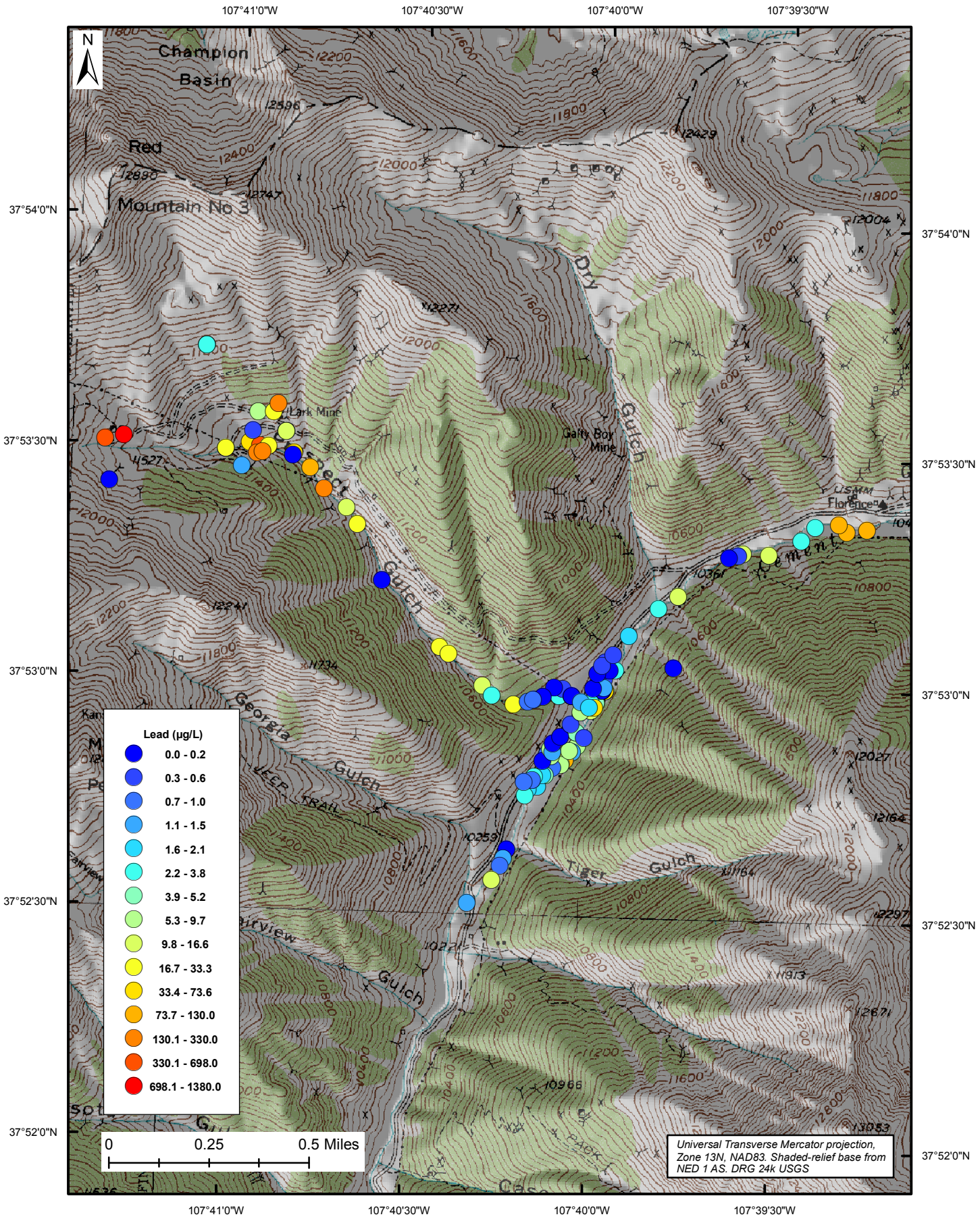

Figure 87: Ground-water lead concentrations in µg/L.

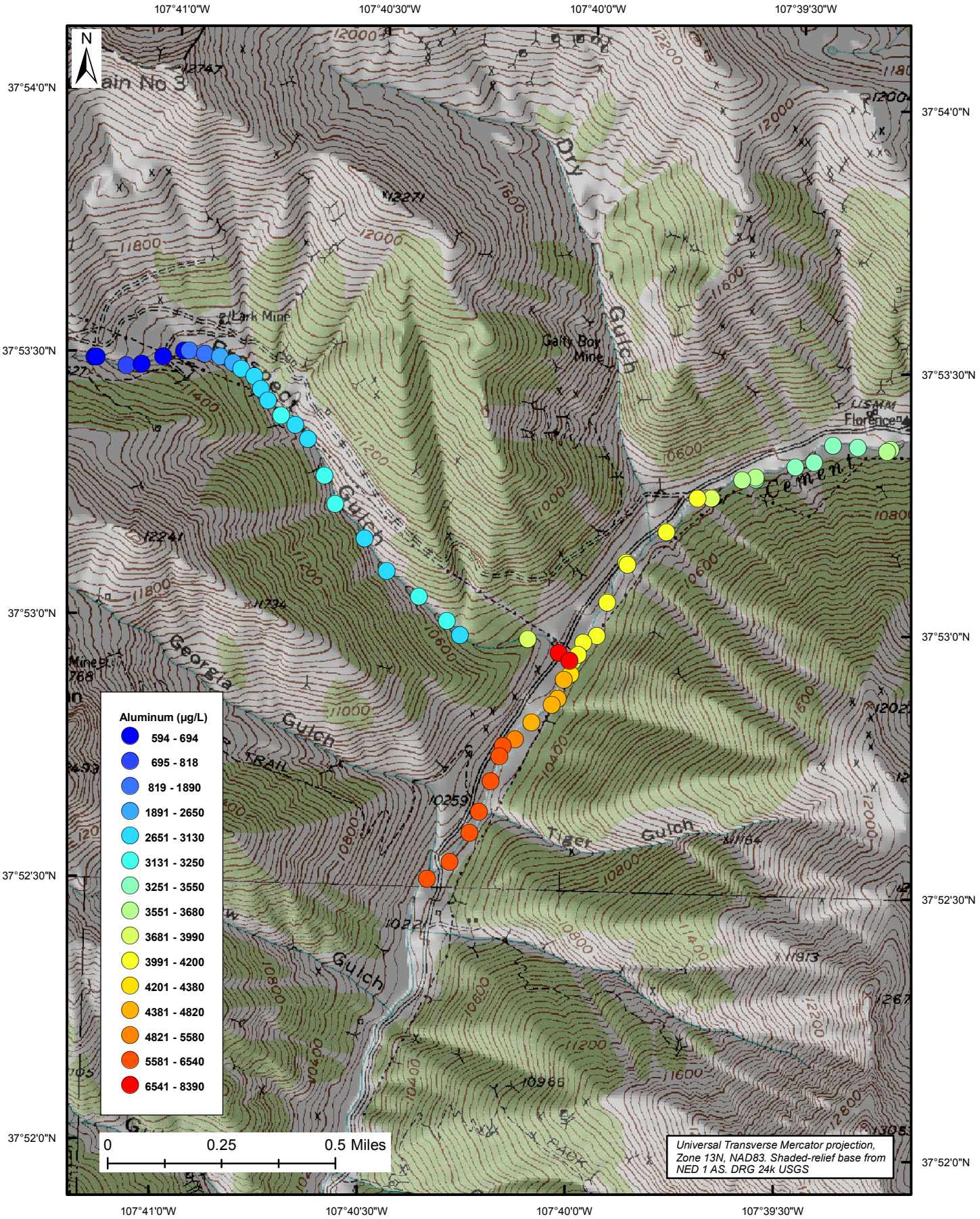

Figure 88: Instream aluminum concentrations in µg/L.

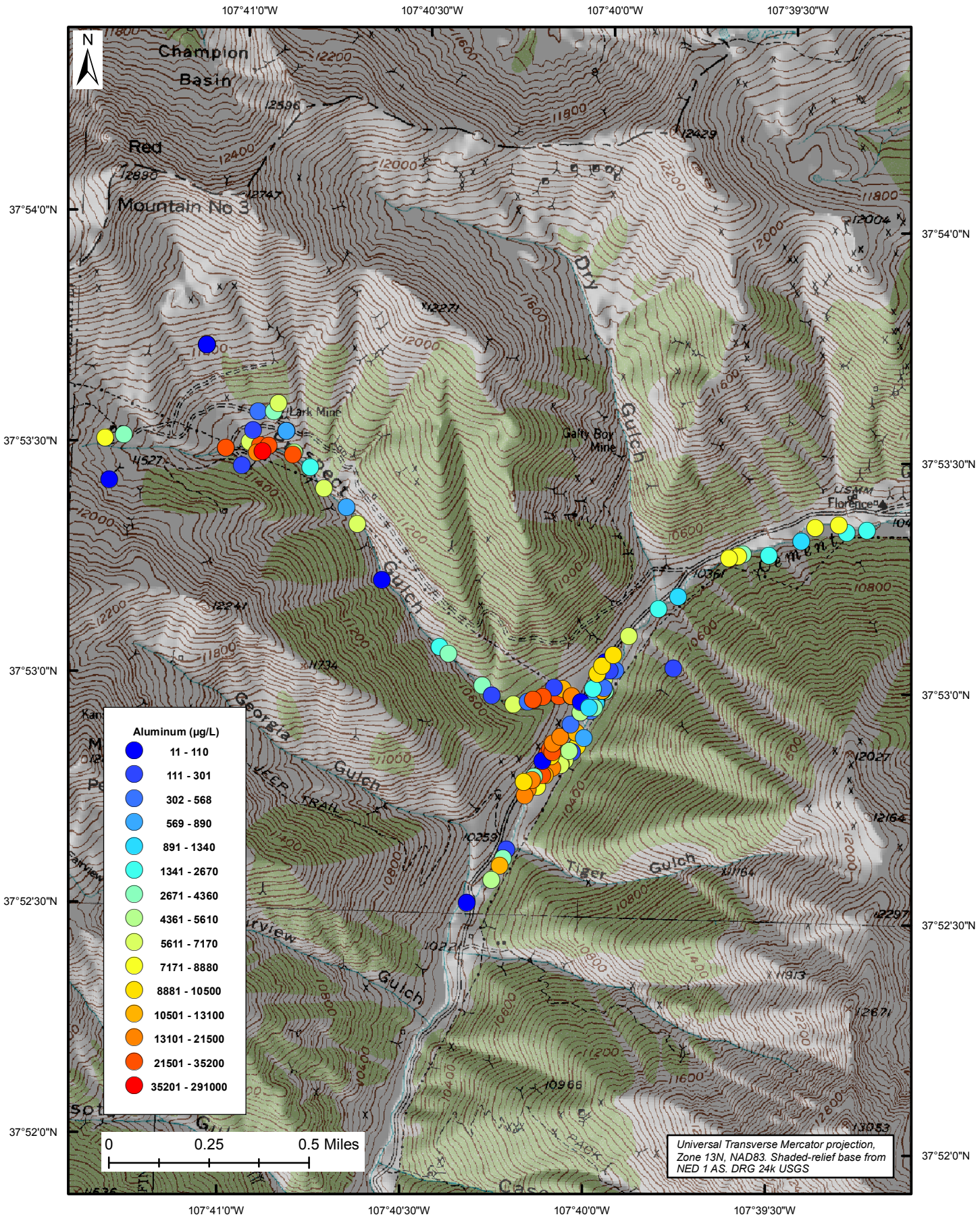

Figure 89: Ground-water aluminum concentrations in µg/L.

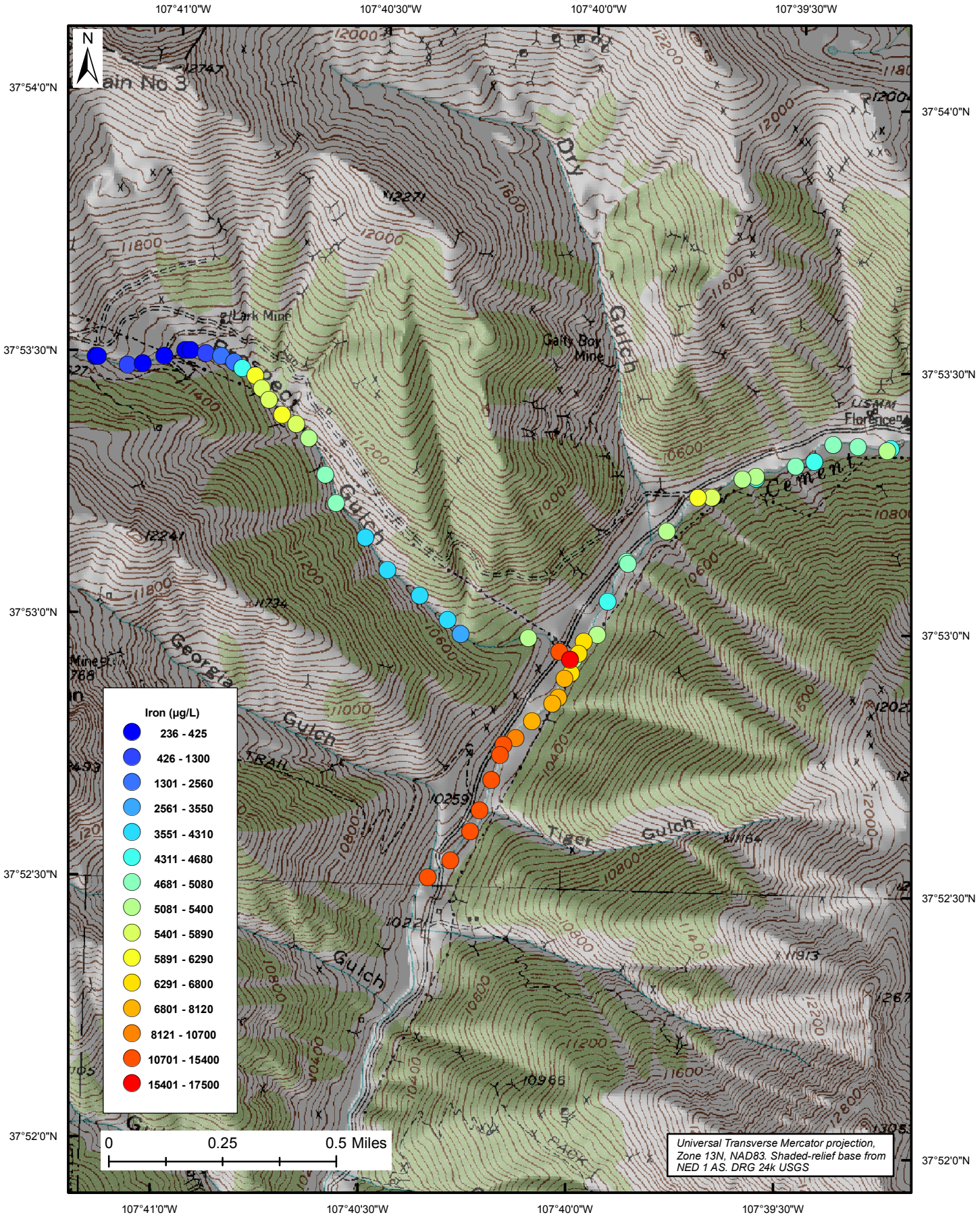

Figure 90: Instream iron concentrations in µg/L.

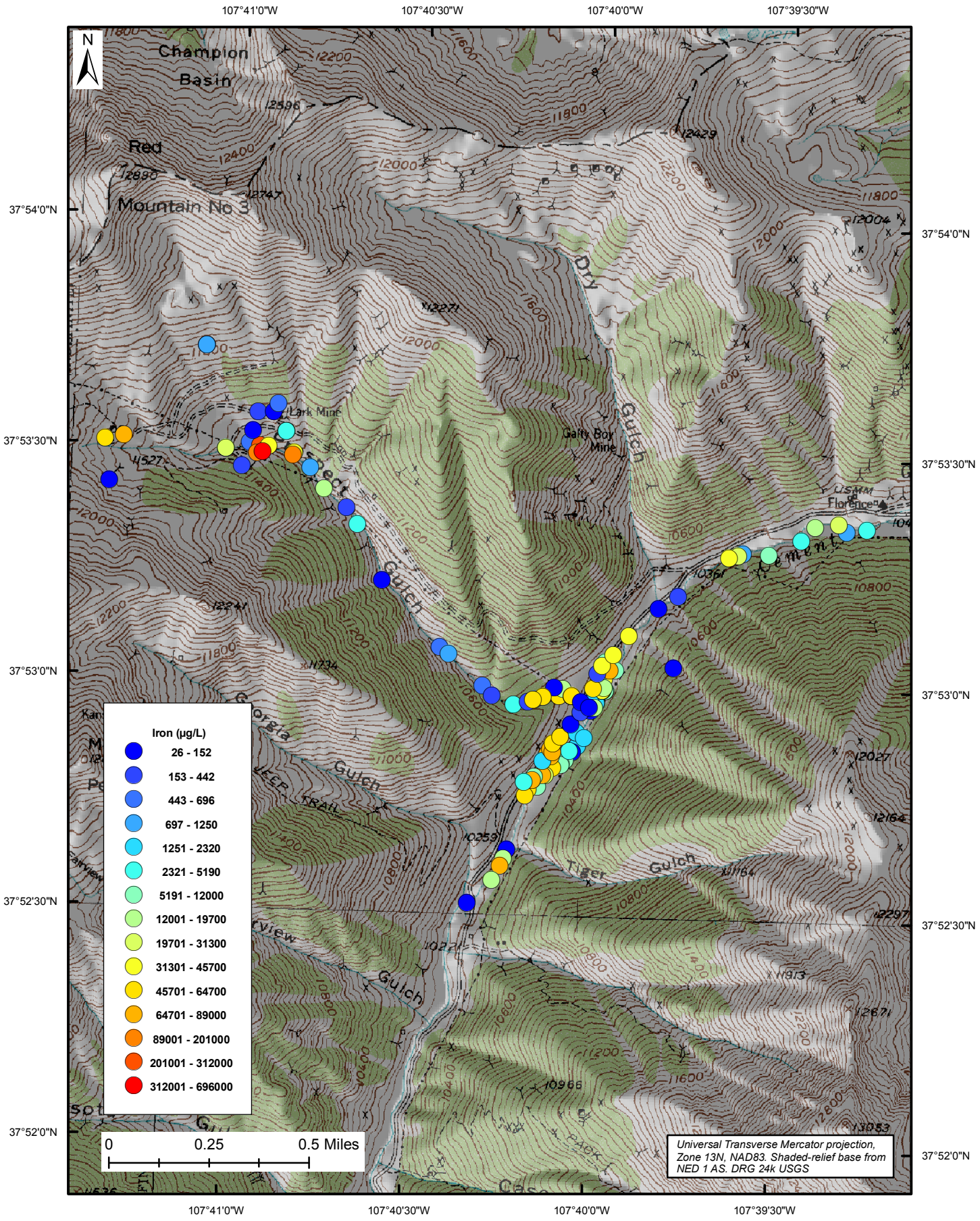

Figure 91: Ground-water iron concentrations in µg/L.

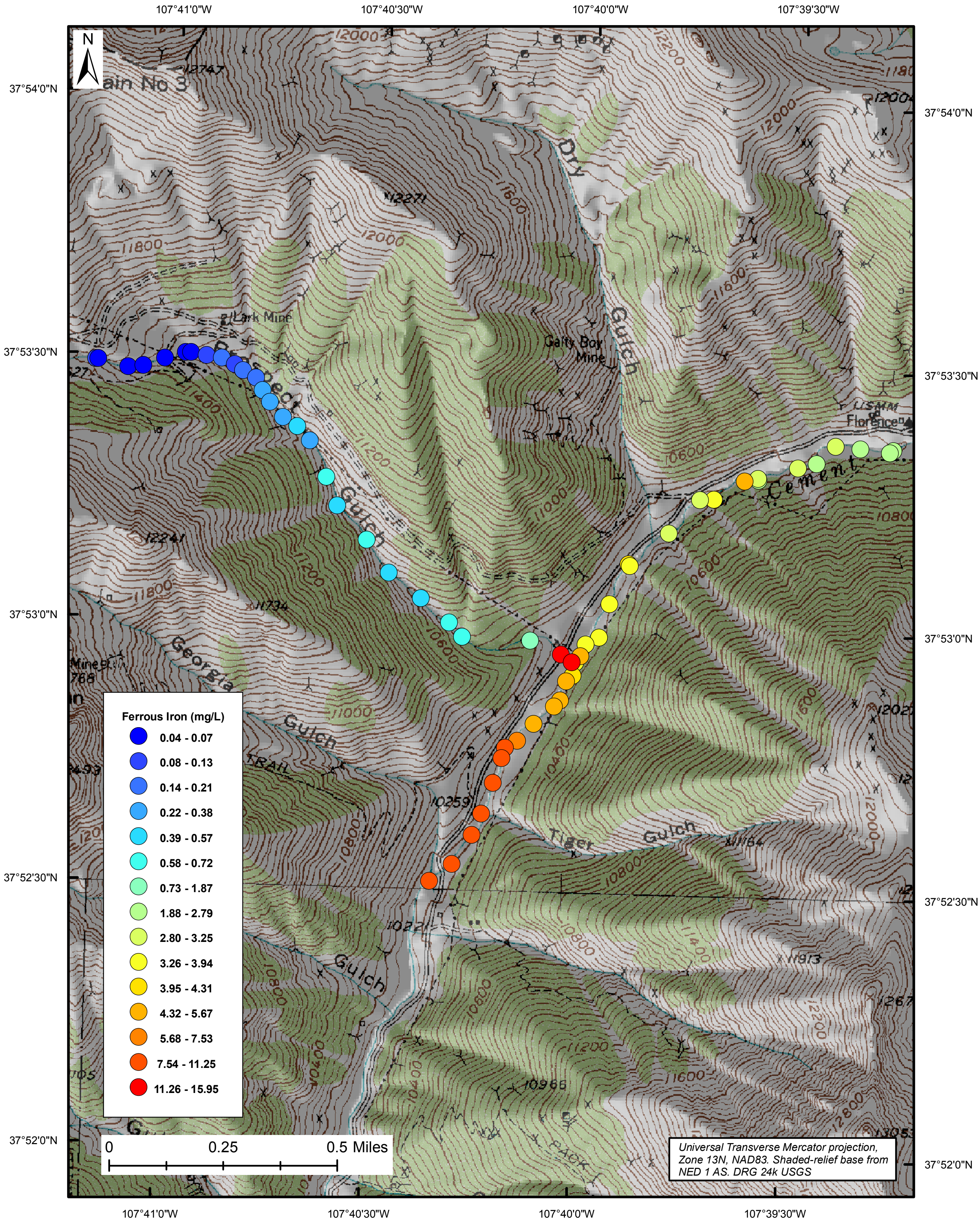

Figure 92: Instream ferrous iron concentrations in mg/L.

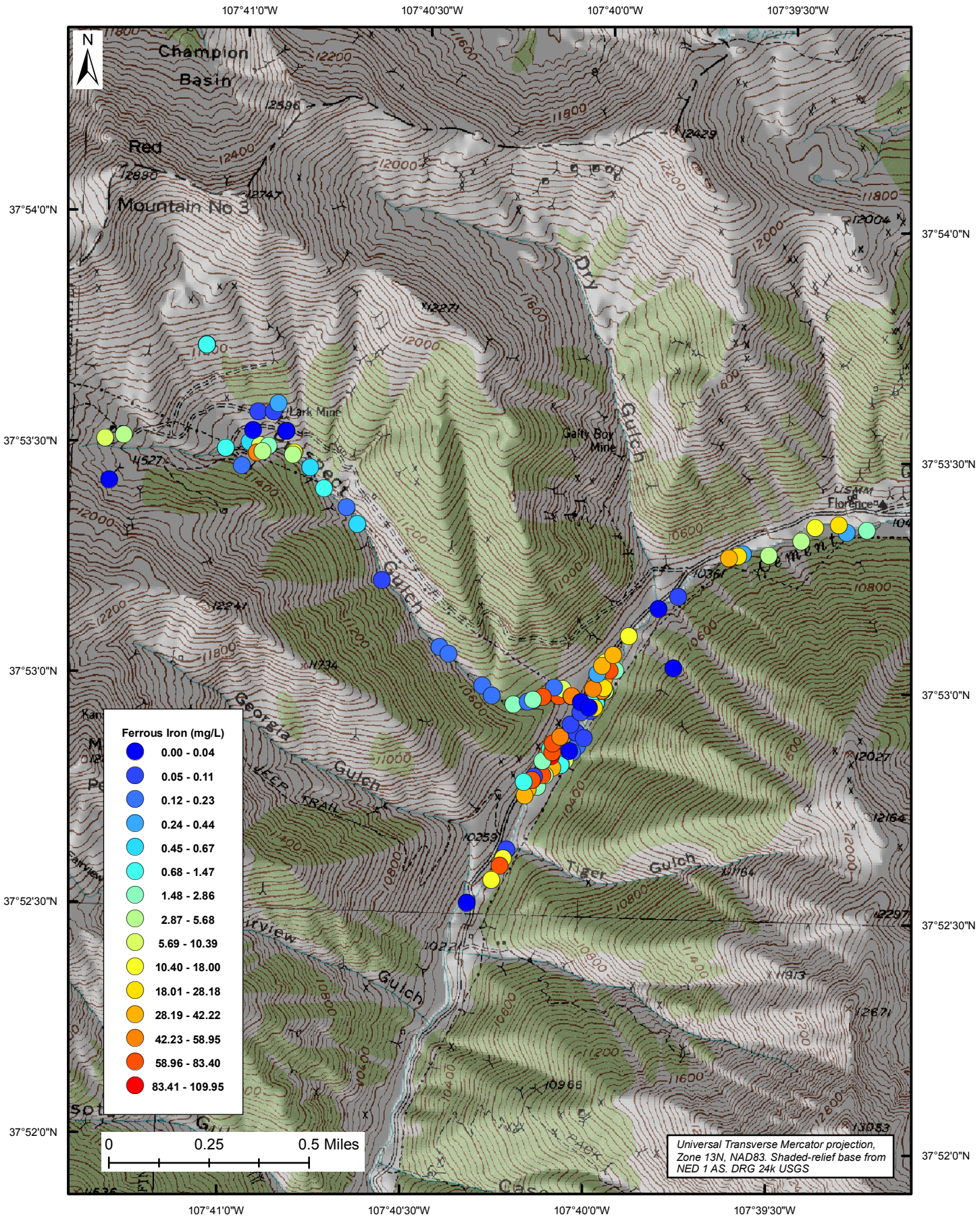

Figure 93: Ground-water ferrous iron concentrations in mg/L.

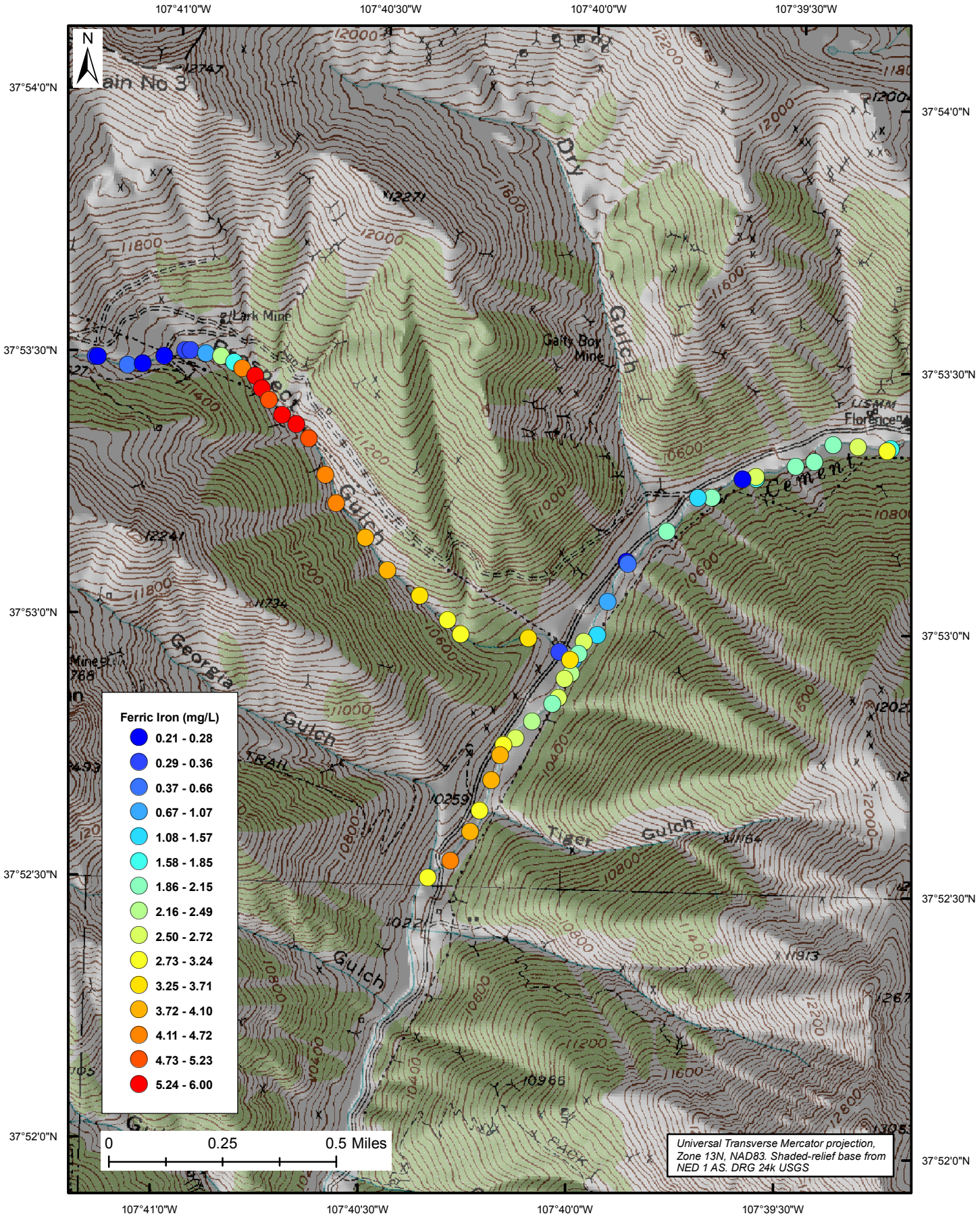

Figure 94: Instream ferric iron concentrations in mg/L.

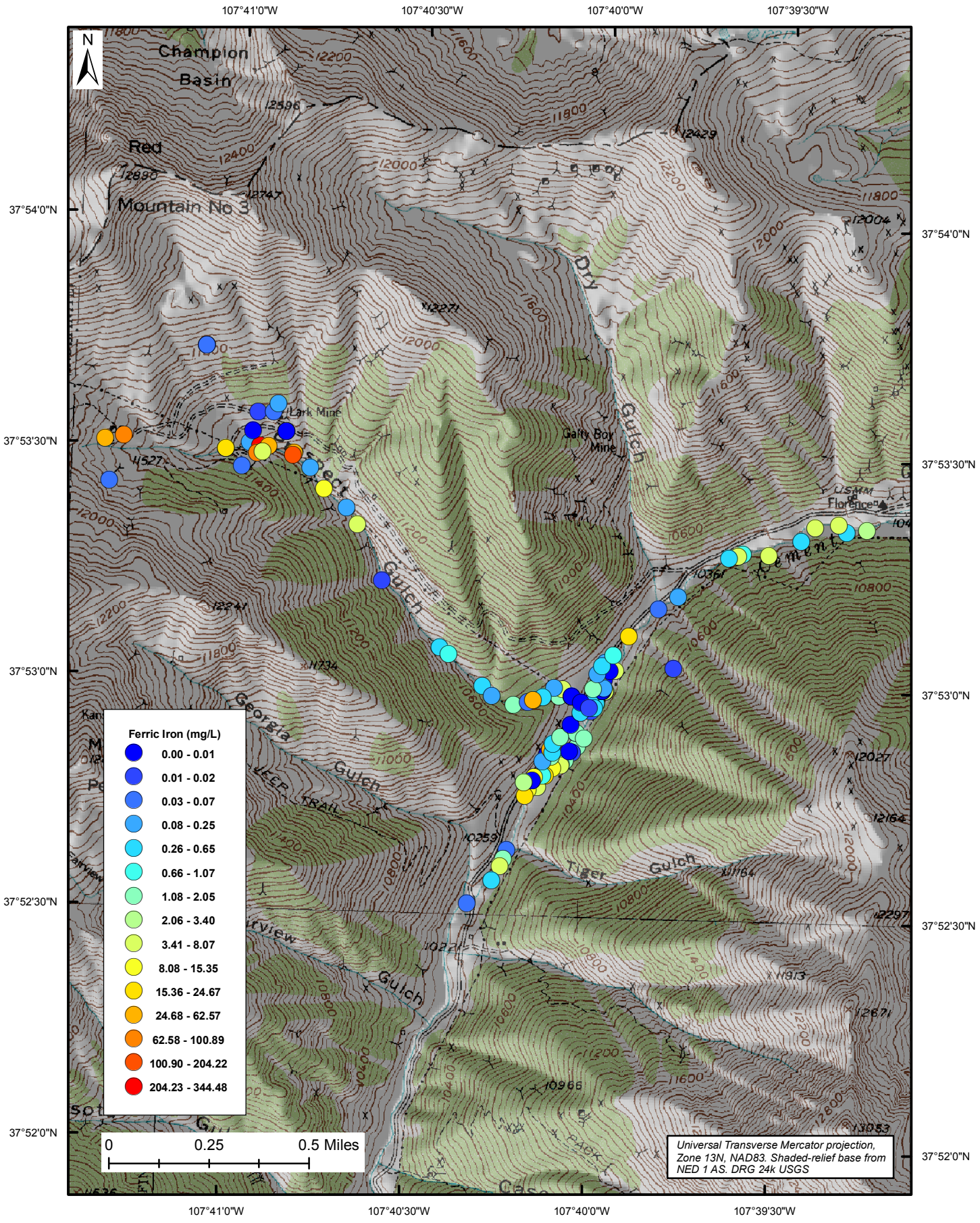

Figure 95: Ground-water ferric iron concentrations in mg/L.

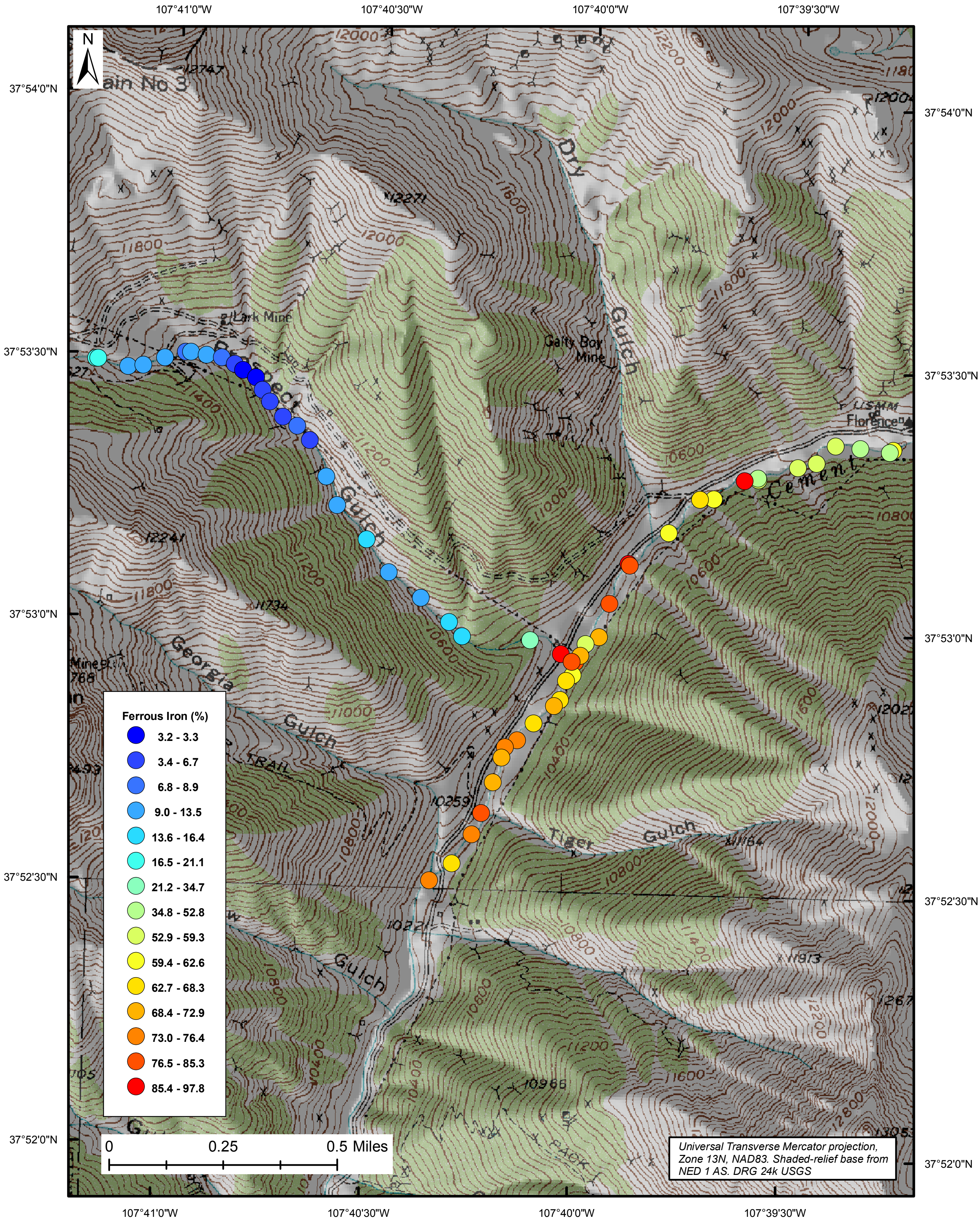

Figure 96: Instream percent ferrous iron.

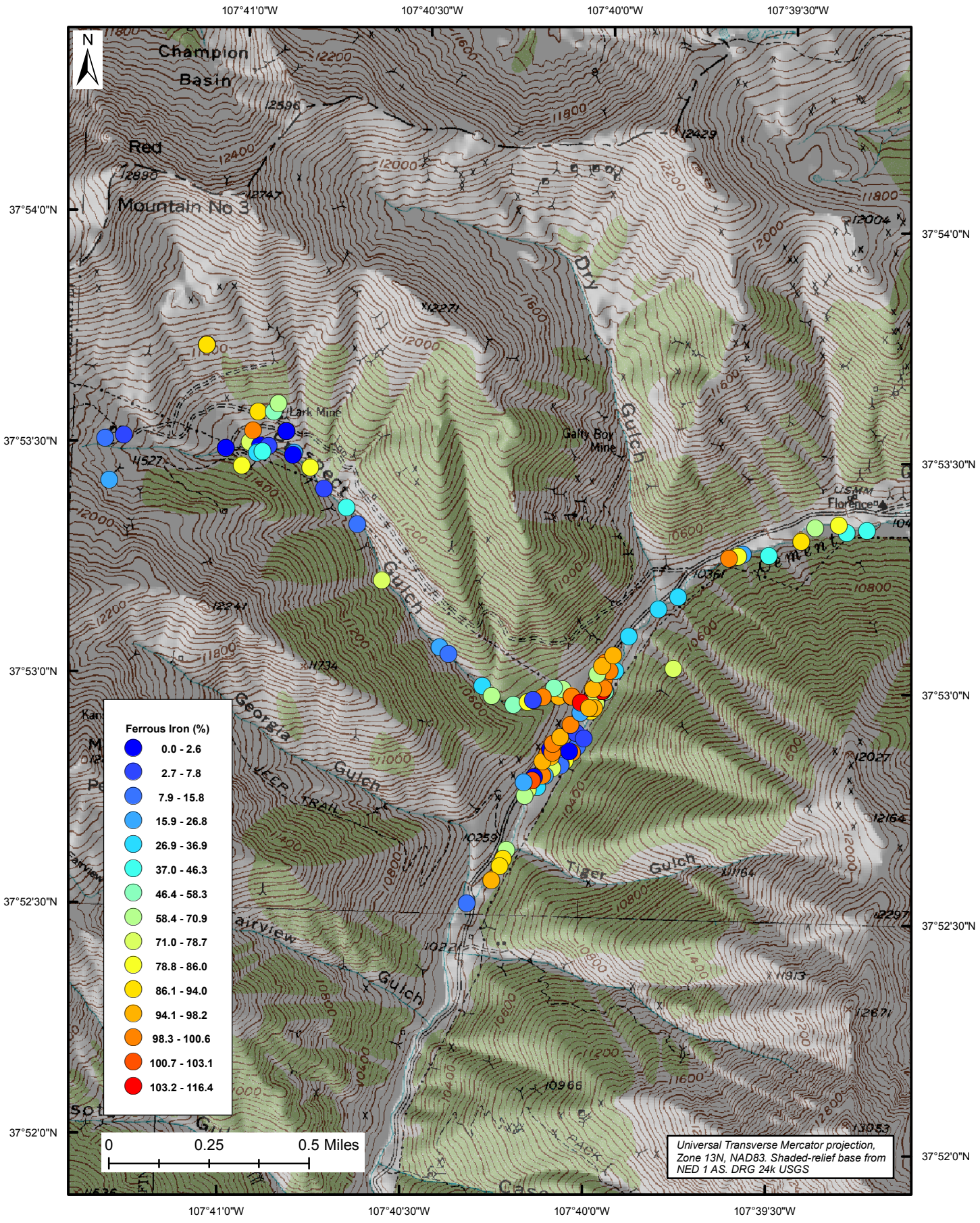

Figure 97: Ground-water percent ferrous iron.

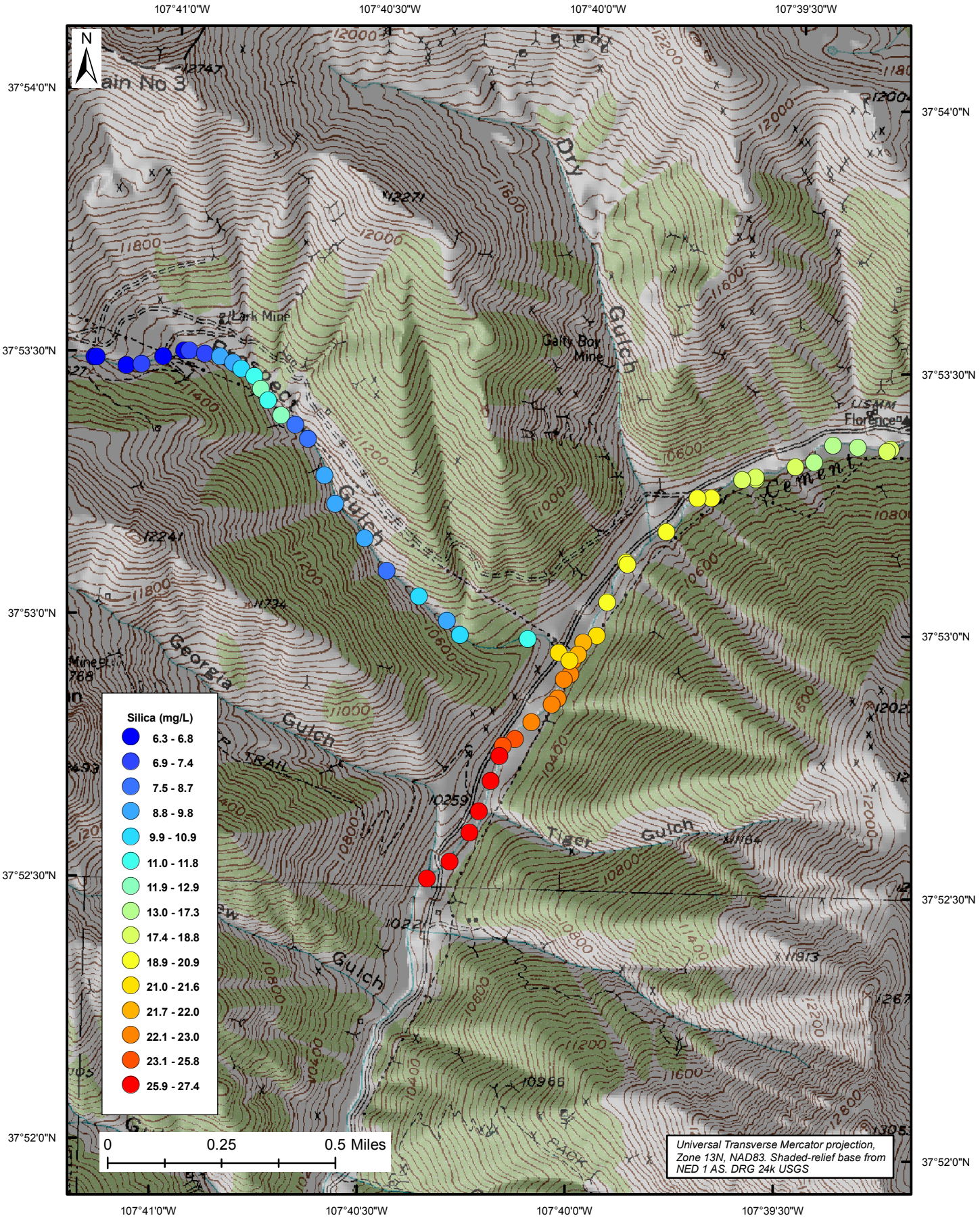

Figure 98: Instream silica concentrations in mg/L.

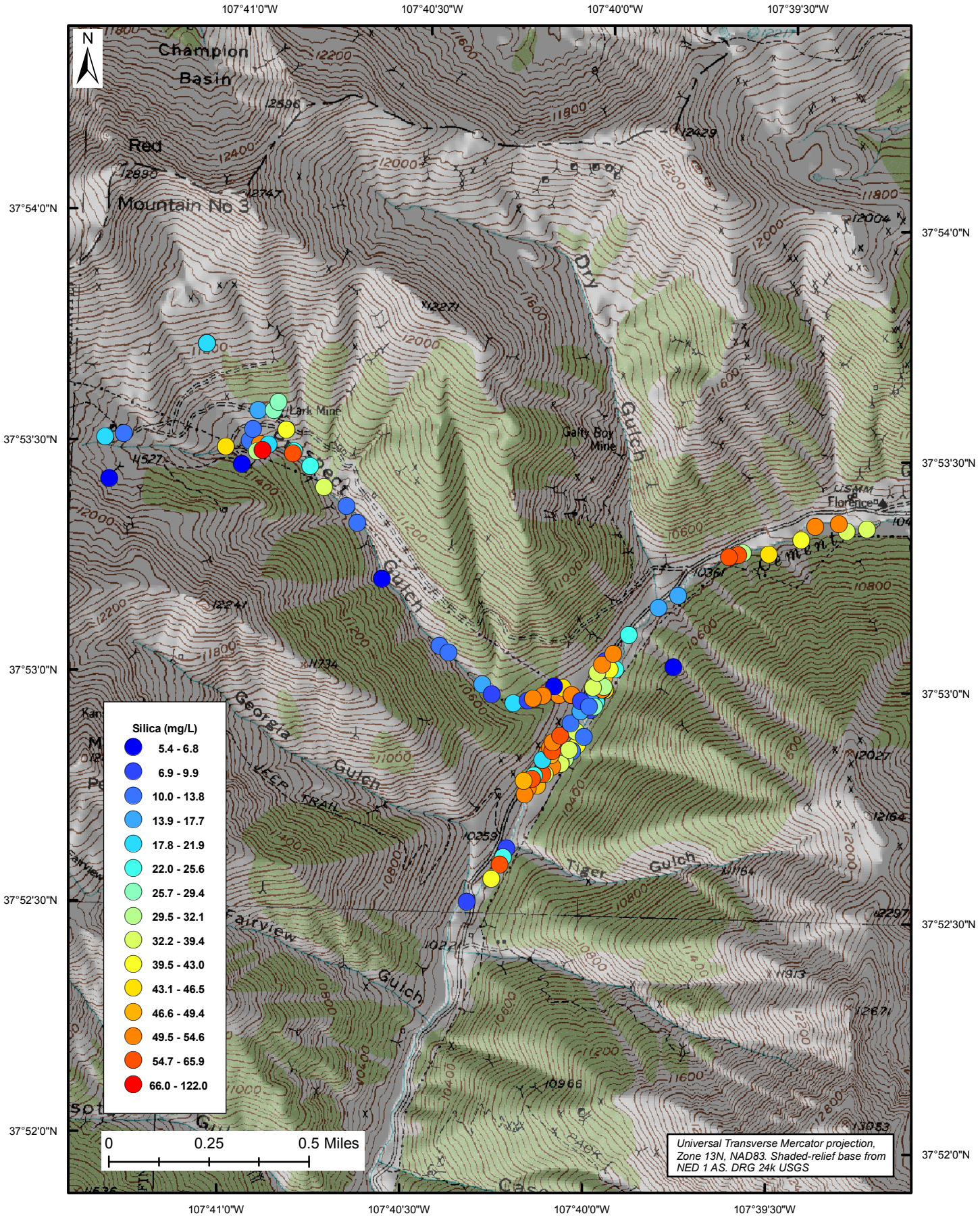

Figure 99: Ground-water silica concentrations in mg/L.

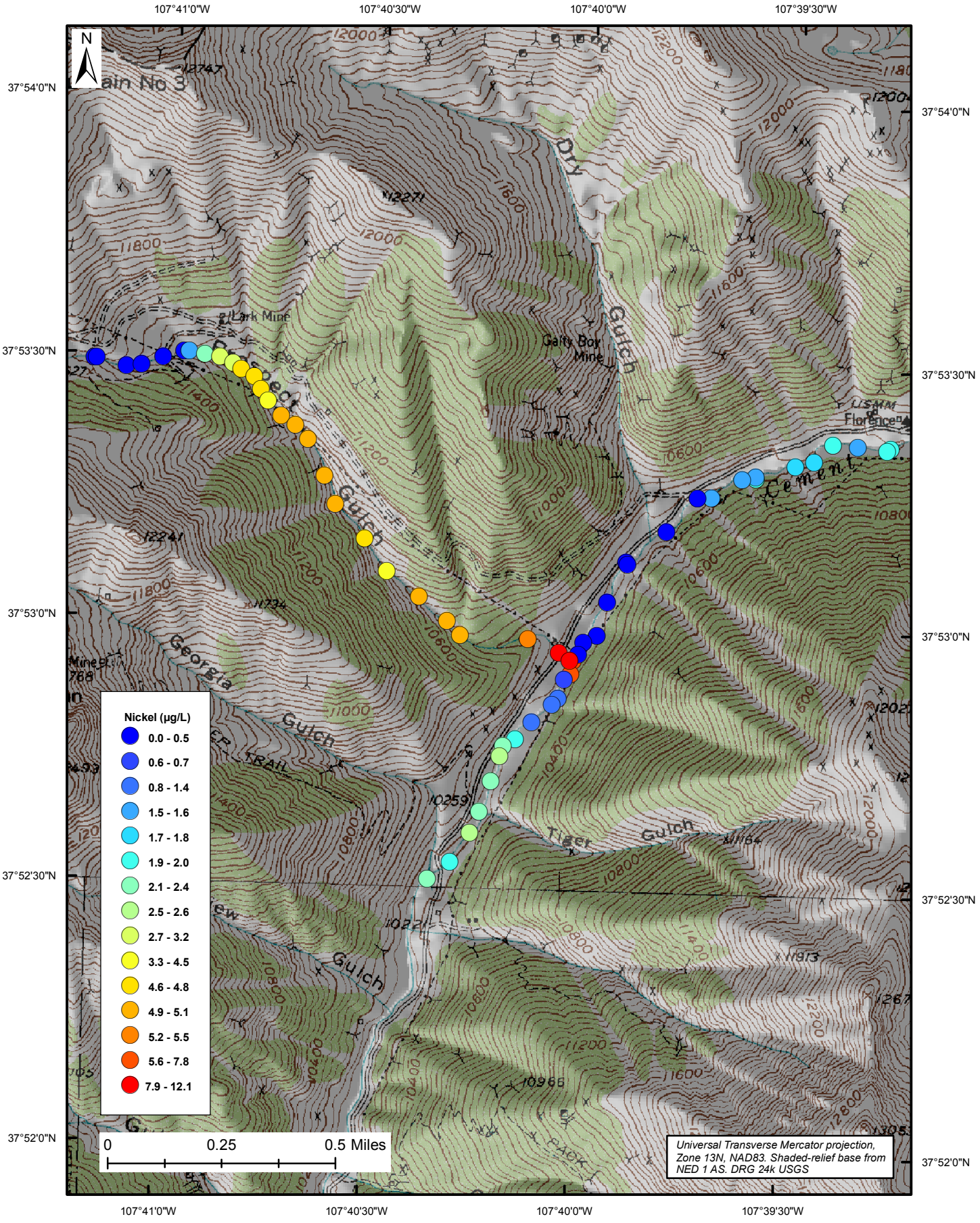

Figure 100: Instream nickel concentrations in µg/L.

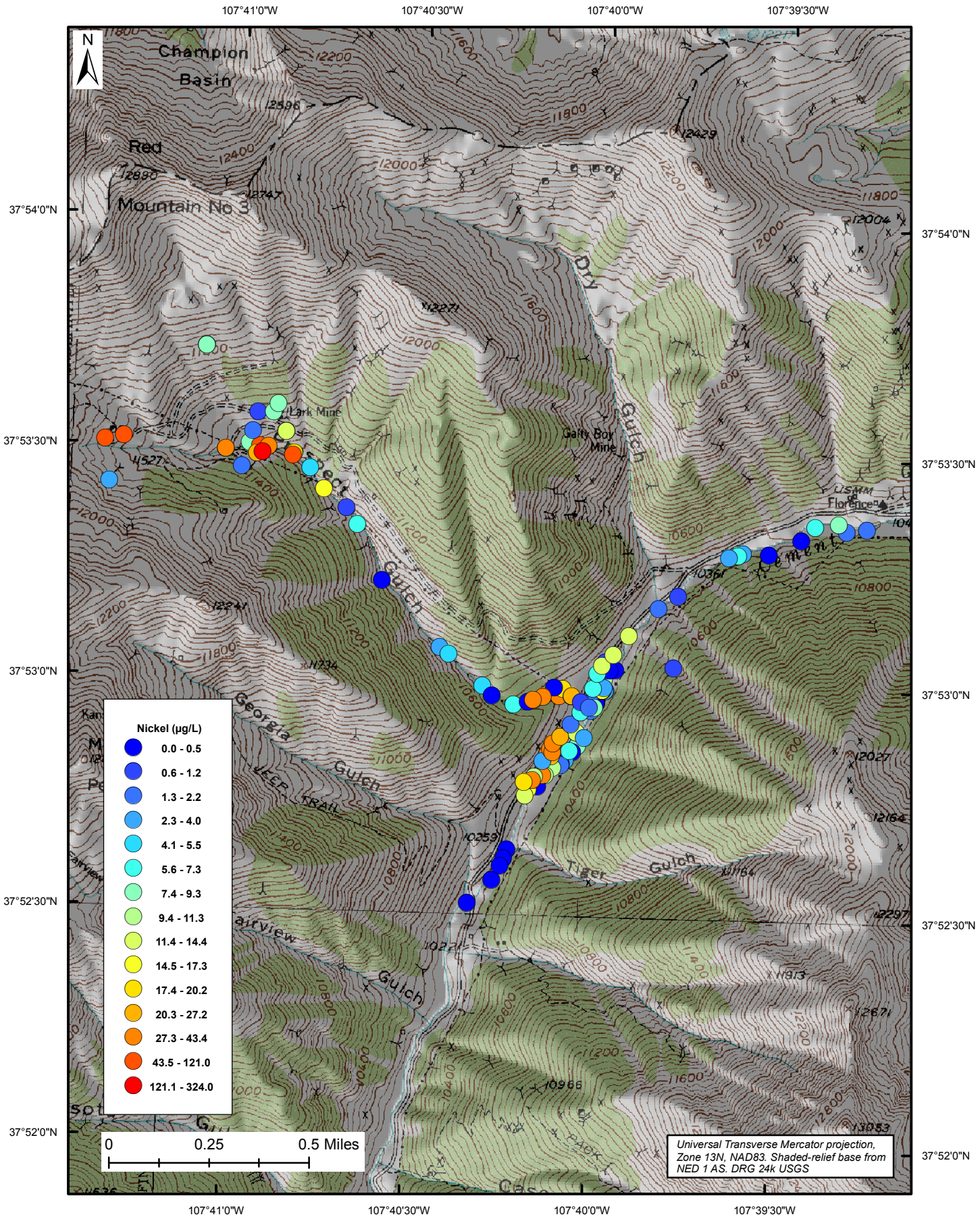

Figure 101: Ground-water nickel concentrations in µg/L.

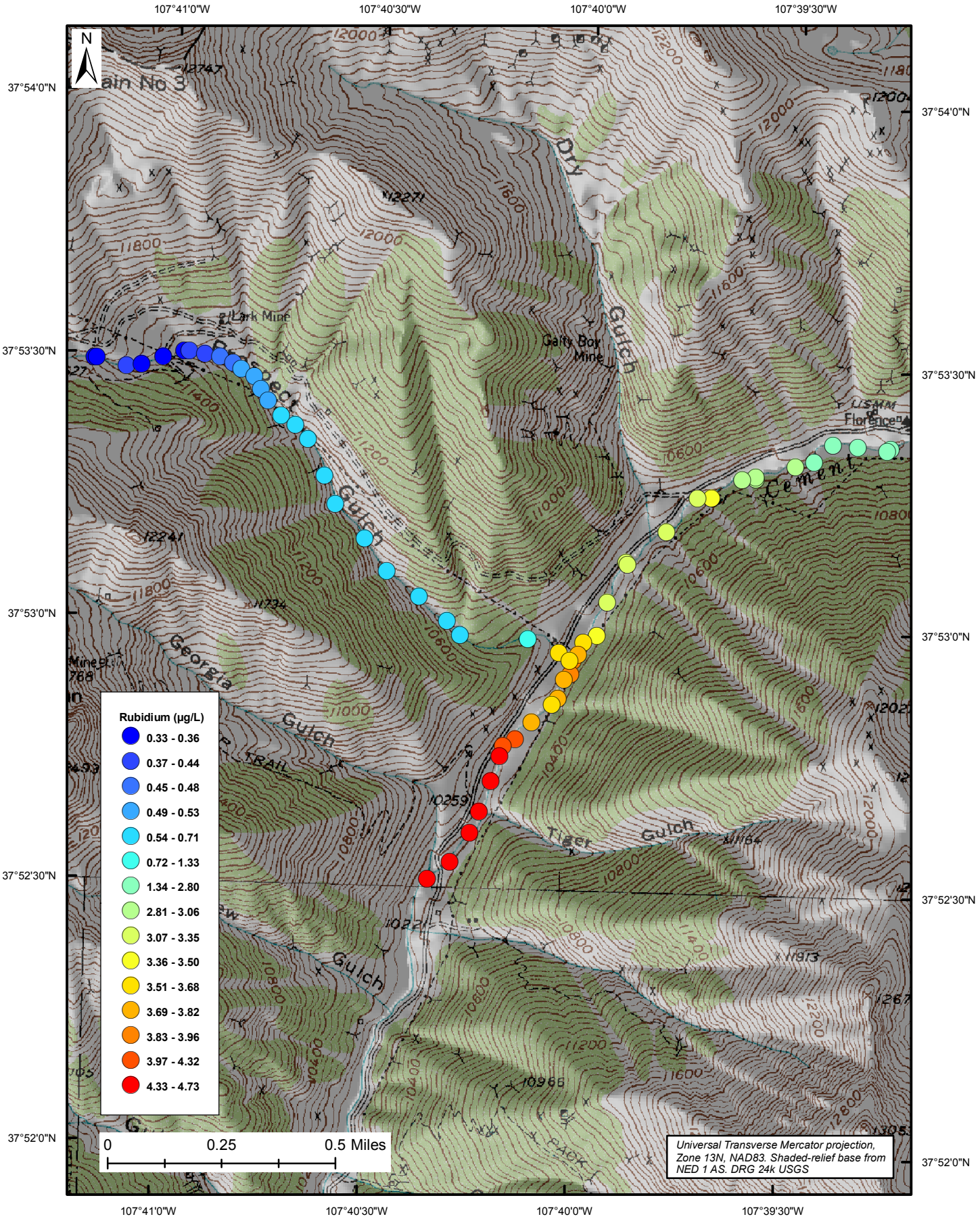

Figure 102: Instream rubidium concentrations in µg/L.

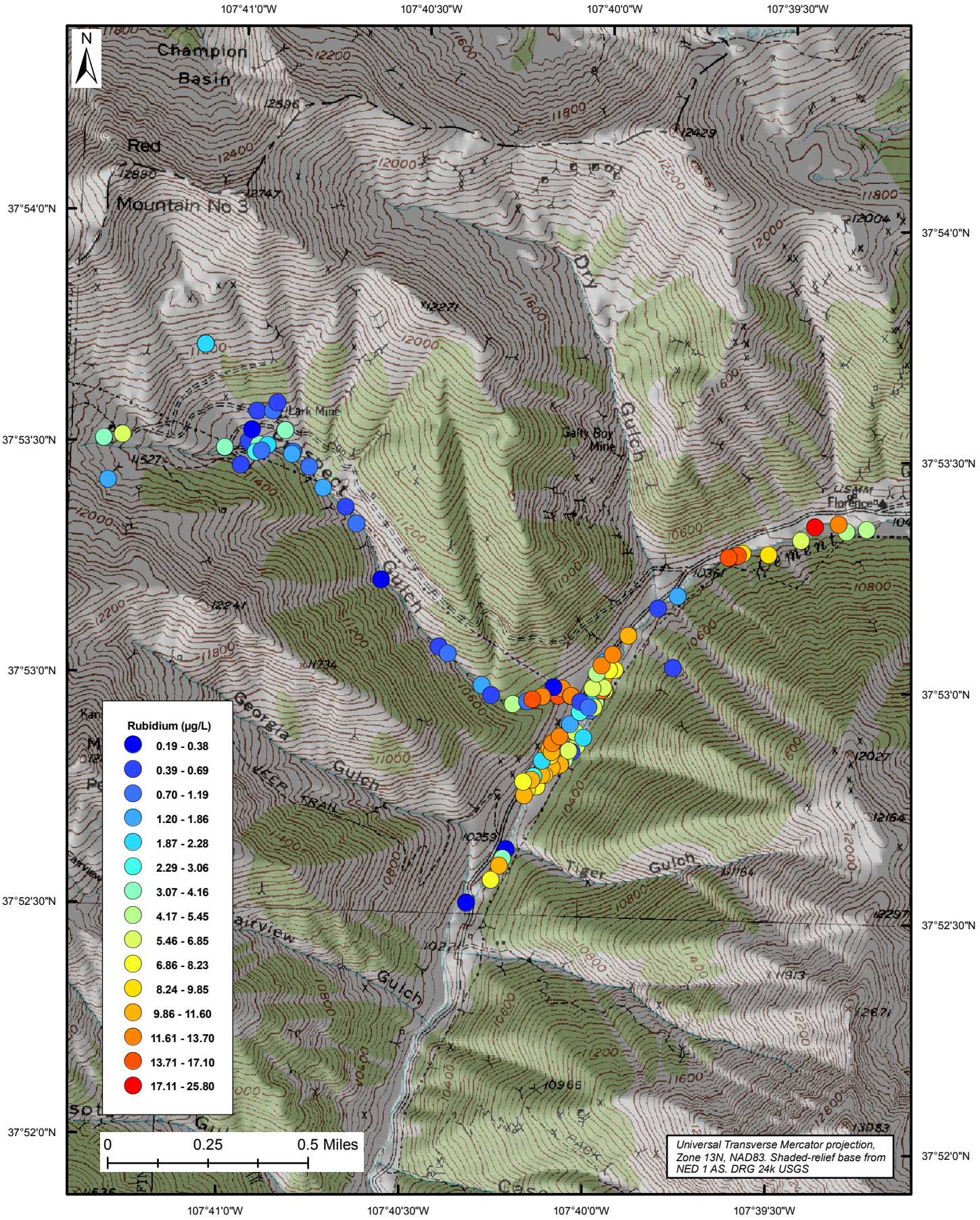

Figure 103: Ground-water rubidium concentrations in µg/L.

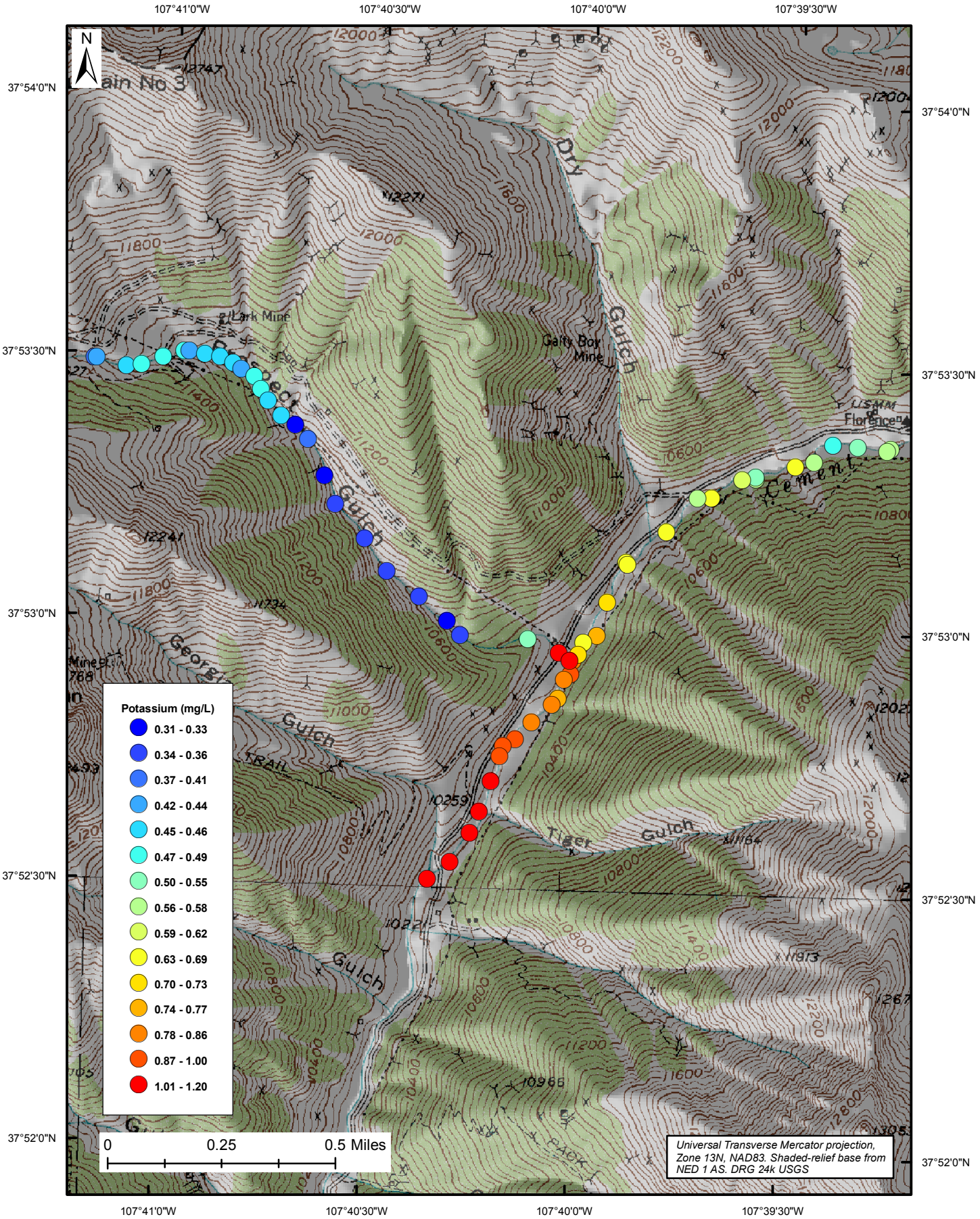

Figure 104: Instream potassium concentrations in mg/L.

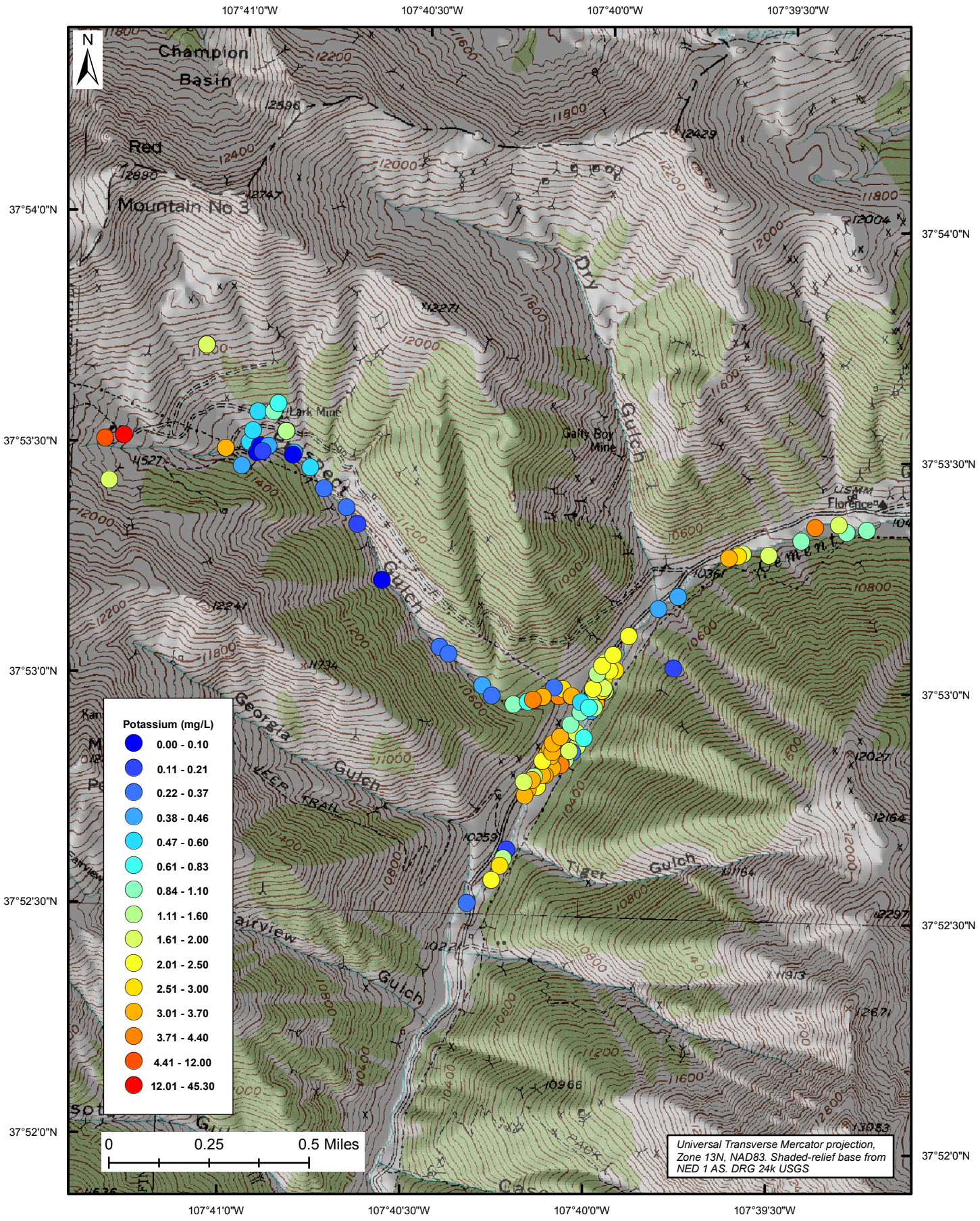

Figure 105: Ground-water potassium concentrations in mg/L.

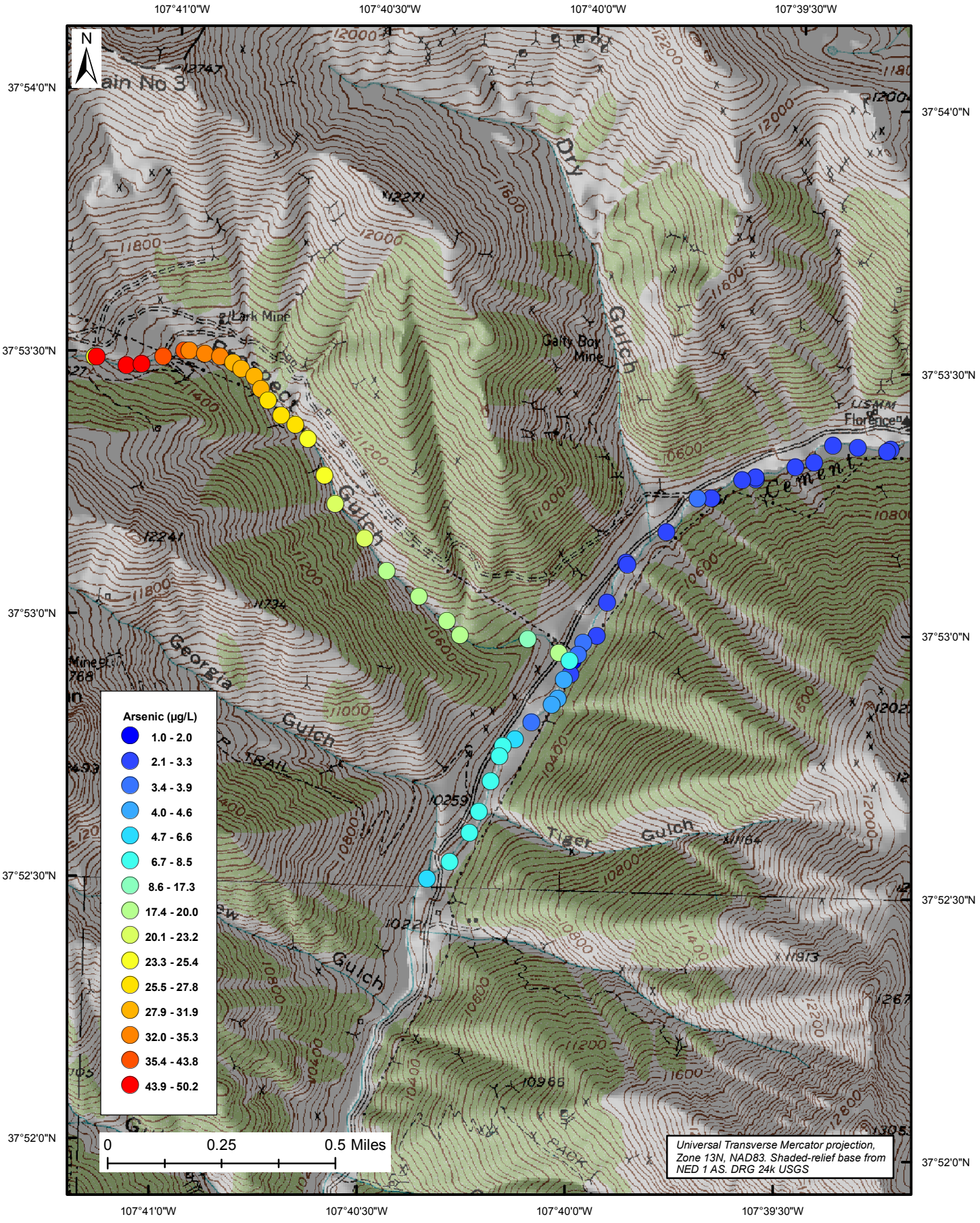

Figure 106: Instream arsenic concentrations in µg/L.

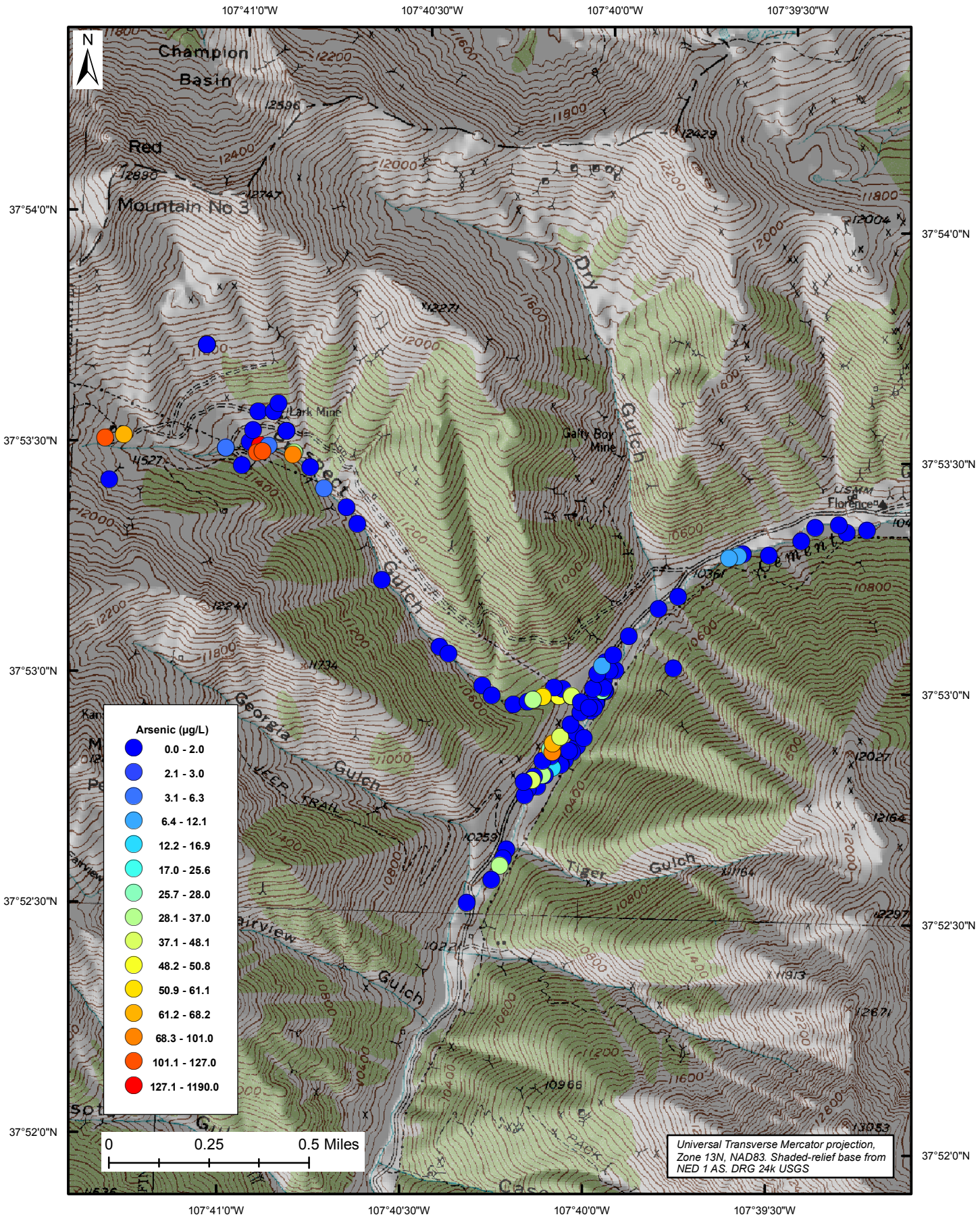

Figure 107: Ground-water arsenic concentrations in µg/L.

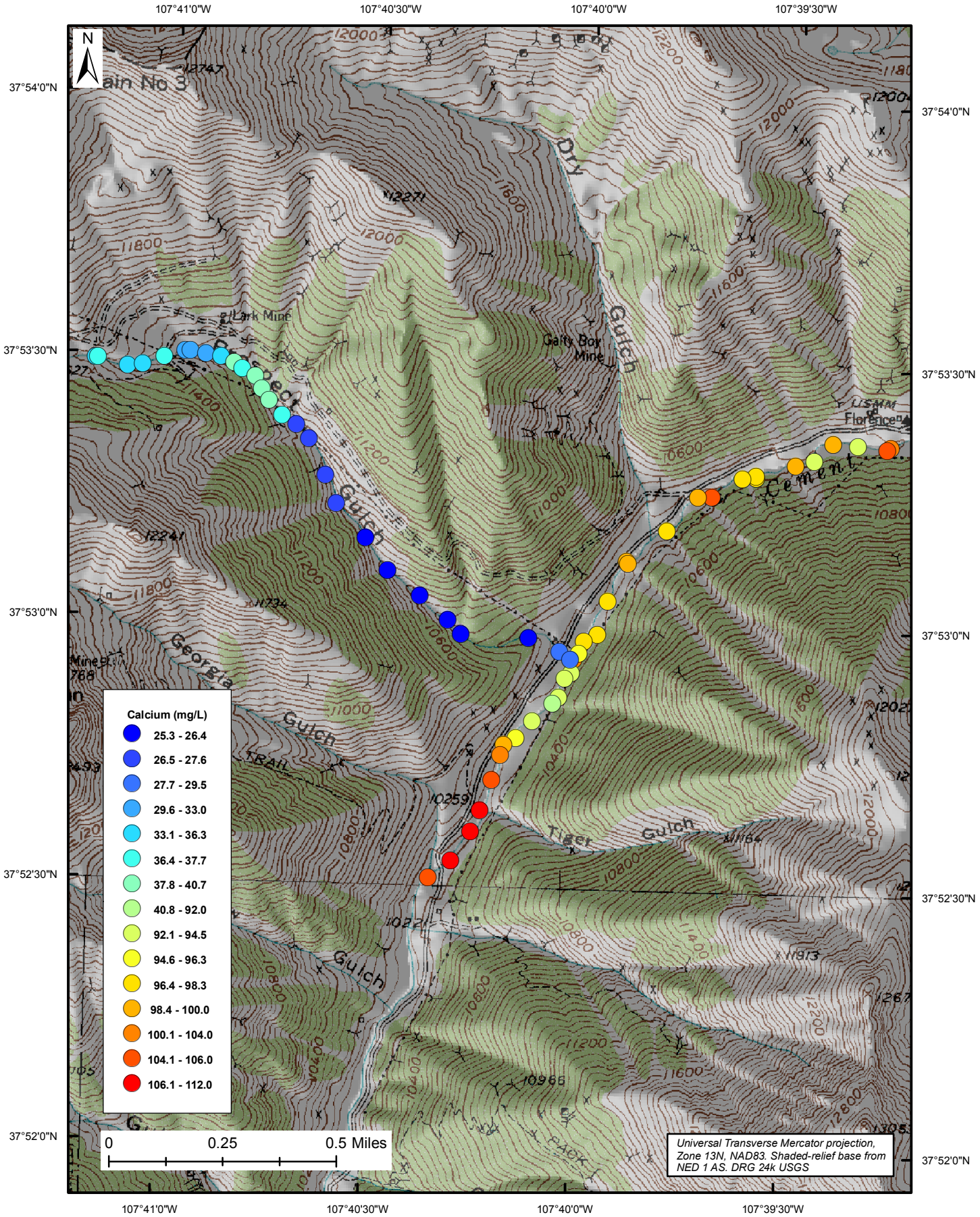

Figure 108: Instream calcium concentrations in mg/L.

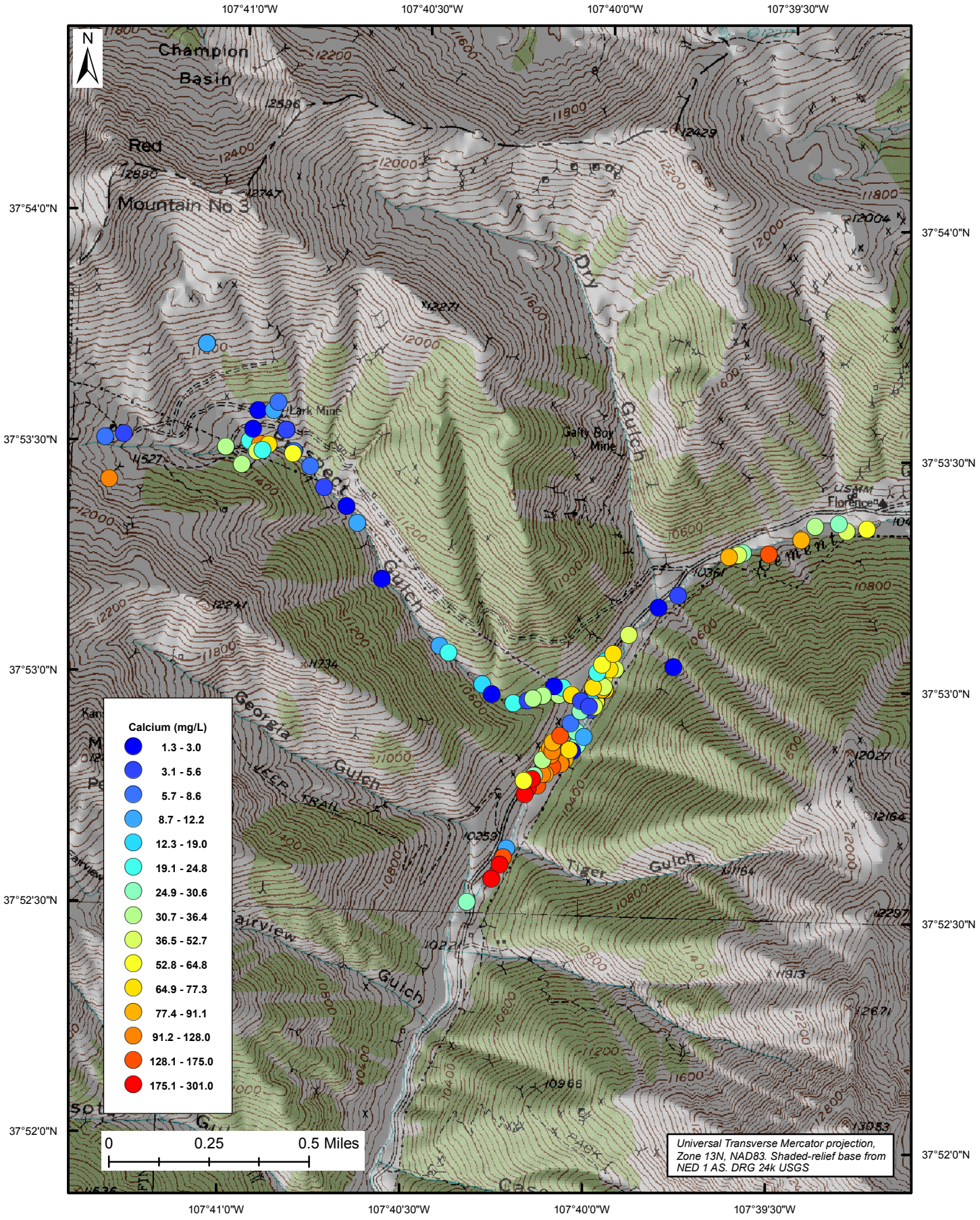

Figure 109: Ground-water calcium concentrations in mg/L.

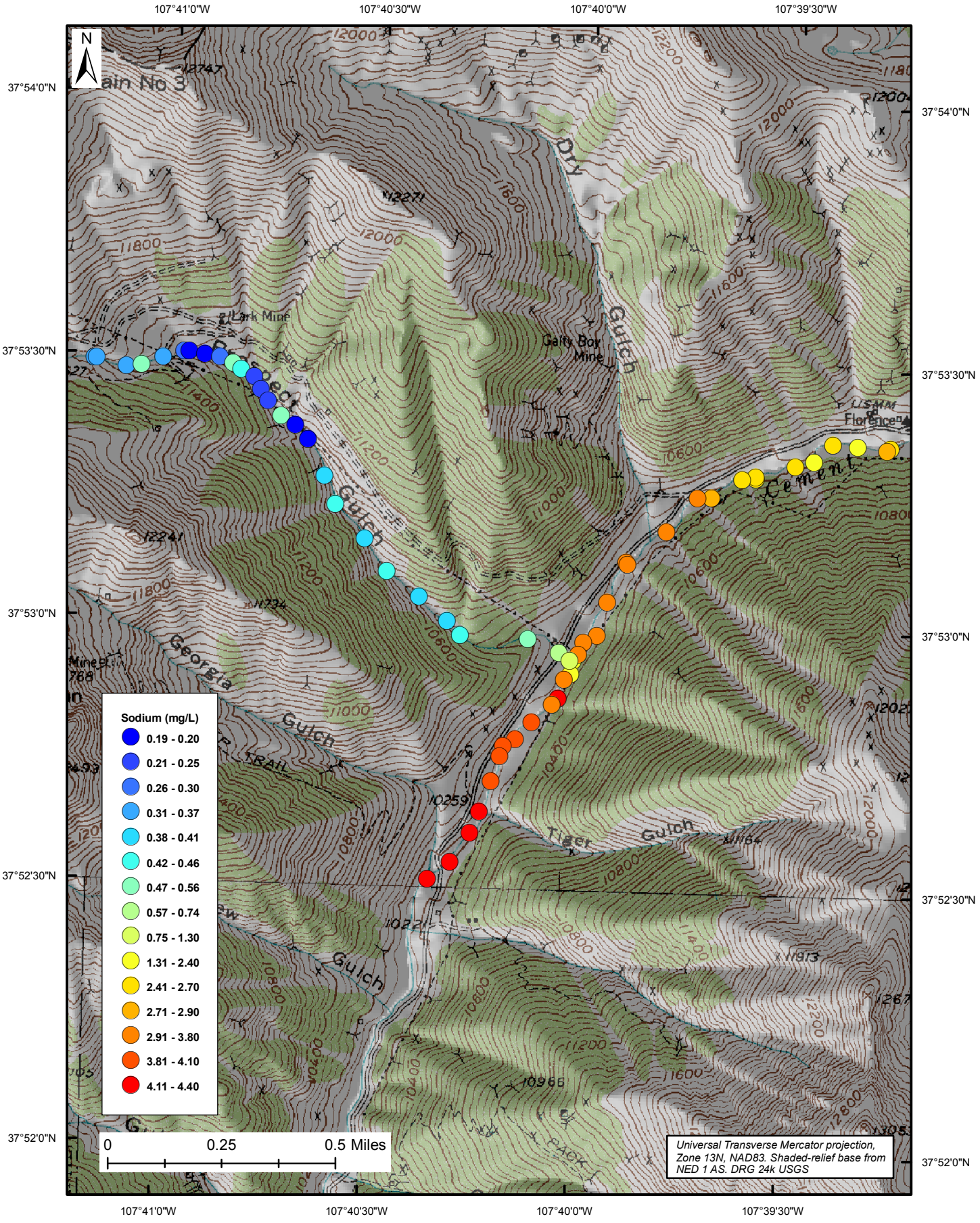

Figure 110: Instream sodium concentrations in mg/L.

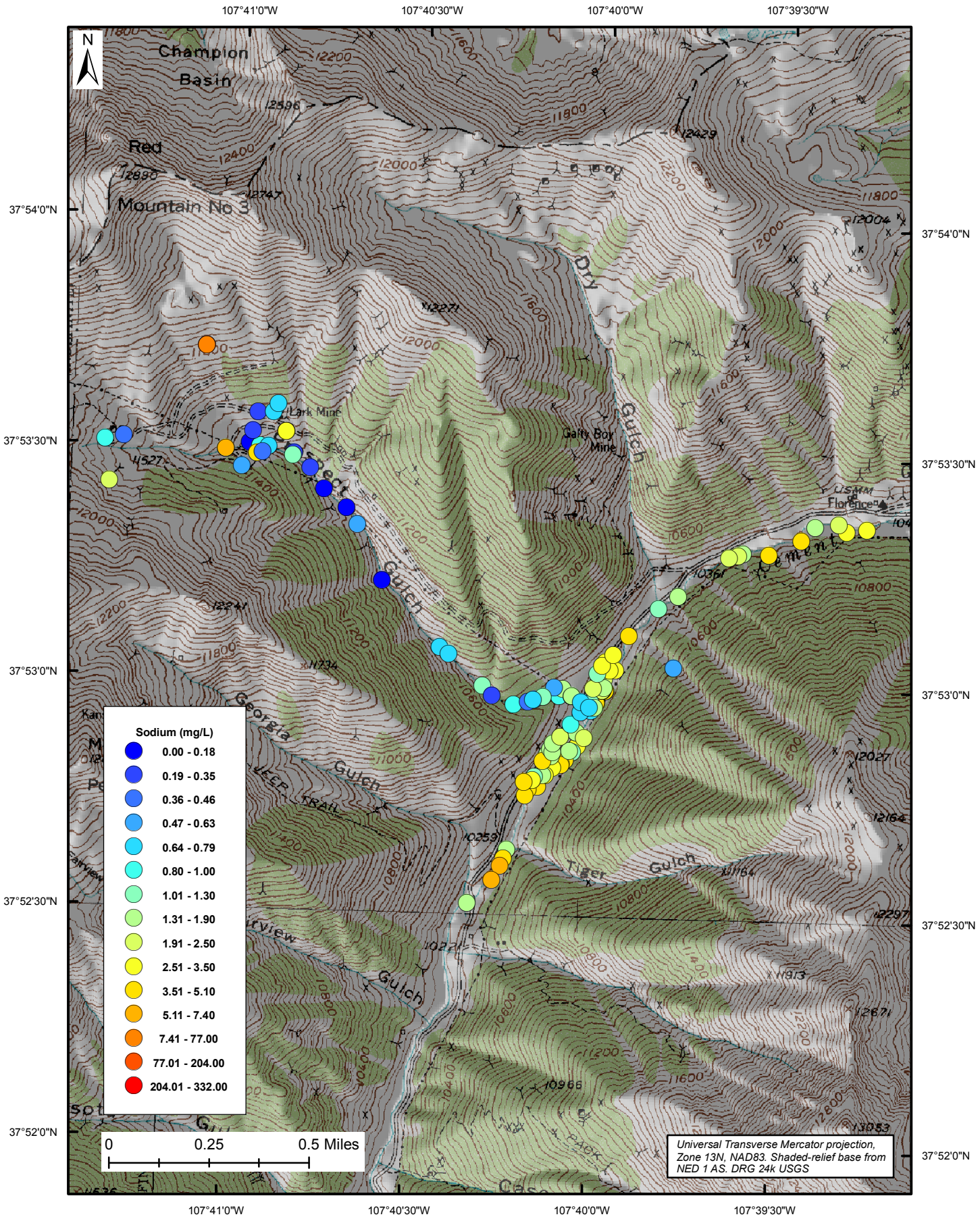

Figure 111: Ground-water sodium concentrations in mg/L.

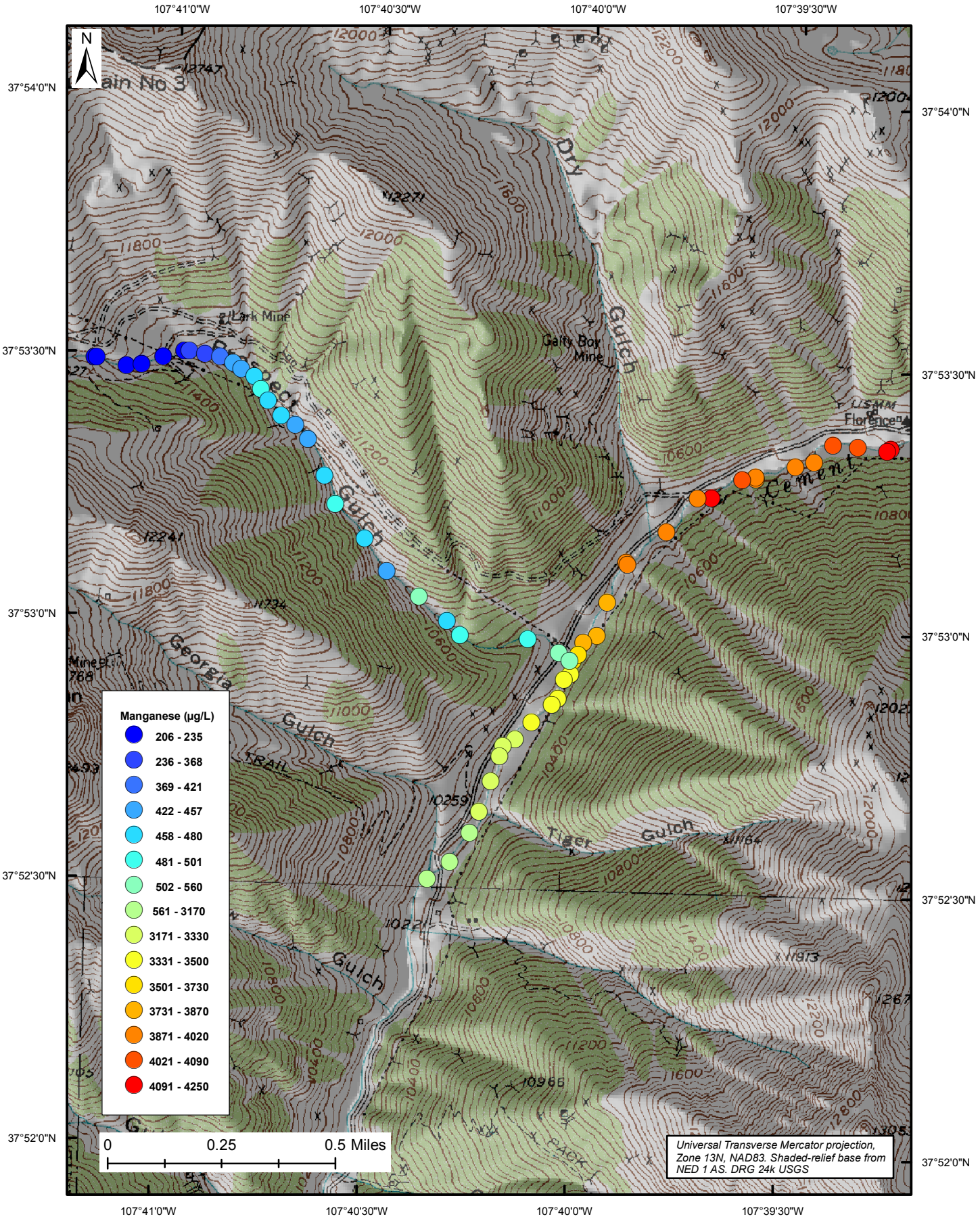

Figure 112: Instream manganese concentrations in µg/L.

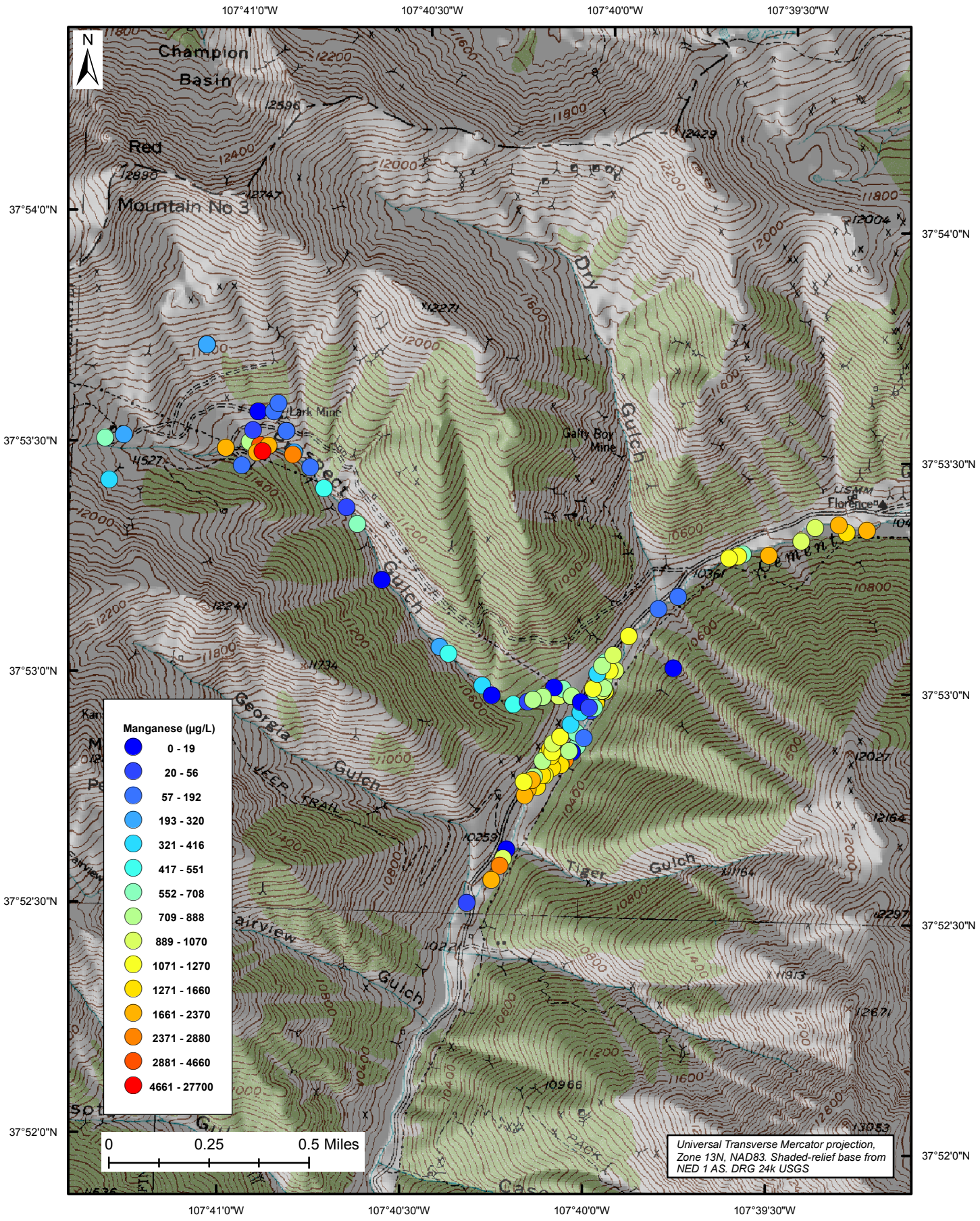

Figure 113: Ground-water manganese concentrations in µg/L.

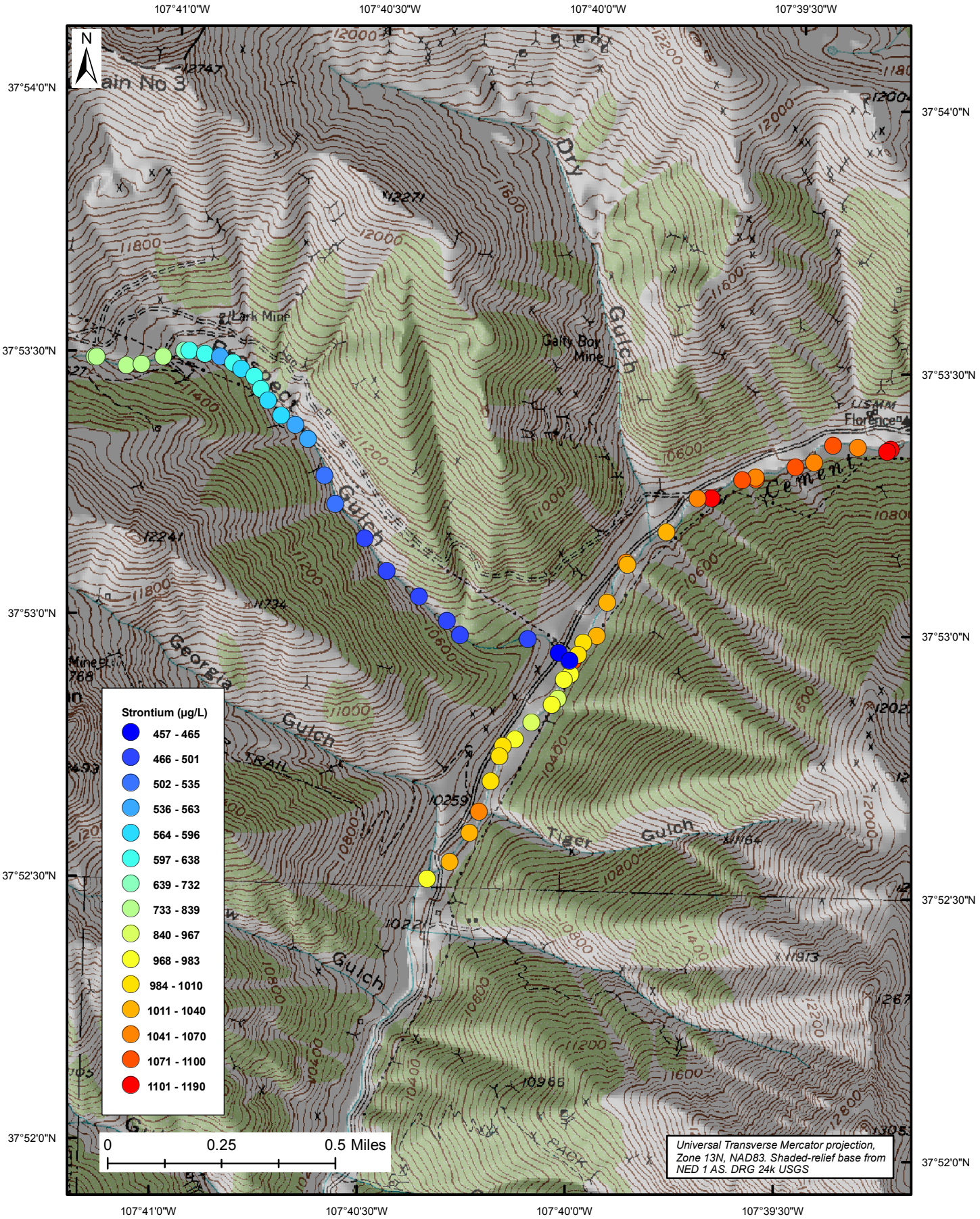

Figure 114: Instream strontium concentrations in µg/L.

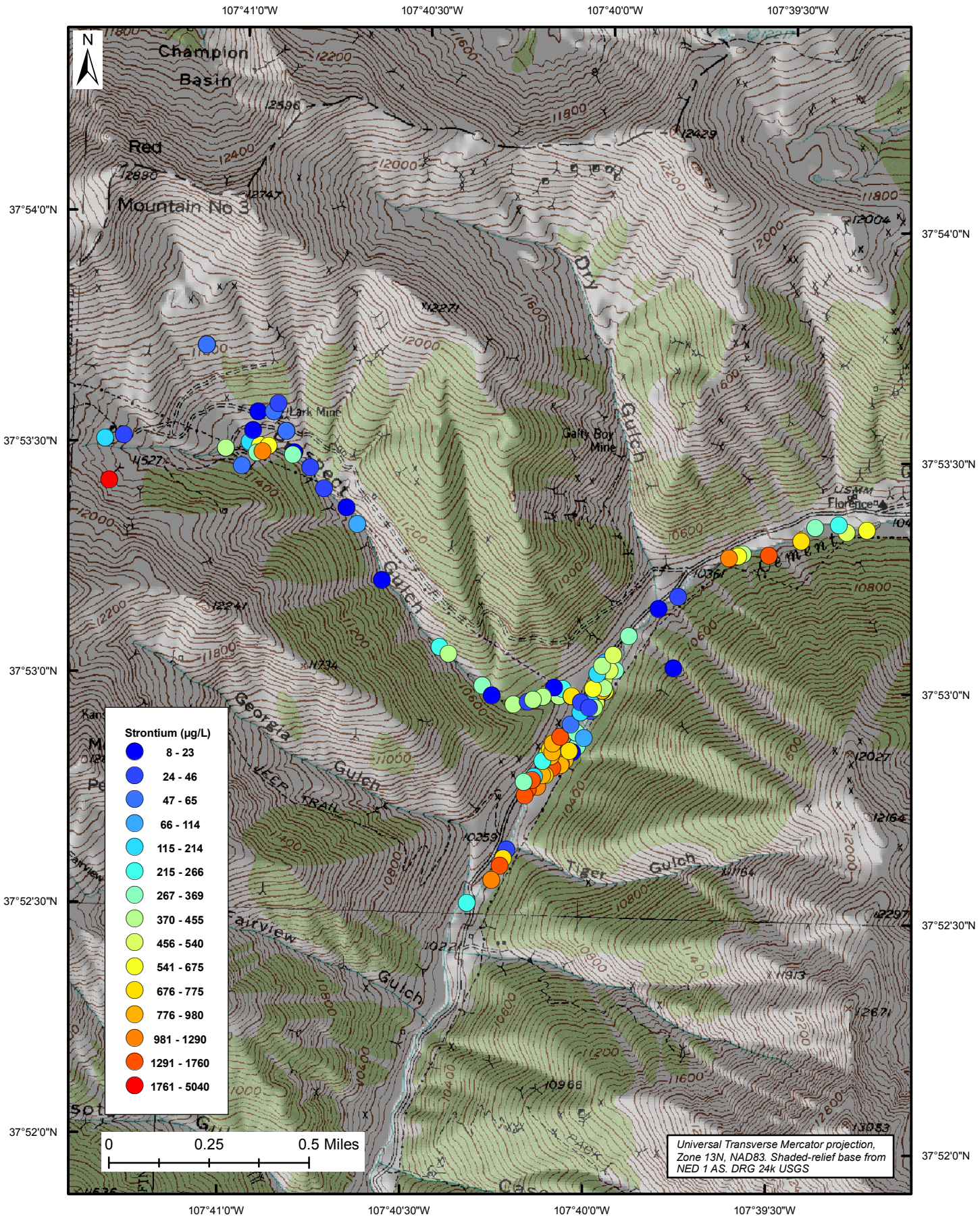

Figure 115: Ground-water strontium concentrations in µg/L.

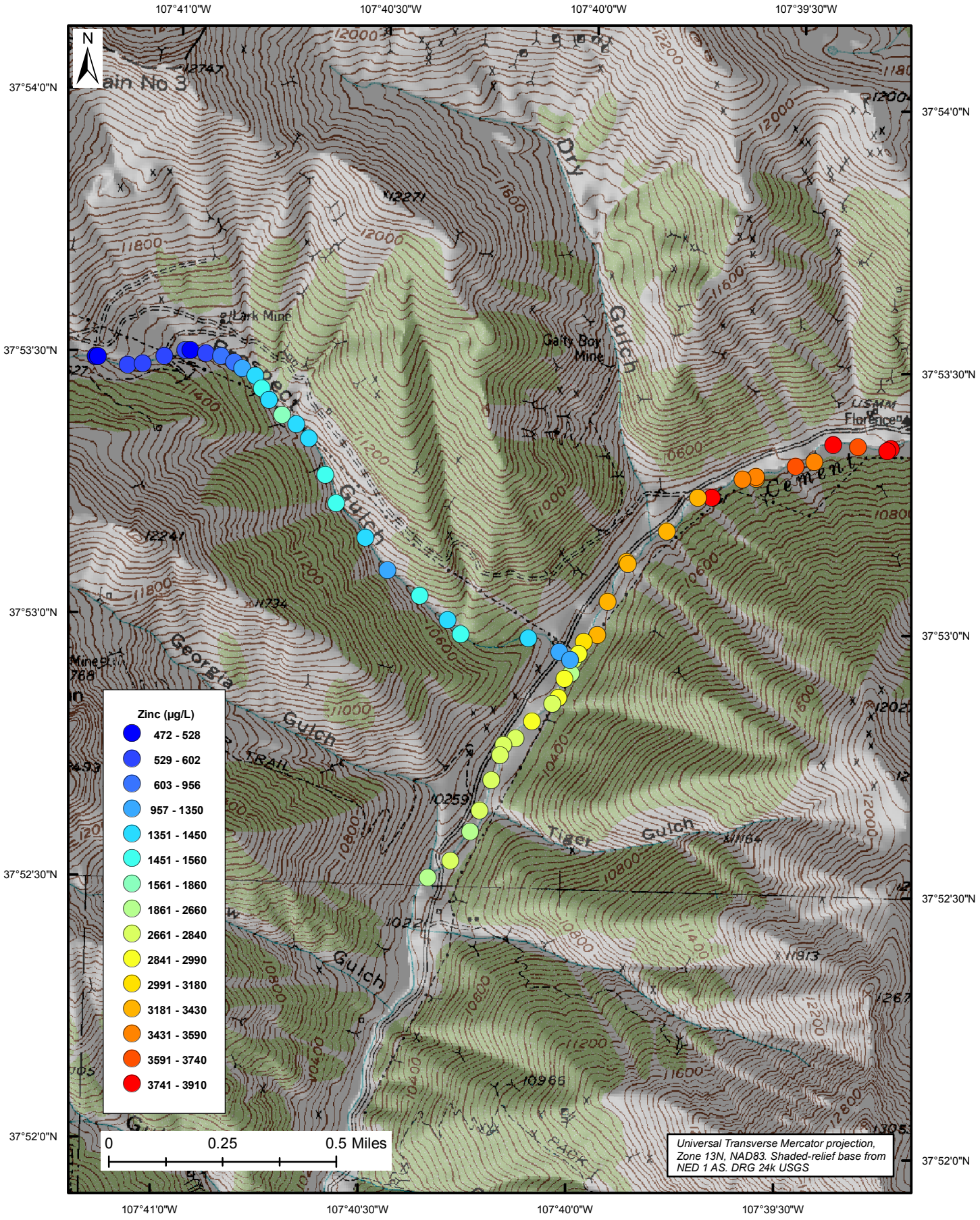

Figure 116: Instream zinc concentrations in µg/L.

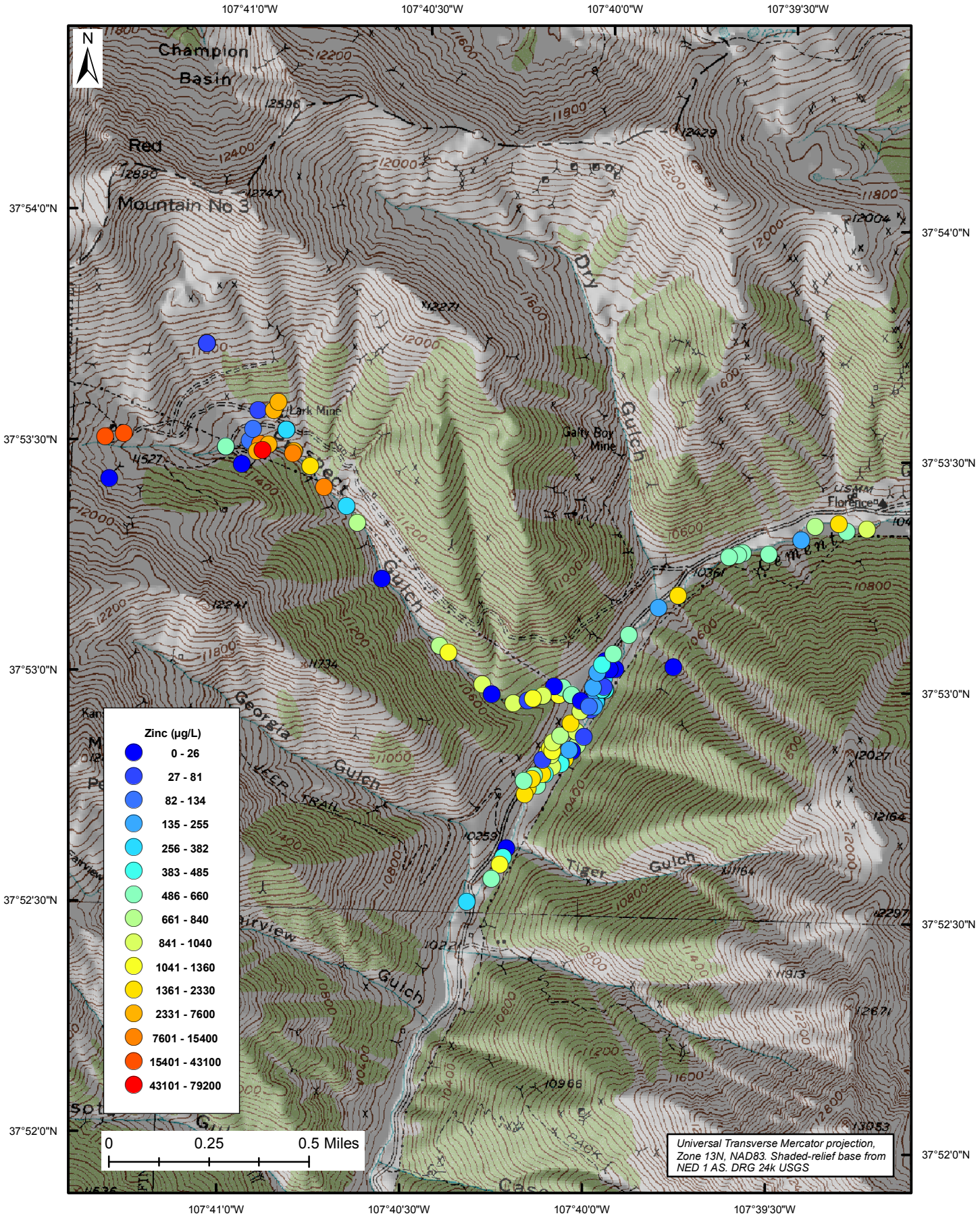

Figure 117: Ground-water zinc concentrations in µg/L.

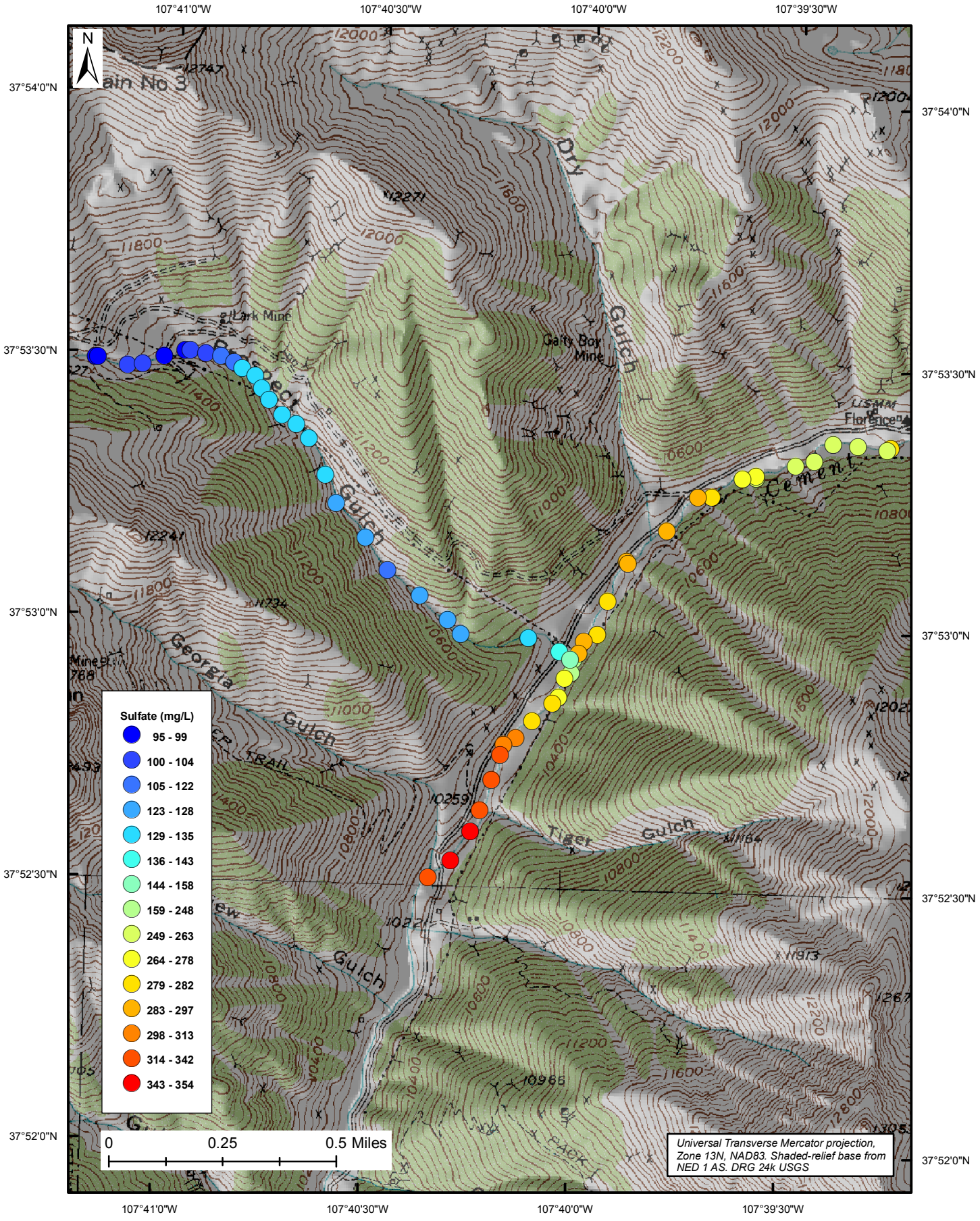

Figure 118: Instream sulfate concentrations in mg/L.

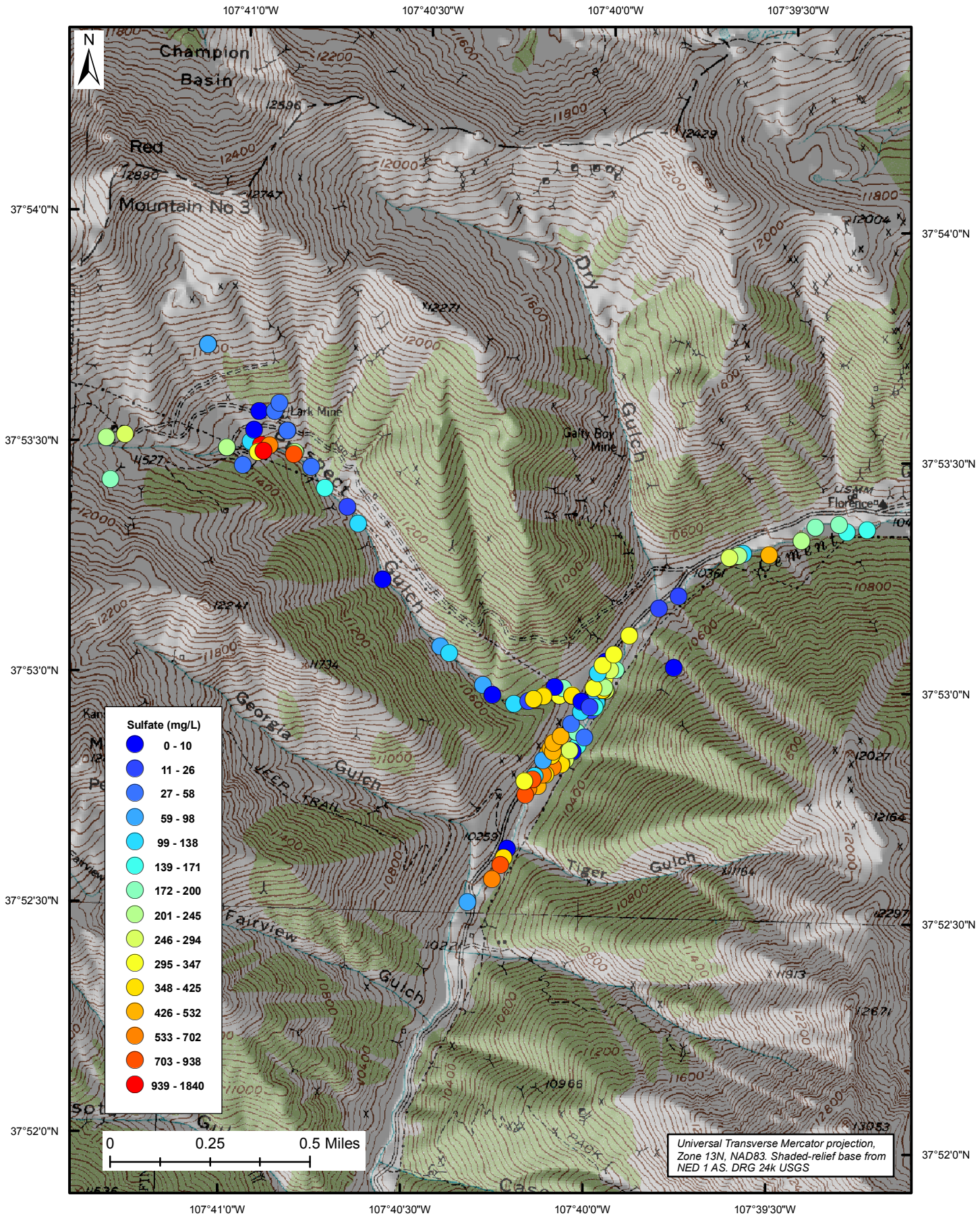

Figure 119: Ground-water sulfate concentrations in mg/L.

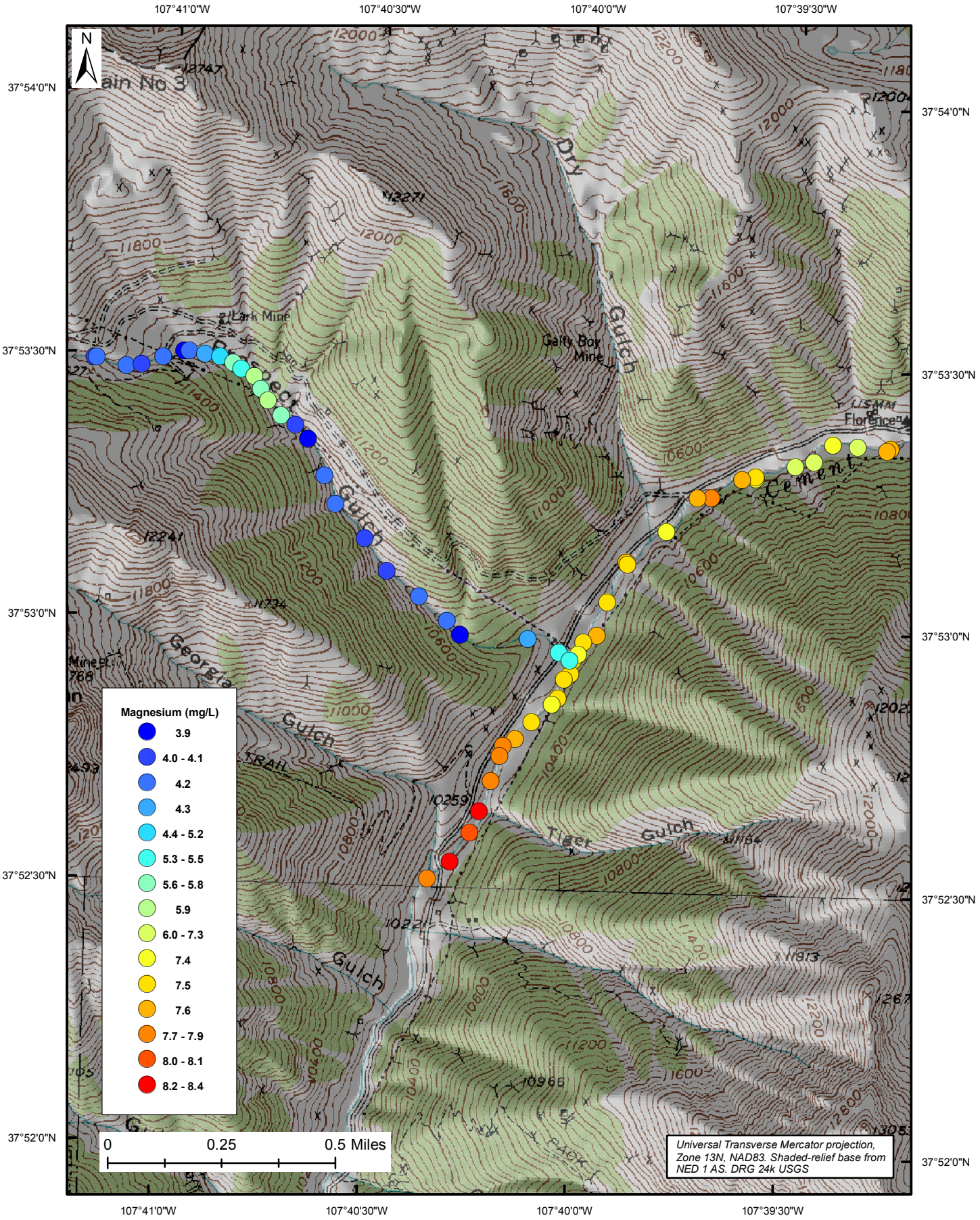

Figure 120: Instream magnesium concentrations in mg/L.

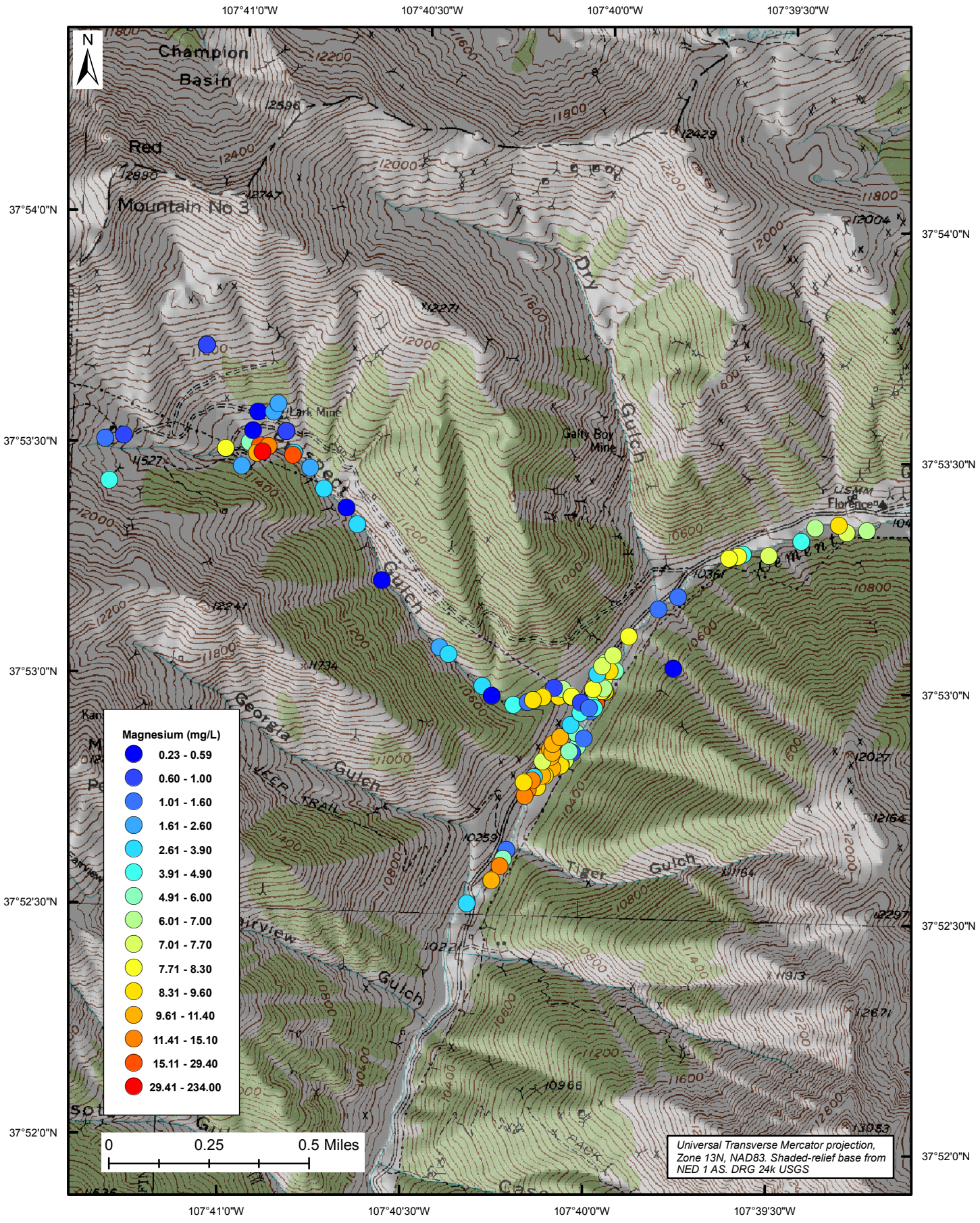

Figure 121: Ground-water magnesium concentrations in mg/L.

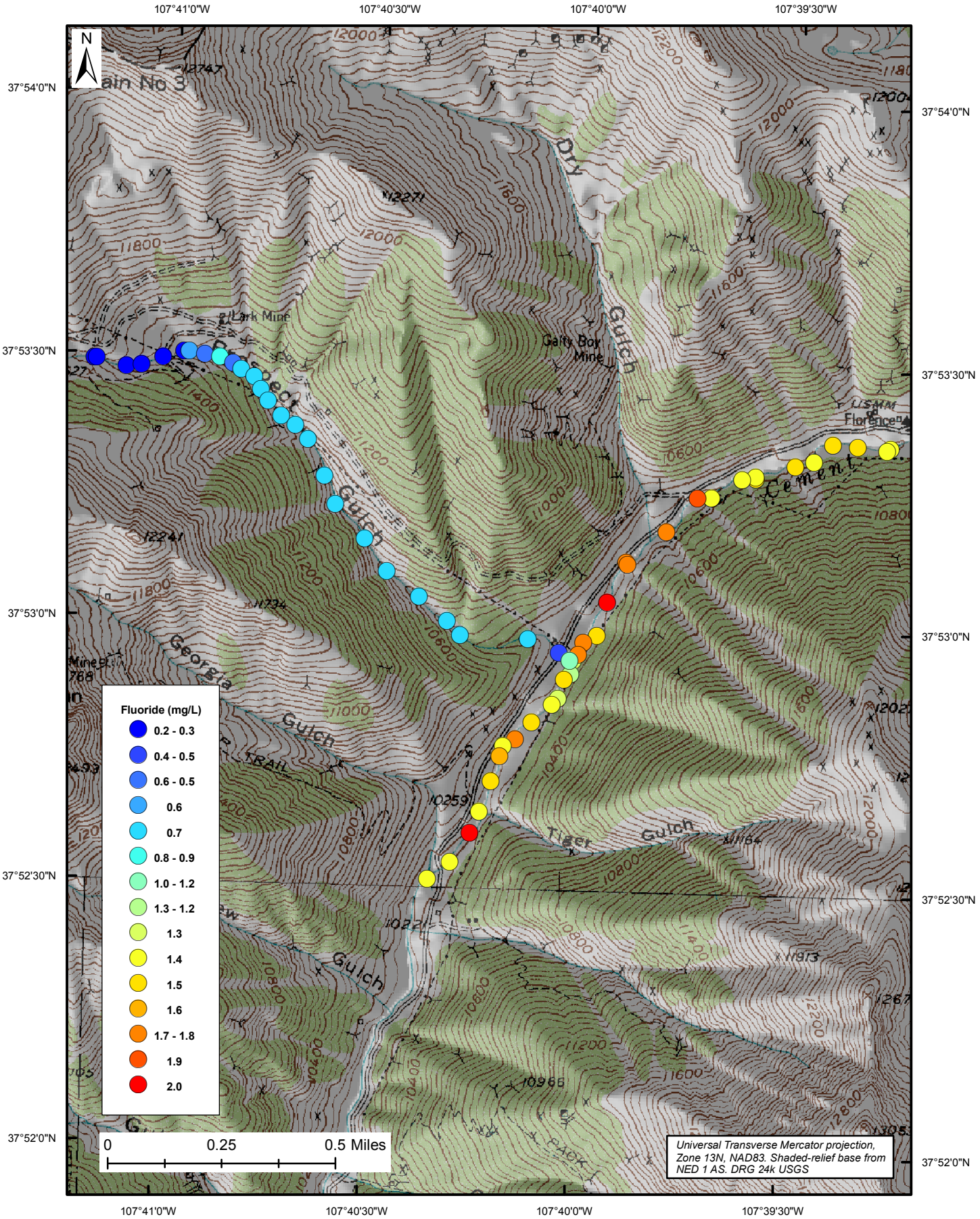

Figure 122: Instream fluoride concentrations in mg/L.

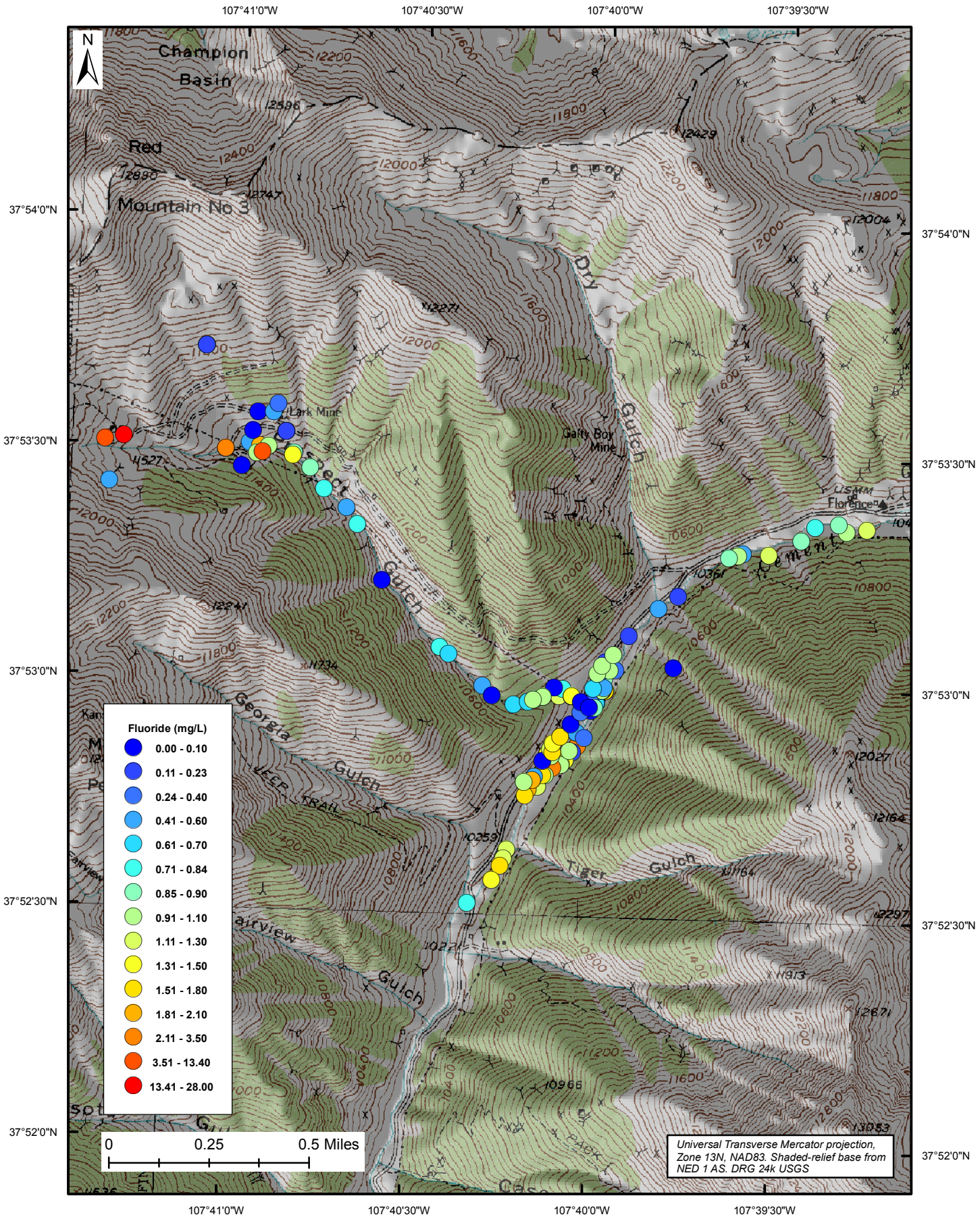

Figure 123: Ground-water fluoride concentrations in mg/L.

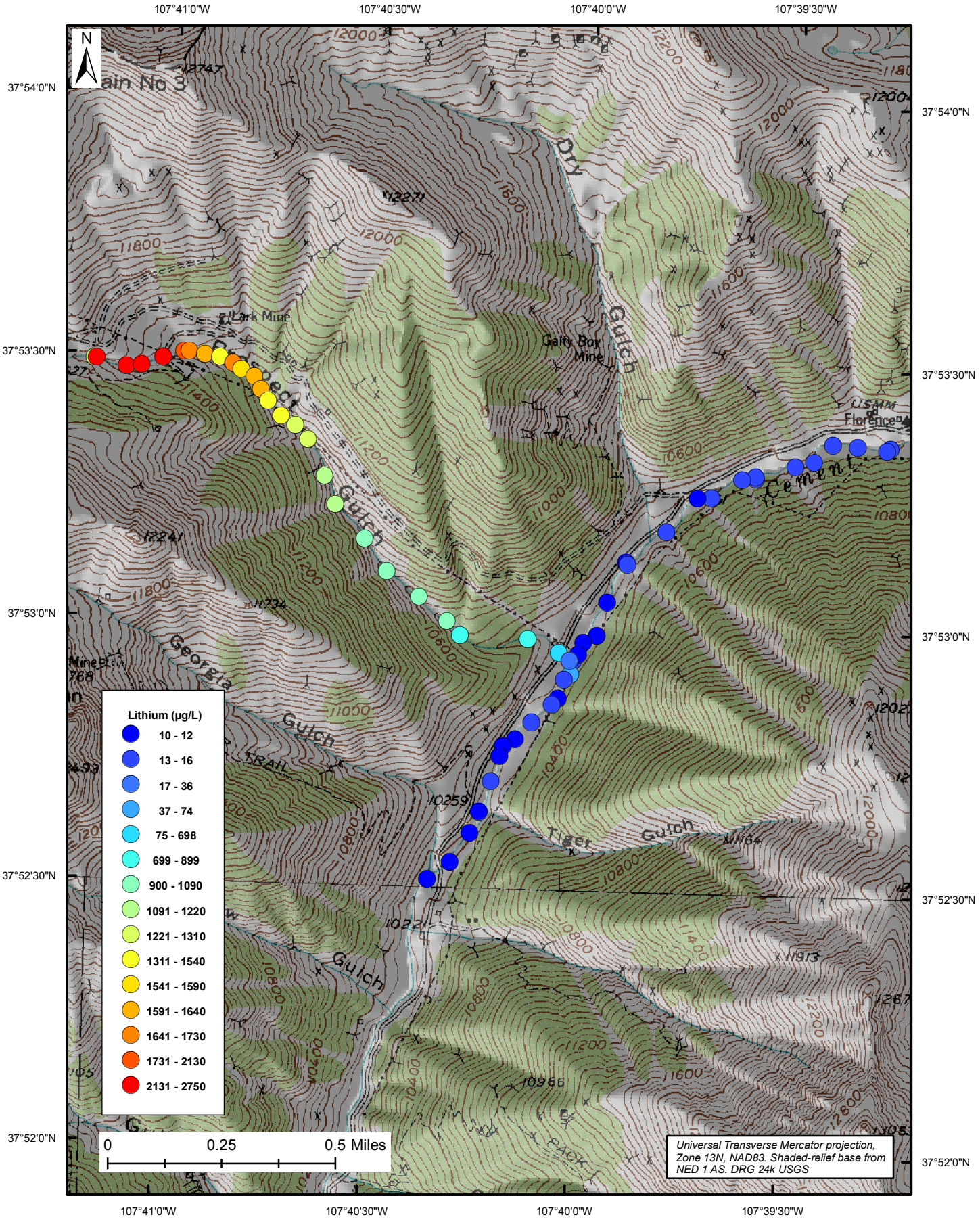

Figure 124: Instream lithium concentrations in µg/L.

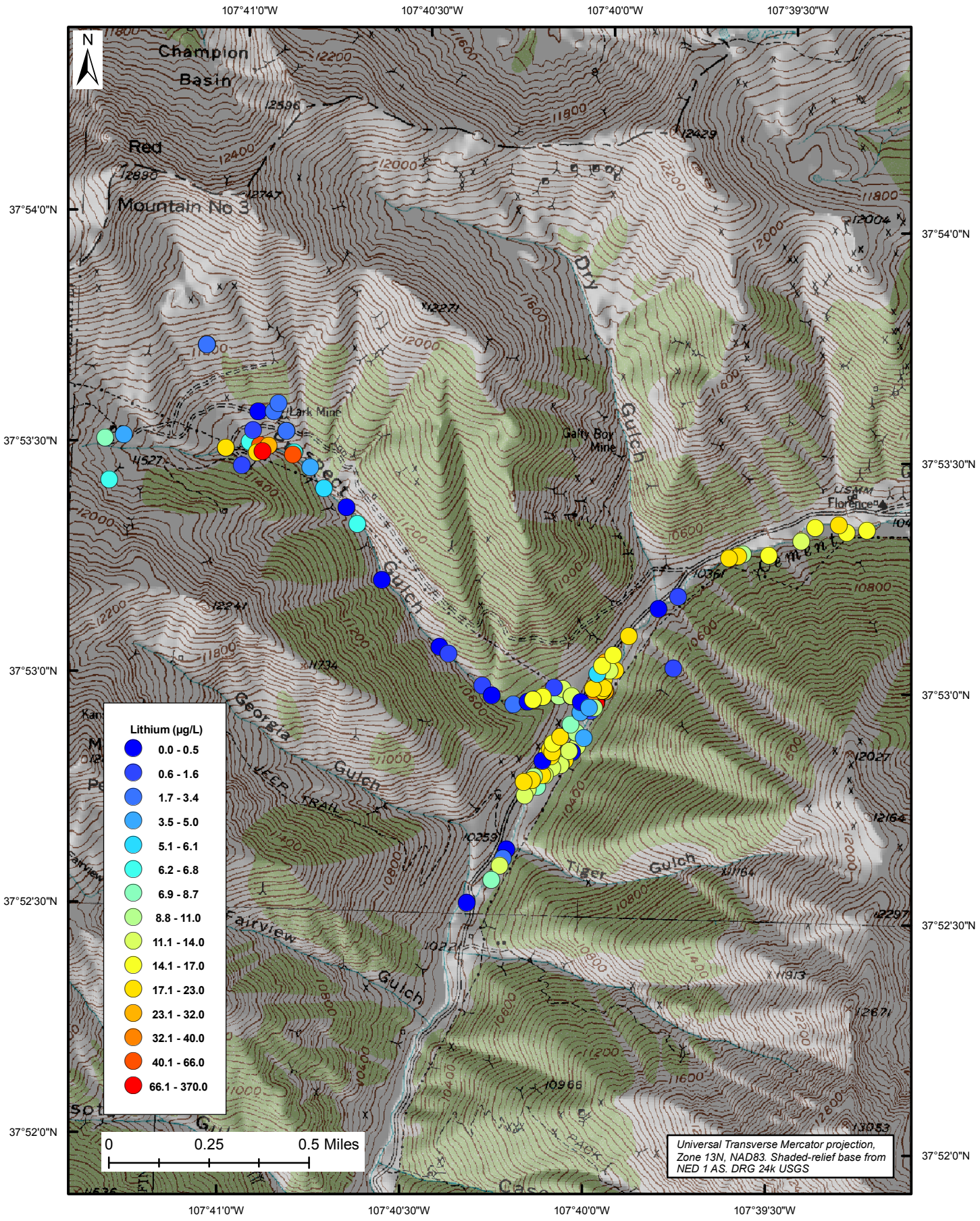

Figure 125: Ground-water lithium concentrations in µg/L.

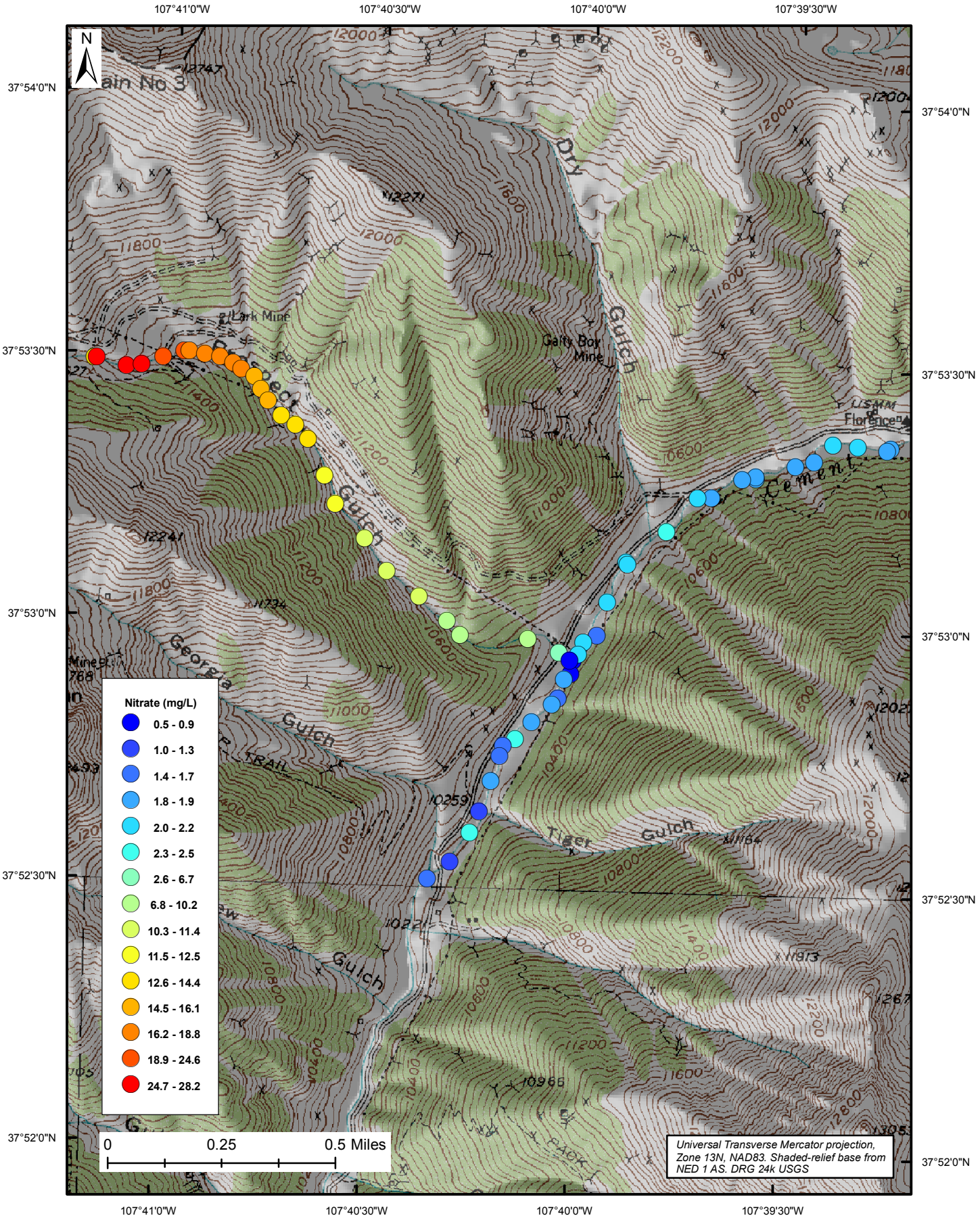

Figure 126: Instream nitrate concentrations in mg/L.

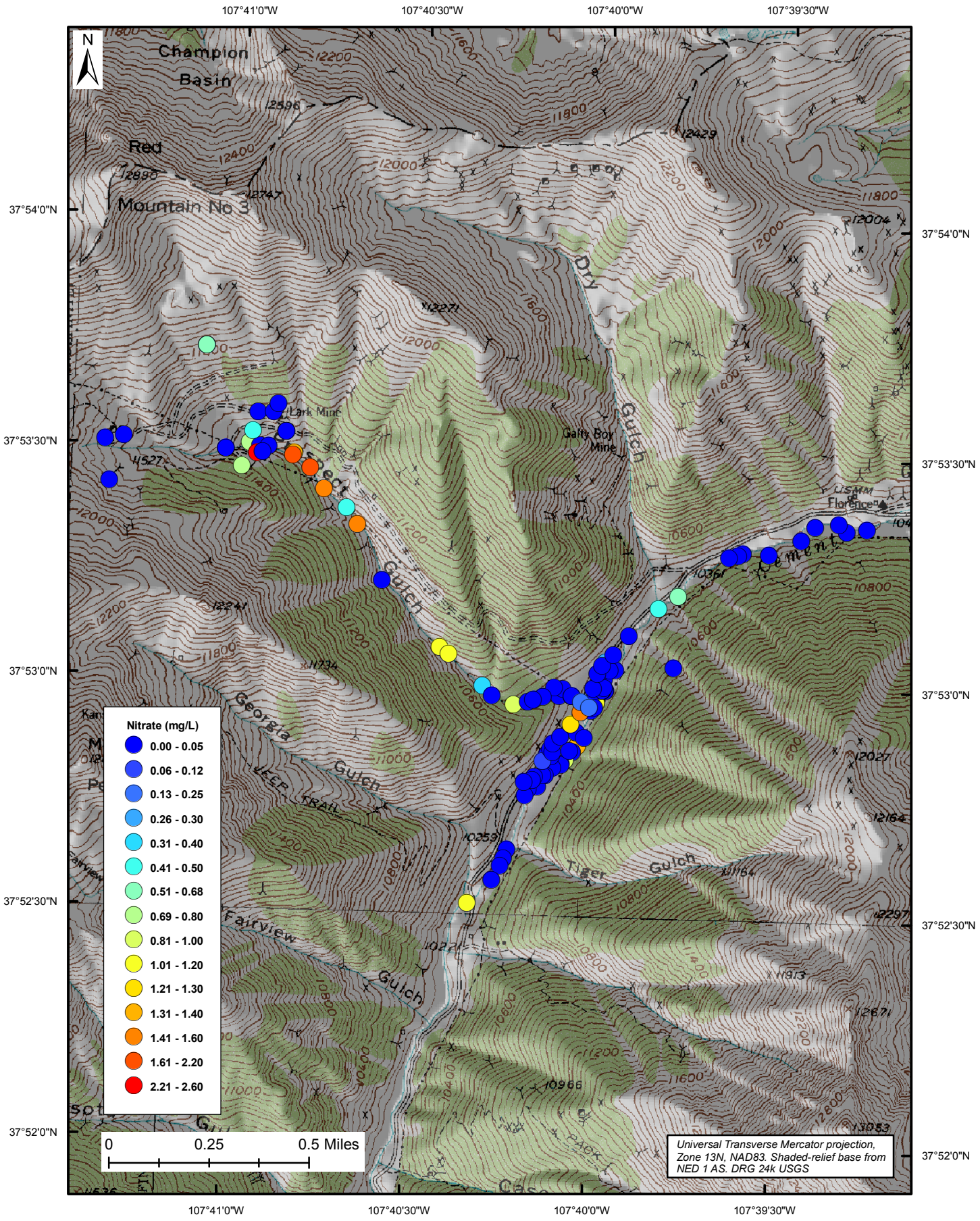

Figure 127: Ground-water nitrate concentrations in mg/L.

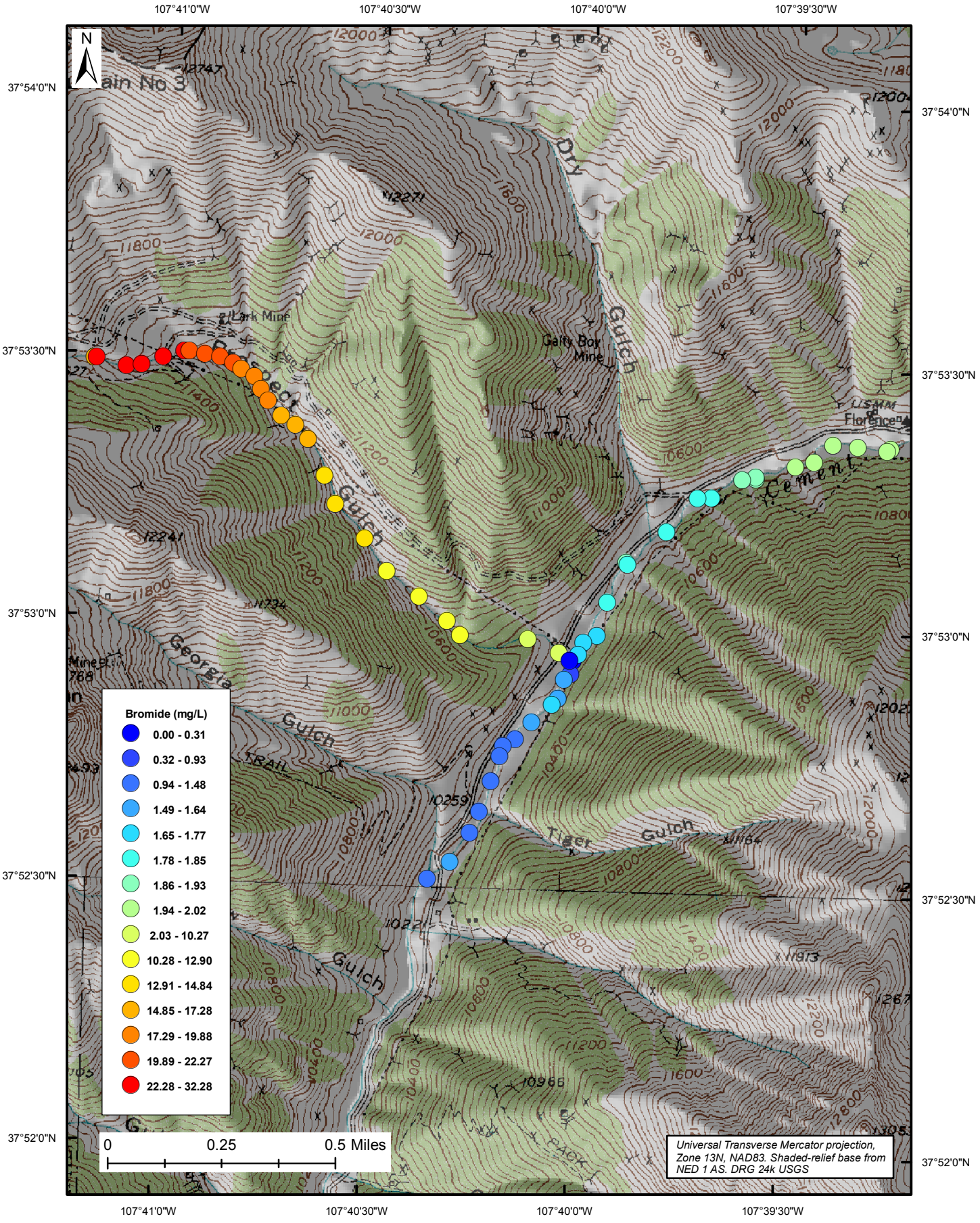

Figure 128: Instream bromide concentrations in mg/L.

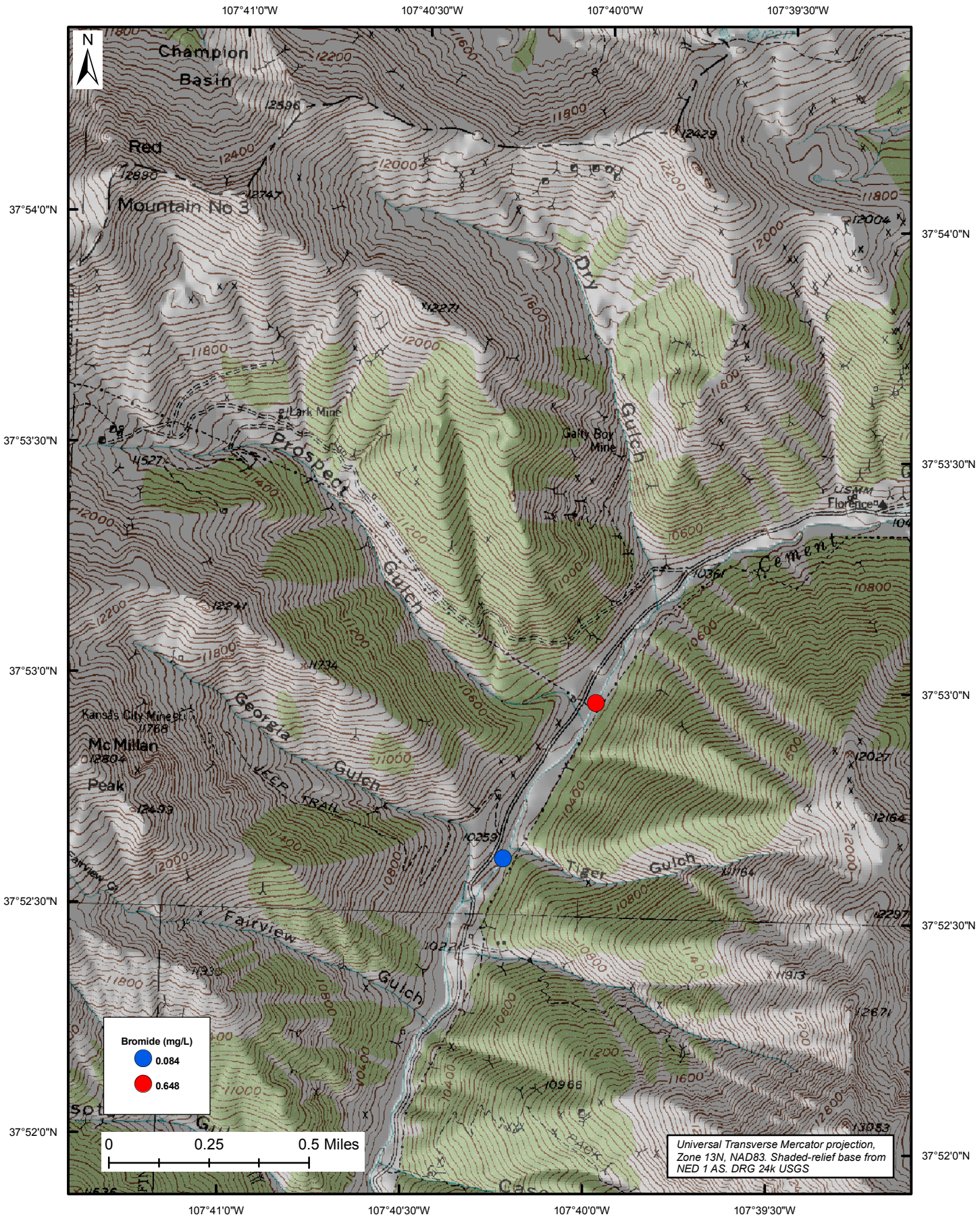

Figure 129: Ground-water bromide concentrations in mg/L.

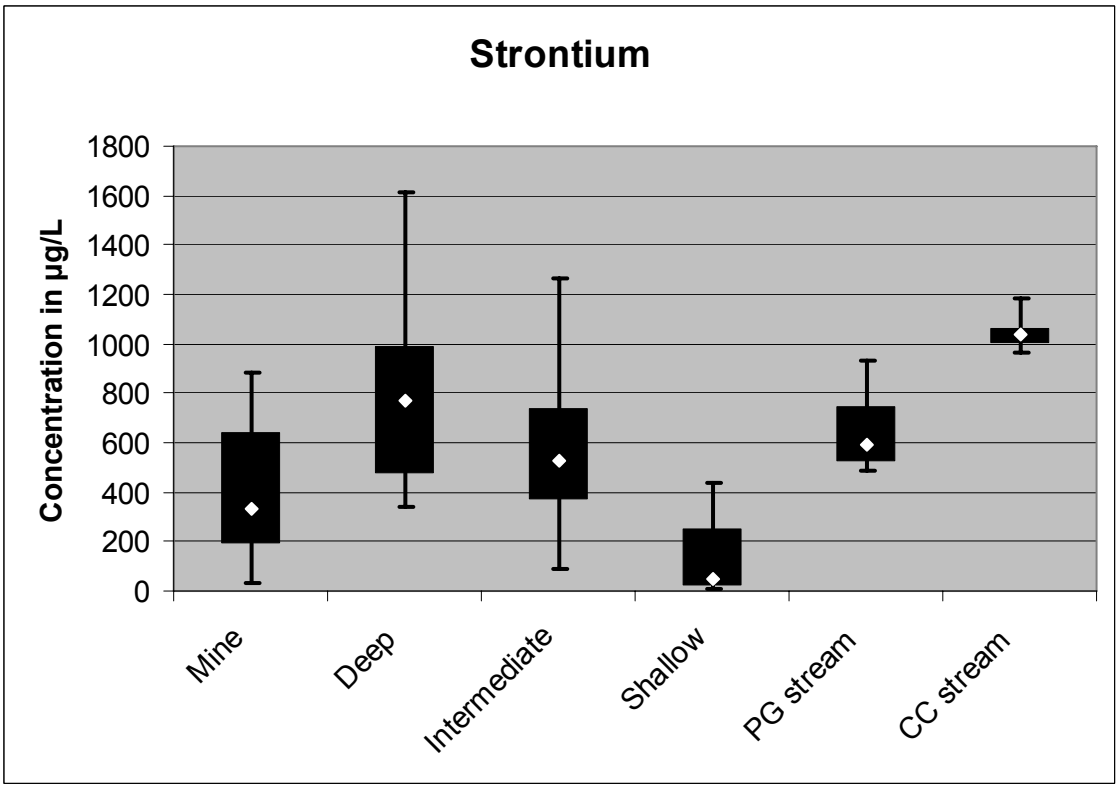

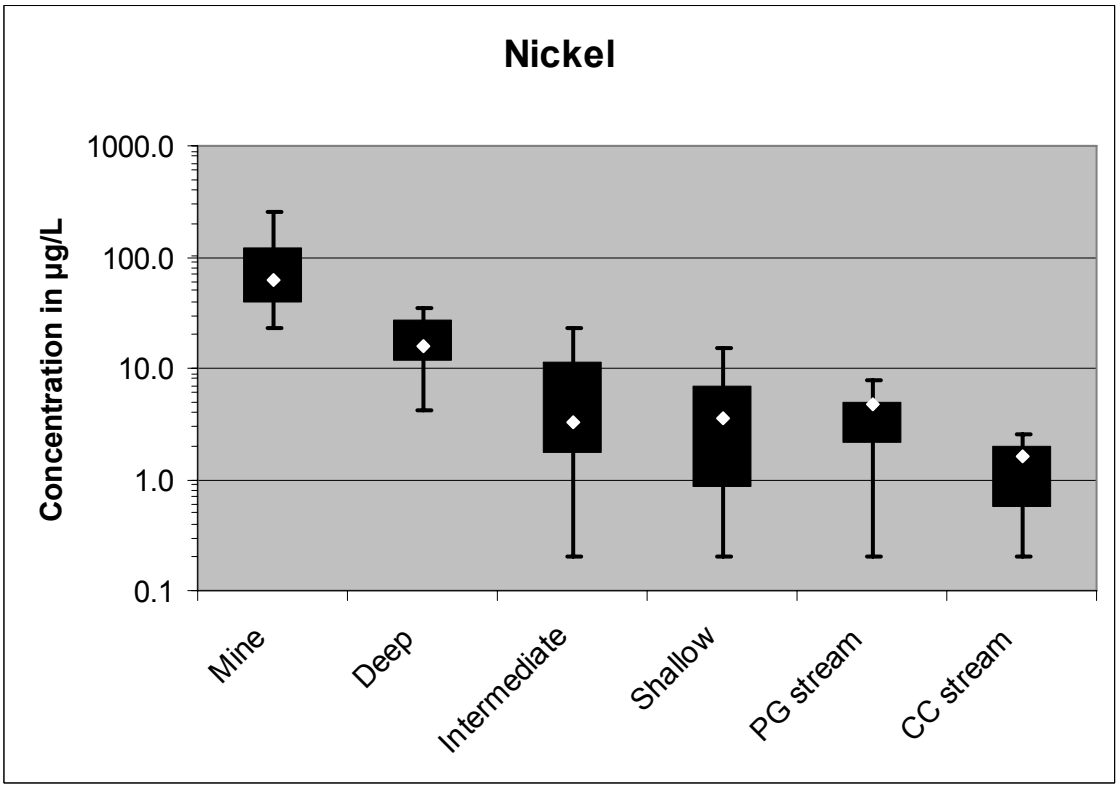

Figure 130: Water category comparisons for strontium and nickel.

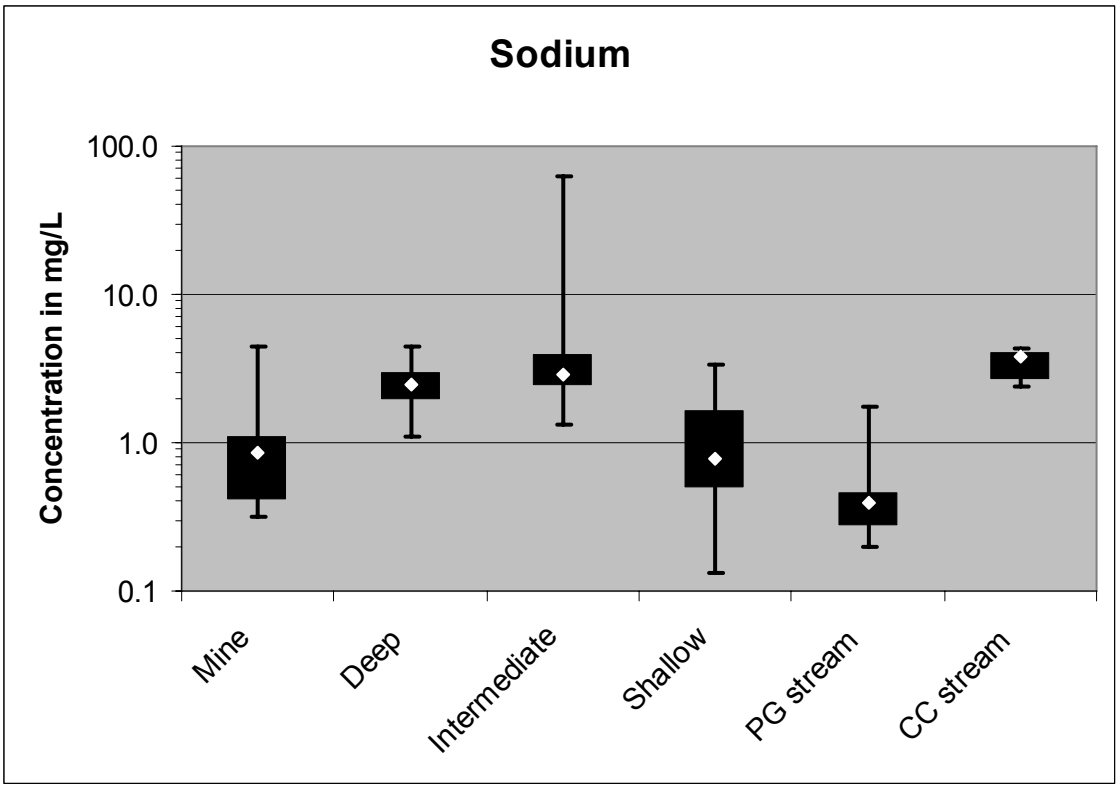

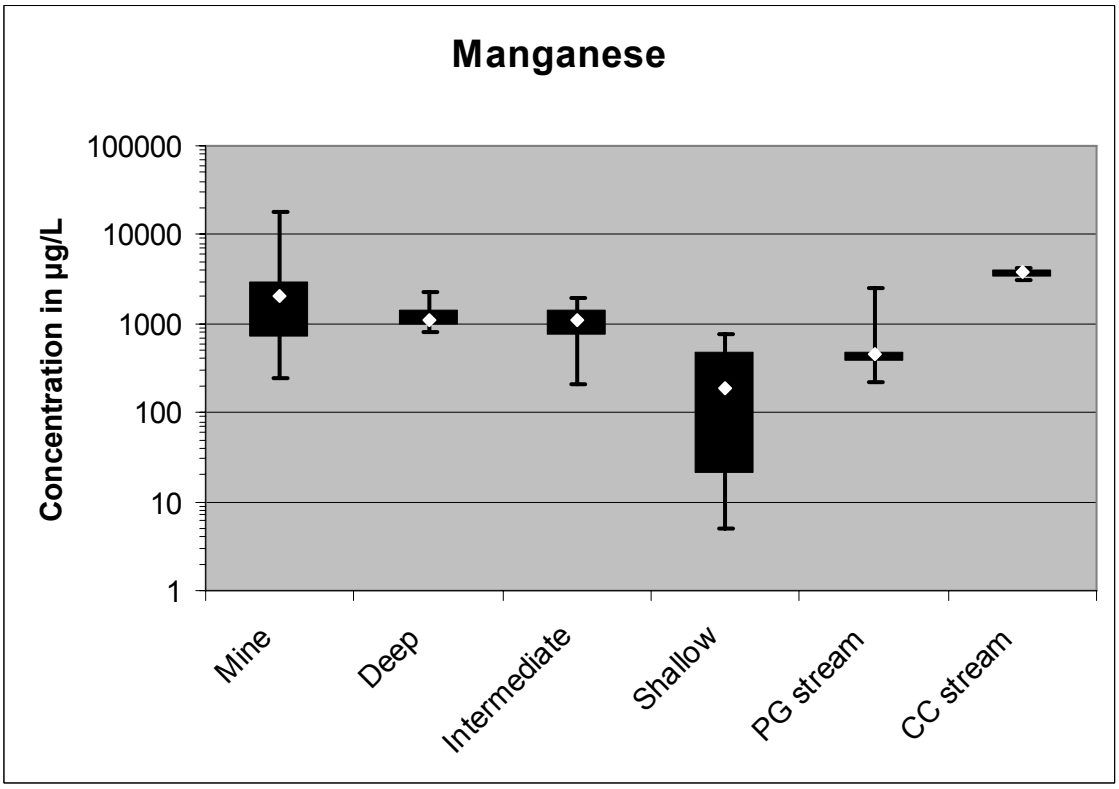

Figure 131: Water category comparisons for sodium and manganese.

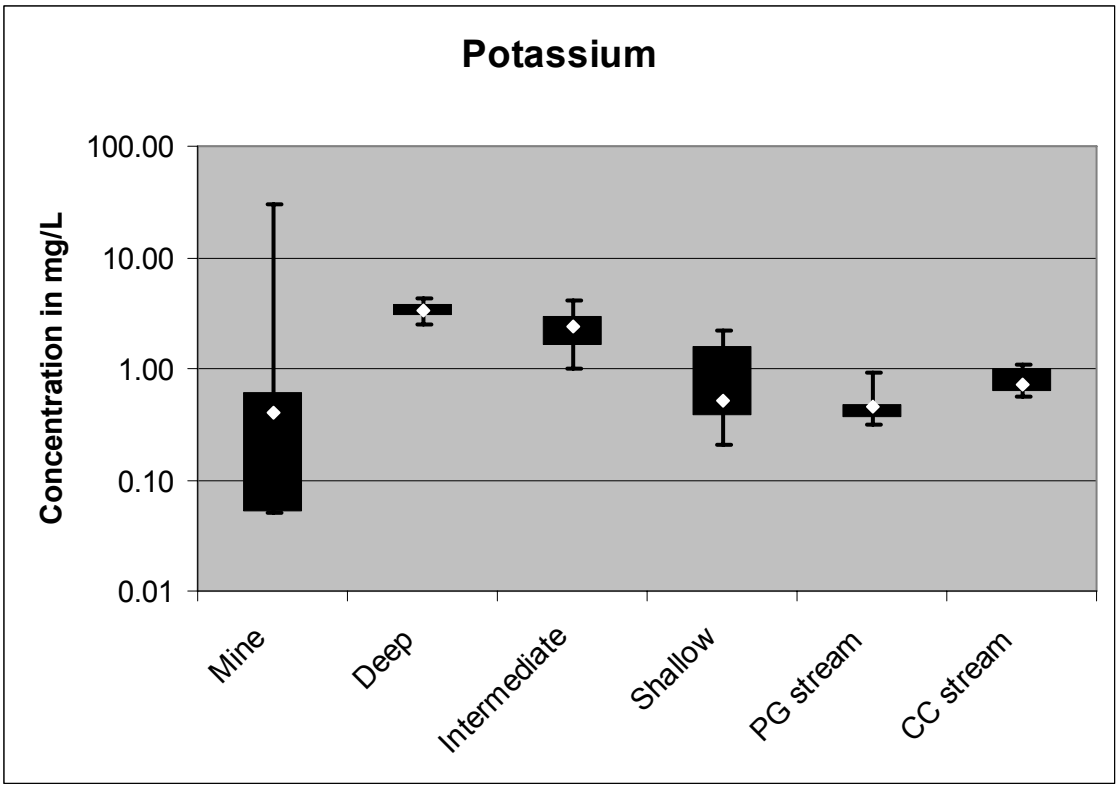

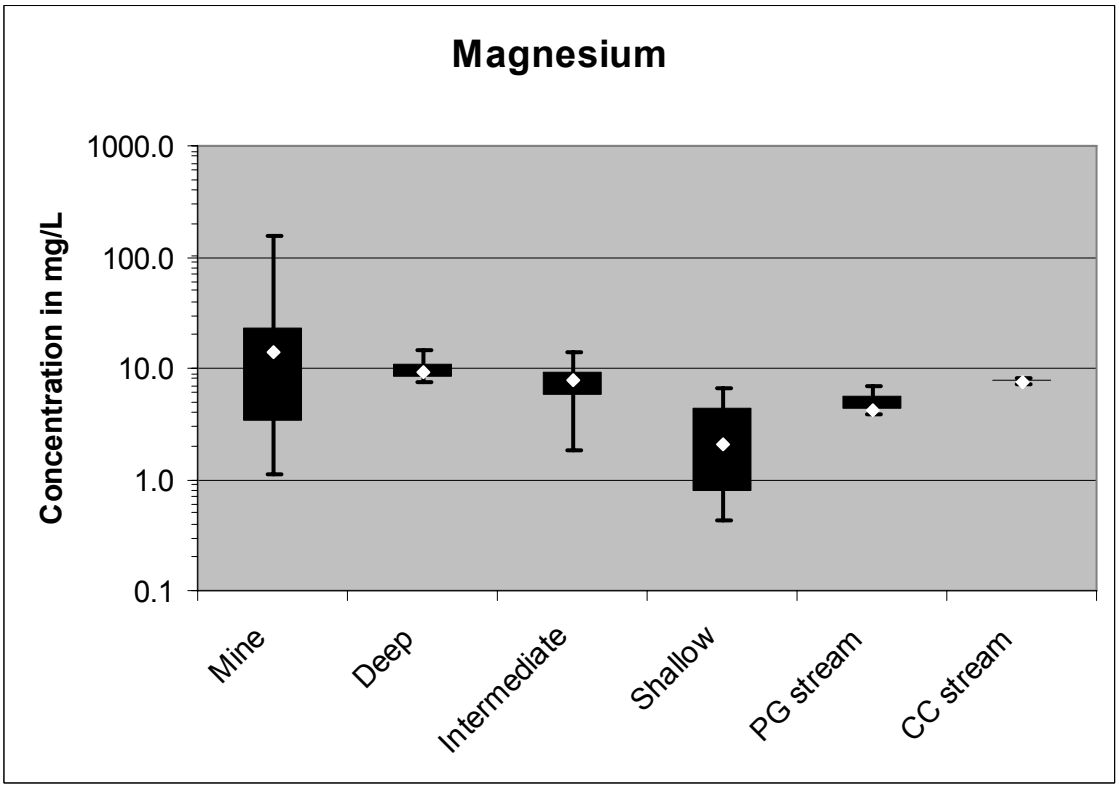

Figure132: Water category comparisons for potassium and magnesium.

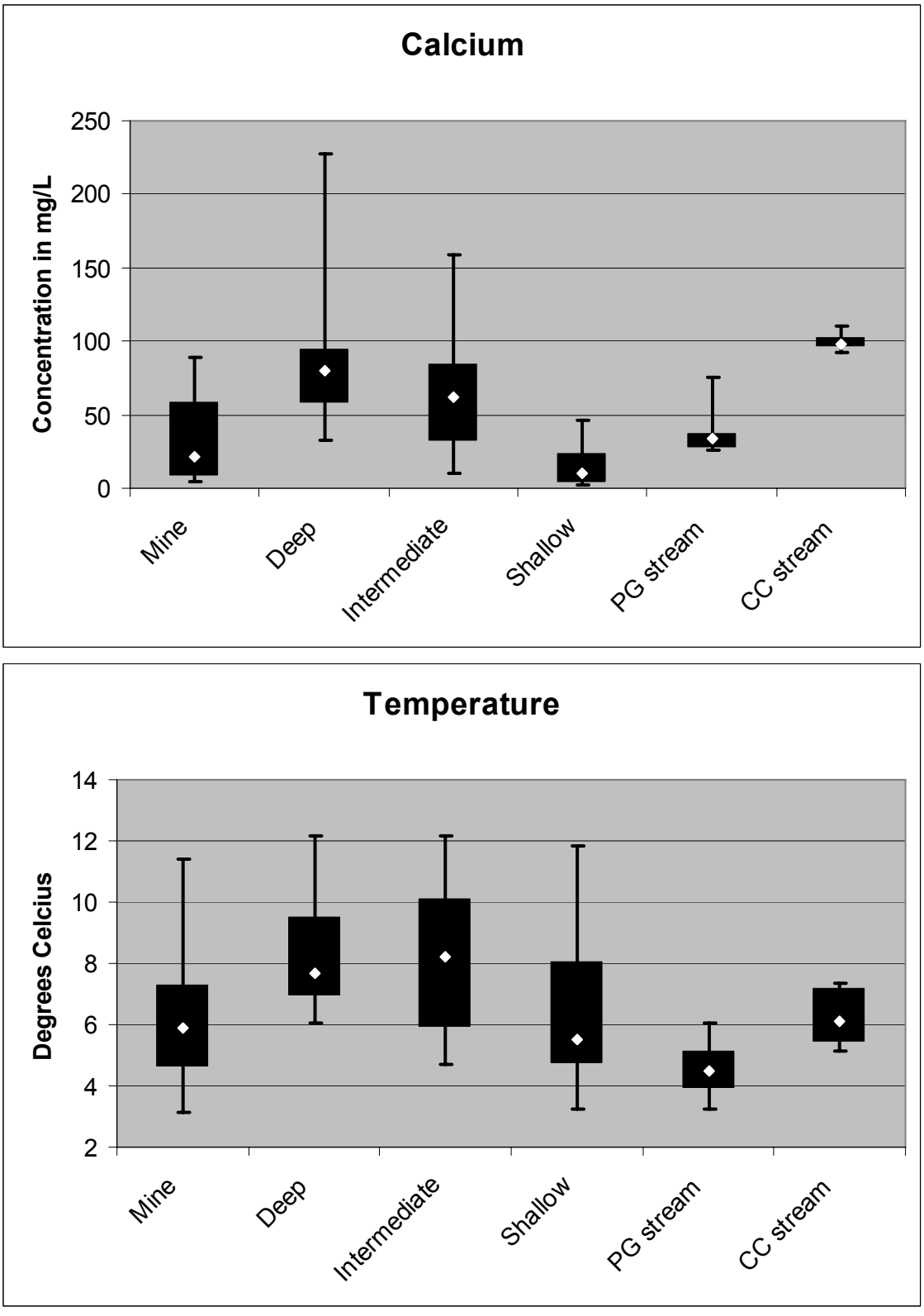

Figure 133: Water category comparisons for calcium and temperature.

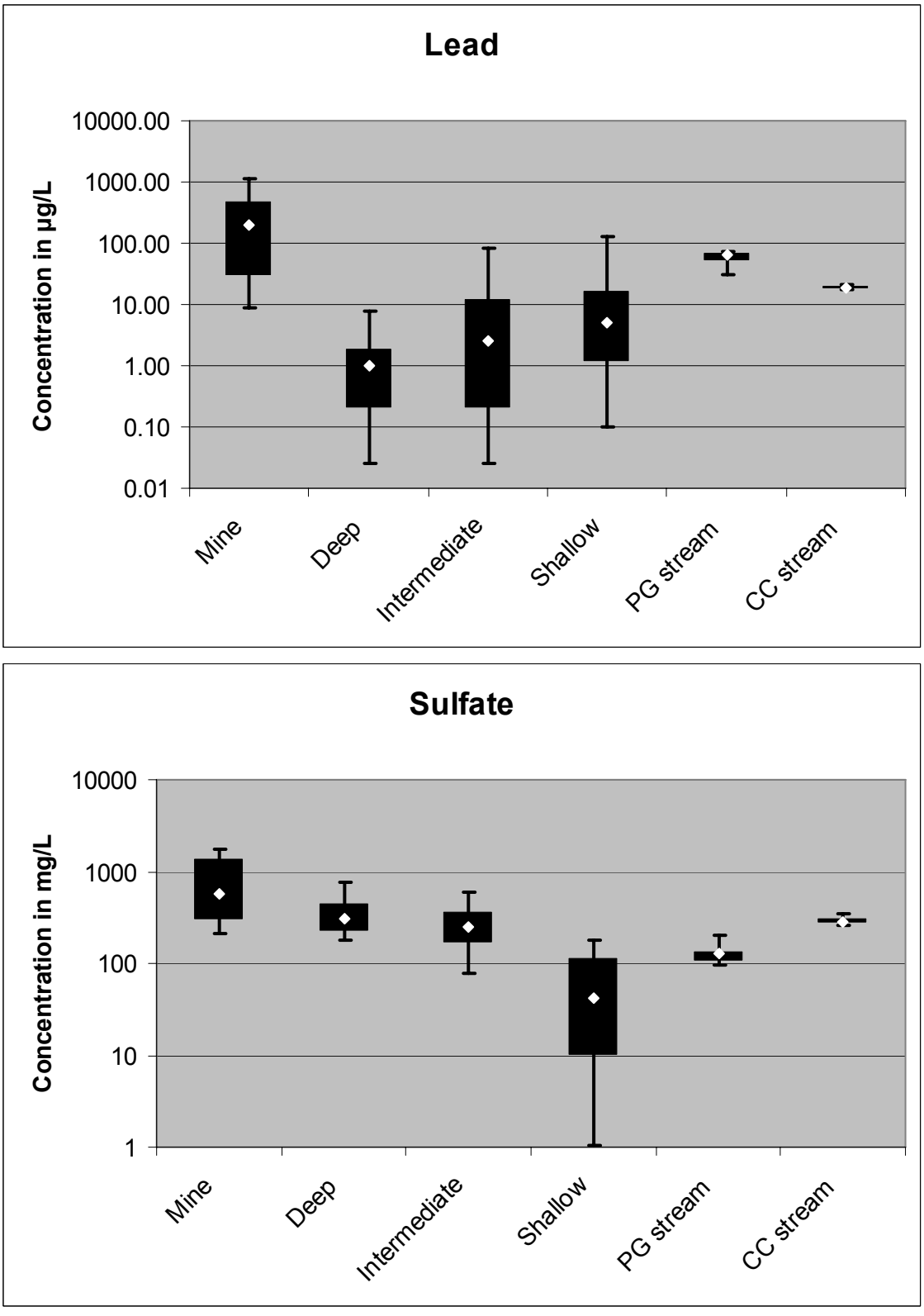

Figure 134: Water category comparisons for lead and sulfate.

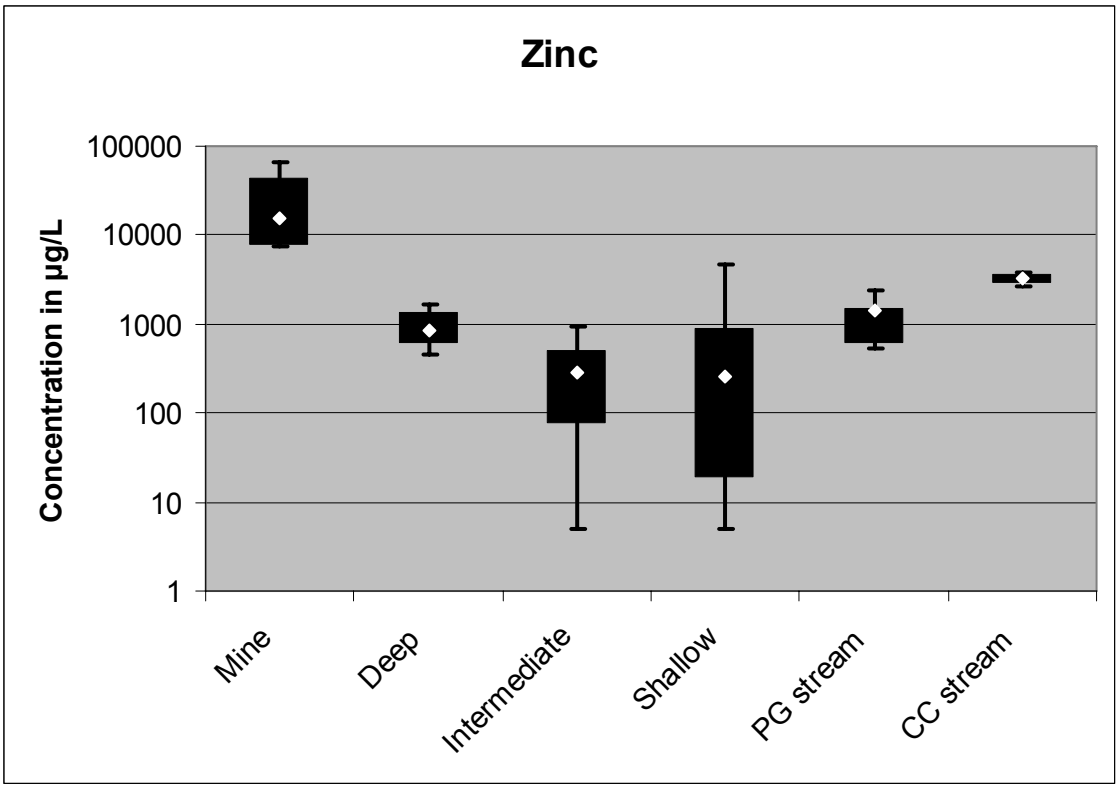

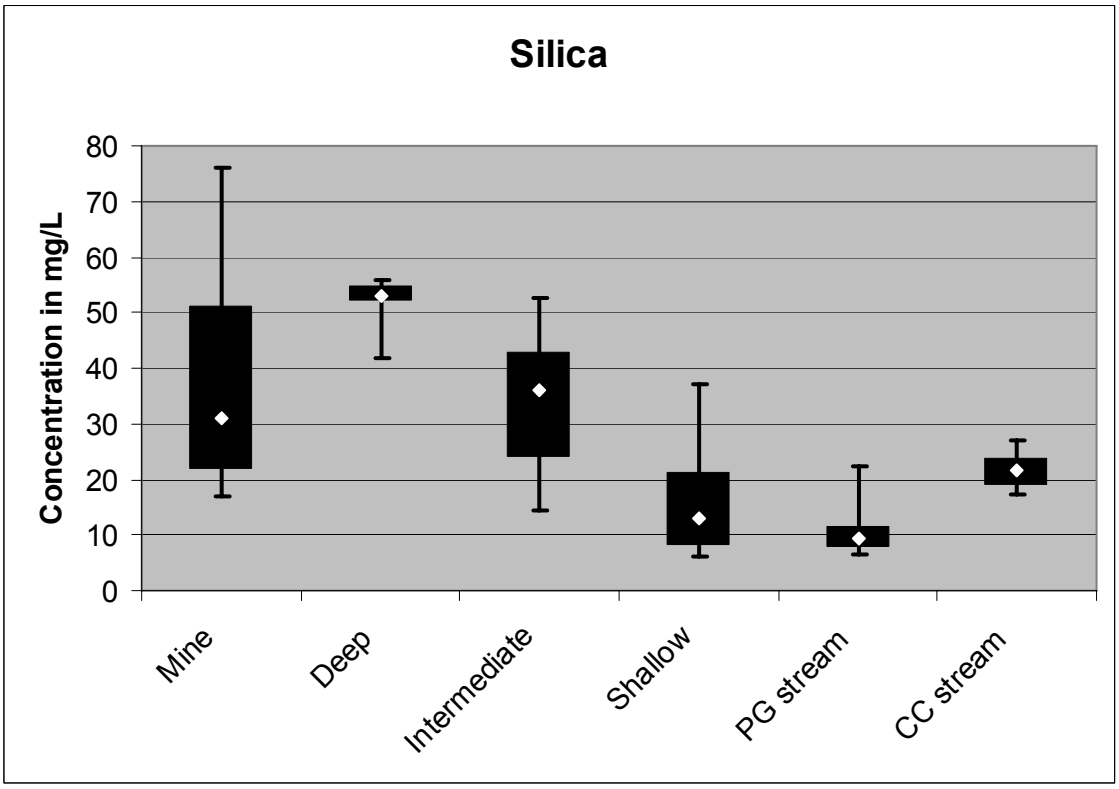

Figure 135: Water category comparisons for zinc and silica.

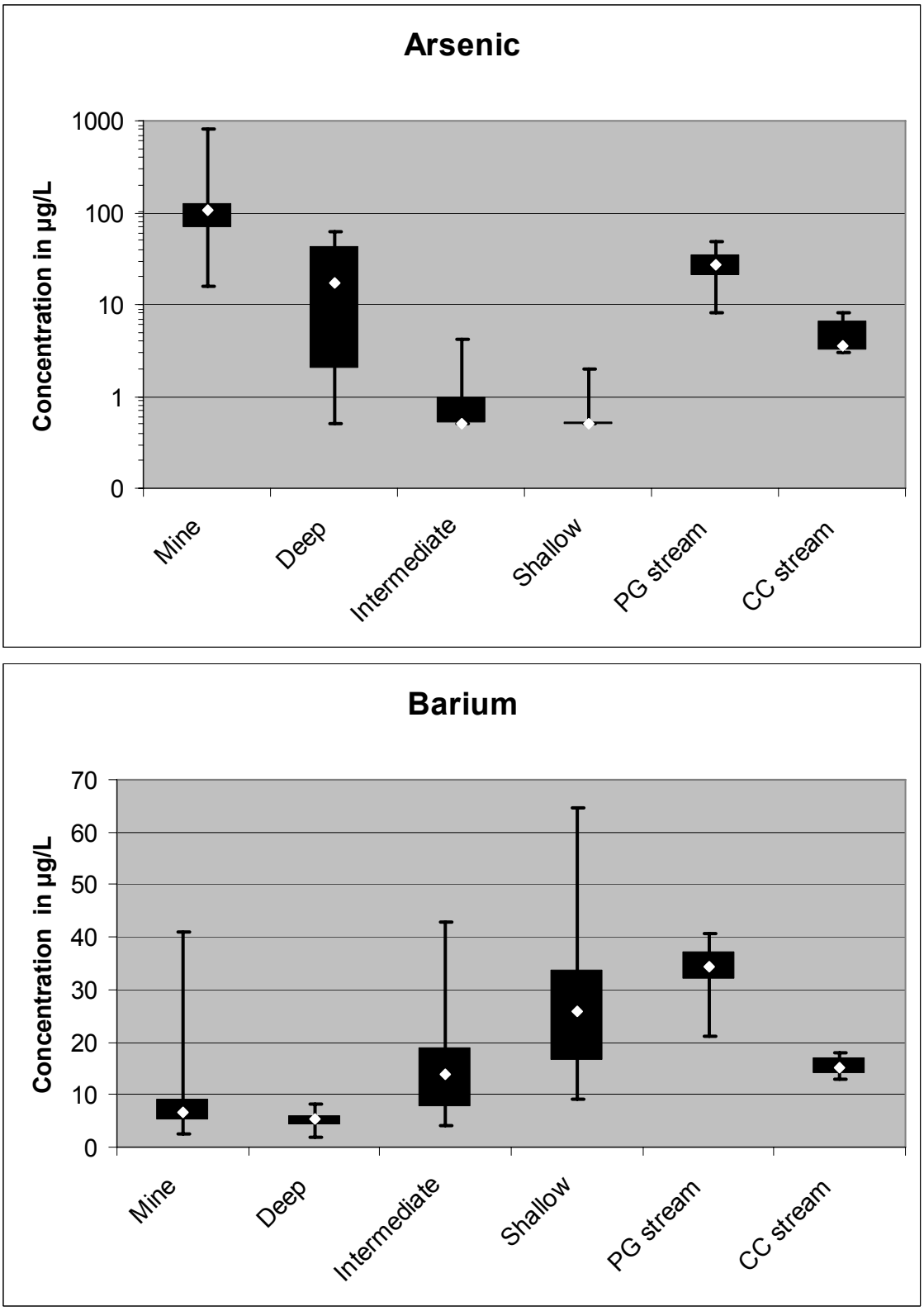

Figure 136: Water category comparisons for arsenic and barium.

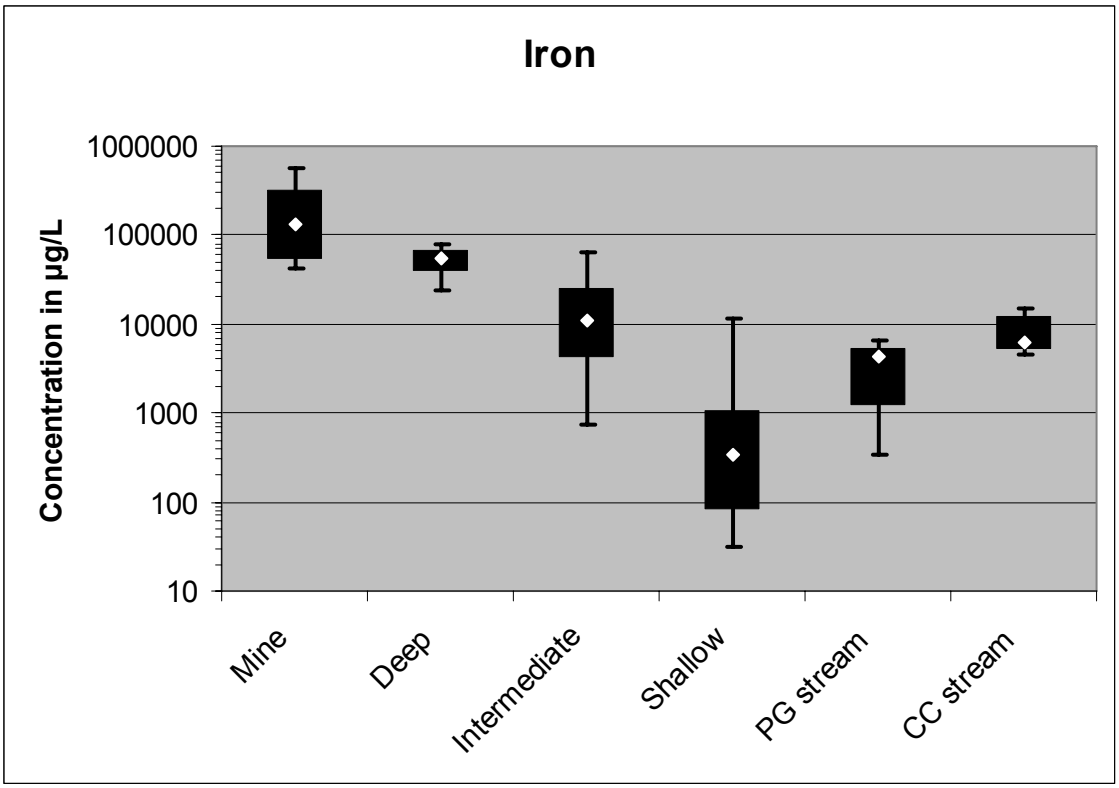

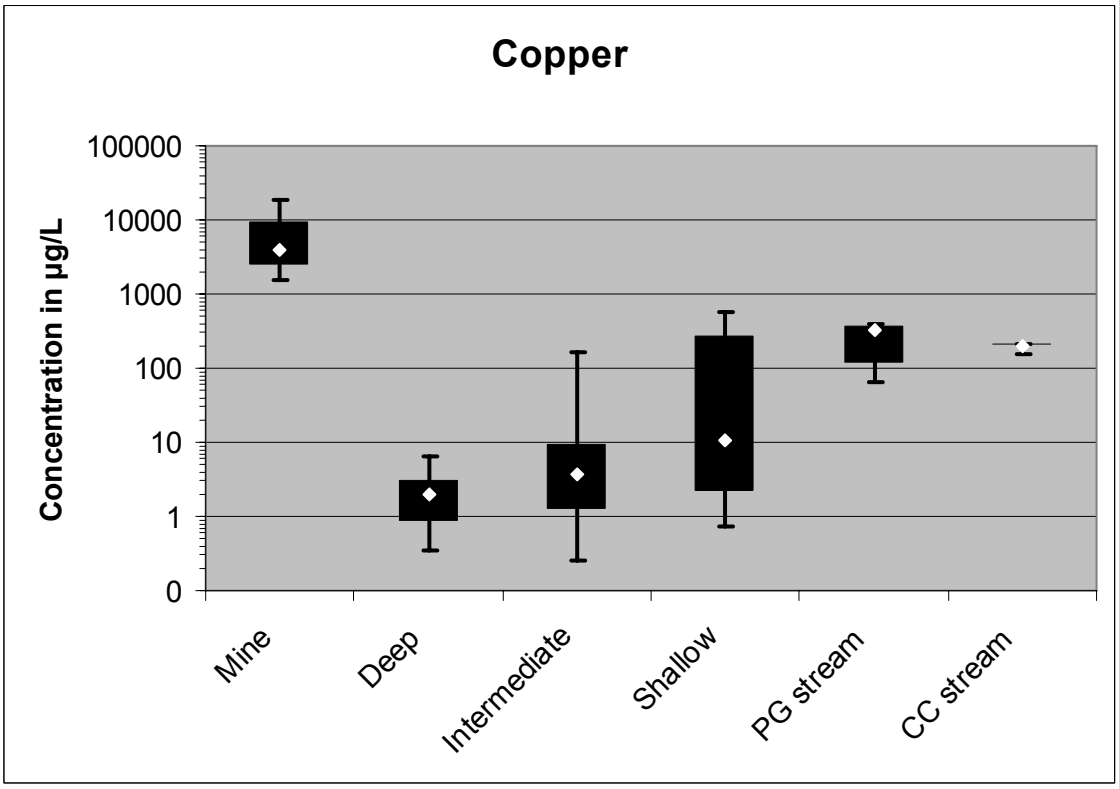

Figure 137: Water category comparisons for iron and copper.

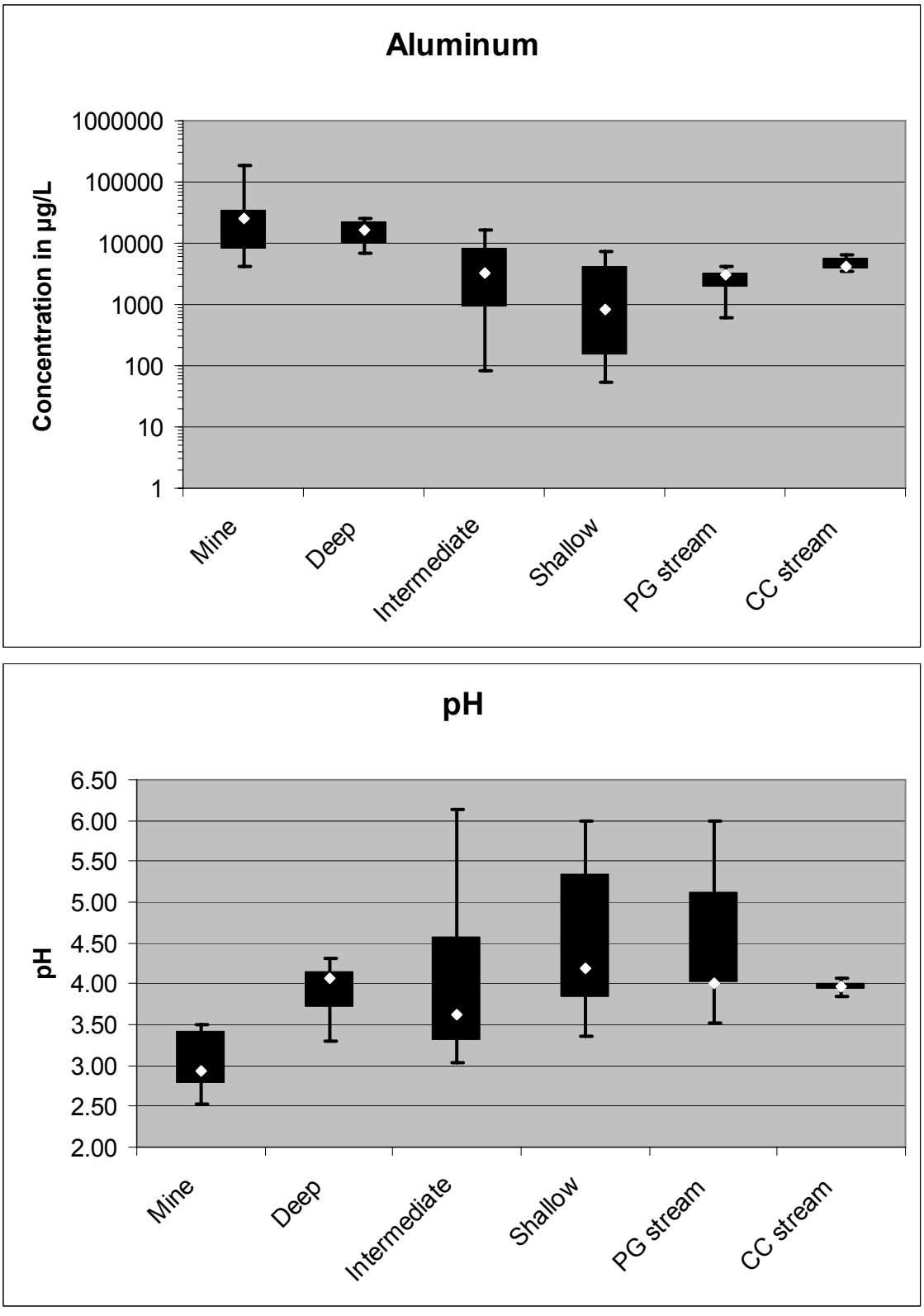

Figure 138: Water category comparisons for aluminum and pH.

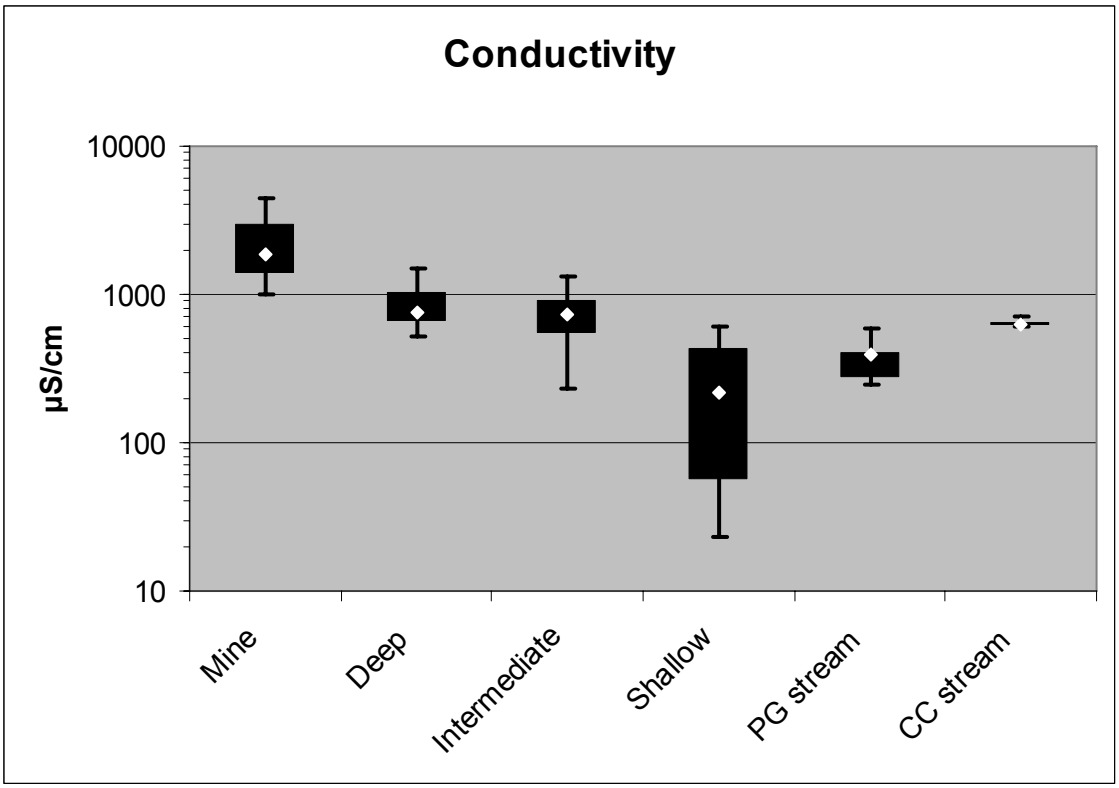

Figure 139: Water category comparison for conductivity.

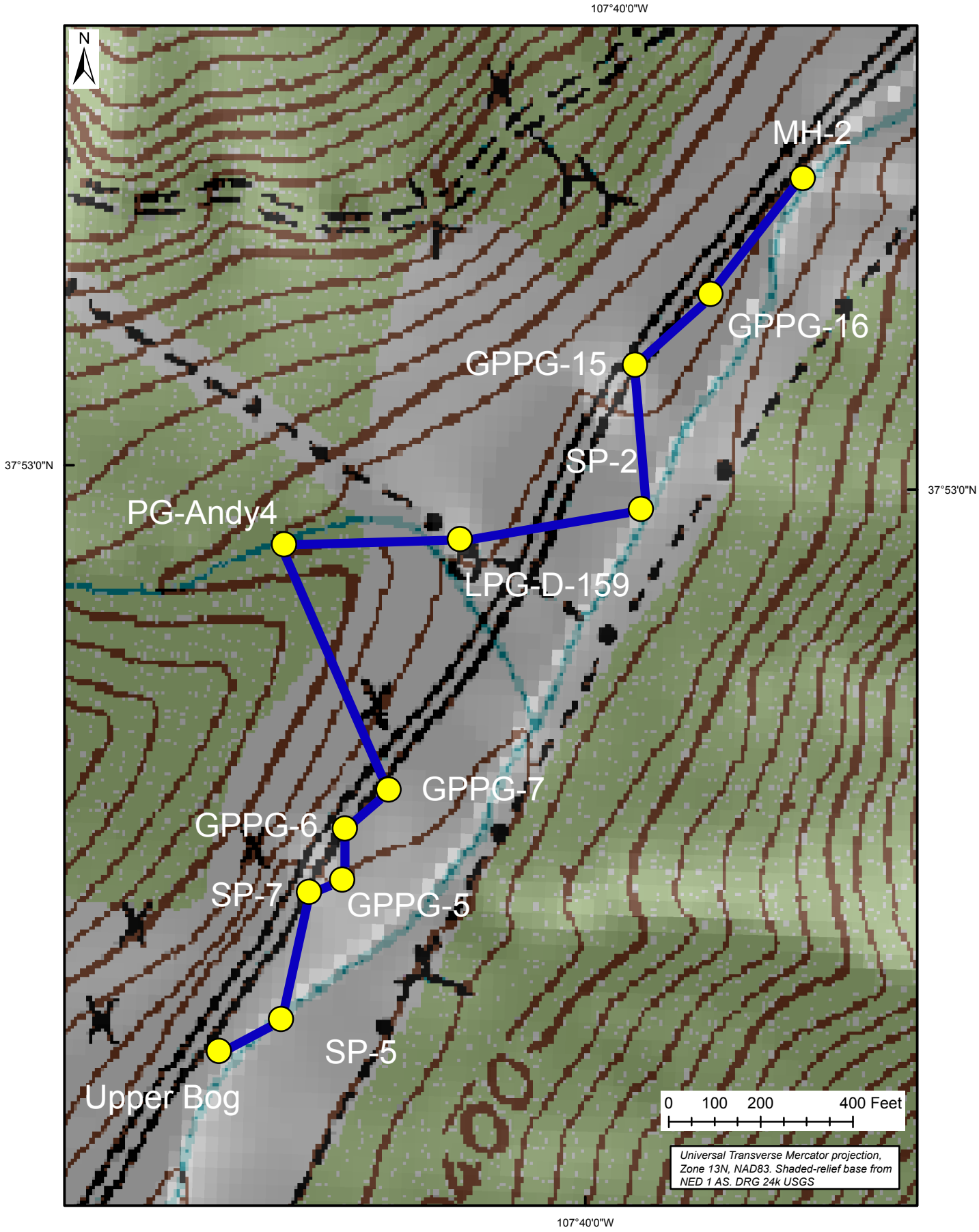

Figure 140: Location map of samples for downstream trend analysis. Line indicates sample order going downstream.

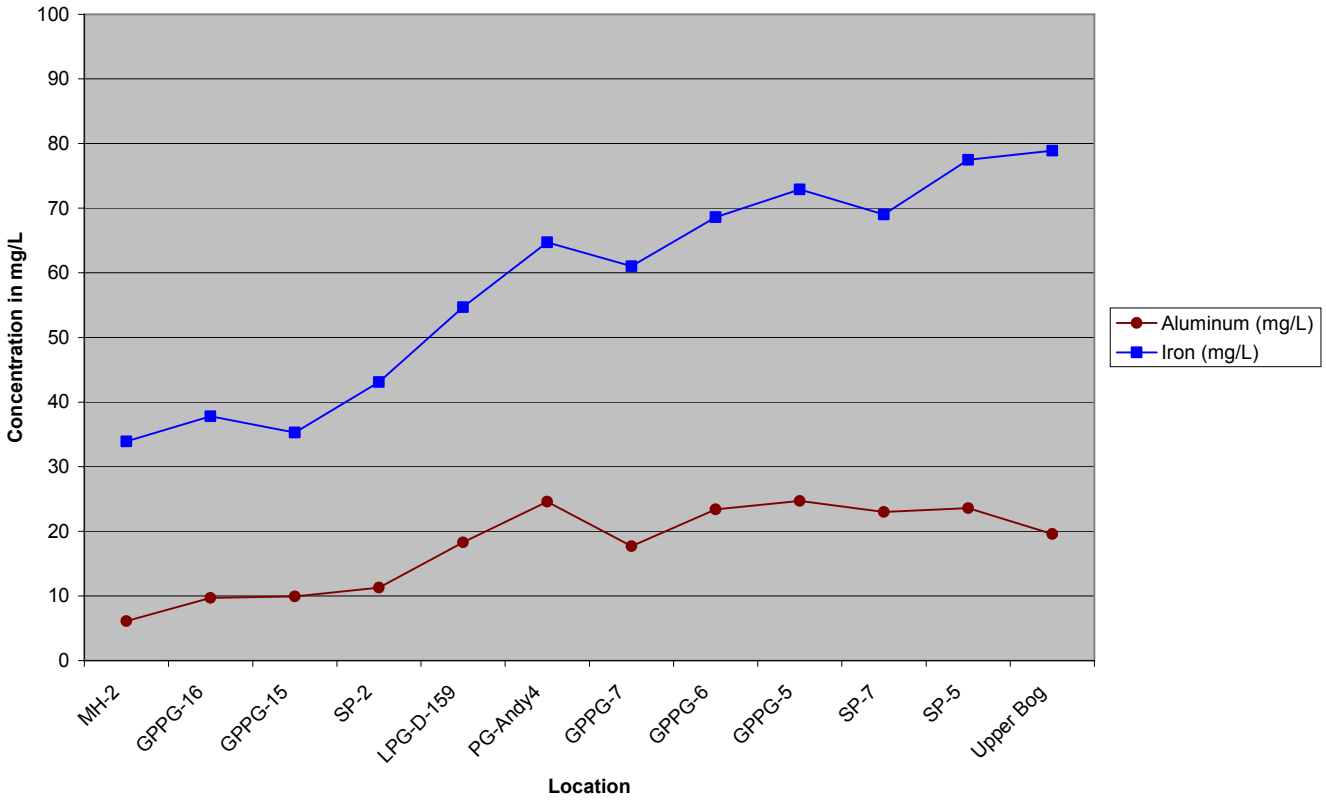

Figure 141: Downstream trend for aluminum and iron along Cement Creek from Gladstone to the Upper Bog.

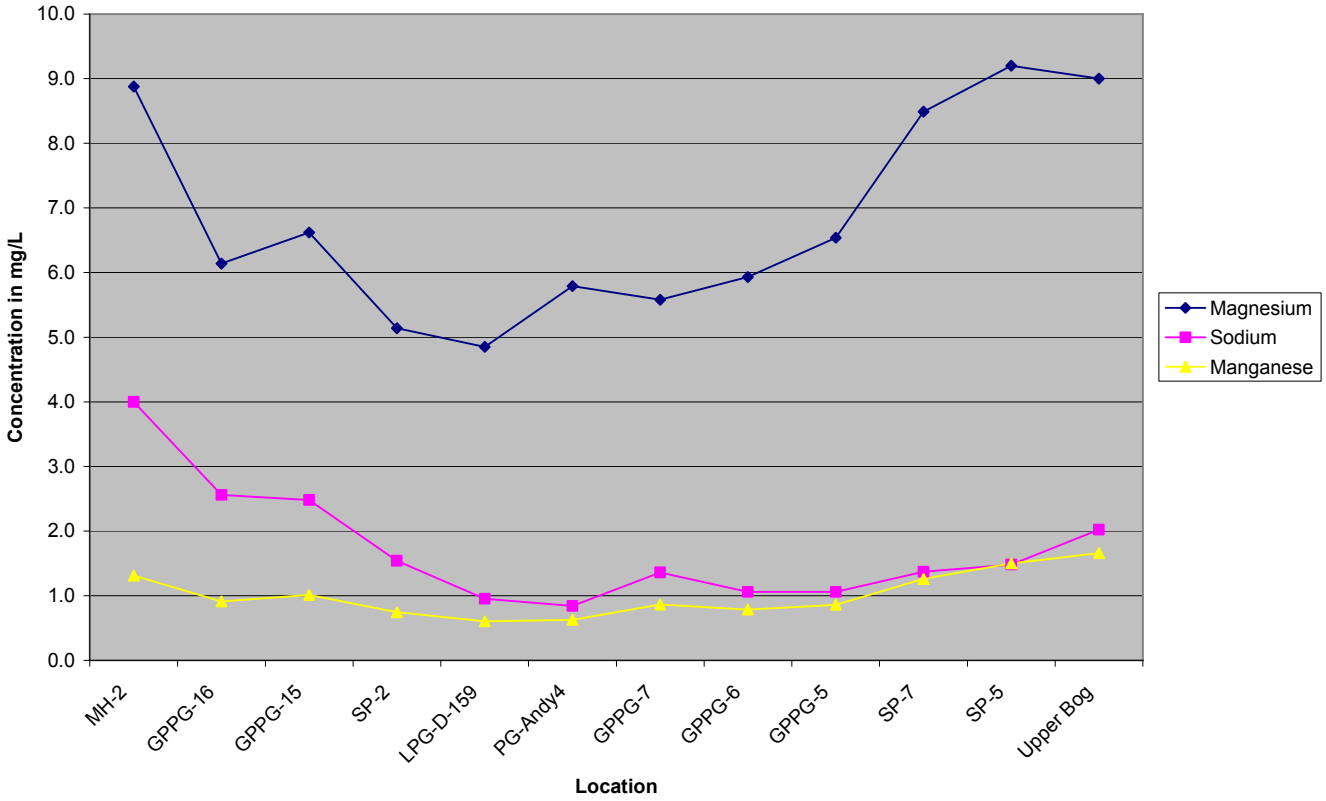

Figure 142: Downstream trend for magnesium, sodium, and manganese along Cement Creek from Gladstone to the Upper Bog.

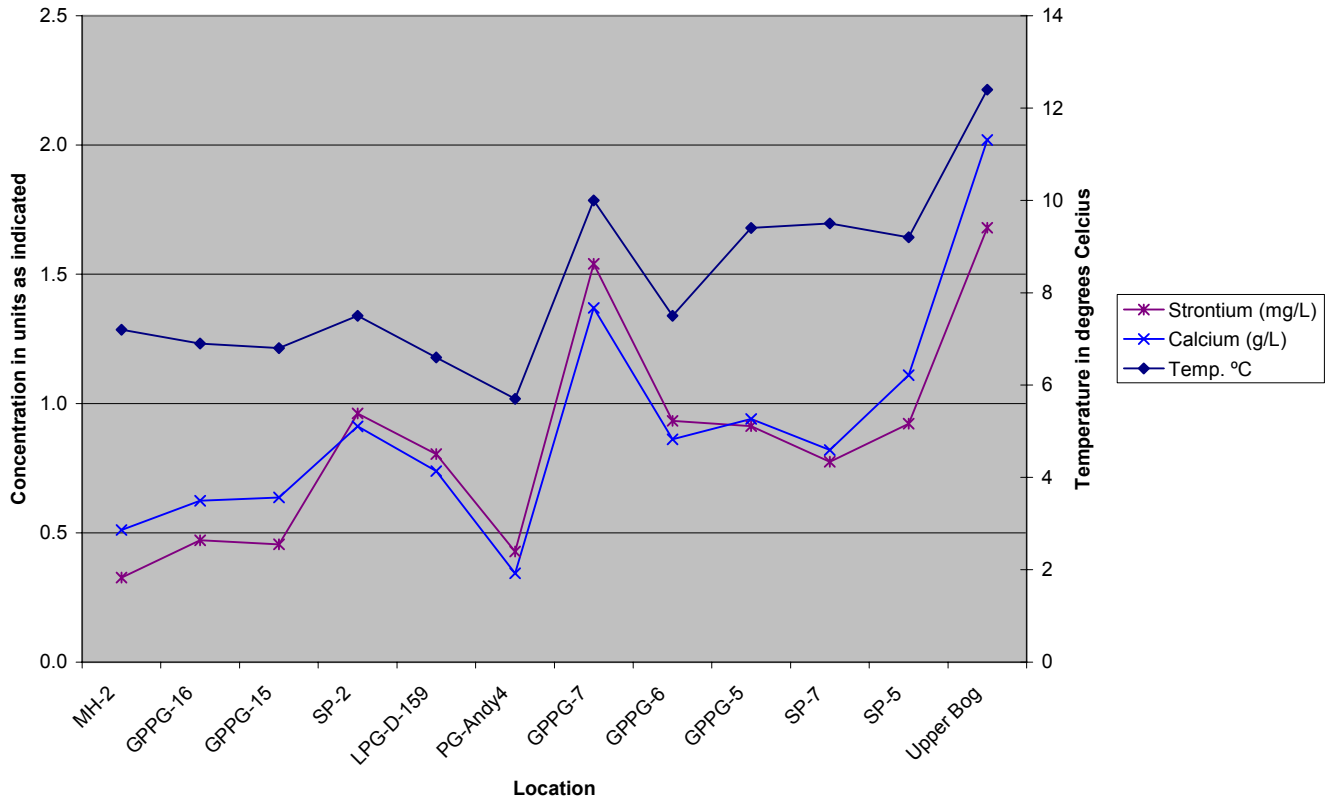

Figure 143: Downstream trend for calcium, strontium, and temperature along Cement Creek from Gladstone to the Upper Bog.

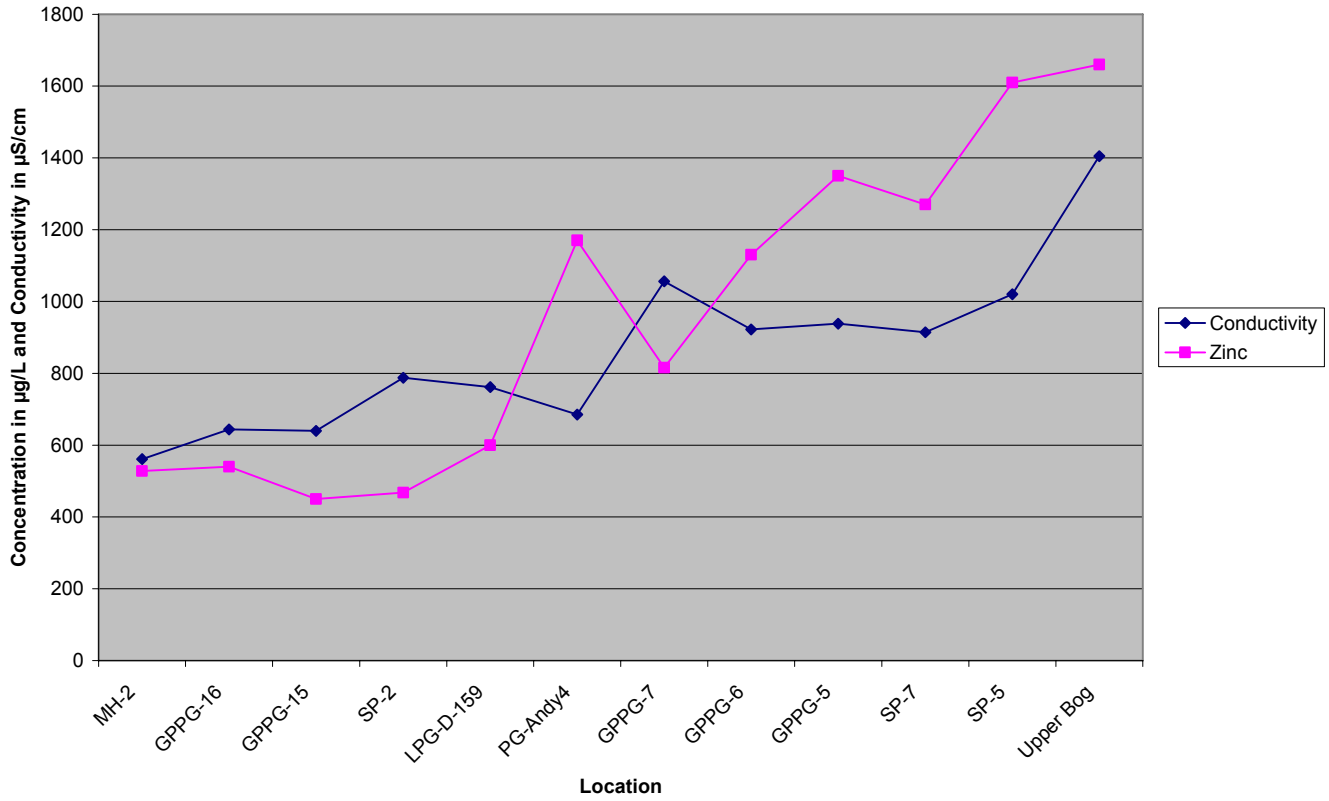

Figure 144: Downstream trend for conductivity and zinc along Cement Creek from Gladstone to the Upper Bog.

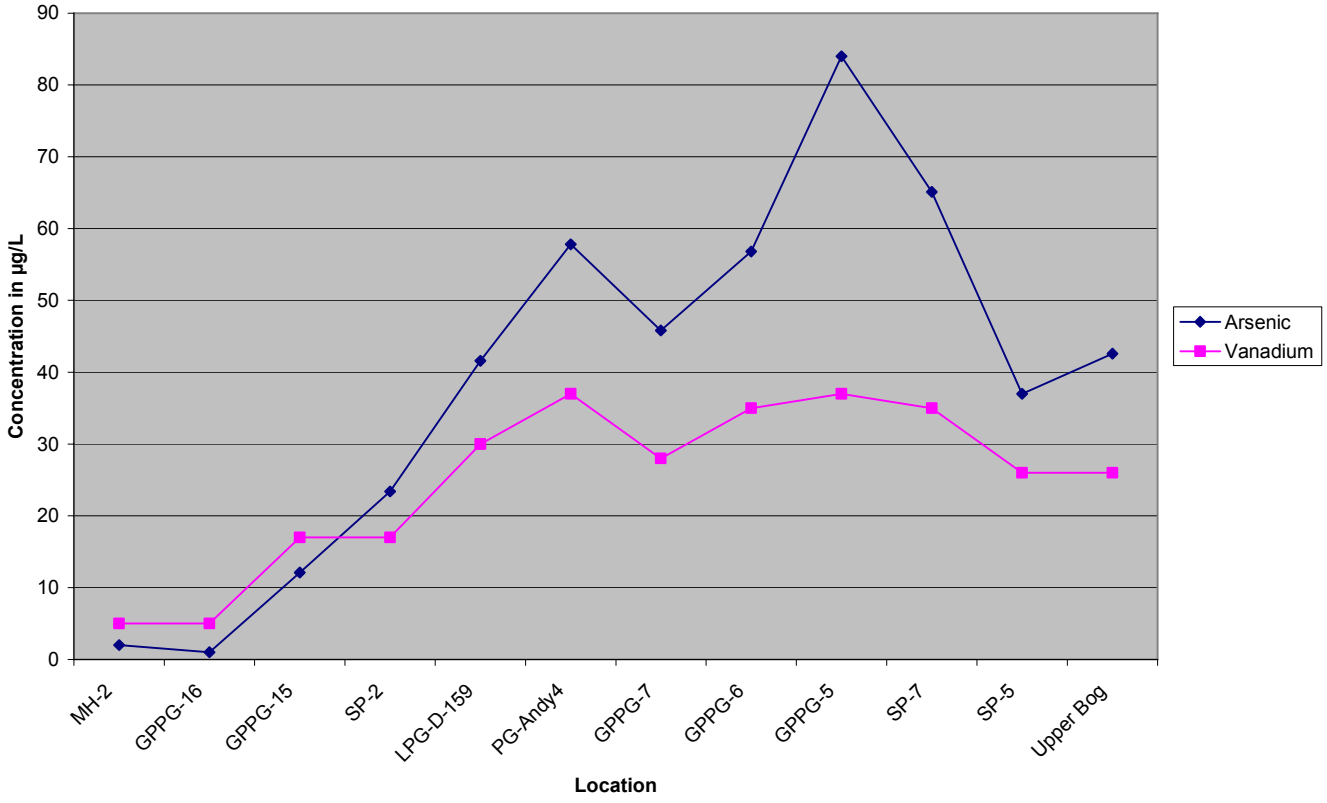

Figure 145: Downstream trend for arsenic and vanadium along Cement Creek from Gladstone to the Upper Bog.

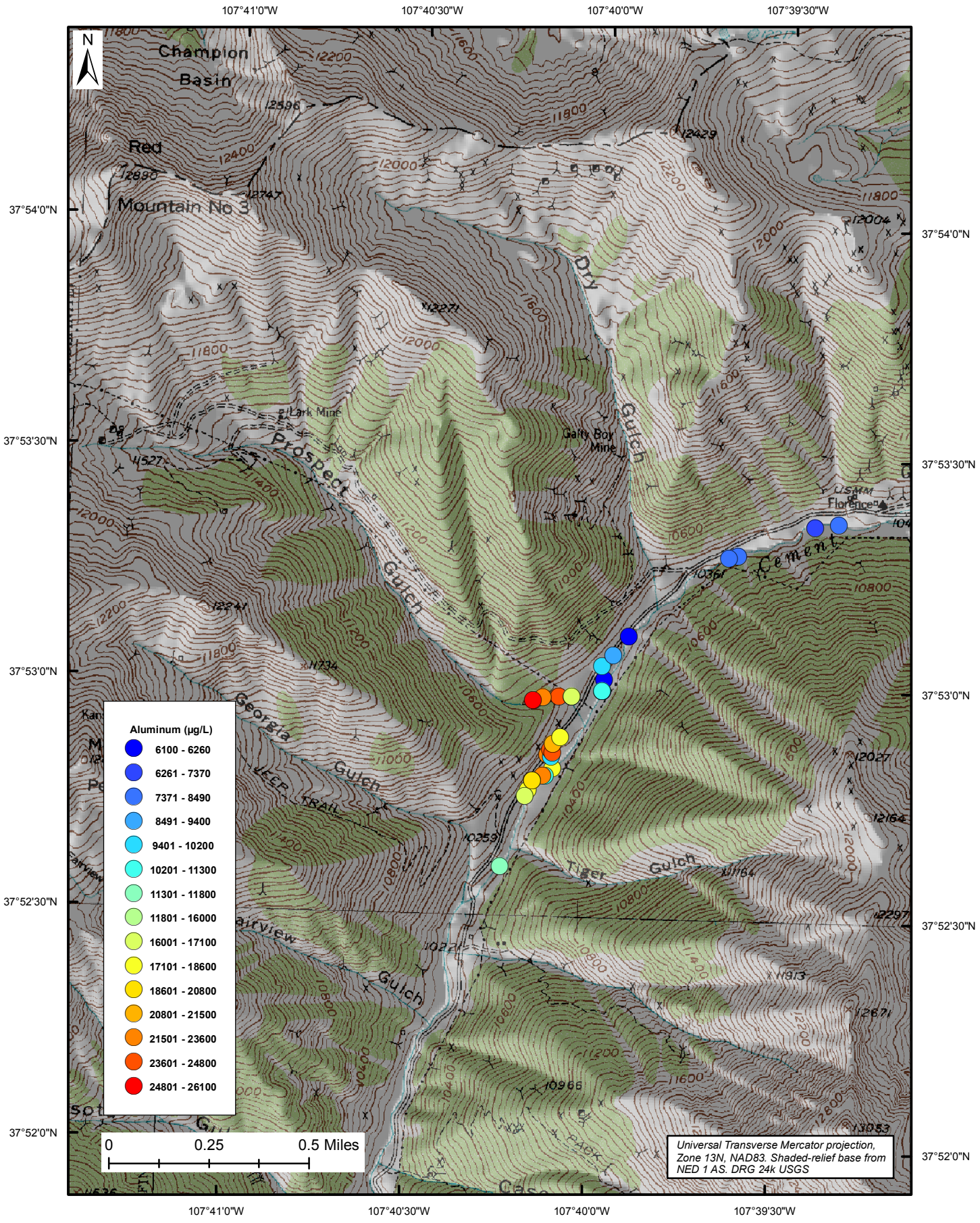

Figure 146: Deep ground-water concentrations of aluminum in µg/L.

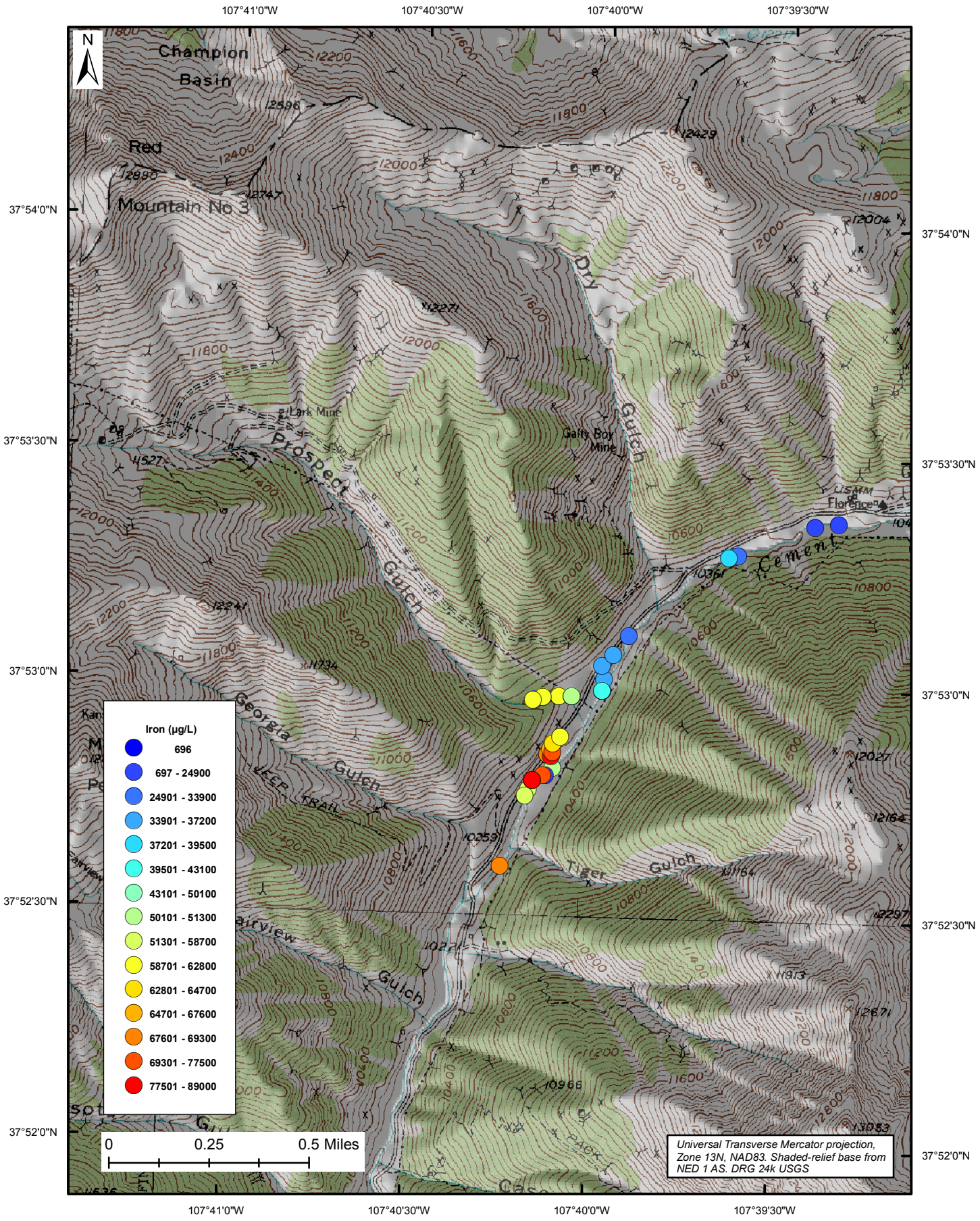

Figure 147: Deep ground-water concentrations of iron in µg/L.

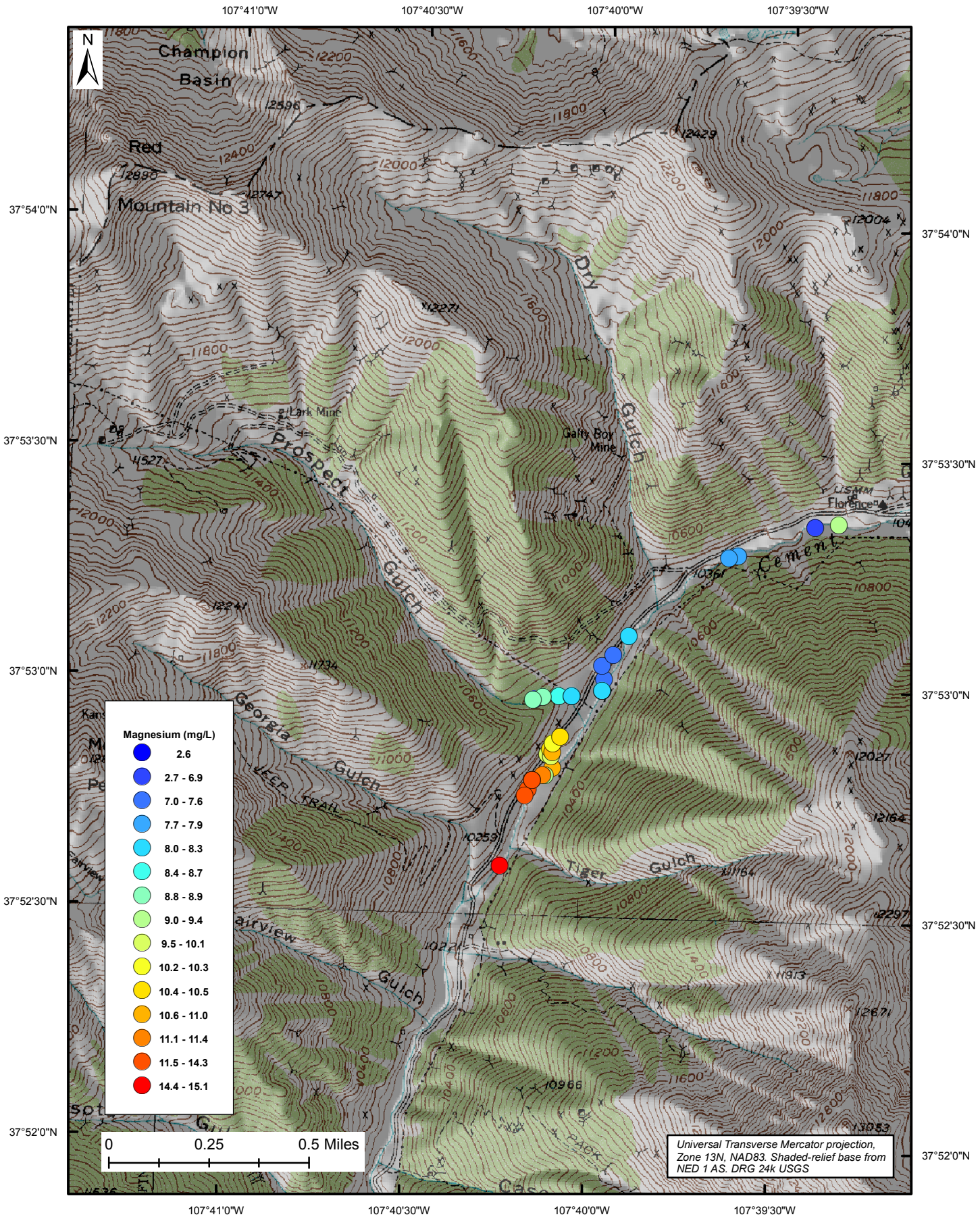

Figure 148: Deep ground-water concentrations of magnesium in mg/L.

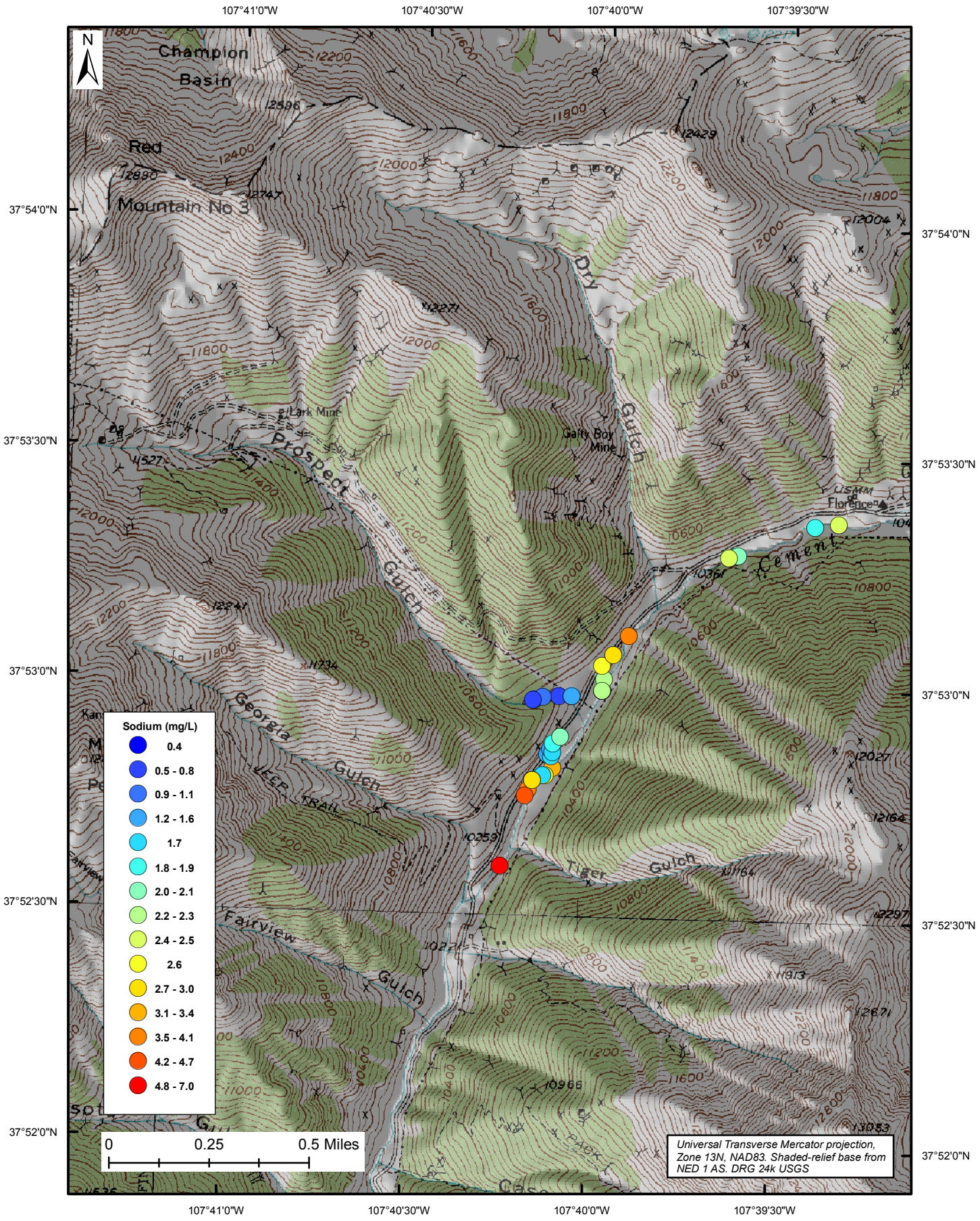

Figure 149: Deep ground-water concentrations of sodium in mg/L.

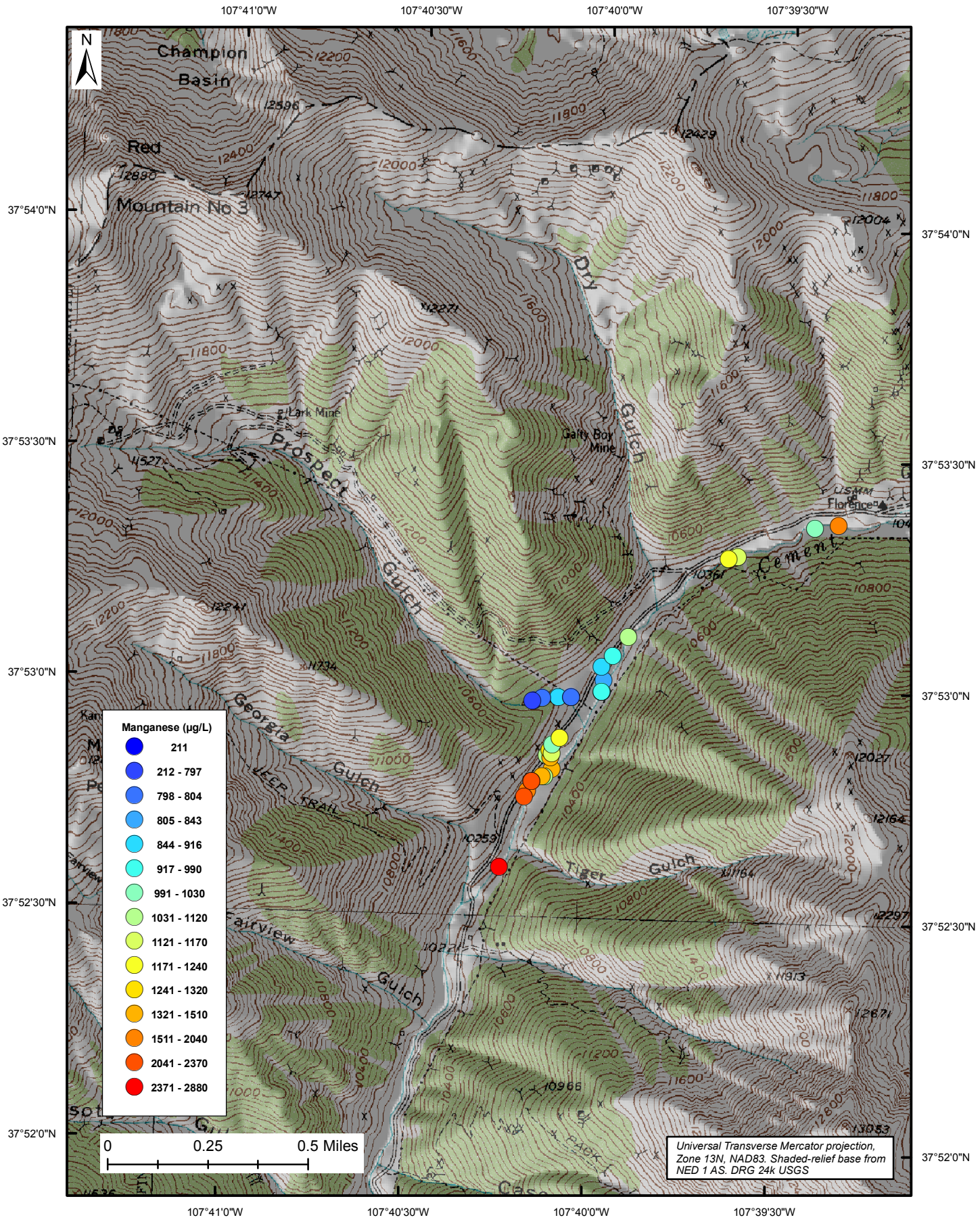

Figure 150: Deep ground-water concentrations of manganese in µg/L.

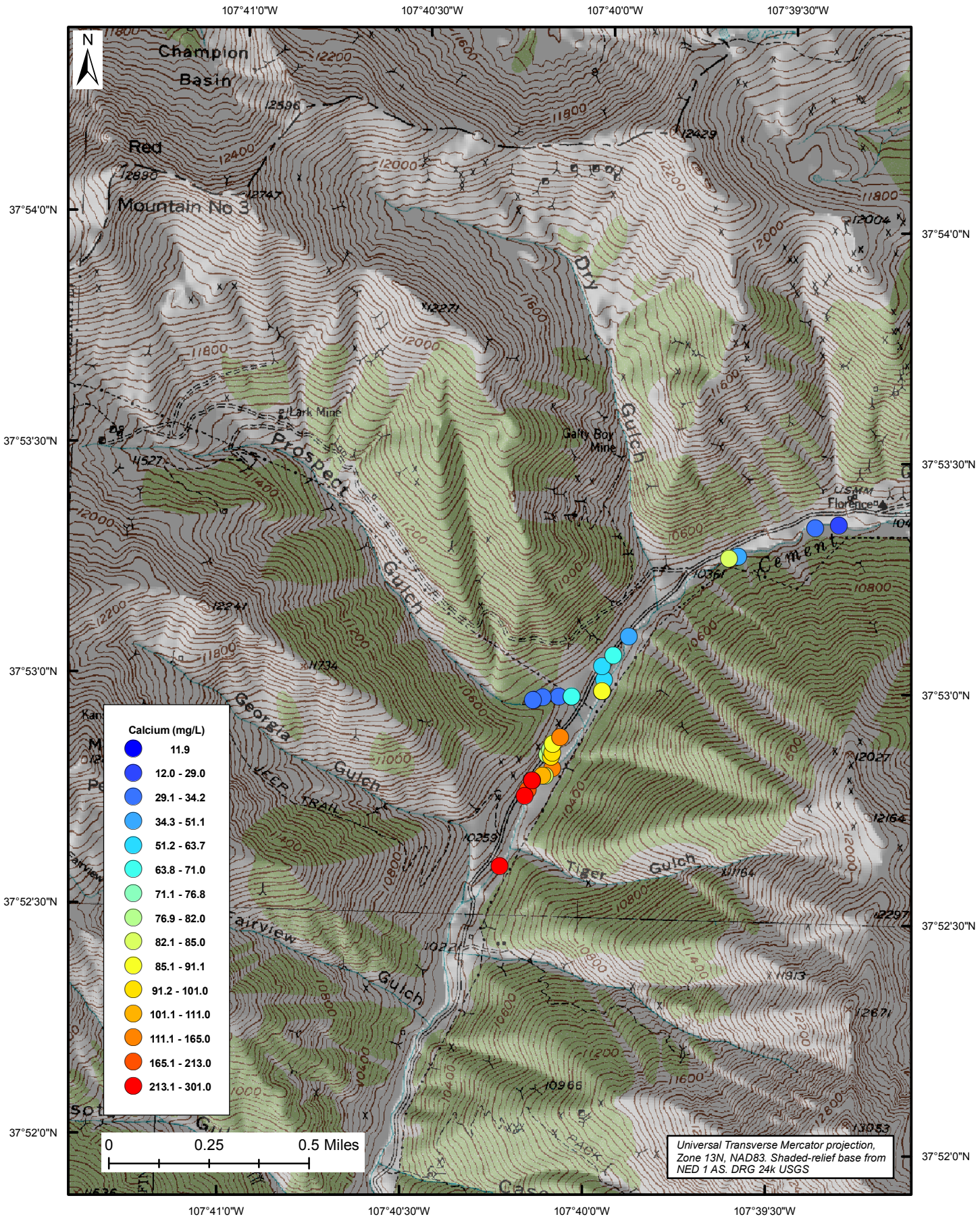

Figure 151: Deep ground-water concentrations of calcium in mg/L.

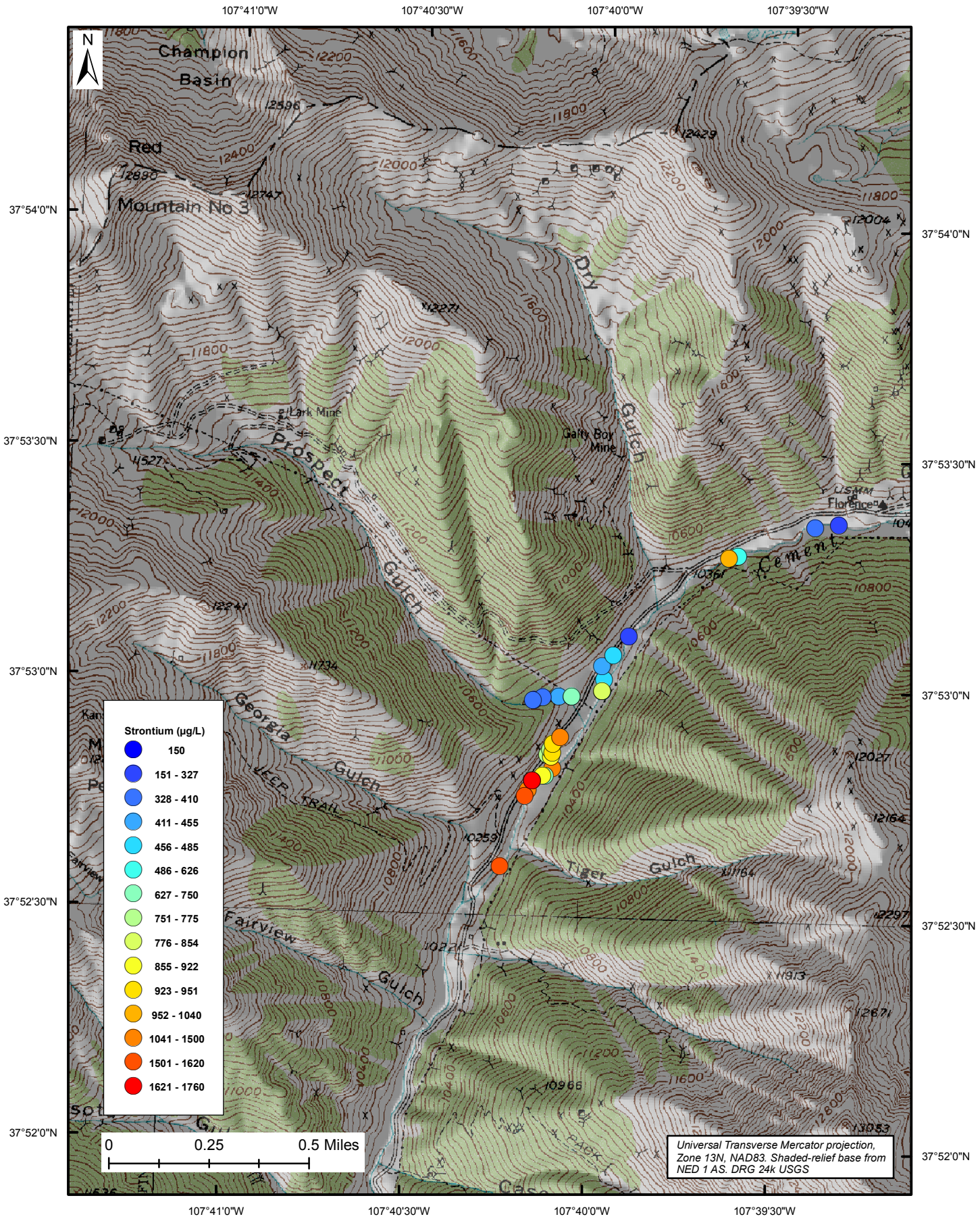

Figure 152: Deep ground-water concentrations of strontium in µg/L.

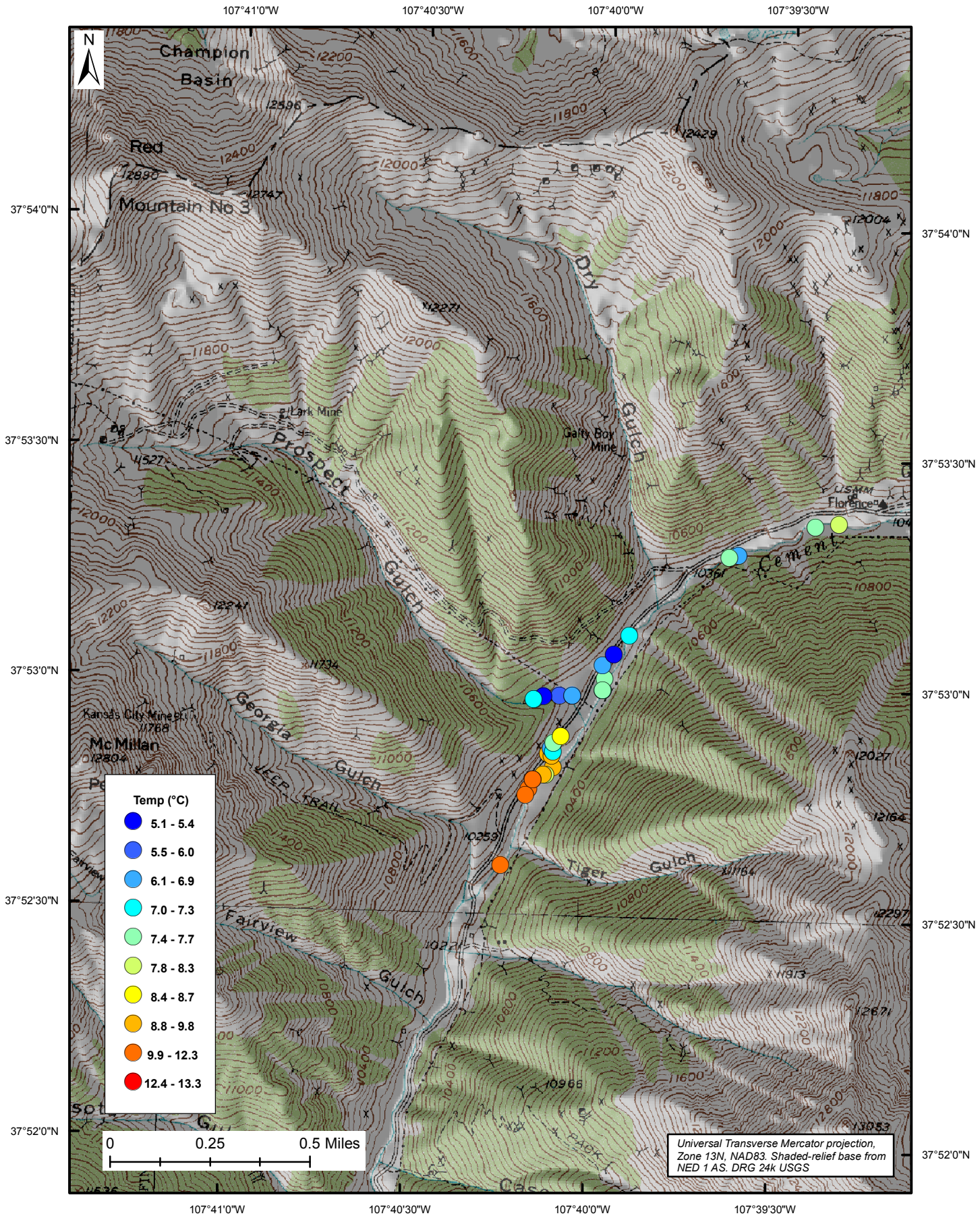

Figure 153: Deep ground-water temperature in °C.

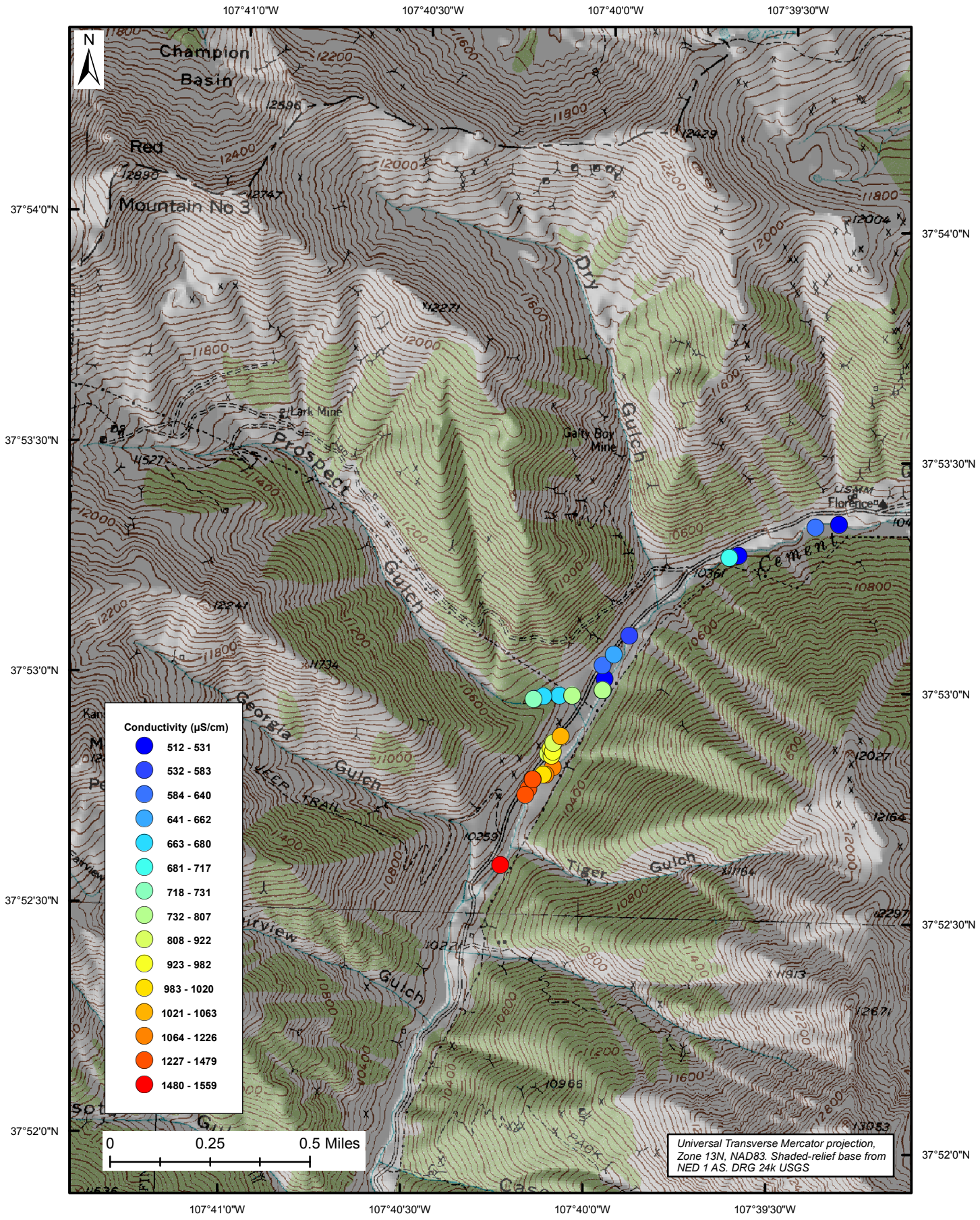

Figure 154: Deep ground-water conductivity in µS/cm.

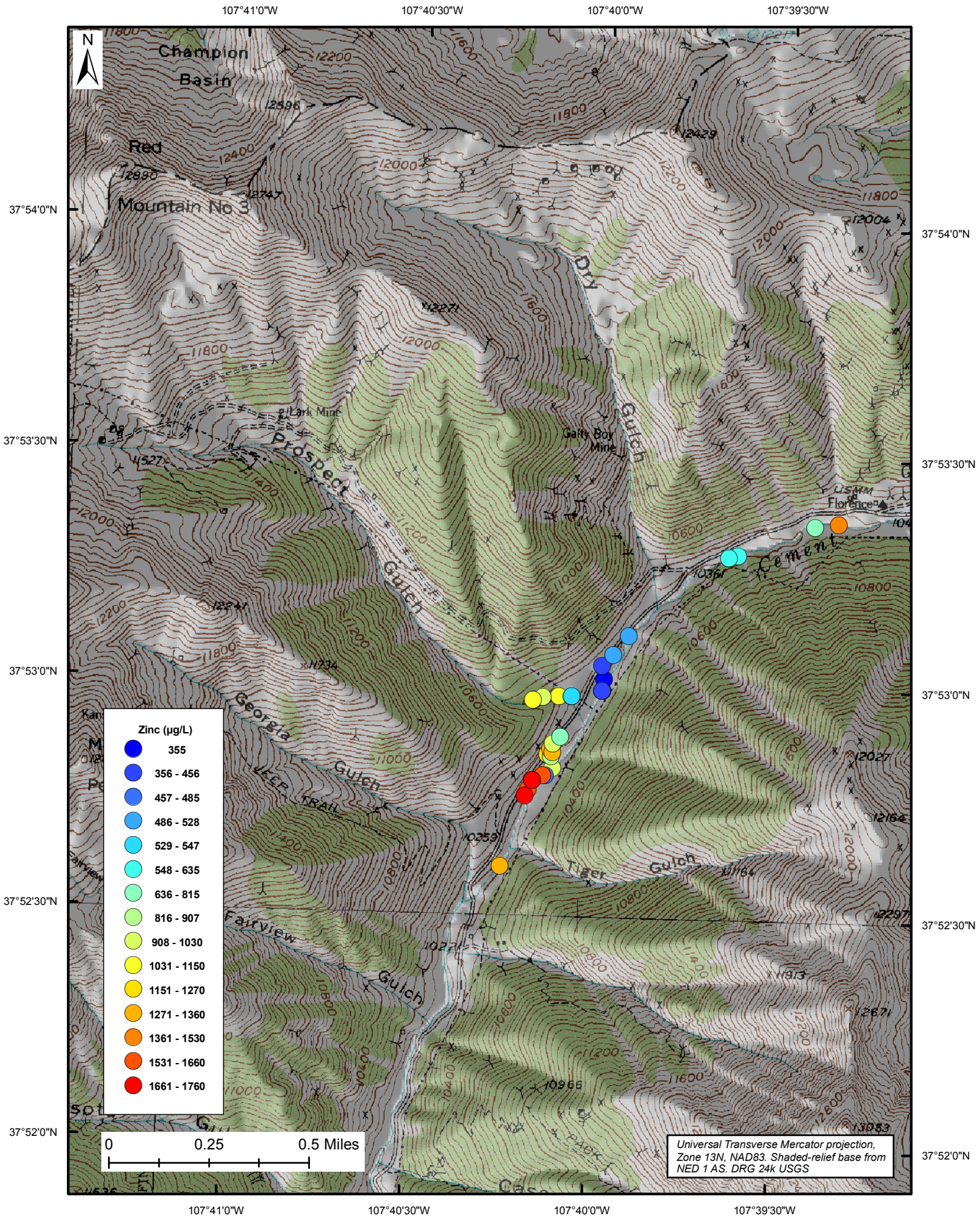

Figure 155: Deep ground-water concentrations of zinc in µg/L.

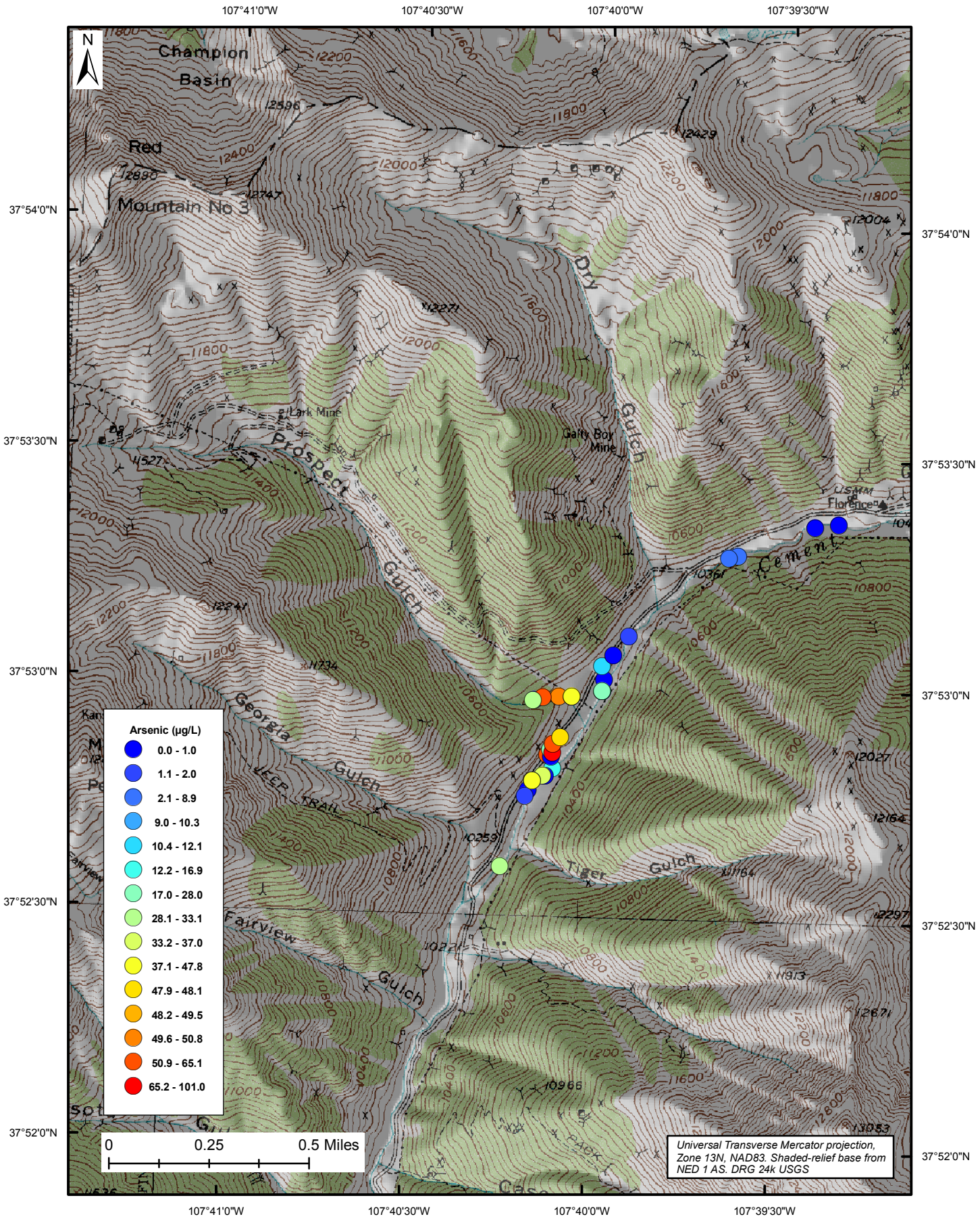

Figure 156: Deep ground-water concentrations of arsenic in µg/L.

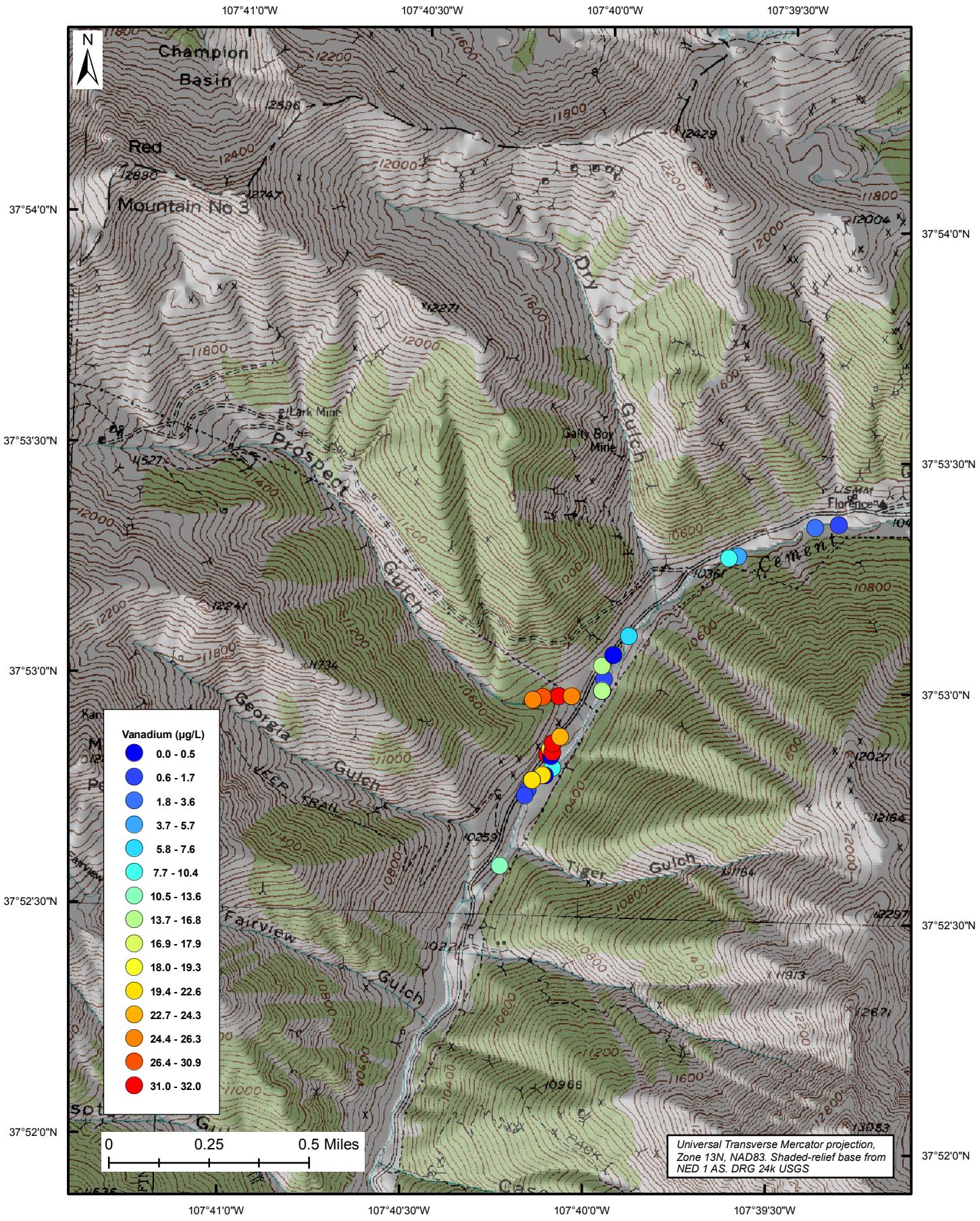

Figure 157: Deep ground-water concentrations of vanadium in µg/L.

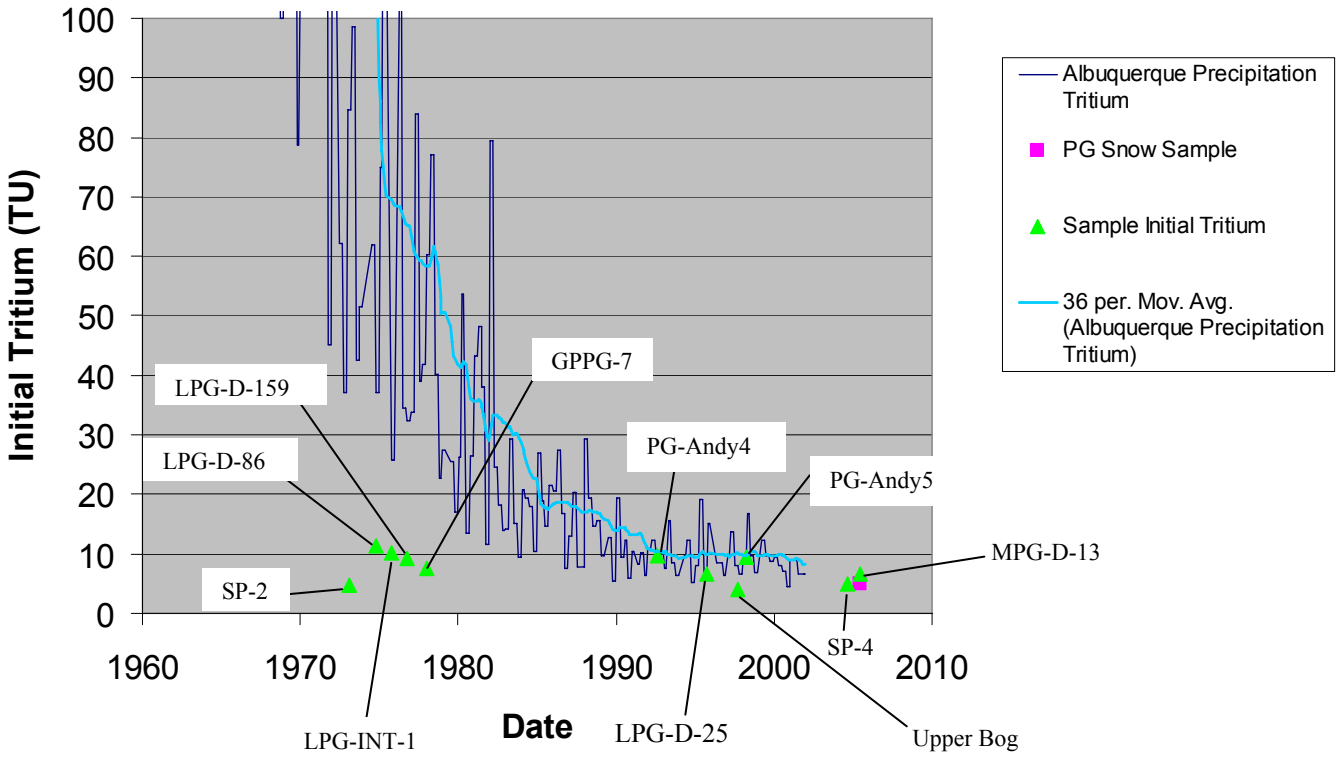

Figure 158: Comparison of Prospect Gulch sample initial tritium (^{3}H) values (measured ^{3}H + modeled tritiogenic ^{3}He) with the precipitation ^{3}H record for Albuquerque, N. Mex. and the PG-Snow-1 sample. Sample initial tritium values are plotted against the apparent recharge year as indicated by the apparent ^{3}H/^{3}He age.

Table 1: Streamflow measurements in cubic feet per second.

Date	Gladstone	Above Prospect	Renoux Bridge	Below Georgia	Prospect Gulch	Cement Creek
August 4, 2004	7.5	8.8	9.6	11.7	0.38	19
August 25, 2004	5.4	6.3	8.1	7.9	0.44	14
September 28, 2004	10.6	12.3	17.5	18.6	0.99	28
October 30, 2004	7.6	8.3	9.5	11.1	0.50	19
January 19, 2005	3.8	5.1*	7.0	7.3*	0.30	13
March 14, 2005	3.6	5.3	7.5	9.1	0.38	16
April 22, 2005	7.9	13.9	18.2	19.5	2.18	51
May 26, 2005	118	124	146	129	32	328
June 29, 2005	48.7	49.1	61.1	59.3	7.21	108
August 16, 2005	11.9	12.7	14.8	13.4	0.77	28

Note:
*January 19, 2005 data for Above Prospect and Below Georgia are estimated using regression curves because of measurement difficulties. Column for Cement Creek is at USGS gauge 09358550 at the mouth of Cement Creek. Locations are indicated in Figure 2.

Table 2: Noble gas and helium/tritium results.
[atm, atmospheres; ft, feet; °C, degrees Celsius; n/a, not available]

Sample ID	Sample type	Collection date	Total dissolved gas pressure (atm)	Assumed recharge elevation (ft)	Modeled recharge temperature (°C)	Modeled delta Neon (percent of solubility)
SP-2	spring	8/23/2004	0.830	11200	12.4	78
Upper Bog	spring	8/25/2004	0.702	11200	0.2	3
SP-4	spring	8/25/2004	0.692	11200	0.0	14
PG-Andy4	spring	8/25/2004	0.718	11200	0.0	17
PG-Andy5	spring	8/25/2004	0.668	11950	3.0	2
LPG-INT-1	well	8/26/2004	1.280	11200	4.0	221
LPG-D-25	well	9/1/2004	n/a	10400	8.3	44
LPG-D-86	well	9/1/2004	n/a	11200	2.6	205
LPG-D-159	well	9/1/2004	n/a	11200	2.7	210
MPG-D-13	well	6/26/2005	n/a	11300	5.9	55
PG-SNOW-1	snow	6/26/2005	n/a	n/a	n/a	n/a
PG-Structure-1	stream	6/26/2005	n/a	n/a	n/a	n/a
GPPG-7	piezometer	6/27/2005	n/a	11200	1.4	65
GPPG-14	piezometer	6/27/2005	n/a	n/a	n/a	n/a

Notes:
All sample locations can be found in appendix A.
Sample PG-Snow-1 was taken near PGdrillwater.
Total dissolved gas pressure is measured in the field with a probe.
delta Neon is the excess air component of Neon.

Table 2: Noble gas and helium/tritium results—*Continued*.
[TU, tritium units; yr, year; n/a, not available]

Sample ID	Modeled terrigenic ^{4}He (percent of solubility)	Modeled tritiogenic ^{3}He (TU)	^{3}H (TU)	Apparent age (yr)	Initial ^{3}H (TU)
SP-2	24	3.94	0.80	31.6	4.7
Upper Bog	10	1.28	2.68	6.9	4.0
SP-4	-1	-0.57	4.88	-2.2	4.3
PG-Andy4	3	4.77	4.95	12.0	9.7
PG-Andy5	0	2.89	6.67	6.4	9.6
LPG-INT-1	16	8.14	2.00	28.8	10.1
LPG-D-25	-1	2.62	4.03	8.9	6.7
LPG-D-86	16	9.15	2.09	29.9	11.2
LPG-D-159	17	7.21	1.90	27.9	9.1
MPG-D-13	0	-0.69	6.71	-1.9	6.0
PG-SNOW-1	n/a	n/a	5.08	n/a	n/a
PG-Structure-1	n/a	n/a	6.18	n/a	n/a
GPPG-7	37	5.91	1.61	27.4	7.5
GPPG-14	n/a	n/a	4.67	n/a	n/a

Notes:

Terrigenic ^{4}He is produced in the subsurface by the radioactive decay of U and Th.
Tritogenic ^{3}He is derived from the decay of ^{3}H.
Initial ^{3}H is the sum of the measured ^{3}H and modeled tritogenic ^{3}He.